ION CONDUCTING POLYMER / GEL ELECTROLYTES BASED SOLID STATE SUPERCAPACITORS
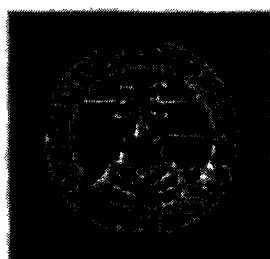
A THESIS SUBMITTED IN PARTIAL
FULFILMENT OF THE REQUIREMENTS FOR
THE DEGREE OF

DOCTOR OF PHILOSOPHY

BY

SANTOSH KUMAR TRIPATHI

Registration Number: 014 of 2003

**School of Science & Technology
Department of Physics
Tezpur University
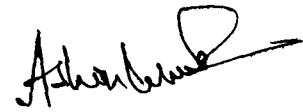Tezpur - 784028
India**

September, 2005

CERTIFICATE

This is to certify that the thesis entitled *"Ion Conducting Polymer/Gel Electrolytes based Solid State Supercapacitors"* which is being submitted by Mr. Santosh Kumar Tripathi for the award of the degree of Doctor of Philosophy to the Department of Physics, School of Science and Technology, Tezpur University is entirely based on the experimental work carried out by him under our joint supervision. The result reported in this thesis embodies the work of the candidate himself. It is original and has not been submitted to any other University or Institute for the award of any degree or diploma.

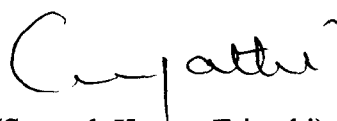(Dr. S. A. Hashmi)

(Dr. Ashok Kumar)

DECLARATION

I hereby declare that the thesis entitled *"Ion Conducting Polymer/Gel Electrolytes based Solid State Supercapacitors"* which is being submitted for the award of the degree of Doctor of Philosophy to the Department of Physics, School of Science and Technology, Tezpur University is based on bonafide experimental work carried out by me. The results embodied in this thesis have not been submitted, in part or in full, to any other university or institution for the award of any degree or diploma.

(Santosh Kumar Tripathi)

Department of Physics
Tezpur University
Tezpur - 784028

DEDICATED
TO

MY FATHER
SRI. PASHUPATI NATH TRIPATHI

MY MOTHER
SMT. DURGAWATI TRIPATHI

MY YOUNGER
MANJU, SANJU, RAKESH AND RENU

ACKNOWLEDGEMENT

(Santosh Kumar Tripathi)

CONTENTS

PREFACE

In recent few decades, a large number of ionic solids have been discovered, whose conductivity is of the order of 10^{-5}-10^{-1} S cm^{-1} at room temperature, which is comparable to that of liquid electrolytes. These solids are termed as Superionic Solids or Solid Electrolytes or Fast Ion Conductors. On the basis of composition, phase and microstructure, the ion conducting solids are classified into different classes such as, crystalline/polycrystalline solids, ion conducting glasses, composite electrolytes, polymer electrolytes and polymeric gel electrolytes.

Recently, polymeric gel electrolytes have been evolved as one of the most important classes of superionic materials formed by the dissolution of salts in polar, high dielectric solvent(s) and adding a neutral host polymer to achieve the mechanically stable and high ionic conductivity. The host polymers are presumed to be rather inert and their role is to entrap/immobilize the liquid electrolyte in their huge matrix. From the device fabrication point of view, it is essential to have good plasticising and adhesive properties as well as good elastomeric nature of the electrolyte materials. The gel electrolytes are of technological importance due to their important advantageous properties such as their (i) ease of synthesis, mostly in the form of thin films, (ii) flexibility useful for proper electrode-electrolyte contacts, (iii) mechanical stability to show solid like behaviour, (iv) higher electrical conductivity owing to their liquid like behaviour etc.

Supercapacitors have recently come up as one of the most important energy storage devices. Basically these are new and innovative type of electrochemical capacitors which have 20-2000 times larger capacitance values as compared to the conventional electrolytic capacitors. These capacitors are similar to batteries except that the nature of charge storage is capacitive. The energy density of these electrochemical capacitors is typically lower than those

i

of advanced batteries (<10 Wh kg^{-1}), but they possess high power density (>500 W kg^{-1}) and longer cycle life (>10^5 cycles). Work on the development of supercapacitors has been started world-wide because of their potential use as power sources in different commercial applications such as, portable electronic equipment, computer memory back-up, medical equipment, power supplies, load levelling, electric vehicles etc.

Most of the reports on the supercapacitors are based on liquid electrolytes, which are encountered with the similar problems as the liquid electrolyte based batteries, in which they are associated with the well known disadvantages of corrosion, self discharge, low energy density and bulky design. All solid-state supercapacitors based on polymer/gel electrolytes have recently attracted growing interest because they offer advantages in terms of proper electrode-electrolyte contact, fabrication in the form of thin film devices, miniaturisation to ensure high energy density and free from corrosion and self discharge. Few studies have been carried out on solid state supercapacitors, which are based on solid polymer/gel electrolyte systems such as poly methyl methacrylate (PMMA)- poly (ethylene oxide) (PEO) / propylene carbonate (PC) / tetralkyl ammonium salts, PEO / PC / LiClO$_4$, poly (acrylonitrile) (PAN)/ PC / tetralkyl ammonium salts, PAN / PC / LiAsF$_6$, Nylon-6 / H$_3$PO$_4$, poly (vinyl alcohol) (PVA)/ H$_3$PO$_4$, PEO / poly(ethylene glycol) (PEG) / LiCF$_3$SO$_3$ etc. Worldwide efforts are continued to develop all solid-state supercapacitors, but still there is a need to optimise various associated parameters for their use at commercial level. These parameters are specific capacitance, working voltage, internal resistance, energy density, power density, cycle life etc.

The present work of the thesis is devoted to the studies on the polymeric gel electrolytes for their application in solid-state electrical double layer capacitors (EDLCs) and electrochemical redox supercapacitors.

Chapter-1 of the thesis describes the general introduction of superionic solids. Emphasis has been given on the polymer based superionic materials. Different types of polymer/gel electrolyte materials and their possible mechanism have been described briefly in this chapter. Possible applications of the ion conducting polymer / gel electrolyte materials have also been discussed in this chapter.

Chapter-2 describes briefly an overview of supercapacitors. Classifications and configurations of different types of supercapacitors depending on the types of materials used in their fabrication have been discussed. Possible mechanisms involved in the capacitive behaviour at electrode-electrolyte interfaces have also been described in brief. Various possible applications of supercapacitors have been discussed, which includes the promising application of supercapacitor in hybrid electrical vehicles. The chapter ends up with the scope of the present thesis.

Chapter-3 deals with the general experimental techniques used to characterize superionic solids, followed by the details of various techniques used to characterise the materials used in the present investigations. Various techniques, such as X-ray, electron and neutron diffraction etc. used for the structural characterisation have been discussed briefly. Technique generally used for the thermal analysis of the materials such as DTA/DSC, TGA etc. have been discussed. Various studies such as impedance spectroscopy, thermoelectric power, pulsed field gradient NMR, light scattering technique etc. have also been discussed in the chapter. A brief description of different transport number measurement techniques have also also been mentioned. Thereafter, various techniques used in the present investigations for the materials preparation, the characterisation of gel electrolytes and the characterisation of supercapacitors have been described. These include a.c. impedance spectroscopy, conductivity

measurement, polarisation method for transport number, cyclic voltammetry, charge-discharge methods etc.

Chapter-4 deals with the studies on polymeric gel electrolytes, which covers the preparation, electrochemical characterisation and optimisation of Poly (vinylidene fluoride-co-hexa fluoropropylene) (PVdF-HFP) and poly methyl methacrylate (PMMA) based gel electrolytes with the binary solvents EC:PC (1:1 V/V) and salts $LiClO_4$, $NaClO_4$ and $TEAClO_4$. Standard solution cast technique was used for the preparation of different polymeric gel electrolytes. The liquid followed by gel electrolytes have been optimised using different physical techniques such as impedance spectroscopy / electrical conductivity as a function of composition and temperature, polarisation technique for transport number evaluation and cyclic voltammetry for the measurement of the electrochemical stability of the polymeric gel electrolytes.

Chapter-5 shows the studies on electrical double layer capacitors (EDLCs) using activated charcoal powder as electrode materials and the optimised polymer gel electrolytes. The performance characteristics of various capacitor cells have been characterised using different techniques as mentioned above. Comparative studies show that the size and type of cations do not play any effective role in capacitive behaviour at electrode-electrolyte interfaces of solid state EDLCs, rather predominant role of anion is possible. Coulombic efficiency is ~ 90-95% for all the capacitor cells, which shows the liquid like electrochemical behaviour of the polymeric gel electrolytes. All the EDLC cells have been found to be stable for about 5000 cycles and even more.

Chapter-6 deals with the studies on solid-state redox supercapacitors using electrochemically prepared p-doped polypyrrole as electrodes and the same polymeric gel electrolytes. Comparative studies again shows that the type and size of cations of the salts used

iv

in the polymeric gel electrolytes does not make any substantial difference in capacitive properties of the supercapacitors, which further indicates the predominant role of anions on the capacitive behaviour of redox capacitor cells. The equivalent series resistance for each capacitor cell under present studies have been found to be of the order of few hundreds ohm cm^2, which is comparatively lower than that of the solid state capacitor cells based on conventional solid polymer electrolyte. Coulombic efficiency has been found to be of the order of liquid electrolytes (~95-100%) based capacitor cells, which confirms the liquid like electrochemical behaviour of all the gel electrolytes under present studies.

Chapter-7 ends up with the summary and conclusions drawn from the present investigations, followed by the future scope of the present studies.

Chapter – 1

General Introduction

GENERAL INTRODUCTION

1.1 Superionic Solids (Fast Ion Conductors)

Solid State Ionics is an interdisciplinary branch of engineering, science and technology that deals with the study of solids having exceptionally large ionic conductivity (of the order of 10^{-5}-10^{-1} S cm^{-1}) at room temperature comparable to that of the liquid electrolytes [1, 2]. This class of materials is referred as "Fast Ion Conductors" or "Solid Electrolytes" or "Superionic Solids". Initially M. Faraday introduced the term "ion" in 1834. The Greek term "ion" means moving and originated from the tribe of Ionians who were moving in ancient Greece from Thessaly to Peloponnese and to the western coast of Asia Minor. In analogy with the term "SOLID STATE ELECTRONICS" entirely new and emerging field of materials science and technology was termed as "SOLID STATE IONICS" by T. Takahashi of Japan in 1970. These superionic solids possess the following characteristics [1, 2]:

1. Bonding in the crystal is generally ionic.

2. Activation energy is low.

3. Electrical conductivity is high of the order of $10^{-5} - 10^{-1}$ S cm^{-1}.

4. Principal charge carriers are ions.

5. Ionic transference number is close to unity i.e. ($t_{ion} \sim 1$).

6. Electronic transference number is small i.e. ($t_e < 10^{-4}$).

7. Internal structure is highly disordered, channelled or layered.

Furthermore, ionic solids may be divided into two different classes depending on the concentration of the defects present in them:

1. "Dilute point defects or low concentration type defects" in which defect concentration is low $< 10^{18}$ cm^{-3}. For example alkali halides (NaCl, KCl etc.).

2

2. "High concentration type defects" in which defect concentration is high $> 10^{20}$ cm^{-3}.

The "high defect concentration type solids" are called superionic solids.

Most of the commonly known ionic solids such as alkali halides (NaCl, KCl etc.) have low room temperature conductivity ($10^{-16} - 10^{-12}$ S cm^{-1}). Thermally generated point defects such as Schottky and Frenkel defects are responsible for the ionic conduction in these types of solids. Major breakthrough in the field of Solid State Ionics took place in 1967 with the discovery of fast sodium ion conduction in β-alumina by Yao and Kummer [3] and silver ion conduction in MAg$_4$I$_5$ (M=K, Rb, NH$_4$ etc.) [4]. Since then thousands of such superionic solids have been discovered suitable for several commercial applications such as solid state batteries, fuel cells, supercapacitors, electrochromic devices, sensors, etc. Many books/reviews are available in literature on these superionic solids [1-14].

Depending on the composition, phase, microstructure and their different physical properties, superionic solids may be divided into different classes as shown in Fig 1.1.
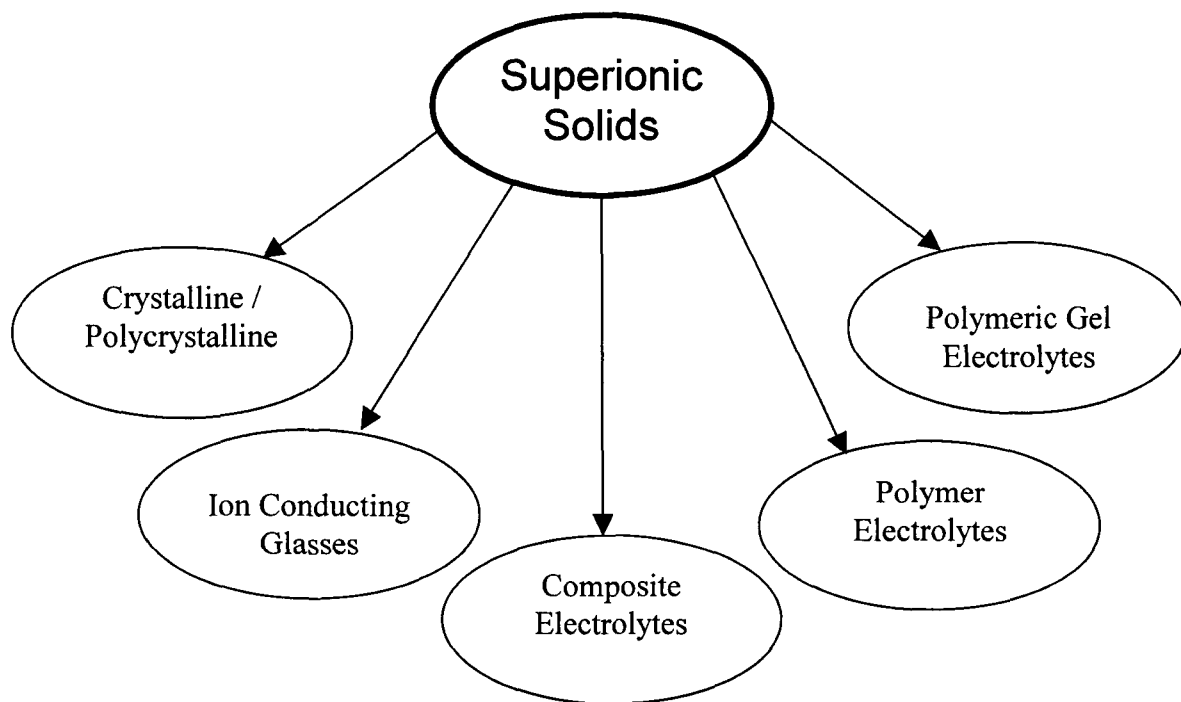
Fig. 1.1: *Classification of superionic solids.*

3

1.1.1 Crystalline / Polycrystalline Solids:

The solids in which ions migrate within their crystalline framework come under this category. Migration of ions within a framework is possible by both cation (alkali ions, copper, silver etc.) as well as anions (fluoride, oxide etc.). The superionic solids involve the migration of monovalent as well as divalent ions. Some of the important crystalline and polycrystalline solids along with their conducting species and conductivity are listed in Table 1.1.

Table - 1.1: Some important crystalline / polycrystalline materials.

(Crystalline / Polycrystalline Solid Electrolytes)	Conducting Species	Conductivity ($S\ cm^{-1}$)	Temperature (^{0}C)	References
α-AgI	Ag^+	2.1×10^{-1}	147	1, 2
Silver β-alumina	Ag^+	6.4×10^{-3}	25	1, 2
$\alpha - Ag_3Si$	Ag^+	20×10^{-1}	240	1, 2
$RbAg_4I_5$	Ag^+	2.6×10^{-1}	22	1, 2
α-Ag_2HgI_4	Ag^+	1.2×10^{-3}	60	15
$AgCrSe_2$	Ag^+	2.0×10^{-1}	225	16
KAg_4I_4CN	Ag^+	1.4×10^{-1}	25	17
$RbAg_4I_4CN$	Ag^+	1.8×10^{-1}	25	17
$Ag_7I_4VO_4$	Ag^+	7.0×10^{-3}	25	18
Ag_8TiS_6	Ag^+	1.0×10^{-3}	25	19
AgI-Ag_3PO_4	Ag^+	6.0×10^{-2}	RT	20
$Na_3MgZr(PO_4)_3$	Na^+	1.0×10^{-3}	27	1, 8-10
Sodium β-alumina	Na^+	1.4×10^{-2}	25	1, 2
$Na_{1+y}Mg_yAl_{1-y}SiO_4$ (y=0.63)	Na^+	5.0×10^{-3}	300	1, 8-10
$Na_{0.8}In_{0.8}Zr_{0.2}S_2$	Na^+	4.0×10^{-6}	200	1, 8-10
$Na_2Ta_2O_5F$	Na^+	6.7×10^{-3}	300	21
$Na_{1.9}Al_{0.3}Ti_{1.7}P_{2.4}O_{12}$ (NASICON)	Na^+	1.3×10^{-2}	400	22
$Na_2ZrSi_4O_{11}$	Na^+	5.0×10^{-7}	300	23
$Na_{1.7}Cr_{1.7}Ti_{6.3}O_{16}$	Na^+	1.0×10^{-2}	200	24
Li_2SO_4	Li^+	10×10^{-1}	800	1, 2

LiAlSiO$_4$	Li$^+$	4.7x10^{-5}	25	1, 8-10
α Li$_4$GeO$_4$	Li$^+$	8.7x10^{-5}	400	1, 8-10
β-LiTa$_3$O$_8$	Li$^+$	1.5x10^{-2}	400	1, 8-10
Lithium β-alumina	Li$^+$	1.3x10^{-4}	25	1, 2
Li$_4$SiO$_4$	Li$^+$	1.0x10^{-3}	400	1, 2
Li$_3$N	Li$^+$	8.8x10^{-3}	400	25
K –β-alumina	K$^+$	6.5x10^{-5}	300	1, 2
K$_3$AlF$_6$	K$^+$	2.0x10^{-5}	425	26
CuF$_2$	F$^-$	4x10^{-2}	700	27
RbBiF$_4$	F$^-$	5x10^{-4}	100	1, 8-10
LaF$_3$	F$^-$	10x10^{-1}	600	1, 2
NH$_4$Sn$_2$F$_5$	F$^-$	5.0x10^{-5}	357	28
PbF$_2$-SnF$_2$	F$^-$	1.0x10^{-3}	25	29
Rb$_4$Cu$_{16}$I$_7$Cl$_{13}$	Cu$^+$	3.4x10^{-1}	R.T	1, 8-10
Cu$_2$S (high chalcocite) T>104 ^{0}C	Cu$^+$	2.0x10^{-1}	400	1, 8-10
α - CuI	Cu$^+$	9.0x10^{-2}	450	1, 2
KCu$_4$I$_5$	Cu$^+$	6.0x10^{-1}	280	30
α - Cu$_2$Se	Cu$^+$	1.1x10^{-1}	150	1, 2
ZrO$_2$-CaO	O^{2-}	5.5x10^{-2}	1000	1, 2
ZrO$_2$-Yb$_2$O$_3$	O^{2-}	8.8x10^{-2}	1000	1, 2
ThO$_2$-Y$_2$O$_3$	O^{2-}	4.8x10^{-3}	1000	1, 2
CeO$_2$-La$_2$O$_3$	O^{2-}	8.0x10^{-2}	1000	1, 2

1.1.2 Ion Conducting Glasses:

In 1973, Kunze [9, 14] accidentally found high Ag$^+$ ionic conductivity in the system AgI-Ag$_2$SeO$_4$. This led to the discovery of superionic conducting glasses. Since then a large number of ion (Ag$^+$, Li$^+$, Na$^+$, F$^-$ etc.) conducting glasses having amorphous internal structure have been reported [31-44], which are used for the fabrication of different solid-state devices.

General composition of glasses can be expressed in the forms of $(MX-M_2O-A_XO_Y)$ which have three components:

1) Glass former, A_XO_Y (usually oxide e.g. B_2O_3, P_2O_5, SiO_2, As_2O_5, V_2O_5, CrO_3 etc.)

2) Glass network modifier, M_2O (usually metal oxides); and

3) Doping salt, MX (usually metal halides).

The addition of glass modifier (within the glass forming range) results in the formation of glass network and the addition of dopant salt results in an increase in carrier concentration and the creation of conduction pathways, which leads to an enhancement in the conductivity. Thus the conductivity of ion conducting glasses can be controlled by controlling the amount of glass former, glass modifier and dopant salt. Sometimes sulphur and selenium compounds [32, 33] are also used as glass formers instead of oxides. Ion conducting glasses possess following advantages over crystalline/ polycrystalline solids:

- Isotropic conduction.

- High room temperature conductivity $(10^{-5}-10^{-2}$ S $cm^{-1})$.

- Tailoring of compositions.

- Ease of fabrication.

- Possible formation in thin film forms, etc.

Some ion-conducting glasses are listed in Table. 1.2.

Table - 1.2: Some important ion conducting glass materials.

Ion Conducting Glasses	Conducting Species	Conductivity (S cm⁻¹)	Temp (⁰C)	Ref.
$50AgBr. 25Ag_2O. 25B_2O_3$	Ag^+	2.7×10^{-3}	25	34
$73AgI. 20Ag_2MoO_4. 7Ag_2Mo_2O_7$	Ag^+	2.2×10^{-3}	25	31
$0.03As_2S_3. 0.47Ag_2S. 0.50AgI$	Ag^+	2.0×10^{-2}	25	35
$40AgI. 30Ag_2O. 30B_2O_3$	Ag^+	1.0×10^{-4}	21	45
$73AgI. 20Ag_2MoO_4. 7Ag_2Mo_2O_7$	Ag^+	2.24×10^{-3}	25	31

$30Ag_2O. 70B_2O_5$	Ag^+	8.0×10^{-9}	50	45
$66.6AgI. 25Ag_2O. 8.33V_2O_5$	Ag^+	5.3×10^{-3}	32	36
$AgI. Ag_2O. B_2O_5$	Ag^+	1.5×10^{-5}	25	31
$40AgCl. 30Ag_2O. 30B_2O_5$	Ag^+	6.3×10^{-4}	25	34
$60AgI. 30Ag_2O. 10B_2O_3$	Ag^+	8.5×10^{-3}	25	46
$4AgI.Ag_2O. B_2O_3. P_2O_5$	Ag^+	1.0×10^{-5}	25	39
$AgI. AgCl. Ag_2O. Cr_2O_3$	Ag^+	2.0×10^{-3}	RT	47
$70AgPO_3. 30Ag_2SO_4$	Ag^+	5.0×10^{-6}	25	40
$AgI. Ag_2O. B_2O_3$	Ag^+	1.0×10^{-1}	370	48
$24Ag_2O. 6Na_2O. 7B_2O_3$	Ag^+	8.0×10^{-10}	50	45
$Ag_2O. B_2O. B_2O_3. AgI$	Ag^+	1.0×10^{-4}	25	49
$29.4Li_2O. 58.8SiO_2. 11.7Li_2SO_4$	Li^+	2.2×10^{-3}	300	41
$10Li_2SO_4. 90LiOH$	Li^+	1.01×10^{-3}	217	50
$Li_2O. B_2O_3. SiO_2$	Li^+	3.0×10^{-4}	253	51
$50(0.4Li_2S. 0.6GeS_2). 50LiI$	Li^+	1.1×10^{-4}	25	41
$40Li_2O.8Al_2O_3.52B_2O_5$	Li^+	6.13×10^{-5}	200	42
$33.3Li_2O.66.6SiO_2$ (Glass Ceramic)	Li^+	1.8×10^{-8}	300	44
$55LiF. 25Ni_2O. 20Al(PO_3)_3$	Li^+	1.0×10^{-3}	200	52
$37Li_2S. 18P_2S_5. 45LiI$	Li^+	1.0×10^{-3}	25	37
$40Na_2O. 50SiO_2. 10B_2O_5$	Na^+	2.0×10^{-3}	300	38
$Na_{3.75}Zr_{1.1}Si_{2.75}P_{0.25}O_{0.2}$ (NaSi-Glass)	Na^+	1.93×10^{-3}	300	43
$InF_3-SnF_2-PbF_2$	F^-	6.3×10^{-4}	150	53
$CuI. Cu_2O. TeO_2. MoO_3$	Cu^+	3.0×10^{-4}	25	54

1.1.3 Composite Solid Electrolytes:

This class of electrolytes are obtained by dispersing a chemically non-interacting and electrically non-conducting fine particle such as Al_2O_3, SiO_2 etc. in an ion-conducting matrix. These are basically two-phase solid system, which was initiated by Liang [55] in order to enhance the conductivity of LiI by adding fine particles of alumina. Although the activated alumina powder is mostly used as the dispersoid, several other second phase materials ranging

7

from semiconducting to insulating particles like NiO, GeO_2, Bi_2O_3, ZrO_2, SiO_2, etc. to electronically conducting particles like Cu, Ni, Ni_3S_2 etc. have also been added as the dispersoids. In order to enhance the ionic conductivity by several orders of magnitude of the ionic solids, different studies were investigated by the addition of suitable adducts [55-65]. Table 1.3 shows a brief list of some important dispersed phase composite solid electrolytes.

Table 1.3: Some important ion conducting composite solid electrolytes.

Composite Solid Electrolytes	Conducting Species	Conductivity $(S\ cm^{-1})$	Temp (^0C)	Ref.
$LiI - Al_2O_3$	Li^+	1.0×10^{-4}	25	55, 56
$LiCl - Al_2O_3$	Li^+	2.5×10^{-5}	182	57
$Li_2SO_4 - MgSO_4$	Li^+	3.6×10^{-3}	500	58
$Li_2SO_4 - CaSO_4$	Li^+	2.1×10^{-3}	500	58
$LiCl - SiO_2$	Li^+	2.2×10^{-6}	182	57
$Li_2SO_4 - Li_2WO_4$	Li^+	4.9×10^{-5}	400	59
$AgI - SiO_2$	Ag^+	1.1×10^{-5}	25	59
$AgI - Fly\ ash$	Ag^+	1.2×10^{-5}	25	59
$AgI - AgBr$	Ag^+	3.2×10^{-4}	25	60
$AgI - Al_2O_3$	Ag^+	1.0×10^{-3}	25	61
$AgCl - Al_2O_3$	Ag^+	4.2×10^{-6}	25	62
$AgBr - Al_2O_3$	Ag^+	1.0×10^{-5}	25	63
$Na_2SO_4 - MgSO_4$	Na^+	2.5×10^{-2}	440	64
$NiCl_2.6H_2O - Al_2O_3$	H^+	1.1×10^{-2}	25	65

1.1.4 Polymer Electrolytes

This class of materials has received tremendous attention in the last few years. It consists of salts in association with polymers such as polyethylene oxide (PEO), polypropylene oxide (PPO), polyethylene glycol (PEG), poly acrylic acid (PAA) etc. Discovery of fast alkali ion transport in such complexes at 100^0C was first observed by Fenton et al. in 1973 [66] and

Wright et al. in 1976 [67]. Thereafter, many interesting observations on these materials have been reported by several workers including Armand et al. in 1978 [68, 69] and Papke et al in 1982 [70], which show that various properties such as ionic conductivity etc. can be controlled by the composition of the electrolytes. Due to advantageous mechanical properties including ease of fabrication as thin films, mouldability and flexibility in electrode-electrolytes contacts in different electrochemical devices, the field of polymer electrolytes has received the attention of researchers worldwide [71-76]. Some examples of ion-conducting polymer electrolytes are given in Table. 1.4.

Table-1.4: Some important polymer electrolytes.

Polymer Electrolytes	Conductivity (S cm⁻¹)	Temperature (⁰C)	References
$(PEO)_x - NaSCN$	1.0×10^{-7}	20	67, 72-76
$(PEO)_x - NH_4SCN$	1.0×10^{-5}	60	67, 72-76
$(PEO)_x - NaI$	1.0×10^{-5}	60	67, 72-76
$(PEO)_x - LiClO_4$	1.3×10^{-7}	27	72-76
$PEO - NH_4CF_3SO_3$	1.4×10^{-6}	30	72-76
$PVAc - LiSCN$	1.0×10^{-3}	100	77
$MEEP - NaCF_3SO_3$	1.0×10^{-5}	25	78
$PEO - LiI$	1.0×10^{-7}	55	72-76
$PEO - NaBF_4$	6.9×10^{-6}	40	72-76
$PEO - LiBF_4$	1.0×10^{-6}	25	72-76
$PEO - ZnBr_2$	1.0×10^{-6}	100	72, 73
$PEO - Cu(ClO_4)_2$	1.0×10^{-6}	25	79
$PEO - CuSCN$	1.3×10^{-6}	30	80
$PEO - AgNO_3$	4.0×10^{-7}	30	81
$(PEO)_{16} - ZnI_2$	3.6×10^{-4}	140	72
$PEO - NH_4I$	1.0×10^{-5}	23	82
$PEO - NH_4ClO_4$	1.0×10^{-5}	30	83
$PEO - (NH_4)_2SO_4$	1.0×10^{-7}	30	84

PEO – NH$_4$HSO$_4$	1.0×10^{-4}	30	85
PVA – H$_3$PO$_4$	1.0×10^{-5}	25	86
PEO – NaPF$_6$	5.7×10^{-6}	30	87
PESc – LiClO$_4$	1.0×10^{-5}	90	88
MEEP – LiClO$_4$	1.7×10^{-5}	20	89
MEEP – LiN(CF$_3$SO$_2$)$_3$	6.5×10^{-5}	20	89
PEO – LiN(CF$_3$SO$_2$)$_2$	1.0×10^{-4}	RT	90
PEO – LiCF$_3$SO$_3$	4.1×10^{-4}	22	91
(PVAc) – LiSCN	1.0×10^{-8}	25	77
(PVAc) – LiCF$_3$SO$_3$	1.0×10^{-9}	40	77
(PPO)$_{12}$ – NaCF$_3$SO$_3$	1.0×10^{-5}	45	72-76
(PEO)$_8$ – Cu(ClO$_4$)$_2$	2.0×10^{-5}	25	92
(PEO)$_8$ – CuCl$_2$	1.2×10^{-9}	25	92
(PEO)$_8$ – ZnCl$_2$	5.2×10^{-6}	25	92
(PEO)$_{24}$ – PbI$_2$	1.0×10^{-7}	75	72, 73
(PEO)$_{15}$ – MgCl$_2$	5.0×10^{-6}	75	72, 73
PEO – LiSCN	5.0×10^{-4}	120	69
PEO – KSCN	1.0×10^{-3}	120	69
PEO – LiCF$_3$SO$_3$	$10^{-4} - 10^{-3}$	100	72-76
PPO – NaCF$_3$SO$_3$	1.0×10^{-5}	45	72-76
PPO – NaCF$_3$SO$_3$	1.0×10^{-4}	100	72-76
PESc – NH$_4$ClO$_4$	1.0×10^{-7}	RT	93
PEO – NaN(CF$_3$SO$_2$)$_2$	1.0×10^{-3}	85	94
PEO – LiN(SO$_2$CF$_2$CF$_3$)$_2$	1.0×10^{-4}	90	95

Polymer electrolytes can be subdivided into different classes: (i) polymer-salt complexes, (ii) polyelectrolytes, (iii) polymer-in-salt or rubbery electrolytes, (iv) solvent swollen polymers, and (v) composite polymer electrolytes.

1.1.4.1   Polymer-Salt complexes:

This class of polymer electrolytes can be formed by dissolving desired salts such as $NaClO_4$, $LiClO_4$ etc. in high molecular weight and low glass transition temperature polymers e.g. PEO, PPO, etc. [71-76]. These materials behave as a solid at macroscopic level due to the absence of low molecular weight solvent whereas at microscopic level polymer chain shows liquid like behaviour under suitable conditions depending on the polymer-salt systems. Since solvent is not present in the polymer-salt complexes, the polymer acts as the solvating species in the system. It overcomes the crystal lattice forces of the salt to facilitate the movement of ions within the system [71-76, 96]. These types of materials are operated in such a range where segmental motion is high and crystalline portion is less. Below glass transition temperature T_g, the segmental motion of the polymer chain is ceased. Between T_g and T_m (melting temperature), there is significant segmental motion of the polymer chains. Above T_m, due to the absence of crystalline region and presence of highly amorphous region, there is comparatively higher segmental motion of the polymer chains. It is well known that the ionic conduction essentially takes place in the amorphous region of the polymers [71-76]. Hence the polymer-salt complexes are operated in such a region where crystallinity is low and segmental motion is high. Many reviews / books are available in literature on polymer-salt complexes [71-76, 96].

1.1.4.2   Polyelectrolytes:

In this class of polymeric materials, anions or cations are chemically bonded with the main chain of polymers [97, 98], whereas small counter ions are associated with fixed ionic charges on the polymer to maintain electro-neutrality as shown in Fig.1.2. These counter ions are firmly bound with the oppositely charged fixed ions on the main polymer chain by coulombic force of attraction in the absence of high dielectric constant solvents (e.g. water etc.). After the uptake of high dielectric solvent, these counter ions are solvated and free to

11
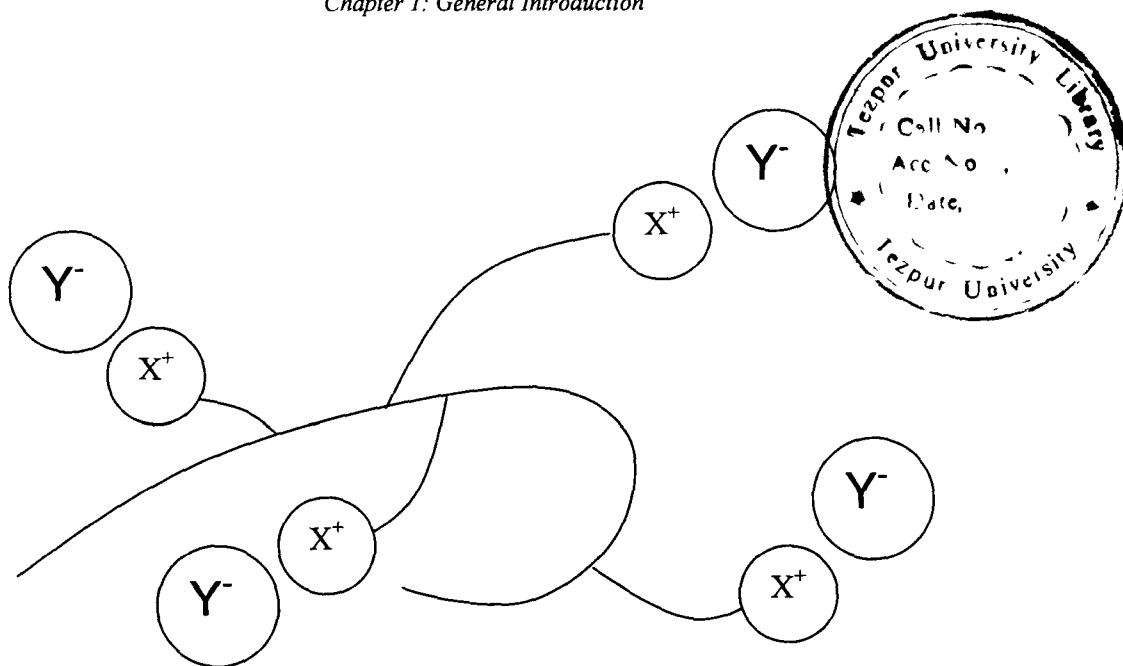
Fig. 1.2: Schematic diagram of polyelectrolytes (poly-bases).

migrate within the polymer matrix. In this type of materials conductivity is due to the migration of only single ions. Ionic conductivity is a function of solvent (mostly water) content. This particular behaviour of these electrolytes makes them a suitable candidate for their application in humidity sensors. Some reviews on polyelectrolytes are available in literature [99, 100]. One of the most important polyelectrolyte is NAFION, which is a good H^+ ion conductor and is commercially used in H_2 / O_2 fuel cells [99].

1.1.4.3 Polymer-in-Salt or Rubbery Electrolytes:

Rubbery polymer electrolytes have conductivities higher than those of conventional polymer electrolytes. In this case high molar mass polymer (PEO, PPO etc.) is dissolved in low temperature molten salt mixtures [101] in order to get a material, which combines the properties of super-ion conducting glass (decoupled cation motion) as well as rubbery properties of polymer electrolytes [102, 103]. These types of rubbery electrolytes are well suited for application in electrochemical devices. They possess the following properties [104]:

12

- The polymer gets dissolve in molten salt mixtures.

- The resulting materials are generally single ion (say cation) conductors.

- T_g of the ionic species is below the room temperature.

- Ionic species are cooled well below room temperature without losing their conducting properties.

The T_g values of rubbery electrolytes are higher than that of the gel electrolytes but due to the decoupling of the cations from the polymer matrix conductivity of these electrolytes are higher. Most of the salts such as $LiClO_4$, $LiClO_3$ etc. lower their T_g value but they are chemically reactive or thermally unstable under ambient conditions. So there is a need to seek chemically and electrochemically stable materials, which can be achieved by going for some composite materials. This is still a great challenge before the research community to form such types of materials.

1.1.4.4 Solvent Swollen Polymers:

In this class of polymeric materials some aqueous or non-aqueous solvents swell the polymer matrix such as polyvinyl alcohol (PVA), polyvinyl pyrrolidine (PVP) etc. and the dopant solutes such as H_3PO_4 etc. are accommodated in the swollen host matrices [86]. Conductivity of these materials depends on the ambient condition and the concentration of the solvent in the swollen matrix, which leads to the instability in the materials.

1.1.4.5 Composite Polymer Electrolytes:

One of the novel techniques adopted to enhance the conductivity of the polymeric electrolytes is to disperse different inorganic or organic additives, which are chemically non-interacting and electrically non-conducting such as Al_2O_3, SiO_2 etc. The resulting electrolytes are generally called as "Composite Polymer Electrolyte (CPEs)" [105]. Several studies have

13

been carried out to enhance the conductivity of polymer electrolytes by using different types of second phase materials (electronically conducting, semiconducting as well as insulating particles). A number of reviews/ articles are available in literature on composite polymer electrolytes [105-113].

From all the above description based on different classes of polymer electrolytes, it is clear that polymer electrolyte is a mixed phase system, which consists of different crystalline phases along with amorphous phase. They have a common feature of ion association, which leads to the formation of ion pairs, triplets, multiplets etc. These possess a lot of complications in the description of their ion transport behaviour in terms of different variables such as degree of hydration, impurity ions from the polymerisation process, ion pairing, inhomogeneity in samples and conduction possibly by both the mobile ions i.e. cations as well as anions etc [71-76]. Hence, there is no any theoretical approach, which has been developed so far that accounts for the ion transport behaviour for a particular group of polymer electrolytes, which is valid universally for all the systems. In this regard, several empirical relations and theories/models have been developed / proposed to explain the ion conduction mechanism in different polymer electrolyte systems such as early phenomenological concepts [68-70], empirical relationships [74, 75], free volume theory [70, 72], static bond percolation theory [72], dynamic bond percolation theory [72] etc. Some ion conduction mechanisms have also been proposed by different workers for composite polymer electrolytes separately, such as Almond-West Formalism-Applicability of the Meyer-Neldel rule [114, 115], Almond-West Formalism-Applicability of the Universal Power law of Jonscher [114, 116], Effective Medium theory (EMT) approaches [117-122] etc.

14

1.1.5 Polymeric Gel Electrolytes:

Polymeric gel electrolytes are one of the most important classes of superionic materials formed by the dissolution of the salts in a polar, high dielectric solvent and adding a neutral polymer to achieve the mechanically stable [104] and very high ion conducting materials. In this case, polymer is dissolved in a liquid electrolyte to obtain a homogeneous and a highly viscous gel of desired consistency [123, 124]. Basically polymeric gel electrolytes consist of polymer, solvent and salts. These constituents of gel electrolytes possess the following characteristics to have high conductivity under the operating conditions.

Essential characteristics of polymers

- Polar in nature.

- Highly amorphous.

- Low glass transition temperature, T_g, etc.

Essential characteristics of salts

- Presence of bulky anion groups etc.

- Soluble in chosen solvents.

Essential characteristics of solvents

- High dielectric constant, imperative for maximising the concentration of free ions.

- Lower viscosity, for better ion transport.

- High boiling point, necessary to prevent solvent evaporation from the electrolyte within the operational temperature range.

- Low freezing point, preferred to avoid the rapid decline of ionic conductivity at low temperature.

- Presence of some chemically active dipoles such as -C=O which induces high polarity.

15

Apart from the above characteristics, several other qualities such as chemical, electrochemical and thermal stability, sufficient chemical compatibility with the electrodes, good plasticising properties of solvents (which help in lowering the T_g of the polymer) and complete miscibility with other polymer are also essential.

In these systems, it is believed that the polymer acts as a stiffener for the solvent which solvates the salt and also acts as the conducting medium [123]. In designing such highly conductive gel electrolytes, which can easily exhibit conductivities greater than 10^{-3} S cm^{-1} at room temperature, the primary step is to synthesize non-aqueous liquid electrolytes based on aprotic polar solvents. The dielectric constant (ε) of the solvent and the lattice energy of the salt govern salt dissociation as well as the subsequent solvation of the ionic species in the solvent [125]. These are quite attractive alternatives to solvent free polymer electrolytes, which can be used in the fabrication of several electrochemical devices [123, 126, 127]. Since gelation of an aprotic liquid electrolyte is the basic concept for the preparation of polymeric gel electrolytes and hence polymer is presumed to be an inert in a gel electrolyte. Its role is to entrap the liquid electrolyte in its huge matrix and acts only as a container for the liquid electrolytes i.e. liquid electrolyte is simply encaged in a polymer matrix. Apart from this, it also possesses various other properties such as high ionic conductivity, fast charge transfer at electrode interfaces and reasonably good electrochemical stability etc. Generally, high ionic conductivity as well as good mechanical strength is incompatible, as one of the two has to be sacrificed to achieve the other. It is the amount of liquid electrolytes incorporated in the gel electrolyte, which dominates ionic conductivity, where as mechanical strength can be improved by increasing polymer content. Hence, we can say that gel electrolytes permit the attainment of an acceptable compromise between good mechanical strength and high ionic conductivity [128].

As the plasticising solvent molecules such as ethylene carbonate (EC), propylene carbonate (PC) etc. also interact and solvate with the ions, the coordinating macromolecules such as polyethers, which are extensively used in polymer-salt complexes may be replaced by more inert polymers [101]. A number of thermoplastic polymers have been proposed as frameworks for gel electrolytes, which includes: poly acrylonitrile (PAN) [129], poly (methyl methacrylate) (PMMA) [123], poly vinylidene fluoride (PVdF) [130, 131], poly vinylidene fluoride-co-hexa fluoro propylene (PVdF-HFP) [132] etc. From device fabrication point of view, it is essential to have a good plasticising and adhesive properties as well as an elastomeric nature of the electrolytes. High amorphicity and low glass transition temperature (T_g) of the polymers are also essential so that the ionic conductivity of the liquid electrolyte is not adversely affected upon polymer addition.

Most of the gel electrolytes exhibit favourable mechanical properties and generally have amorphous morphology, when atactic polymers like PAN, PMMA etc. are used [133]. These electrolytes are generally resistant to decomposition even under harsh conditions [134]. These show the improved low temperature performance as compared to the pure polymer systems, as the magnitude of the conductivity is determined by the fluidity of the ionic environment in the polymer matrix, which in turn is determined by the melting point of the solvates formed between the salts and the plasticizer solvents. The melting point of the solvates can be decreased by using solvent mixtures, as they lead to the formation of eutectics which provide an ionic environment with increased fluidity at low temperatures and consequently, high conductivity [133, 135]. There is a need to improve several aspects of gel electrolytes such as the cationic transport number is generally less than 1, sometimes even less than 0.5 for most of the polymer as well as the solution electrolytes. There is also a need of improvement in the area of material processing, cell engineering and manufacturing on a commercial scale [135, 136].

In order to enhance the cell performance and to resolve the fundamental problems, we have to understand ionic conduction mechanisms properly in these gel electrolytes. All those factors, which govern the conduction mechanisms, have to be estimated independently so as to understand the differences that exist in the structural chemistry of liquid as well as gel electrolytes and to see that how these properties affect the electrolyte conductivity [123, 137]. For the purpose the main factors which need to be focussed are the ion transport dependence on macroscopic as well as microscopic viscosity, nature of salt anion and its size, carrier concentration, degree of dissociation of the salt, extent of ion-association in pairs/triplets or higher order aggregates, structural dynamics of liquid and gel electrolytes, nature of salt-polymer interaction, solvation mechanisms and the degree of amorphicity of the polymer etc. Some of the important polymeric gel electrolytes are given in Table 1.5.

Table-1.5: Some important ion conducting polymeric gel electrolytes.

Materials (Polymer Gel Electrolytes)	Conductivity (S cm^{-1})	Temperature (^{0}C)	References
PVdF – EC/PC/γ-BL – LiClO$_4$	$10^{-7} - 10^{-5}$	25	72
PAN – EC/PC – LiClO$_4$	4.5×10^{-3}	25	138
PAN – EC/PC – LiN(CF$_3$SO$_3$)$_2$	2.0×10^{-3}	25	138
PMMA – EC/PC – LiCF$_3$SO$_3$	8.0×10^{-4}	25	138
PAN – EC/PC/PEGDA – LiClO$_4$	1.2×10^{-3}	20	139
PAN – EC/PC – LiCF$_3$SO$_3$	1.1×10^{-3}	20	89
PVP – Tetraglyme – LiClO$_4$	8.0×10^{-4}	20	89
PVP – EC/PC – LiCF$_3$SO$_3$	4.0×10^{-4}	20	89
PAN – EC/PC/γ-BL – LiAsF$_6$	3.9×10^{-3}	20	89
PAN – EC – LiClO$_4$	2.0×10^{-3}	25	131
PVdF – DMSO – LiCF$_3$SO$_3$	4.6×10^{-3}	RT	140
PVdF-HFP – EC/DEC – TFSI	1.0×10^{-3}	RT	141
PMMA – PEG – LiCF$_3$SO$_3$	1.0×10^{-4}	25	142
PMMA – PC – NaClO$_4$	1.0×10^{-3}	RT	143

PMMA – EC/PC – NaClO$_4$	1.0×10^{-3}	RT	143
PMMA – PC/DMC/DEC – LiCF$_3$SO$_3$	5.0×10^{-3}	20	144
PMMA – EC/DMC/DEC – LiCF$_3$SO$_3$	7.0×10^{-3}	20	144
PAN – EC – LiClO$_4$	2.14×10^{-3}	25	129
PEGDA – EC/PC – LiClO$_4$	4.0×10^{-3}	20	145
PMMA – PC – LiClO$_4$	2.3×10^{-3}	25	123
PVC – EC/PC – LiClO$_4$	1.2×10^{-3}	20	146
PMMA – PC – LiClO$_4$	1.6×10^{-3}	22	147
PAN – EC/PC – LiAsF$_6$	5.0×10^{-3}	20	148
PAN – EC/PC – NaClO$_4$	1.5×10^{-3}	25	148
PAN – EC/PC – LiClO$_4$	7.0×10^{-4}	25	148
(PEO-PAN) – EC/BL – LiClO$_4$	2.0×10^{-3}	30	149
PEGDA – EC/PC – LiAsF$_6$	1.7×10^{-4}	25	150
PEGDA – EC/PC – LiClO$_4$	2.8×10^{-3}	25	150
PAN – EC/DMC – NaClO$_4$	1.8×10^{-3}	-	151
PMMA – EC/PC – LiClO$_4$	1.0×10^{-3}	25	152
PAN – EC/BL – LiClO$_4$	2.16×10^{-3}	22	153
PAN – EC/PC/BL – LiClO$_4$	2.79×10^{-3}	22	153
PAN – EC/BL/DMF – LiClO$_4$	4.09×10^{-3}	22	153
PAN – EC/DMC – LiAsF$_6$	2.1×10^{-3}	-	151
PAN – EC/PC – LiClO$_4$	9.0×10^{-4}	30	154
PMMA – EC/PC – LiClO$_4$	5.0×10^{-4}	30	154
PVdF-HFP – EC/PC – LiPF$_6$	1.2×10^{-3}	-	155
PVdF – EC/PC – LiBF$_4$	1.32×10^{-3}	RT	156
PMMA – EC/PC – SA	2.55×10^{-5}	25	157
PMMA – EC/PC/MF – SA	2.52×10^{-5}	25	157
PMMA – EC/PC – TOS	1.36×10^{-4}	25	157
(PEO-PMMA) – PEGDE – MgClO$_4$	1.0×10^{-4}	-	158
PMMA – EC/PC – Benzoic Acid	1.6×10^{-5}	-	159
PVdF-HFP – EC/DEC – LiN(CF$_3$SO$_2$)$_2$	1.0×10^{-2}	70	160
PVdF – EC/PC – LiBF$_4$	6.4×10^{-3}	RT	161

PAN – EC/PC – LiClO$_4$	8.0x10^{-4}	20	162
PVdF-HFP – EC/PC – LiClO$_4$	3.0x10^{-3}	20	162
PMMA – PC – LiClO$_4$	2.0x10^{-2}	20	163
PMMA – PC – Zn(ClO$_4$)$_2$	4.2x10^{-2}	20	163
PMMA – PC – Mg(ClO$_4$)$_2$	1.6x10^{-2}	20	163
PMMA – γBL/DMA/DMF – LiClO$_4$	1.3x10^{-2}	RT	164
(PEO-PMA) – EC/DMC – Mg[(CF$_3$SO$_2$)$_2$N]$_2$ (Magnesium Imide)	1.0x10^{-3}	RT	165
PMMA – EC/PC/DMA – Chloroacetic Acid	1.0x10^{-3}	25	166
PVdF-HFP - EC/PC/DMA -Hydroxybenzoic Acid	10^{-3} – 10^{-4}	RT	167
(PAN-PMMA) – EC/γ BL – LiBF$_4$	2.2x10^{-3}	20	168
PVdF-HFP – PC – Mor$_{1,4}$TFSI	1.0x10^{-2}	60	169

Mor$_{1,4}$TFSI is N-Butyl-N-methylmorpholinium bis (trifluoro-methane-sulfonyl) imide

1.2 Applications of Superionic Solids

Superionic solids can be used in the fabrication of a variety of solid sate energy storage, energy

conversion and electrochemical devices as shown in Fig 1.3. They have a potential

Fig. 1.3: Solid state electrochemical devices [1, 2].

PAN – EC/PC – LiClO$_4$	8.0×10^{-4}	20	162
PVdF-HFP – EC/PC – LiClO$_4$	3.0×10^{-3}	20	162
PMMA – PC – LiClO$_4$	2.0×10^{-2}	20	163
PMMA – PC – Zn(ClO$_4$)$_2$	4.2×10^{-2}	20	163
PMMA – PC – Mg(ClO$_4$)$_2$	1.6×10^{-2}	20	163
PMMA – γBL/DMA/DMF – LiClO$_4$	1.3×10^{-2}	RT	164
(PEO-PMA) – EC/DMC – Mg[(CF$_3$SO$_2$)$_2$N]$_2$ (Magnesium Imide)	1.0×10^{-3}	RT	165
PMMA – EC/PC/DMA – Chloroacetic Acid	1.0×10^{-3}	25	166
PVdF-HFP - EC/PC/DMA -Hydroxybenzoic Acid	$10^{-3} – 10^{-4}$	RT	167
(PAN-PMMA) – EC/γ BL – LiBF$_4$	2.2×10^{-3}	20	168
PVdF-HFP – PC – Mor$_{1,4}$TFSI	1.0×10^{-2}	60	169

Mor$_{1,4}$TFSI is N-Butyl-N-methylmorpholinium bis (trifluoro-methane-sulfonyl) imide

1.2 Applications of Superionic Solids

Superionic solids can be used in the fabrication of a variety of solid sate energy storage, energy

conversion and electrochemical devices as shown in Fig 1.3. They have a potential
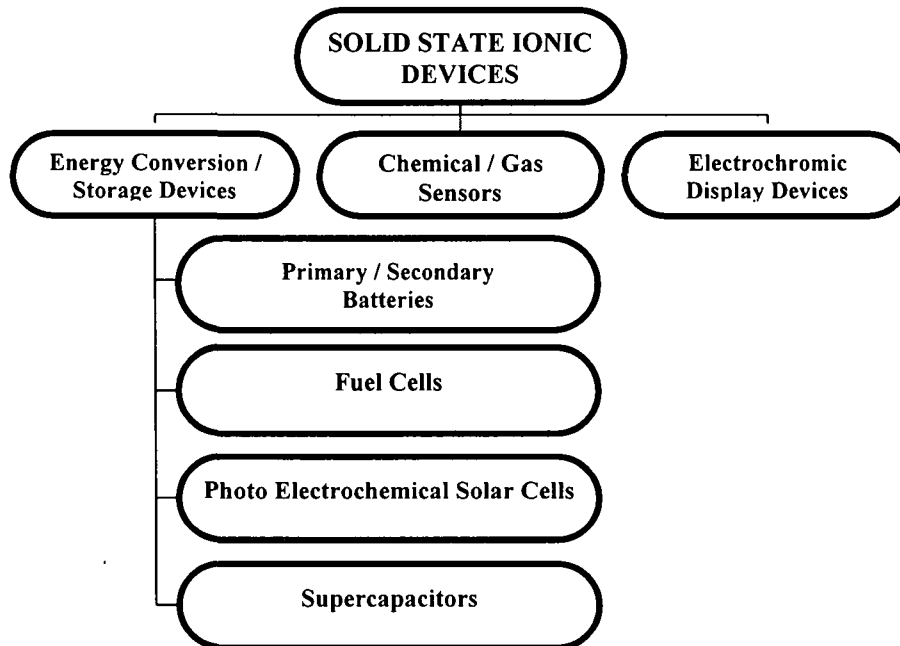
Fig. 1.3: Solid state electrochemical devices [1, 2].

capability to replace their liquid counterparts in several electrochemical devices. The polymer/gel electrolytes based ionic/electrochemical devices possess various advantages over the devices based on other ion conducting materials. They show good adhesive property, desirable mouldability and flexibility, proper electrode-electrolyte contacts, good mass efficiency etc. and these can easily be prepared in the form of thin films, which enable the miniaturization of devices, helpful in transportation.

Thus, the polymer/gel electrolytes in solid-state electrochemical devices open a new door for the researchers to look for high energy density devices. Nowadays, several types of energy storage/conversion devices are fabricated using different polymer/gel electrolytes. Some important applications are described below:

1.2.1 Solid State Batteries:

Battery is an electrochemical device, having a capability to convert chemical energy into electrical energy by the process of electrochemical reactions at the electrode-electrolyte interfaces. A schematic representation of solid-state battery is shown in the Fig. 1.4. All the components in the figure i.e. cathode, anode and electrolyte are in the solid-state form. It consists of three compartments, in which two electrodes (i.e. anode and cathode) are separated by electrolyte material, which possesses high ionic conductivity with sufficient mechanical, electrochemical and interfacial stability with the two electrodes under operating conditions.
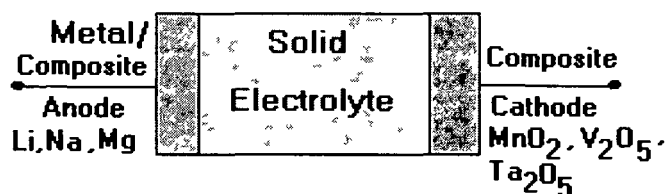
Fig 1 4 Typical configuration of solid-state battery

The e.m.f. developed in the battery cell is given by mathematical expressions:

$$\Delta G = -nFE \qquad \text{.....................} \qquad (1.1)$$

where ΔG is the Gibb's free energy for the electrode reactions between respective electrode/ electrolyte interfaces taking place in the cell under consideration, n is the valency of the conducting species and F is the Faraday's constant and E is the e.m.f. of the cell. Hence in order to develop a high energy density battery, the value of ΔG should be towards negative side. For the purpose, electrode should be as light as possible. In the fabrication of battery, generally anode is chosen to be of pure materials or alloys e.g. in lithium batteries, the anode is of pure lithium and cathode is made up of some insertion types of materials such as TiS_2, MoO_3, V_6O_{13} etc. [170-172]. A number of reviews, books and articles on different types of solid-state batteries are available in literatures [173-178].

1.2.2 Electrochemical Supercapacitors:

Supercapacitors are new and innovative types of electrochemical capacitors, which have 20-2000 times larger capacitance values as compared to the conventional electrolytic capacitors. From the configuration point of view, these are similar to the rechargeable
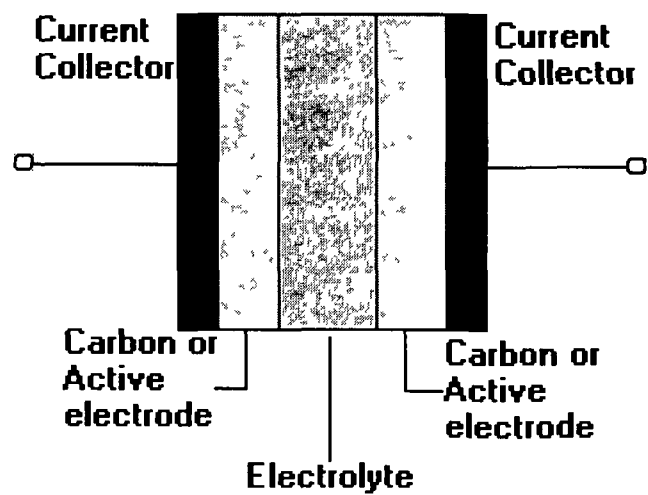
Fig 1 5.   Typical configuration of supercapacitors

batteries, the main difference being that in the case of batteries two different electrode materials (anode and cathode) are used whereas in supercapacitors generally two identical electrode materials are used as shown in the Fig 1.5. Details of the different types of supercapacitors are described in Chapter 2.

1.2.3 Fuel Cells:

These are the electrochemical sources of energy in which the chemical energy of a fuel and an oxidant is converted into electrical energy by a process involving essentially invariant electrode-electrolyte system [1,2]. The general configuration of H_2/O_2 fuel cell is given in Fig 1.6.
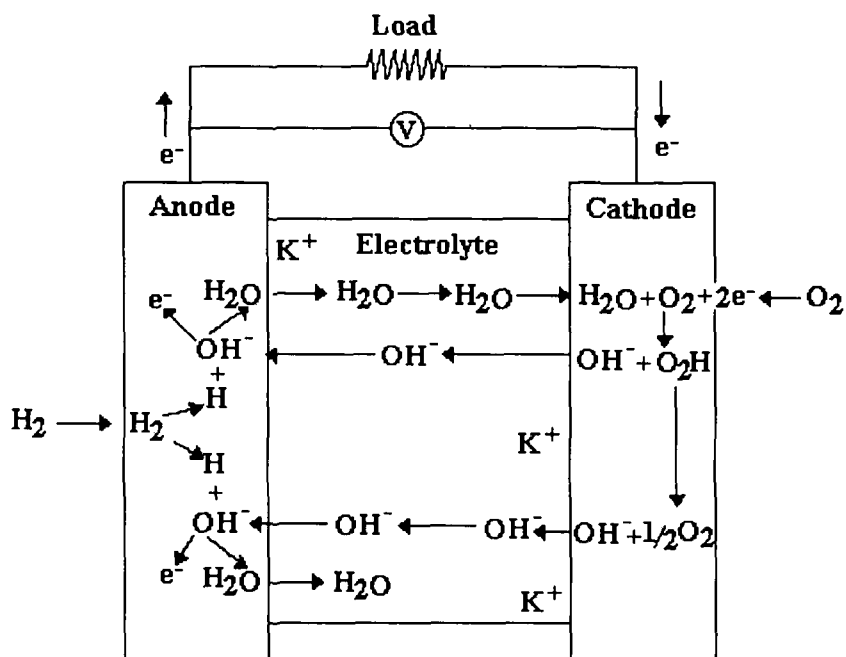
Fig 1.6:   General configuration of H_2/O_2 fuel cell.

The main difference between the fuel cell and the battery is that in the case of fuel cell, the fuel is provided continuously from the external source to the electrode materials, whereas in the case of battery the reactants are already stored in the cell. Electrical energy can be drawn from the fuel cell as long as an oxidant or fuel is available. The fuels, which are generally used

in the fuel cell, are H_2, CH_4, NH_3, N_2H_4, CH_3OH, H_2-rich gas derived from coal/oil or recovered from biomass etc. The oxidants are generally preferred for this purpose are O_2, air, H_2O_2, halogens etc. Depending on the types of electrolyte materials used, fuel cell may be categorised in the different groups such as, phosphoric acid fuel cell (PAFC), alkaline fuel cell (AFC), molten carbonate fuel cell (MCFC), solid oxide fuel cell (SOFC), solid polymer electrolyte fuel cells (SPEFC) etc. The comparison of these fuel cells is shown in Table 1.6 [179, 180].

Table-1.6: Comparison of different types of fuel cells.

Fuel Cell	Typical Electrolyte	Operating temperature	Equilibrium potential (V)	Over Potential	Conductivity of electrolyte $(S\ cm^{-1})$	Stack operating potential (V)	
						1 atm.	Under pressure
SPEFC	$-(CF_2)_m-$ SO_3H	80	1.160	0.28	0.1-0.2	-	0.75
AFC	KOH	100	1.150	0.22	0.17	-	0.86
PAFC	H_3PO_4	200	1.130	0.30	0.15	0.65	0.71
MCFC	Li_2CO_3 $-K_2CO_3$	650	1.020	0.06	0.14	0.66	0.75
SOFC	$Zr_{0.92}Y_{0.08}$ $O_{2.96}$	1000	0.925	0.05	0.12	0.60	-

Out of these fuel cells, solid polymer electrolyte fuel cells (SPEFCs) are most popular, in which proton conducting polymer electrolytes (polymeric ion-exchange membrane) such as hydrated Nafion or other hydrated perfluorinated ionomeric materials are used. Operating temperature range in these types of fuel cells is $\sim 100^0C$. There also exist direct methanol SPE fuel cells, which use dynamic hydrogen reference electrode [181] and acid doped polybenzimidazole [182] as the polymer electrolyte showing about hundreds of mA current density at $\sim 70^0C$ and 200^0C.

1.2.4 Electrochromic Display Devices (ECDs):

An electrochromic display device is basically an electrochemical cell, in which the energy output can be observed in the form of optical (colour) change. Basically, there exist some materials, which show the phenomenon of a reversible and persistent change in their optical properties upon application of an electric field [183]. This phenomenon is called electrochromism and the materials, which show this phenomenon, are referred to as electrochromic materials. Consequently, devices based on these electrochromic materials allow an arbitrary control over their optical reflectance and transmittance in response to the variation in brightness of the environment [175]. These properties make electrochromic materials of considerable interest for optical devices of several types such as elements for information displays, anti dazzling rear view mirrors for automobiles, cars, aircrafts, ships, smart windows, energy efficient large area architectural glazing, sky-lights in buildings, sunglasses, sunroofs etc [73, 183, 184]. The basic design of an electrochromic devices (ECDs) is shown in Fig 1.7.

$$WO_3 + xM^+ + xe^- \rightleftharpoons M_xWO_3$$

(bleached/transparent)   (Coloured/Blue)
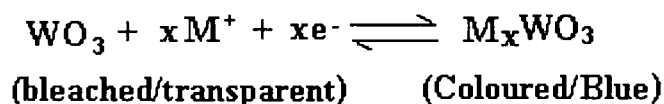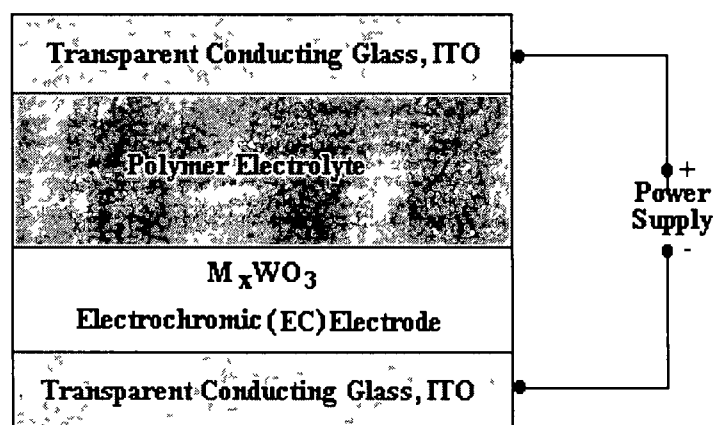
Where $M = H^+, Li^+, Na^+$

Fig 1.7: General configuration of ECD cell.

The most popular electrochromic oxide is WO_3, which shows a mixed conduction of ions and electrons and therefore, if ions are introduced from the electrolyte by the application of a suitable voltage between the two transparent electrical conductors, there is a corresponding charge balancing counter flow of electrons from the transparent electron conductor as shown in the Fig 1.7. These electrons will remain in the electrochromic film as long as the ions reside there and the electrons will then evoke a persistent change of the optical properties. When the polarity of the voltage is reversed, the original optical state of the device is recovered [183]. Colouration and bleaching of WO_3 films are synonymous with intercalation and deintercalation of small alkali metal ions (e.g. H^+, Li^+ and Na^+) into the film and can be expressed as shown in the Fig 1.7. For practical devices, the ion conductor or the electrolyte is preferentially used in the form of a polymer/ gel electrolyte materials.

1.2.5 Photo-electrochemical Solar Cells (PESCs):

Photo-electrochemical solar cells (PESCs) are the devices based on the junction of a semiconductor and an electrolyte containing a redox couple such as $I^- / I_3^- / I_2$ or $S^{2-} / S_x^{2-} / S_{x+1}^{2-}$ etc [72, 73]. The electrodes in such a cell are made of n-type semiconductors and transparent conducting materials such as ITO. In conventional photocells involving liquid electrolytes, illumination produces photo-generated holes that oxidise the complex anions in solution, while electrons travel from the semiconductor through an external load to reduce the species at the transparent illuminated surface. The electrochemical cycle is completed by re-diffusion of the species in the electrolyte. But the system suffers from a common problem of photo-corrosion and side reactions at the semiconductor interface that limits its working life. The use of polymer/gel electrolytes in PESCs eliminates these problems upto certain extent and offers ease in a number of ways such as miniaturization, time stability, transportability, etc. A general diagram of PESCs is shown in Fig 1.8.
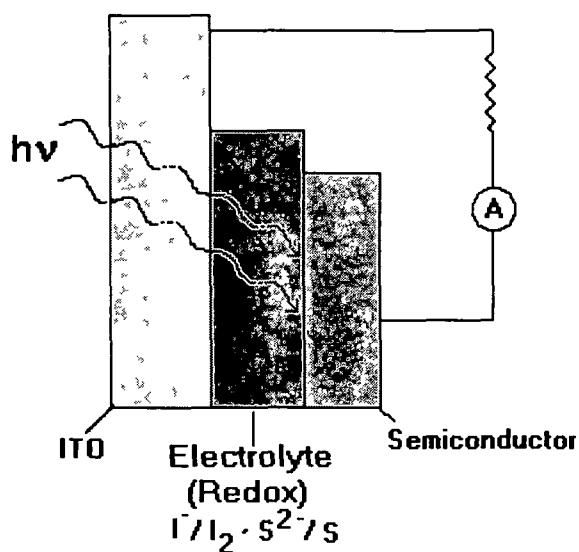
Fig 1 8   General configuration of photo-electrochemical solar cell

Several photo-electrochemical solar cells based on different types of polymeric gel electrolytes have been reported in the literature [72, 73].

1.2.6 Electrochemical Transistors:

Chao and Wrighton [185] were the first to develop a solid-state electrochemical transistor using conducting polymer [poly (3-methyl thiophene)] and polymer electrolyte ($PEO_{16}LiCF_3SO_3$). The diagram of the electrochemical transistor is shown in Fig 1.9. The device can be cycled by doping the poly (3-methyl thiophene) between a conducting state (oxidised, "on") and an undoped insulating state (reduced, "off") by cycling the applied potential. The oxidation of the neutral poly (3-methylthiophene) occurs with the insertion of a triflate anion from the electrolyte. The redox schemes are shown in the Fig 1.9. The device is turned on at a potential of +0.4 V vs. Ag. A change in the electrolyte structure occurs on exceeding +0.6 V due to the depletion of anions with a seven fold increase in the electrolyte resistance. However, the switching times are slow in this case at ~ 5 s as compared to ~ 5 µs for

a solution electrolyte. The slow switching appears to be due to slow diffusion in the electronic polymer and not from the electrolyte conductivity [185].

(a) Reduced Polymer, Device "Off"   (b) Oxydised Polymer, Device "On"
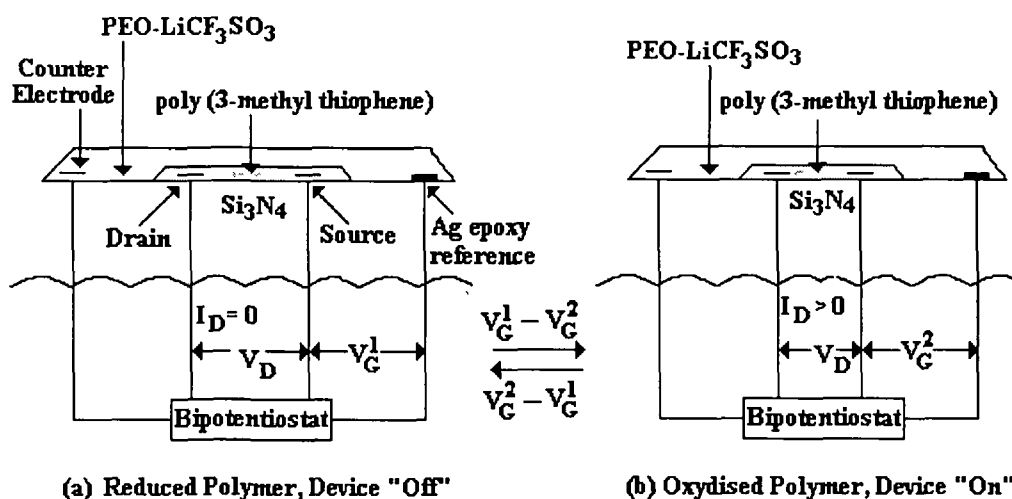
Fig 1.9:   *General configuration of electrochemical transistor using poly (3-methyl-thiophene) and $PEO_{16}LiCF_3SO_3$ polymer electrolyte.*

1.2.7 Solid State Sensors:

Nowadays, sensors have been playing very important role in various applications for measurement and control of temperature, pressure, in the field of agriculture, biosensors, environmental pollution from different gases e.g. SO_x, CO_x, No_x, etc. Its principle is based on the changes in the electrical properties of the electrolyte materials (systems) under different environment [12, 73]. Depending on the mechanisms involved and type of configuration, sensors can be broadly divided into two different classes:

(a) Electrochemical type:

In this type of sensors, the parametric changes produced due to the electrochemical reactions induced at the electrode-electrolyte interface are monitored. Electrochemical sensors may further be divided into three types: (i) potentiometric, (ii) amperometric, and (iii) coulometric.

(b) Impedance type:

In this type of sensors, the conductivity changes induced at the electrode-electrolyte interfaces are monitored.
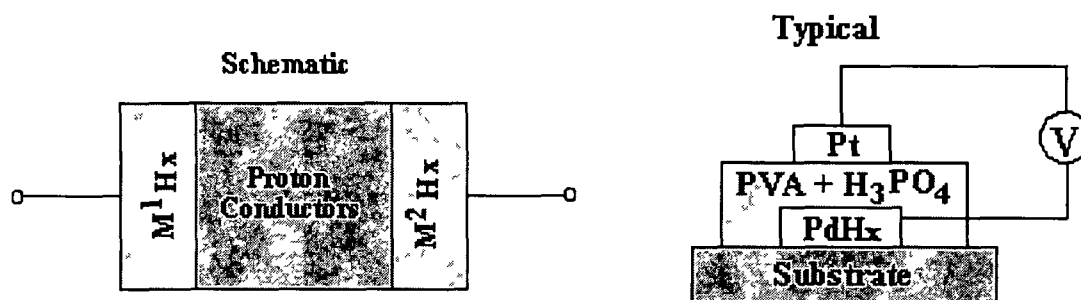
Fig 1.10: Schematic diagram of solid state H_2 sensors.

The polymeric electrolyte sensors developed so far, are only for humidity and gases. The moisture sensitivity of ionic conductivity in polymeric electrolytes makes them a suitable candidate for humidity sensors. Typical designs of potentiometric hydrogen sensor using PVA-H_3PO_4 as an electrolyte are shown in the Fig 1.10. Various types of sensors are commercially available for different applications [12, 73, 86, 186-188].

Some others examples of solid state sensors are (i) oxygen sensors for steel industries, (ii) CO_x, NO_x, SO_x sensors for environmental pollution control, (iii) Humidity Sensors, (iv) ammonia Sensors, (v) H_2S Sensors, etc.[12, 73].

Various other applications of solid-state ionic materials include electrochemical switching, thermo-electric generators, solid-state reference electrodes, steam electrolyser, dehumidifier, hydrogen pump, etc. [1, 2, 12, 73].

Chapter – 2

Supercapacitors: An Overview

SUPERCAPACITORS: AN OVERVIEW

2.1 Supercapacitors: A Brief Review

Capacitor is a device having a capacity to store the electrical energy. After the advent of ICs and LSI chips in the market, the continued existence of capacitors was once considered to be technologically doubtful. However, digitalisation of electronic and electrical appliances, has led to a strong demand for capacitors with low impedance in a high frequency range, small size, and large capacitance. In the beginning, capacitors were used primarily in electrical and electronic products, but today they are used in various fields ranging from high frequency to low frequency applications such as industrial application to automobile, aircraft and space, computers, games, mobile, power supply circuits and other power electronics. In view of its quite versatile applications the demand of capacitor market shows a tendency of steady growth worldwide. Depending on the types of materials used, their configuration and different charge storage mechanisms, capacitors may be broadly classified into three different categories, viz. (i) conventional capacitors, (ii) electrolytic capacitors, and (iii) electrochemical capacitors.

2.1.1 Conventional Capacitors:

The configuration of conventional capacitors, as shown in Fig. 2.1, is simple in which mica/paper/ceramic film is sandwiched between two metallic electrodes, which are obviously electronic conductors. They are attractive as pulse power discharge energy storage system because of their fast discharge times and high peak power. The film and mica capacitors are quite large in size and difficulties are encountered in obtaining a large capacitance. The layers built ceramic capacitors have poor temperature characteristics when they are manufactured in a small size and large capacitance.

31

Dielectric: Paper/Mica/Ceramic

Metal Electrodes
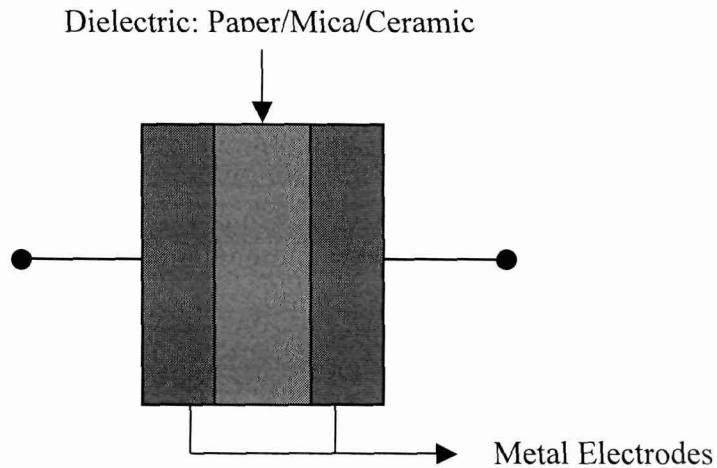
Fig. 2.1: Conventional capacitors

2.1.2 Electrolytic Capacitors:

Electrolytic capacitors are usually asymmetric and polarity dependent, i.e. they have a preferred arrangement of anode and cathode. These capacitors have one metallic electrode, and an electrolyte as the opposite electrode. An insulating oxide layer is electrochemically formed on the surface of the metal electrode, which acts as the dielectric. In this case one of the plate is electronically conducting and other may be ionically conducting or semiconducting, providing an electrolytic or semiconducting dielectric interface respectively. Generally there are two types of electrolytic capacitors, commonly available, namely:

(a) Tantalum electrolytic capacitors, and

(b) Aluminium electrolytic capacitors.

These capacitors use liquid as well as solid electrolytes. The solid electrolyte based capacitors are more popular due to their various advantages over liquid electrolyte such as no leakage, improvement in frequency as well as temperature response, heat resistance, miniaturisation, easy transportability etc.

(a)   Tantalum Electrolytic Capacitors:

There are two types of tantalum electrolytic capacitors available in the market: wet electrolytic capacitors, which use sulfuric acid as the electrolyte material, and solid electrolytic capacitors, which use MnO_2 as the solid electrolyte [Fig. 2.2].
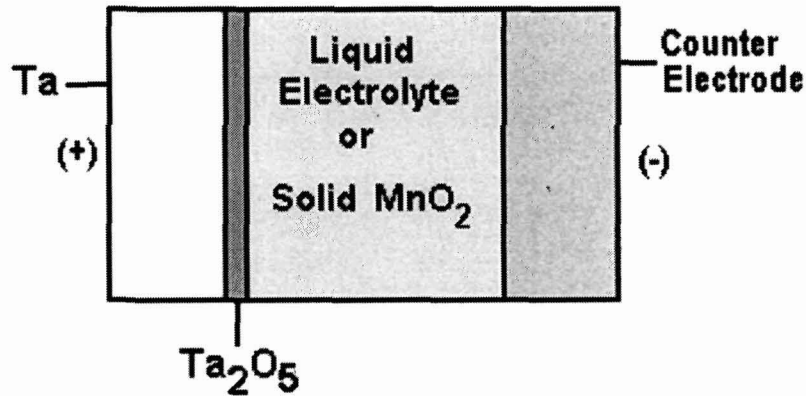
Fig. 2.2: Configuration of tantalum electrolytic capacitor

Till 1970, the wet type electrolytic capacitors were primarily used in circuits requiring a relatively high level of reliability, such as communications equipment and telephone switchboards. However, in recent years, with communications equipment consuming less power and being smaller in size as a result of the development of ICs, LSI chips, and VSLI chips, it has become possible to ensure sufficient reliability and long life for solid electrolytic capacitors. Most of today's tantalum electrolytic capacitors use manganese dioxide as the solid electrolyte. In addition, although there is no lack of research and development being done on solid electrolytic capacitors based on organic materials [189-191], because of the insufficient capacity achievement rate, this type of capacitors, are yet to reach practical applications.

(b)   Aluminium Electrolytic Capacitors

Most of the aluminium electrolytic capacitors reported worldwide for different applications are of the wet type. Aluminium solid electrolytic capacitors still account for a

share of only less than 1%. This type of capacitor incorporates an organic solid membrane as the solid electrolyte. There are two main types of solid electrolytes: a functional polymer e.g. polypyrrole (pPy), and an organic semiconductor (TCNQ salt) [192-194]. A disadvantage with the TCNQ complexes, which are generally applied to the oxidized metal surface in the molten state, is that they can only be worked or melted at temperatures at which their stability limit allows, and when overheated they decompose to hydrocyanic acid and therefore have a toxic and corrosive effect. A major challenge in the implementation of a conductive polymer as the
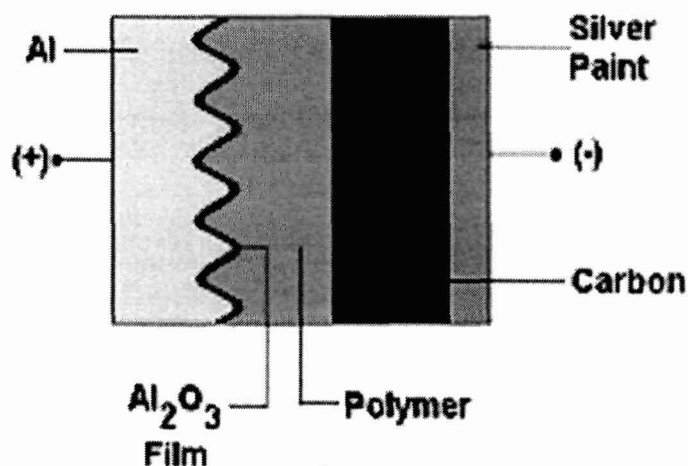
Fig. 2.3: Configuration of aluminium electrolytic capacitor

solid electrode is its efficient placement into the anode, which generally has a highly porous surface structure. Using an electrochemical or chemical polymerisation in-situ process usually circumvents this issue. Fig. 2.3 shows the schematic diagram of a typical aluminium solid electrolytic capacitor incorporating a polymeric electrolyte. The surface of an aluminium foil is etched and then oxidized in order to form a dielectric layer of Al_2O_3. A layer of manganese dioxide solid electrolyte material is then formed on the surface of the dielectric followed by a layer of organic solid electrolyte material, which is formed by electrochemical synthesis. The positive and negative electrodes are mounted to complete the electronic component.

Table 2.1 shows specifications and possible applications of some conventional and electrolytic capacitors.

Table 2.1: Some important conventional and electrolytic capacitors and their possible applications.

Types of Capacitors	Specification	Application
Paper	~ 400 V, < 0.1 μF	High frequency electronic circuits.
Mica	~ 100 V, < 1 μF	High frequency electronic circuits.
Ceramic	~ 50 V, < 0.1 μF	High frequency electronic circuits.
Thin Film	~ 50 V, < 0.01 μF	High frequency electronic circuits.
Tantalum Electrolytic (Liquid)	~ 50 V, > 1 μF	Medium frequency electronic circuits, Power supply filters etc.
Aluminium Electrolytic (Liquid)	~ 50 V, > 1 μF	Medium frequency electronic circuits, Power supply filters etc.
Tantalum Electrolytic (Solid)	~ 25 V, > 10 μF	Medium frequency electronic circuits, Power supply filters etc.
Aluminium Electrolytic (Solid)	~ 25 V, > 1 μF	Medium frequency electronic circuits, Power supply filters etc.

2.1.3 Electrochemical Supercapacitors:

Electrochemical capacitor, also referred to as "supercapacitor", is a symmetric device in which the electrolyte is placed between the two identical electrodes. It stores the electrical energy in an electrochemical double layer formed at a solid electrode/liquid or solid electrolyte interface. Positive and negative ionic charges within the electrolyte accumulate at the surface of the solid electrode and compensate for the electronic charge at the electrode surface. They are unique energy storage devices, which have the following specific characteristics:

- Large value of capacitance (~20-2000 times per gram or per cm^2 of electroactive materials).

- High power storage as well as delivering ability.

Historically, in 1879 Helmholtz first considered the storage of charge at electrode-electrolyte interface and regarded the double layer as equivalent to a parallel plate capacitor. The concept of a double layer corresponds to a model consisting of two array layers of opposite charges, separated by a small distance having atomic dimensions, and facing each other, as on the plates of a two plate hardware capacitor. Initially this model was used to describe the distribution of opposite charges, quasi-2-dimensionally, at the interface of colloidal particles. Fig. 2.4 (a) shows the structure of Helmholtz double layer model [195].

In the original model for colloidal interfaces, the charges on the surface side of the double layer arise either from acid-base ionisation, as with proteins or polyelectrolytes, or on account of the adsorption of ions, as at lyophobic colloids. On the solution side of the double layer, counter ions of opposite sign of charge accumulate to balance the charge on the colloid, forming a double layer array of positive and negative charges. The Helmholtz model was later adapted to the case of electrode interfaces, where, on the metal side, a controllable surface density of excess negative or positive charge can arise that corresponds to an excess or deficiency of electron charges of the delocalised electron plasma of the metal.

After the proposal of Helmholtz model, it was realised further that the ions on the solution side of the double layer would not remain static in a compact array as in Fig. 2.4 (a), but would be subject to the effect of thermal fluctuations [196] according to the Boltzmann principle [197]. Further Gouy [196] introduced this thermal fluctuation factor into a modified representation of the double layer. In this model, the ions were assumed to be a point charges. A schematic representation of Gouy model is shown in Fig. 2.4 (b).

In the next stage of development of the theory of double layers, the problem associated with the Gouy-Chapman treatment i.e., overestimation of the double layer capacitance was
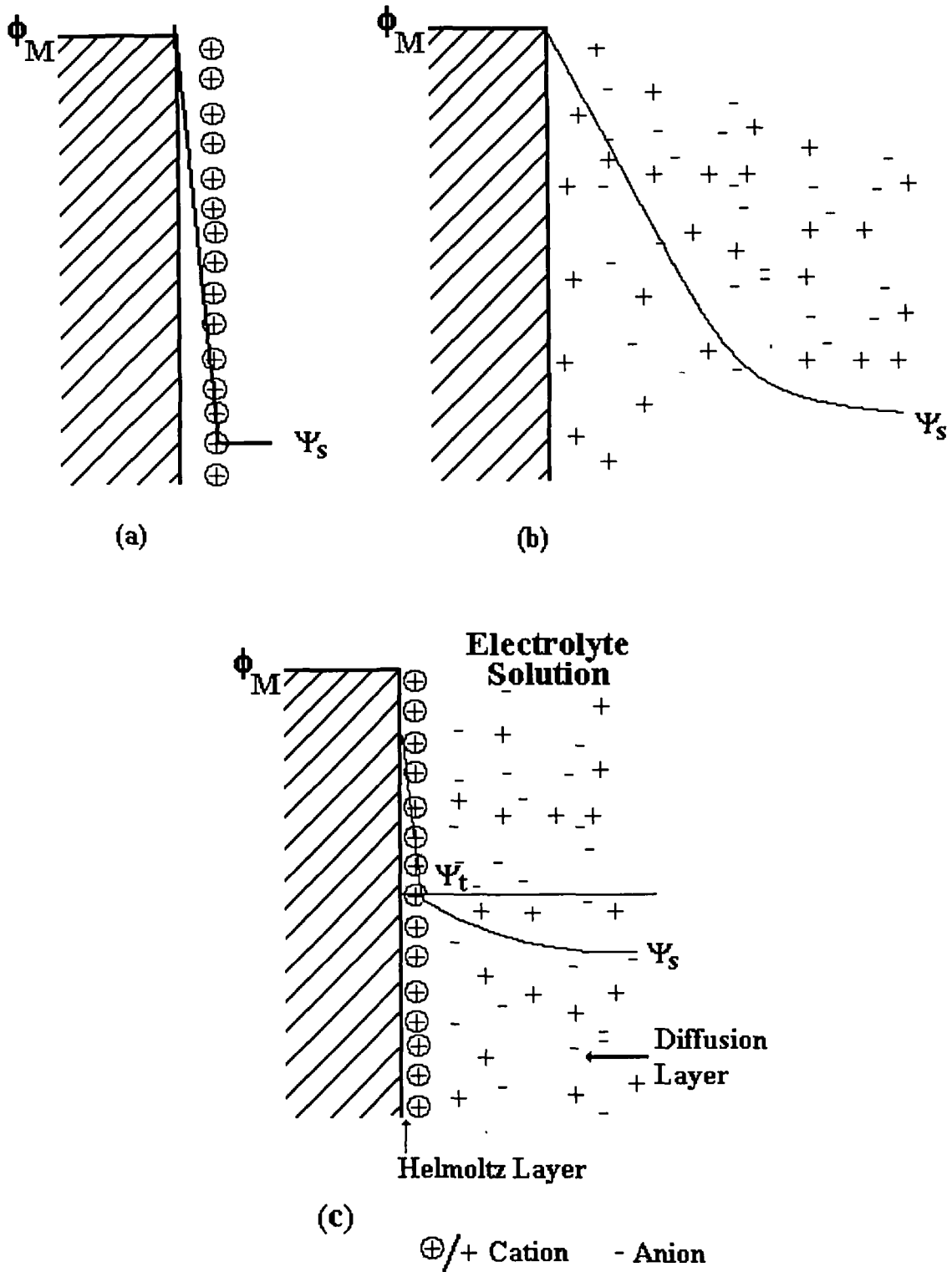
Fig. 2.4: General representation of Helmholtz double layer and its potential profile.

overcome by stern in 1924 [198]. In this model it was recognised that the inner region of the ion distribution could be treated in terms of an adsorption process according to Langmuir's adsorption isotherm, and the region beyond this inner layer, into the solution could be validly treated in terms of a diffuse region of distributed ionic charge [Fig. 2.4 (b)] as treated by Guoy [196] and Chapman [199]. In addition, if the ions were recognised as having finite size, it was easy to define a geometrical limit to the compact region of adsorption of ions at the electrode surface [Fig. 2.4 (c)]. Accordingly, the overall double layer capacitance, C_{dl}, is associated with the Helmholtz type of compact double layer having a capacitance C_H and the remaining ionic charge density beyond this compact ion array (referred to as the "diffusion" region), having a capacitance C_{diff}, connected in series. The C_{dl} can be expressed by the relation:

$$\frac{1}{C_{dl}} = \frac{1}{C_H} + \frac{1}{C_{diff}} \qquad \dots \dots (2.1)$$

According to the Helmholtz and other models described above, typical capacitance values were found to be in the range of 20-40 μF cm^{-2} for electrode-liquid electrolyte interfaces. Further, Rayleigh in 1966 [200] reported a substantially higher capacitance of ~ 200 μF cm^{-2} for the interface of platinum and AgBr. This higher value was explained in terms of the specific adsorption of a layer of electrolyte ions on the electrode surface. Thereafter in 1980 NEC Corporation, Japan reported and commercialised the Electrical Double Layer Capacitors (EDLCs) having a specific capacitance value of about several hundred of mF cm^{-2}, which was composed of large surface area activated carbon electrodes and sulphuric acid electrolyte with a brand name 'SUPERCAPs'. This led to the discovery of Supercapacitors, which attracted global attention of research community towards their further investigation at commercial scale. Since then, different research groups in the literature have reported supercapacitors of various types using different electrode and electrolytes [201-206].

The configurations of the supercapacitors are almost similar to the batteries. In both the cases electrolyte is sandwiched between two electrode materials, as shown in Fig. 2.5. The main difference between them is that in the case of supercapacitors two identical electrode materials (blocking / active) are generally used, whereas in batteries two different electrode

Battery

Active Electrode (Anode)	Electrolyte	Active Electrode (Cathode)

Supercapacitor

Blocking Electrode or Active Electrode	Electrolyte	Blocking Electrode or Active Electrode
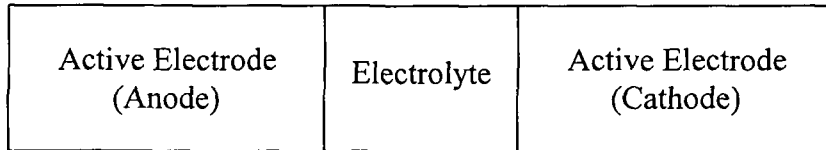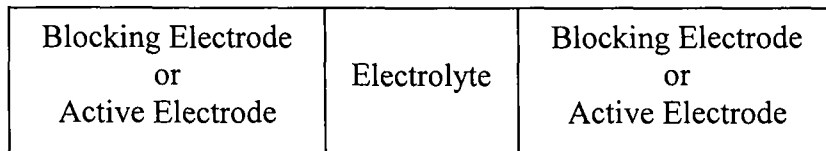
Fig. 2.5: Configuration of batteries and supercapacitors.

materials (anode and cathode) are used, which is involved in the interfacial reactions leading to an overall electrochemical process of the cell.

In the battery system, the energy can be expressed as: $E = Q.\Delta V$, where Q is the Faradic charge associated at the interfacial reaction and ΔV is the Nernstian cell potential, which is ideally constant during charge or discharge until all the reactant materials are electrochemically consumed. On the other hand, the energy of a charged capacitor is expressed as: $E = \frac{1}{2} Q.\Delta V$ or $\frac{1}{2} C (\Delta V)^2$, where Q is the charge accumulated and the electrode surfaces and ΔV is voltage difference across the capacitor. The ΔV rises while charging and declines while discharging linearly due to the electrostatic reason. A comparative picture of the potential variation while charge/discharge of battery and capacitor is pictorially shown in Fig. 2.6 [201].
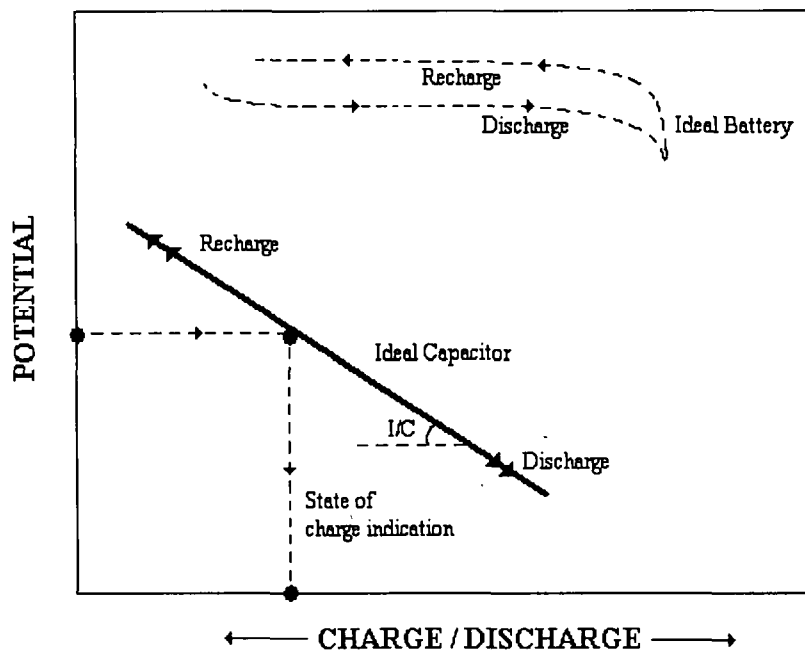
Fig. 2.6: A comparative charge-discharge plots of battery and supercapacitor[201]

An overall comparison of a battery and a supercapacitor is summarised in Table 2.2.

Table 2.2: A comparison of battery and electrochemical capacitor characteristics.

Battery	Electrochemical Capacitor
E.M.F is ideally constant during charge and discharge	Potential is related to state of charge
Behaviour is not capacitive	Behaviour is capacitive
Discharge at constant current arises at a constant potential approximately	Discharge at constant current gives mainly linear decline of potential with time, which is characteristic of capacitor
Has moderate or good energy density	Has relatively poor energy density
Has relatively poorer power density	Has good power density
Has less cycle life	Has excellent cyclability or cycle life
Has internal IR due to electrolyte and active materials	Has internal IR due to high area matrix and electrolytes
Has poorer life time due to degradation or reconstruction of active materials	Has longer life time except for corrosion of current collectors etc.

40

Table 2.3 shows the comparison of energy density, power density and cycle life of

batteries, conventional capacitors as well as supercapacitors quantitatively.

Table 2.3: Comparison of characteristics of energy storage devices.

Parameters	Battery	Conventional Capacitors	Supercapacitors
Energy Density, $(Wh\ Kg^{-1})$	30-300	0.03-0.3	3-30
Power Density, $(kW\ Kg^{-1})$	0.1-0.5	$10-10^4$	$1-10^3$
Cycle Life	$<10^4$	$>10^6$	$>10^5$

On the basis of the types of electrode materials used and charge storage mechanisms

supercapacitors may be divided into two different classes as shown in Fig. 2.7.
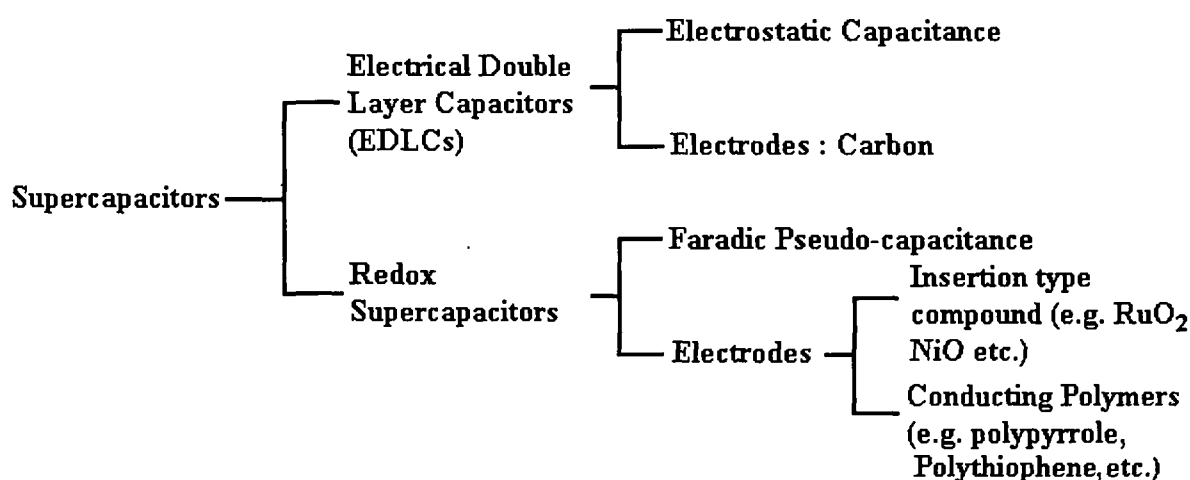
Fig. 2.7: Types of supercapacitors

2.1.3.1   Electrical Double Layer Capacitors (EDLCs):

The capacitors, which employ the carbon or other similar materials as blocking

electrodes, are referred as "electrical double layer capacitors (EDLCs)." Reasons for using

carbon are manifold such as its (i) low cost, (ii) availability in different physical types (powder,

paper, fibre, fabric) with larger surface area, (iii) availability in different forms (activated

carbon, graphite, acetylene black, glassy carbon, etc.), and (v) established electrode production technologies.

Electrodes, which do not participate in any electrochemical reaction including charge transfer at the electrode-electrolyte interface (within the voltage limit of electrochemical stability range of electrolyte), are able to accumulate (store) charges on application of electric potential. These electrodes are termed as polarisable or blocking. In general, large surface area carbon electrodes are used in EDLCs. Several electric double layer capacitors using large surface area electrodes with different types of carbons have been developed with liquid and polymer/gel electrolytes [200-236]. In particular, activated carbon powders/fibres/fabrics, which can be produced with large surface area up to 2000-2500 m^2 g^{-1}, have attracted much attention for the fabrication of double layer capacitors due to their corresponding very high capacitance values of 400-500 Fg^{-1}. The charge storage mechanism in EDLCs is electrostatic in nature resulting from the separation of charged species at the interfacial double layers. The charge storage mechanism and the operational principle of EDLCs are shown in Fig. 2.8.
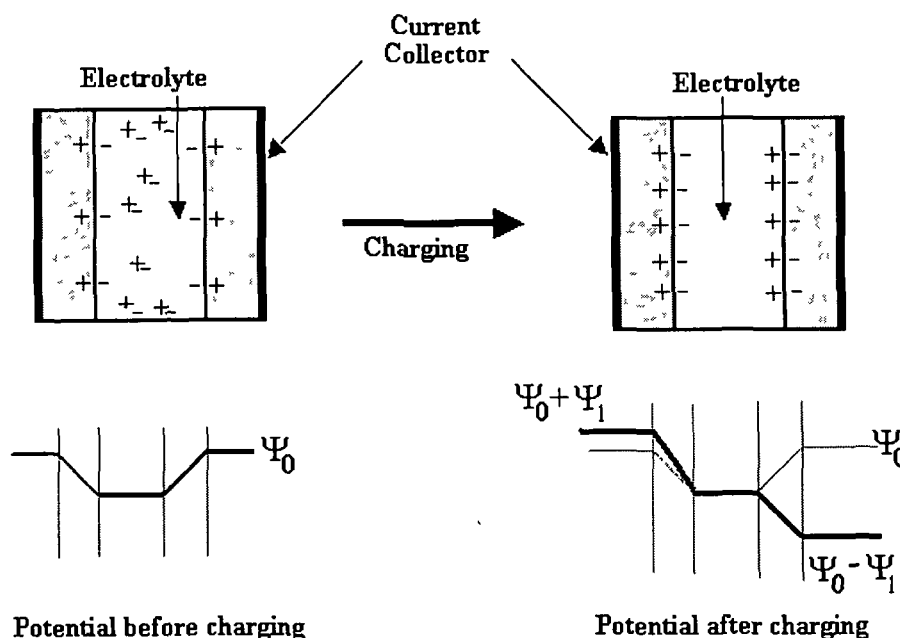
Fig. 2.8: Structure of electric double layer capacitor, after Nishino [204].

The capacitance C and the charge Q accumulated in the electrical double layer formed at the interface between the blocking (polarisable) electrodes and electrolyte is expressed as [204]:

$$Capacitance \ C = \left[\iint \frac{\varepsilon}{4\pi\sigma} \right] dS \qquad .... (2.2)$$

$$Accumulated \ charge \ Q = \left[\iint \frac{\varepsilon}{4\pi\sigma} dS \right] (2\psi_1) \qquad .... (2.3)$$

where ε is dielectric constant of the electrolyte, σ is distance from the electrode interface to the centre of ions and S is electrode surface area.

Some important examples of EDLCs are given in Table 2.4.

Table 2.4: Some important Electrical Double Layer Capacitors and their characteristics.

Capacitor Cells	Capacity		Energy (Wh Kg⁻¹)	Power (kW Kg⁻¹)	References
	(F g⁻¹)	(mF cm⁻²)	(Wh Kg⁻¹)	(kW Kg⁻¹)	
ACF | Nylon 6-10-H$_3$PO$_4$ | ACF	70	-	1.4	-	207
Ni-ACF | PC-LiClO$_4$| Ni-ACF	95	-	-	-	208
ACF | PMMA-PEO-(C$_2$H$_5$)$_4$NBF$_4$-PC | ACF	20	570	16.2	-	209
ACF | PAN-(C$_2$H$_5$)$_4$NBF$_4$-PC | ACF	16	370	-	-	210
ACF | PEO + PEG + LiCF$_3$SO$_3$ | ACF	4	20	-	-	211
ACF | PVA + H$_3$PO$_4$ | ACF	70-90	360-470	14-18	-	211
AC | PVdF-HFP-EC-PC-(C$_2$H$_5$)$_4$NBF$_4$ | AC	123	-	-	-	212
HD-ACF | KCl (aq.) | HD-ACF	28	-	-	-	213
C | KOH (aq.) | C; (C : aerogel)	20-40	-	-	7.7	201, 206
ACF | KOH (aq.) | ACF	30-48	-	-	-	201, 206
CE | PEO + PEG + LiClO$_4$ | CE (CE : Carbon Black + PE)	60	-	6.2	0.3	201, 206
C | PC-EC-LiAsF$_6$-PAN | C	-	0.02-0.06	-	-	201, 206
C | PEO-PC-LiClO$_4$ | C	-	0.44	-	-	201, 206
ACF | PEO-PMMA-PC-TEABF$_4$ | ACF	-	200-400	-	-	201, 206

ACF | PEO-PMMA-PC-TEAClO₄ | ACF	-	200-400	-	-	201, 206
AC/C | H₂SO₄ (aq.) | AC/C	20	-	1.0	0.67	201, 206
PAN-MF | 5M KOH | PAN-MF	-	-	3.0	0.1-1.0	201, 206
PAN-MF | 0.5M LiClO₄+ CH₃CN | PAN-MF	-	-	15.0	0.3-5.0	201, 206
AC-CNT | TEABF₄ | AC-CNT	95	-	-	110	214
AB | PVdF-EC-PC-TEABF₄ | AB (Acetylene Black)	4.1	-	-	-	215
ACP | PVA-HClO₄ | ACP (ACP: activated carbon powder)	44	-	-	-	216
ACF | PVP-PVAc-PC-TEABF₄ | ACF	38	-	-	-	217
C | H₂SO₄ | C	150	-	-	-	218
AC | H₂SO₄ | AC	180	-	-	-	219
C | ACN-TEABF₄ | C	100	-	-	-	220
C-MN | H₂SO₄ | C-MN MN: Mica Nanocomposite	180	-	-	-	221
ACF | PC-TEABF₄ | ACF	169	-	-	-	222
C(Rice Husk) | KCl | C(Rice Husk)	210	-	-	-	223
CNT | ACN-TEABF₄ | CNT	66	-	-	-	224
C(Aerogel) | H₂SO₄ | C(Aerogel)	104	-	-	-	225
C (Porous) | EMICF₃SO₃ | C (Porous)	-	14 F Cm⁻³	-	-	226
CB | PEO-PEG-LiClO₄ | CB	60	-	20 KJ/L	300 W/L	227
C(Aerogel) | 4M KOH | C(Aerogel)	-	24 F Cm⁻³	-	7.7	228
AC | KOH | AC	412.8	-	-	-	229
ACF | KCl | ACF	28	-	-	-	230
Pb₂Ru₂O₆.₅ | H₂SO₄ | Pb₂Ru₂O₆.₅	40	-	-	0.75	231
C | KOH | C	166	-	-	-	232
CF | KOH | CF (Carbon Fiber)	28	-	-	-	233
CB | KOH | CB (Carbon Black)	108	-	-	-	234
CF | H₂SO₄ | CF (Carbon Fabric)	170	-	-	-	235
AC | PC-TEABF₄ | AC	58.76	-	-	-	236

ACF : Activated Carbon Fabrics, Ni-ACF : Nickel loaded ACF, HD-ACF : High Density ACF, AC : Activated Carbon Powder, AC/C : Activated Carbon + Carbon Composite, PAN-MF : Polyacrylonitrile Microcellular Foam, Pb₂Ru₂O₆.₅: Lead ruthenate pyrochlore .

2.1.3.2   Redox Supercapacitors:

Capacitors, which employ the electroactive materials such as insertion type compounds (noble metal oxides e.g. RuO_2, NiO etc.) [237-239] or conducting polymers (e.g. polypyrrole, polythiophene etc.) [240-259] as active electrodes are referred as 'redox supercapacitors'. In redox supercapacitors, a fast faradic charge transfer process takes place which gives rise to a 'pseudocapacitance.' Recently a new class of supramolecular materials (e.g. 1,5 Diamino-anthraquinone oligomer, etc.) have been introduced as promising electrodes for redox supercapacitors, which exhibit high specific capacity with aqueous and non-aqueous liquid electrolytes [260, 261].

Conducting polymers have been shown to be potential electrode materials for redox supercapacitors because they offer several advantageous properties over the other noble metal oxides or carbon electrode materials, which include [201, 202, 205, 206]:

- Charging / Discharging through volume

- Large value of charge density (500 C g^{-1})

- High energy density comparable to noble metal oxides

- Low cost

- Easy synthesis

Particularly for electrochemical capacitors, the ability to charge (or discharge) through the whole volume is most attractive aspect of conducting polymers compared to the large area carbon materials. Hence, the combination of all these advantages over other electrode materials (carbon and metal oxides) make conducting polymers feasible and quite attractive electroactive materials for their application in electrochemical supercapacitors.

It is well known that conducting polymers exist in p-doped (oxidised) and n-doped (reduced) states. The mechanism of electrochemical doping of a conducting polymer is described schematically in Fig. 2.9 [240].
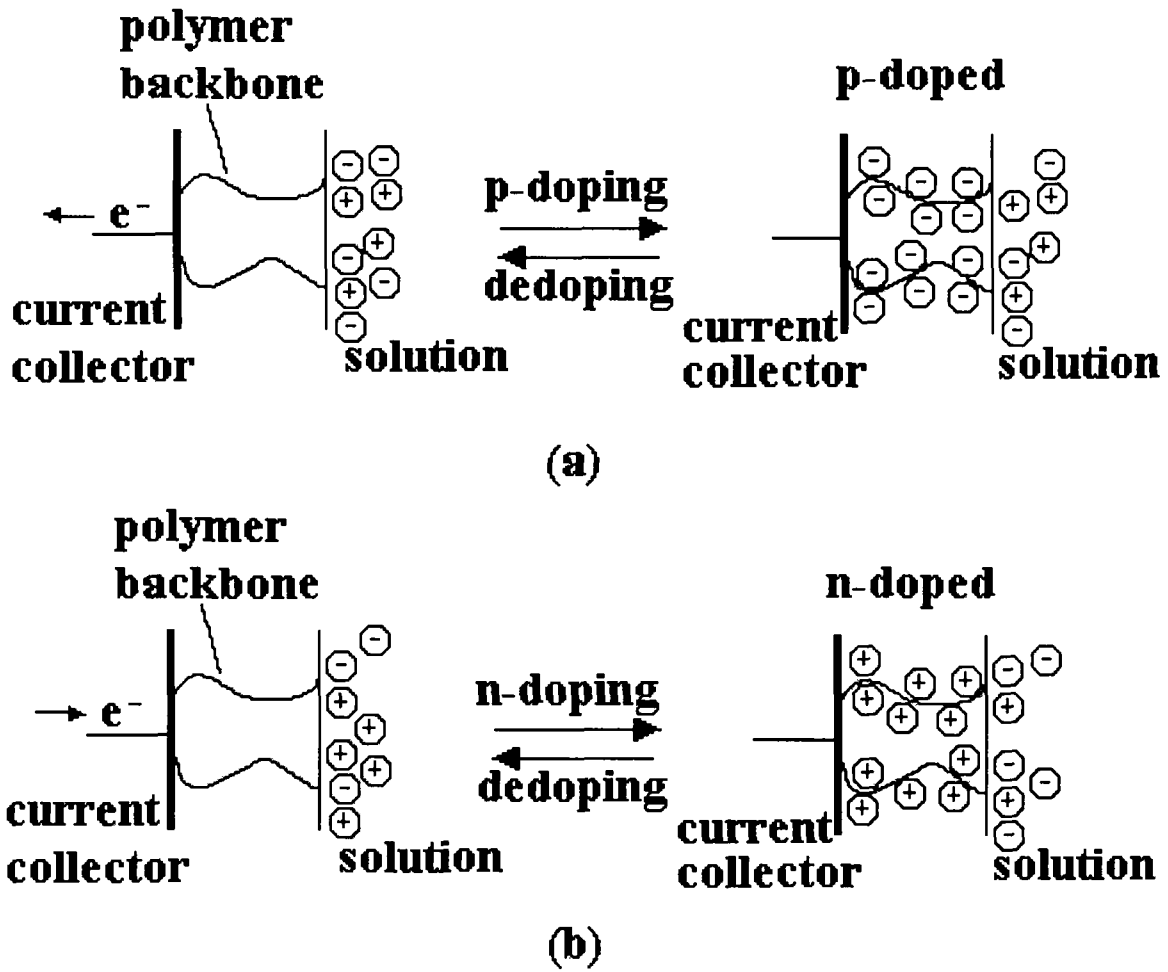
Fig. 2.9: Schematic representation of the charging and discharging processes at conducting polymer electrodes associated with (a) p-doping and (b) n-doping [240].

Electrochemical p-doping of conducting polymers takes place by abstraction of electrons from the polymer backbone through the external circuit and incorporation of an anion from solution into the polymer film to counter balance the positive electronic charge [Fig. 2.9 (a)]. On the other hand, in the case of n-doping, electrons are transported onto the polymer backbone by the external circuit, and cations enter the polymer from the solution phase in order to maintain overall charge neutrality [Fig. 2.9 (b)].

In view of the two types of conducting polymers, Rudge et al. (1994) [240] proposed three schemes of configuration of conducting polymers based redox capacitors, classified namely as types I, II and III, as shown in Fig. 2.10. Two identical p-dopable polymers are employed as active electrodes in type I capacitors. In the fully charged state, one electrode will be in the fully p-doped (positive) state and the other in the uncharged state. In this type, a potential difference of 0.8-1.0 V is obtained between the electrodes, with half this range being available for capacitor charge and discharge [Fig. 2.10 (a)]. The type II capacitors are comprised of two different p-dopable conducting polymers sandwiching the electrolyte materials, that have different ranges of potentials for oxidation and reduction [Fig. 2.10 (b)]. In type III capacitors, a configuration of n- and p- doped forms of the same polymers (e.g. poly-3-(fluorophenyl)-thiophene [240], etc.) is used [Fig. 2.10 (c)]. This type of capacitor system offers a wider range of operating voltage upto 3.1 V, which leads to the approximately nine-fold enhancement of energy density with respect to the type-I capacitor systems. Table 2.5 gives a comparison of various parameters such as, voltage range, charge and energy densities for different types of capacitor systems. Although the type-III capacitors are attractive from the operating voltage and energy density point of view, but it is seldom reported in literature as the preparation of n-doped conducting polymer is difficult due to various reasons including chemical / electrochemical instability at the ambient temperature.

(a) TYPE-I

Conducting Polymer (1) | Electrolyte | Conducting Polymer (1)
(p-doped)   (p-doped)
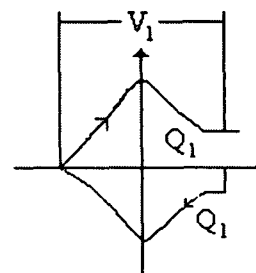
(b) TYPE-II

Conducting Polymer (1) | Electrolyte | Conducting Polymer (2)
(p-doped)   (p-doped)
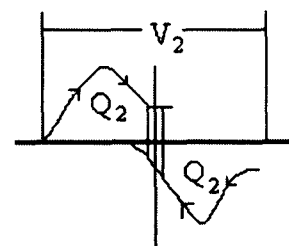
(c) TYPE-III

Conducting Polymer | Electrolyte | Conducting Polymer
(p-doped)   (n-doped)
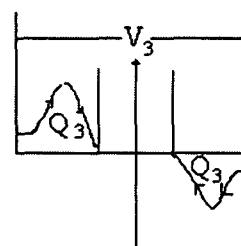
Fig. 2.10: Schematic representation of charge and discharge operation of different electrochemical supercapacitors, (a) Type-I supercapacitors, (b) Type-II supercapacitors and, (c) Type-III supercapacitors [240].

Table 2.5: A comparison of Type I, II and III redox supercapacitors [240].

Types	Voltage (V)	Charge Density		Energy Density		
		$C\ cm^{-2}$	$C\ g^{-1}$	$J\ cm^{-2}$	$J\ g^{-1}$	$W\ h\ Kg^{-1}$
I	1.0	1.2	86	0.56	41	11
II	1.5	2.2	120	1.9	100	27
III	3.1	1.3	52	3.5	140	39

Some important redox supercapacitors are listed in Table 2.6.

Table 2.6:   Some important redox supercapacitors and their characteristics.

Capacitor Cells	Capacity (F gm^{-1})	(mF cm^{-2})	Energy (Wh Kg^{-1})	Power (kW Kg^{-1})	References
$RuO_2.xH_2O$ | H_2SO_4 (aq.) | $RuO_2.xH_2O$	720	-	26.7	-	237
Ni-NiO | 1M KOH (aq.) | Ni-NiO	50-64	-	7.2-11.0	4.0-17.0	238
pPy | PMMA-EC-PC-LiClO$_4$| PANI	13	-	4.0	0.7	241
pPy | PVA + H$_3$PO$_4$ | pPy	39-84	1.5-5.0	12.0	-	242
pMeT | PEO-PEG-LiCF$_3$SO$_3$ | pPy	25-30	3.0-3.5	10.0-12.0	-	243
pDTT | PEO-PC-(C$_2$H$_5$)$_4$NBF$_4$ | pDTT	25-35	5.0-7.0	3.0-7.0	0.2	244
PEDOT | ACN-LiClO$_4$ | PEDOT	-	-	1.0-4.0	2.5	245
pPy / graphite | KCl (aq.) | pPy / graphite	400	-	-	-	246
Li-PANI | ACN-(C$_2$H$_5$)$_4$NBF$_4$ | Li-PANI	60-100	-	-	-	247
pPy(p) | PAN-gel electrolyte | pPy(p)	20-50	-	1.5-10	0.3-7.0	201, 206
pFPT | ACN-Me$_4$NCF$_3$SO$_3$ | pFPT	-	-	-	35.0	201, 206
pPy (p) | PC+LiClO$_4$ | pPy (p)	-	-	2-20	0.2-4.0	201, 206
pMeT (p) | PC+LiClO$_4$ | pMeT(p)	-	-	2-20	0.2-4.0	201, 206
pDTT(p)|PC+TEABF$_4$| pDTT(n)	-	-	2-20	0.2-4.0	201, 206
PANI | 4M HBF$_4$ | PANI	64-75	-	1.7-3.1	-	201, 206
PANI | Me$_4$NCF$_3$SO$_3$ + CH$_3$ CN| PANI	-	-	5.0	1.2	201, 206
MnO$_2$-pPy | PMMA-Gel electrolyte | MnO$_2$-pPy	-	10-18	-	-	248
AC | PYR$_{14}$TFSI | pMeT	100	-	24	14	249
RuO$_2$/TiO$_2$ | KOH | AC	120	-	5.7	1.207	250
pPy | PMMA-EC-PC-NaClO$_4$ | pMeT	-	12	-	-	251
PANI | NaClO$_4$ + HClO$_4$ | PANI	815	-	-	0.5	252
pMeT | PC-TEABF$_4$ | pTh	200	-	-	-	253
PANI | HBF$_4$ | PANI	75	-	2.7	1.0	254
pMeT | PC-TEABF$_4$ | pMeT	240	-	25	-	255
CNT/pPy | H$_2$SO$_4$| CNT/pPy	170	-	-	-	256

PANI | TEABF$_4$ | PANI	150	-	3.5	1.3	257
PANI | KOH | AC	380	-	18	1.25	258
PANI | HClO$_4$ + NaClO$_4$ | PANI	1300	-	-	0.5	259
pDAAQ | PC-(C$_2$H$_5$)$_4$NClO$_4$ | pDAAQ	-	-	25.0-46.0	10.2-30.5	260
pDAAQ | PMMA-EC-PC-(C$_2$H$_5$)$_4$NClO$_4$ | pDAAQ	3.7-5.4	125-184	92-135	-	261
CNT/RuO$_2$ | H$_2$SO$_4$ | CNT/RuO$_2$	560	-	-	-	262
AC/RuO$_2$ | H$_2$SO$_4$ | AC/RuO$_2$	308	-	-	-	263
Ru$_{(1-y)}$Cr$_y$O$_2$. xH$_2$O | H$_2$SO$_4$ | Ru$_{(1-y)}$Cr$_y$O$_2$. xH$_2$O	840	-	-	-	264
Pb$_2$Ru$_2$O$_{6\,5}$ | H$_2$SO$_4$ | Pb$_2$Ru$_2$O$_{6\,5}$	56	-	5	0.75	265
a-RuO$_2$/WO$_3$ | H$_2$SO$_4$ | a-RuO$_2$/WO$_3$	560	-	-	-	266
SnO$_2$/RuO$_2$ | KOH | SnO$_2$/RuO$_2$	710	-	-	-	267
RuO$_2$/C | H$_2$SO$_4$ | RuO$_2$/C	407	-	17.6	4	268
RuO$_2$/ VO$_2$ | H$_2$SO$_4$ | RuO$_2$/VO$_2$	1200	-	-	-	269
CoAl | KOH | CoAl	77	-	15.5	-	270

pPy : Polypyrrole, PANI : Polyaniline, Li-PANI : Lithium doped PANI, pMeT : Poly (3-methyl thiophene), pDTT : Poly (thieno [3,4-b : 3',4'-d] thiophene), PEDOT : Poly (3,4 ethylene-dioxythiophene), pDAAQ : poly (1,5-diaminoanthraquinone), pFPT : poly-3-(4-fluorophenyl) thiophene, CNTs : Carbon nanotubes, Me$_4$NCF$_3$SO$_3$: Tetramethyl ammonium trifluoromethane sulfonate, ACN : Acetonitrile, PFPT: Poly-3-(4-fluorophenyl)-thiophene, TMATFMS: Tetra methyl ammonium trifluoro methane sulfonate, PYR$_{14}$TFSI: N-Butyl-N-Methyl-Pyrrolidinium bis (trifluoromethane sulfonyl imide), CoAl: Cobalt-Aluminium.

2.2 Applications

The reason why electrochemical capacitors were able to raise considerable attention are visualised in Fig. 2.11, where typical energy storage and conversion devices are presented in the so called 'Ragone Plot' in terms of their specific energy and specific power. Batteries and low temperature fuel cells are typically low power devices whereas conventional capacitors may have a power density of > 10^6 watts per dm^3 at very low energy density. Electrochemical capacitors are basically low voltage devices. They bridge the energy density gap between rechargeable batteries and electrolytic capacitors or metallised film capacitors, by offering

energy density higher than capacitors and power density higher than rechargeable batteries. The energy density for electrochemical capacitor is two orders of magnitude lower than that for batteries, but power densities are several orders higher.
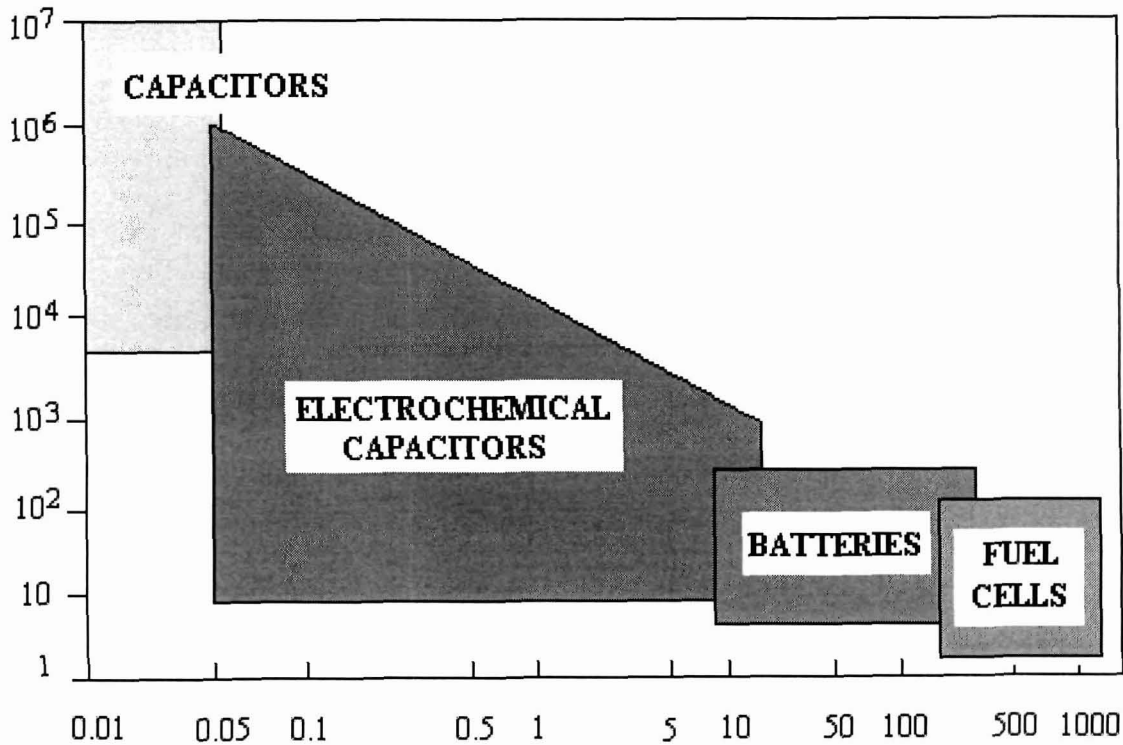
Fig. 2.11: Sketch of Ragone plot for various energy storage and conversion devices. The indicated areas are rough guidelines.

From application point of view it can be used as a power sources in different commercial applications [201-206] such as:

- Portable electronic equipment

- Computer memory backup

- Medical Equipment

- Power supplies

- Load Levelling

- Escalators

51

One of the most promising applications of supercapacitor is in hybrid power design for electrical vehicles, in which the main battery system provides power for the continuous motion of electrical vehicles, whereas supercapacitors connected in parallel to the battery ensures peak power delivery for acceleration, etc. Fig. 2.12 shows the schematic operation of supercapacitors based electrical vehicle. The supercapacitors would be discharged at a high rate during
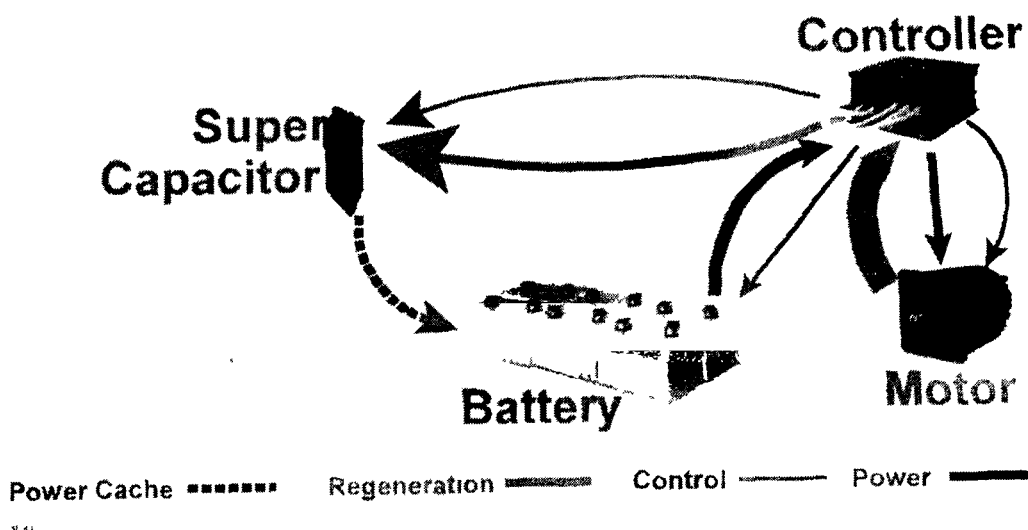
Fig. 2.12: Schematic operation of electrical vehicles.

acceleration and hill climbing, and recharged when travelling at constant speed, either from the battery or by the regenerative braking. It also acts as load levelling device by protecting the battery from deep-discharge cycles [201-206].

2.3 Scope of the Thesis:

In the present work, the polymeric gel electrolytes comprising of PVdF-HFP or PMMA (20 wt%) - EC:PC (1:1 V/V) - salts ($LiClO_4$, $NaClO_4$ and $TEAClO_4$) have been synthesized for their application in all solid-state electrical double layer capacitors (EDLCs) and redox supercapacitors. Salts of different cationic sizes and common anion (ClO_4^-) were used in the preparation of polymeric gel electrolytes to study on the effect of cations on the capacitive

behaviour of the capacitor cells. Different experimental techniques were used to characterise and optimise the gel electrolytes to achieve their acceptable electrical conductivity and mechanical stability. These are mentioned below (see Chapter 3 for details):

- The measurements of electrical conductivity were carried out as a function of composition and temperature.

- The transport number measurements of the gels were estimated using "polarisation technique"

- The electrochemical stability (i.e. potential window) of the electrolyte materials was tested using linear sweep cyclic voltammetry.

The optimised electrolytes have been used in the fabrication of EDLCs based on activated charcoal powder electrodes and electrochemically deposited polypyrrole based redox supercapacitors. The performance characteristics of the capacitor cells were studied using the following experimental techniques:

(i)   The a.c. impedance spectroscopy was carried out to find the overall equivalent circuit in the frequency range of 10 mHz-100 kHz. Various related parameters e.g. capacitance, bulk and charge transfer resistances, etc. have been evaluated.

(ii)   The linear sweep voltammetry was carried out to study the scan rate dependence and cyclic efficiency of the capacitor cells.

(iii)   The capacitor cells were also characterised using galvanostatic charge-discharge methods. Various associated parameters e.g. discharge capacitance, internal resistance, coulombic efficiency, energy and power densities, etc. have been evaluated.

Details of the studies on all solid-state EDLCs and redox supercapacitors are described in chapters 5 and 6.

Chapter – 3

Experimental Techniques

EXPERIMENTAL TECHNIQUES

Though most of the experimental techniques used to characterize different materials would certainly give some information about its structure and properties but for a particular system some techniques are more useful than others. Superionic solids show fast ionic motion due to its specific structure. Almost all the experimental techniques used to characterize superionic solids may equally be useful to characterize polymeric gel electrolytes. Most of these techniques are described in detail in literature [1, 2, 5, 271, 272]. The following section briefly describes the general experimental techniques used to characterize superionic solids at macroscopic as well as microscopic level and followed by experimental techniques used in the present studies.

3.1 General Experimental Techniques used to Characterize Superionic Solids

3.1.1 Structural Characterization:

Structural characterization shows the details of the three-dimensional arrangements of the constituent atoms in a solid at its microscopic, along with its macroscopic external structures (external morphology, cracks etc.). Some of the different structural characterization techniques are given in Table 3.1. The standard techniques used to characterize superionic solids macroscopically are (i) optical / electron microscopic studies, and (ii) diffraction studies. Both the techniques are standard and widely used by research community. They are described briefly in the following sections.

3.1.1.1 Microscopic Studies:

Microscopic studies (optical, electron, scanning electron etc.) are generally used to study the morphology or surface structure of the materials. X-ray topography is also used for

such characterization. These studies are quite informative from device point of view as they

provide several technological information such as surface reactivity, corrosion, cracks,

Table 3.1: Structural characterization and measurement techniques.

Information regarding structural properties	Measurement techniques used
Phase identification	Optical microscopy, X-ray diffraction, electron microscopy and diffraction for small amounts.
Distinguish amorphous and crystalline materials	Microscopy, X-ray diffraction.
Structural changes or transitions	Differential thermal analysis, microscopy, or in-situ X-ray diffraction.
Macroscopic morphology, crystal system information	Goniometry, Optical microscopy.
Unit cell and space group	X-ray (neutron, or electron) diffraction.
Site symmetry in crystalline and amorphous materials	Visible and infrared absorption, X-ray emission or diffraction, resonance methods.
Position of atoms, thermal vibration amplitudes,	X-ray (neutron, or electron) diffraction.
Imperfections	Microscopy, X-ray topography, indirect and resonance methods, absorption spectroscopy.
Spin configuration	Neutron diffraction and magnetic properties, magnetic resonance methods, Mossbauer techniques.
Bonding (electron dynamics)	Electron density by X-ray diffraction, spin density by neutron diffraction, dynamics by indirect methods.

strength of the materials etc. The microscopy techniques are based on the principle of the

scattering of the incident waves by the sample, which results in the formation of an image in

momentum space (k-space) obtained by either reflection or transmission of the scattered light,

thereafter it is transformed back again in the real space (**r**-space) using suitable lenses. Depending on the types and nature of radiation involved in the formation of image as well as the mode in which imaging is carried out for the characterization of surface properties of the materials, microscopic techniques are broadly divided into different categories (Fig. 3.1).
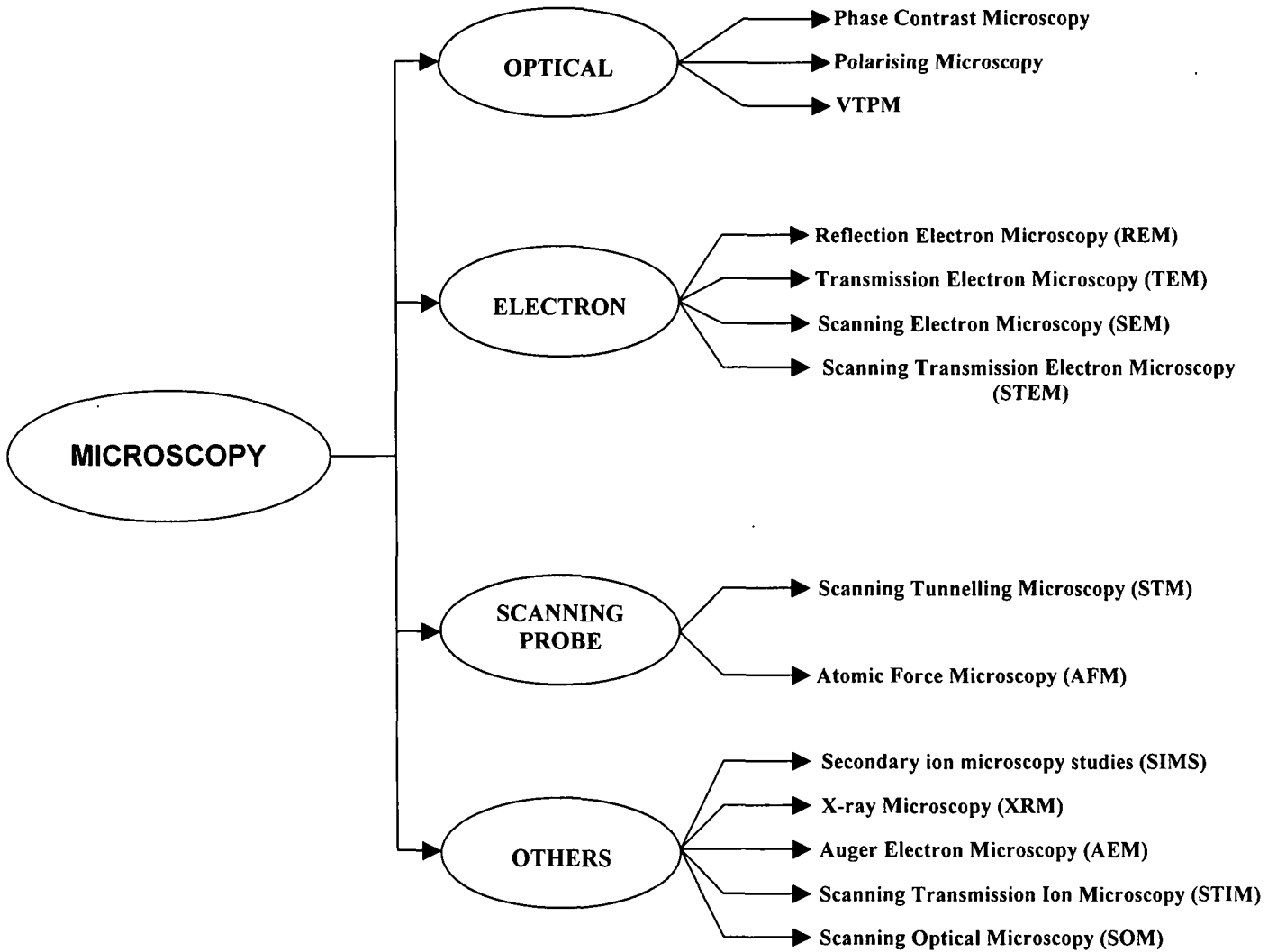
Fig 3.1: Microscopic techniques for characterization of superionic materials.

All the above techniques are quite useful in the surface characterisation of materials for which a lot of information is available in the literature [273-278].

3.1.1.2 Diffraction Studies:

Diffraction studies are useful to determine the bulk structure of the materials such as the arrangement of atoms and their orientation in space. It is helpful in distinguishing between amorphous and crystalline phases of the materials.

The precise measurement of lattice parameters such as crystal plane, lattice spacing, crystallite size, lattice disorder and preferred orientation etc. can be performed to locate any dislocation or imperfection, which drastically changes the behaviour of the materials using these techniques. Generally three different types of diffraction techniques are used, (1) X-Ray diffraction (XRD), (2) neutron diffraction, and (3) electron diffraction studies. The types of information that can be obtained from each of the diffraction techniques are listed in Table 3.2.

Table 3.2. Possible structural information using different diffraction techniques [279-281].

Information regarding structural properties	X-ray Diffraction	Neutron Diffraction	Electron Diffraction
Energy required for diffraction beams having $\lambda = 1\text{Å}$. $\lambda \sim 1\text{-}10\text{Å}$ to produce observable diffraction effects.	~ 10 KeV.	~ 0.1 eV.	~ 100 KeV.
Phase identification and structural changes with distinction between crystalline and amorphous phases in materials.	✓	X	✓
Unit cell, space group and crystal system information.	✓	✓	✓
Position of atoms and thermal vibration amplitudes.	✓	✓	✓
Site symmetry in crystalline and amorphous materials.	✓	X	X
Electron density and nature of bonding.	✓	X	X
Spin density, spin configuration and magnetic properties.	X	✓	X

(a) <u>X-ray Diffraction (XRD)</u>

X-Ray Diffraction is one of the powerful tools for the structural determination of the materials [281]. In addition to the determination of crystal structure, XRD is applied to explore various other problems such as chemical analysis, stress measurement, phase equilibria, measurement of particle size, determination or orientation of single crystals or the ensemble of orientations in a polycrystalline/polymeric aggregate, order-disorder transformation etc. In the case of polymeric material XRD is used to determine the proportion of crystalline and amorphous phases in terms of degree of crystallinity. This technique is based on the scattering of X-rays by crystals. Thus, the crystal structure of a given specimen can be identified with this technique. Bragg's law defines the conditions for obtaining X-ray diffraction from a crystalline material, according to the equation:

$$n\lambda = 2d\sin\theta \qquad\qquad ....(3.1)$$

where 'n' is the order of diffraction, 'λ' is the wavelength of the characteristic line X-rays (usually the CuK_α doublet with $CuK\alpha_1 = 1.5405$ Å), 'd' is the distance (Å) between a set of parallel lattice planes and 'θ' is the angle between the incident collimated X-ray beam and an atomic lattice plane in the crystal. The reflection angle for a particular set of lattice planes (hkl) is:

$$2\theta = 2\sin^{-1}(\lambda/2d_{(hkl)}) \qquad\qquad ....(3.2)$$

where, (hkl) are the Miller indices defining the orientation of the plane with respect to the crystallographic axis. When X-rays of a known wavelength impinge on a crystal (sample) whose lattice planes are separated by a distance 'd', strong reflection occurs only at those angles where scattering from successive lattice planes is in phase. This requires the path difference to be an integral multiple 'n' of the wavelength i.e. Bragg's condition has to be satisfied [281]. The major instrument for x-ray diffraction that is used to analyse virtually all

59

types of materials is the focussing X-ray diffractometer with scintillation or proportional

counter detector. The basic arrangement of the instrument is shown in Fig. 3.2. The curved

monochromator reflects about 50 % CuKα. The detector rotates around the point 'O', where

the sample is kept at twice the angular speed of the specimen so that the specimen surface is

always at 'θ' and the receiving slit at '2θ'. The XRD pattern obtained corresponds to diffraction

from a particular set of interatomic planes whose spacing 'd_{hkl}' may be calculated from Bragg's

equation, as X-rays of known wavelength are used [281].
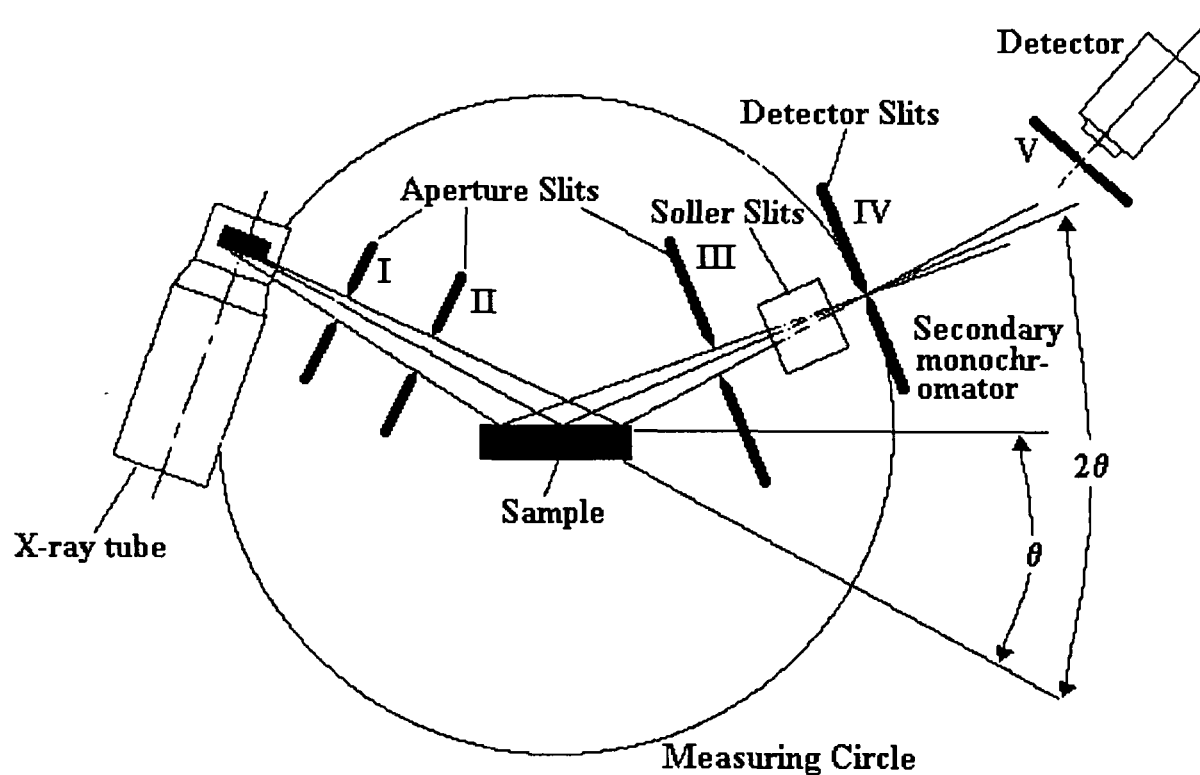
Fig. 3.2: *Basic arrangement of an X-ray diffractometer*

Since the diffraction studies alone cannot give the complete picture of the internal

structure and transport relationship in the materials, the different complementary studies such

as scattering methods, magnetic resonance methods etc. are also required for the determination

of the true picture of the materials.

(b) <u>Neutron and Electron Diffraction</u>

Since a crystal diffracts waves, so instead of x-rays, neutrons and electrons can also be used for diffraction purpose provided their wavelengths are in the range of 1 - 10 Å. The wavelength for neutrons and electrons is given by the de-Broglie relation, $\lambda = h / (2mE)^{1/2}$, where E is the kinetic energy of the particle.

For neutron, $\lambda = 0.286 / (E)^{1/2}$; where λ is in Angstroms and E is in electron volts. Thus the energy of a neutron of wavelength of 1 Å is ~ 0.08 eV. The thermal neutrons in a nuclear reactor have the same energy at room temperature and hence can be used for crystal diffraction studies.

Similarly, for electrons, $\lambda = 1.227 / (E)^{1/2}$; where λ is in Angstroms and E is in kilo electron volts. The spreaded energy of thermal neutrons from the atomic reactors have to be monochromatized and then allowed to fall on a crystal and then after selecting a particular reflected beam, it is allowed to fall on the test sample under examination. The intensity of the scattered beam is measured through a counter.

Though the neutron diffraction studies are more or less similar to those of X-rays, there are many differences. Neutrons are scattered by nuclei unlike x-rays that are scattered by electrons. Many low atomic weight elements can be studied by neutron diffraction due to the above properties, where X-rays are incapable of giving precise results. Since, neutron possesses a magnetic moment and hence has an additional scattering due to magnetic ordering. Thus neutron diffraction studies are quite important in magnetic structure determinations. X-rays or electron diffraction studies does not reveal this structure. This technique also affords a method of studying lattice vibrations. Electrons can also be used like X-rays or neutrons. However, the electrons are much more easily scattered and hence the penetration depth is small. These are therefore used in surface studies - bonds, defects, energy states, etc.

A comparison of XRD, electron diffraction and neutron diffraction are given in the Table 3.2. The main difference lies in the magnetic order and isotope detection by the neutron technique. On the other hand X-rays are easier to produce, compared to neutrons, which requires an atomic reactor.

3.1.2 Thermal Studies:

For the studies on phase transition and thermodynamic behaviour, thermal techniques are useful and well established. These are described briefly in the following sections:

3.1.2.1 Phase Transition Studies:

Most of the superionic solids are formed due to the mixing of two or more compounds forming solid solutions. Some of these solids undergo phase transition. The transition temperature can be determined by observing a sudden change in any of the physical properties of the solids such as specific heat, latent heat, electrical conductivity, thermal expansion, structure etc. Generally transitions occur at a particular temperature, but sometimes it may also be observed over a temperature range of hundreds of degrees. Phase transition is generally related with the structural change of the materials, which leads to the enhancement in electrical conductivity, by several orders of magnitude. The type of phase transition occurring at lower temperature in solid from insulating to conducting phase is generally referred to as β to α phase transition. Many reviews are available in literature [1, 2, 271], which deal with the various aspects of phase transition of solids. To study the phase transition in solids, various experimental techniques are used such as conductivity technique [282, 283], variable temperature XRD [284], resonance techniques such as NMR and NQR [1, 2, 271, 272], acoustical techniques [285], thermal analysis techniques [1,2] etc. The most widely used methods in the determination of phase transition in solids are thermal analysis techniques,

which show the changes in its physical and chemical properties as a function of temperature. There are three important thermal analysis techniques which are generally used for the determination of phase transition [23], namely; (a) Differential Scanning Calorimetry (DSC), (b) Differential Thermal Analysis (DTA); and (c) Thermo-Gravimetric Analysis (TGA), which are described briefly below:

(a) Differential Thermal Analysis (DTA) / Differential Scanning Calorimetry (DSC)

The differential thermal analysis (DTA) is a technique, which is based on the measurement of the difference in temperature of a sample with respect to an inert reference material (usually alumina powder) as a function of temperature or time [1, 2, 286]. Both the test sample and an inert reference material undergo a controlled heating or cooling, which is usually linear with respect to time. A zero temperature difference between the sample and the reference material is observed when the former does not undergo any chemical or physical change. If, however any reaction takes place, then a temperature difference ΔT will occur between the sample and the reference material.

When the heat or energy released is measured quantitatively, the technique is referred as differential scanning calorimetry (DSC). In this technique mainly the energy necessary to establish a zero temperature difference between the sample and a reference material is recorded as a function of temperature or time. The experimental arrangement is shown in Fig. 3.3. By measuring just how much more heat it has to put out in order to keep the temperature of the sample increasing at the same rate, as the reference sample is what we measure in a DSC experiment. Finally, we plot heat output of the two samples (test and reference) at a given temperature as the temperature increases.

63

Polymer Sample

Sample Pan   Reference Pan

Computer to monitor temperature
and regulate heat flow
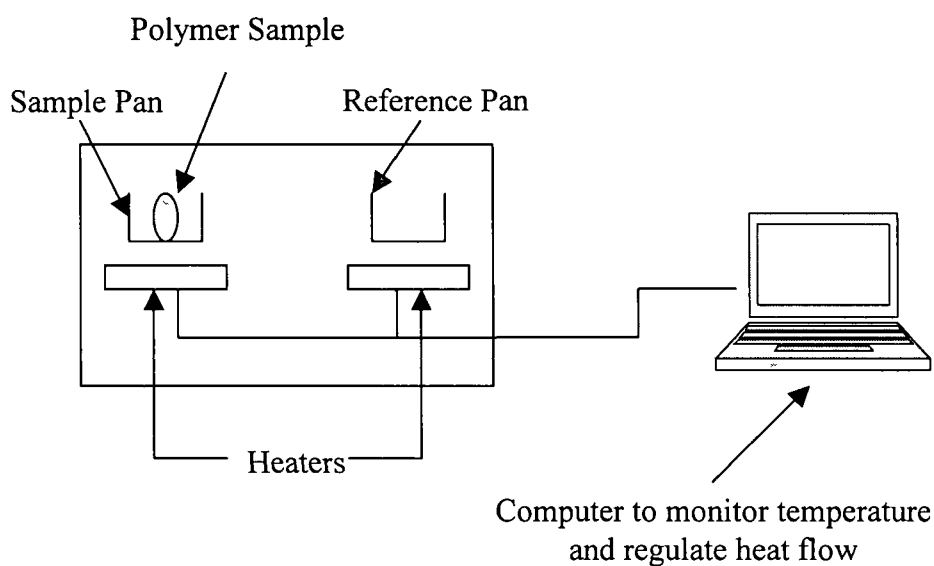
Fig. 3.3:   Experimental set-up for DSC.

Various useful information such as heat capacity, glass transition temperature, degree of

crystallization of polymeric materials, endothermic reaction, exothermic reaction,

crystallization temperature, melting temperature, decomposition temperature, melting enthalpy

etc. can be figured up using this study.

(b) Thermo-Gravimetric Analysis (TGA)

Thermo-gravimetric analysis (TGA) is a technique in which a change in the weight of a

substance is recorded as a function of temperature or time [286]. The basic instrumental

requirement for thermo-gravimetry is a precision balance with a furnace programmed for a

linear rise of temperature with time. The results may be presented as, (i) a thermo-gravimetric

(TG) curve, in which the weight change is recorded as a function of temperature or time, or (ii)

as a derivative thermo-gravimetric (DTG) curve where the first derivative of the TG curve is

plotted with respect to either temperature or time. In TG plots the horizontal portions indicate

the regions, where there is no weight change, the curved portions are indicative of weight

losses. The stoichiometry of a material can be made at any given temperature using this technique.

3.1.2.2 Thermodynamic Studies:

Thermodynamic studies [1, 2, 271] are useful to explore the physical and chemical phenomena associated with the solid materials. The important quantities necessary for thermodynamic descriptions are specific heat or heat capacity, Gibbs free energy and phase diagram.

(a) Specific heat or heat capacity:

When we give a certain amount of heat to a body, its temperature will rise and the amount of heat required attaining the temperature increase is called as heat capacity of the body. Mathematically, the heat capacity C* may be written as:

$$C^* = \lim_{\Delta t \to 0} \left(\frac{\Delta Q}{\Delta T} \right) \qquad \dots (3.3)$$

where ΔQ is the amount of heat given to a body of mass m, and; ΔT is the rise in temperature. Specific heat, C, is defined as the heat capacity per gram.

$$C = \frac{C^*}{m} = \frac{1}{m} \lim_{\Delta T \to 0} \left(\frac{\Delta Q}{\Delta T} \right) = \frac{1}{m} \left(\frac{dQ}{dT} \right) \qquad \dots (3.4)$$

It is well known from the first law of thermodynamics that the specific heat of a substance at constant volume, C_v is defined as the temperature derivative of its internal energy, U.

$$C_v = \left(\frac{\partial U}{\partial T} \right)_V \qquad \dots (3.5)$$

From the value of C_v, it can be predicted that how the internal energy is distributed among the different modes of thermal excitation. Hence the value of C_v, which is a function of

temperature, gives us a lot of information about the degree of disorder in superionic solids and the knowledge of order-disorder phase transformation.

Though the main aim is to determine the value of C_v, practically it is quite difficult to maintain the constant volume of solid with varying temperature. However, it is possible to maintain the constant ambient pressure, therefore a quantity called specific heat at constant pressure, C_p, is measured and then co-related with C_v, with the following mathematical expression:

$$C_P - C_V = \frac{V_m \alpha^2 T}{\beta} \qquad \dots (3.6)$$

where V_m is the molar volume, α is the thermal volume expansion coefficient and β is the compressibility. β may be calculated using the Nernst-Lindemann relation:

$$C_P - C_V = A C_P^2 T = \frac{V_m \alpha^2 T}{\beta} \qquad \dots (3.7)$$

where, A is a constant, which may be calculated by having the value of V_m, α, β at any temperature T. Various techniques are available in literature for the determination of C_v [1,2].

(b) <u>Energy of Formation or Gibbs Free Energy</u>:

During the formation of any compound, some energy is always involved and this energy is known as Gibbs Free energy, ΔG, for that chemical reaction or for the formation of the compound. One of the most direct methods for the measurement of energy of formation is by measuring the electrochemical cell voltage developed in any particular reaction. It may also be evaluated by having the amount of coulumbic charge (current) flowing through the cell.

Most of the superionic solids undergo phase transition on application of temperature, which has already been discussed in section.

3.1.3 Macroscopic Studies for Ion Transport Mechanism in Solids:

3.1.3.1 Impedance Spectroscopy and Electrical Conductivity:

The electrical conductivity measurement techniques and the impedance spectroscopy studies are described briefly in section 3.2.1.2 (a).

3.1.3.2 Thermoelectric Power:

Thermoelectric power is one of the most important parameter for the ion transport studies in solids. It gives the information about the migration of ions, *i.e.* its *electrical* conductivity under the action of temperature gradient [1]. It is one of the methods to determine the activation energy of the conducting species in solids. The thermoelectric power 'Q' can mathematically be expressed as:

$$Q = \frac{\Delta V}{\Delta T} = \left(-\frac{E}{nT}\right) + H \qquad \qquad \dots (3.8)$$

where ΔT is the temperature difference between the two faces of the sample, E is the activation energy/heat of transport, n is the amount of charge under transport, T is the temperature, and H is a constant term, which depends on the electrode contact potentials.

It is based on the principle that ions in a solid electrolyte become mobile when a temperature gradient is maintained, which leads to the development of a thermo e.m.f. across the two faces of the electrodes.

A schematic representation of the experimental arrangement for measurement of thermoelectric power is given in Fig 3.4. In this method, the sample is sandwiched between two electrodes. One of the electrodes is heated by a small heater to maintain the temperature gradient of ΔT. Suitable arrangement of thermocouples is made to measure the temperature difference ($\Delta T = T_1 - T_2$) at the two faces of the electrode (Fig. 3.4). The voltage across the two electrodes ΔV is measured by a potentiometer. In order to study the temperature dependence of
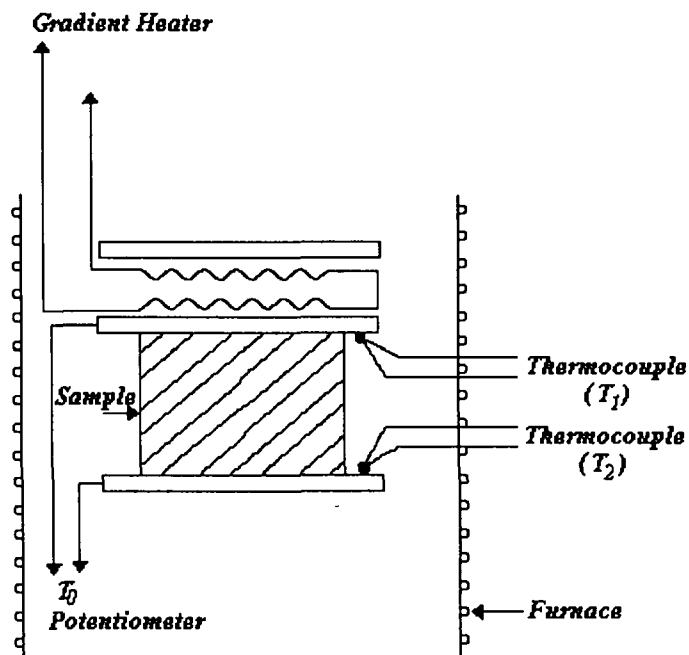
Fig 3.4: Experimental arrangement for measurement of thermoelectric power.

thermoelectric power, the whole assembly is put in the furnace till the equilibrium state is attained. A plot of Q vs. $\frac{1}{T}$ is a straight line for most of the solid electrolytes, the slope of which gives the value of heat of transport/activation energy. This method has many advantages over other techniques such as (i) contribution of ions and holes to the overall conduction can be determined, (ii) effect of contact polarisation can be eliminated, (iii) effect of inter-particle resistances can be eliminated, (iv) effect of inter-granular resistances can be avoided, (v) capacitance values do not affect the value of activation energy in the case of polycrystalline materials etc.

3.1.3.3   Diffusion:

Diffusion is a process in which migration of particles from higher to lower concentration regions occurs within a system to maintain a uniform concentration gradient throughout the system. It is related with the ionic conduction. Actually, the ions are randomly

mobile from one lattice point to another lattice point or interstitial site [1, 2, 271], which results in the establishment of concentration gradient of mobile ionic species within the system. On the application of external field, these ionic species start migrating in the direction of applied external field. The motion of these particles as the result of a concentration gradient is called as diffusion. The diffusion flow is entirely dependent on concentration gradient (∇C) and can be expressed mathematically according to Fick's first law:

$$J = -D(\nabla C) \qquad\qquad .... (3.9)$$

where J is the net number of atoms of the diffusing species passing through unit volume in unit time, C is the concentration of atoms of this species at the plane and D is the diffusion coefficient.

The diffusion measurement is quite useful in providing important parameters such as electrical conductivity (σ) and activation energy (ΔE) for diffusion over a wide temperature range as per Nernst-Einstein and Arrhenius equations given below:

$$D = \frac{\sigma KT}{Nq^2} \qquad\qquad .... (3.10)$$

$$D = D_0 \exp\left(-\frac{\Delta E}{KT}\right) \qquad\qquad .... (3.11)$$

where D is Diffusion coefficient, D_0 is constant pre-exponential factor, N is Avogadro number, K is Boltzmann constant and q is the charge of the conducting species. A wide variety of experimental methods are available for the measurement of diffusion coefficient and can be grouped as:

(a) Direct Methods

In these methods the mass flow or concentration of the diffusing species is measured as a function of distance or time. A number of different physico-chemical methods [1, 2, 271] are available for the measurement of concentration of diffusant as a function of the depth of

penetration. These include mass spectrometry, characteristic light absorption measurement due to diffusant, spectrophotometric methods, electron spin resonance signal intensity measurements, radioactive tracer technique etc.

Out of these methods, radioactive tracer technique is much reliable [1, 2, 271], as other techniques have been found to be lacking in their reproducibility in the measurement of diffusion coefficient. In this experiment, the radioactive isotope of the material is allowed to diffuse into the specimen for the different intervals of time and its amount penetrating to different depths are measured by standard nuclear radiation counting equipment sampling different sections of the specimen. Initially radioactive or stable tracer atoms are deposited on one side of the surface of the materials in the form of very thin layer. Then the specimen is heated for a certain time at fixed temperature so that diffusion can take place. As soon as the tracer atoms start diffusing, a concentration gradient is created along the x-axis. Let us recall Fick's first law according to which, if C is the concentration of the tracer atoms inside the sample having chemically homogeneous matrix, D_{Tr} is the diffusion coefficient of the tracer atom then flux J, which is the net numbers of tracer atoms of the diffusing species passing through unit surface area in unit time, can be written as:

$$J = -D_{Tr} \frac{\partial C}{\partial x} \qquad \qquad .... (3.12)$$

It has been considered that diffusion is taking place along the direction of x-axis.

In the tracer diffusion method, the flux of the tracer atom within the sample changes along the direction of diffusion with time according to Fick's second law:

$$\frac{\partial C}{\partial t} = -\frac{\partial J}{\partial x} \qquad \qquad .... (3.13)$$

$$\frac{\partial C}{\partial t} = \frac{\partial}{\partial x}\left(D_{Tr}\frac{\partial C}{\partial x}\right) = D_{Tr}\left(\frac{\partial^2 C}{\partial x^2}\right) \qquad .... (3.14)$$

By considering that D_{Tr} is independent of x.

For planar diffusion, the concentration of the diffusant at different penetration depths, x can be obtained by solving the above Fick's eqn. (3.14), which comes out to be:

$$c(x,t) = \left(\frac{C_0}{\sqrt{4\pi D_{Tr}t}}\right) \exp\left(-\frac{x^2}{4D_{Tr}t}\right) \qquad \dots (3.15)$$

Here C_0 is the initial concentration of the tracer atom on the sample surface at x = 0 (i.e. at the starting of the diffusion) and t is the time for which diffusion anneal has been allowed to proceed. The above solution (3.15) is equally valid for all t > 0. The concentration distribution has been shown in Fig 3.5. From the plot of log C versus x^2, the value of tracer diffusion coefficient, D_{Tr}, can be easily calculated.
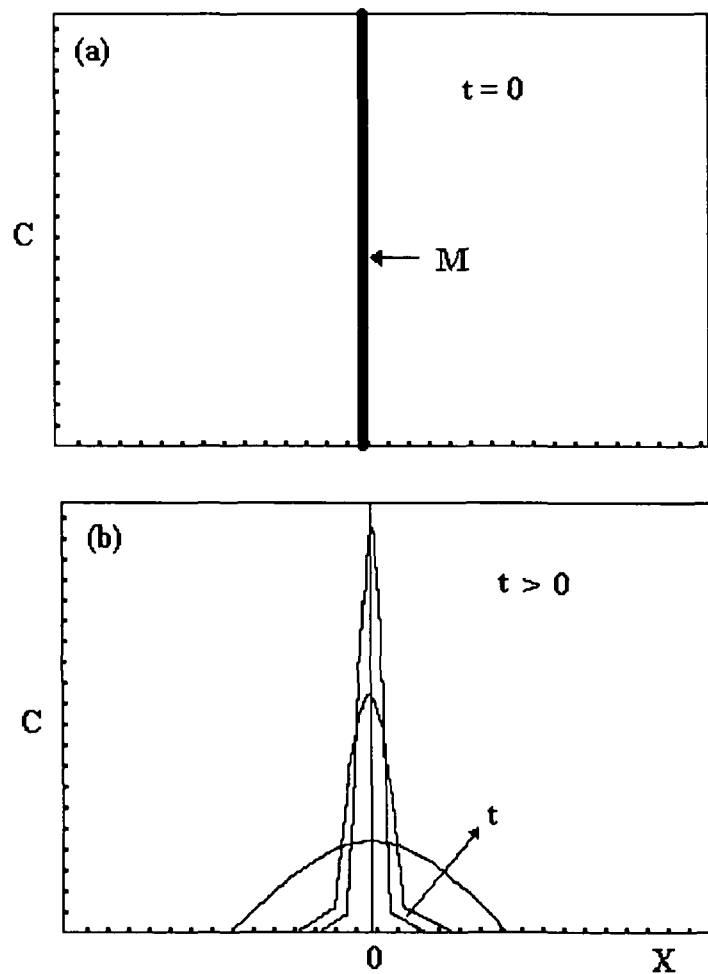
Fig. 3.5: Concentration distribution of the tracer atoms [2].

71

(b) Indirect Methods:

In this method the jump frequency or relaxation time is measured in order to obtain the diffusion coefficient,

$$D \approx \frac{1}{6} f \lambda^2 \upsilon \qquad \qquad \dots (3.16)$$

where λ is the jump length, υ is the jump frequency and f is the correlation factor [1,2, 272, 287], signifying the fact that individual atomic jumps are often correlated. The value of υ (or $1/\tau$) can be determined by relaxation measurements like:

- Light Scattering (Laser Raman) Technique

- Nuclear Magnetic Resonance (NMR) or Pulsed Field Gradient NMR (PFG-NMR)

- Diffuse Neutron or X-ray Scattering.

Out of all the above techniques, two techniques i.e. pulsed field gradient NMR [2, 272, 288] and light scattering techniques are the frequently used techniques by the research workers, which are described as follows: .

(i) Pulsed Field Gradient (PFG) NMR Technique:

Stejskal and Tanner [288] initially developed the pulsed field gradient NMR (PFG-NMR) technique for the measurement of translational diffusion coefficients. This technique is based on the fact that when the field gradient pulses are applied on the material between two radio frequency pulses (RF pulses), a nuclear magnetic resonance (NMR) pulse is developed with a $\pi/2 - \pi$ radio frequency pulse sequence, which results in spin-echo signal as shown in Fig. 3.6.

In this method, the magnetic field gradient pulses of amplitude G having width δ and separated by a distance Δ are applied between the radio frequency pulses and the echo. The experiment is performed with and without applying the gradient pulses. In the absence of

gradient pulses, the first radio frequency pulse (RF$_1$) rotates the magnetisation through 90^0. The second radio frequency pulse (RF$_2$) rotates and rephases the magnetisations causing spin-
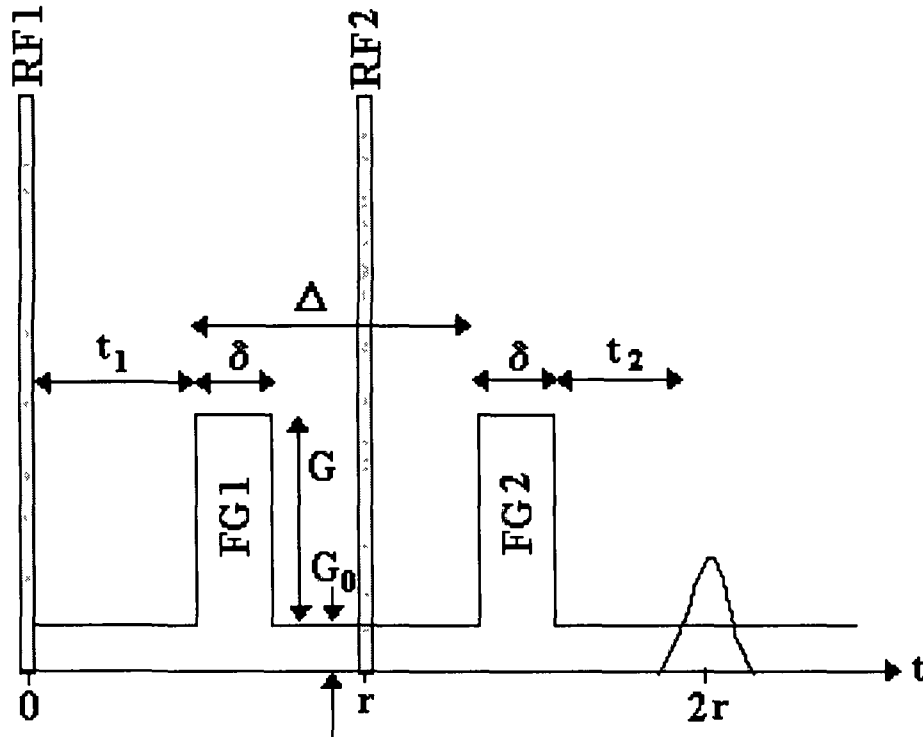
Fig. 3.6: Experimental arrangement for the measurement of translational diffusion coefficient by PFG-NMR technique [272].

echo amplitude. If there is no diffusion, the second gradient pulse (FG$_2$) opposes the effect of first gradient pulse (FG$_1$). As a result, the amplitude of the echo remains unchanged. On the other hand, if the nuclei are mobile and diffusion takes place within the time interval between gradient pulses FG$_1$ and FG$_2$, then an incomplete phasing will be observed, which results in the reduction of echo amplitude.

Further, it was shown by Stejskal and Tanner [288] that the two spin echo amplitudes are related to the diffusion coefficient of the mobile species by the following mathematical expression:

$$\log_e\left(\frac{A_0}{A}\right) = -D\gamma^2\delta^2\left(\Delta - \frac{1}{3}\delta\right)G^2 \qquad \ldots(3.17)$$

where A_0 is spin-echo amplitude with pulsed field gradient (PFG), A is spin-echo amplitude without PFG, γ is gyromagnetic ratio, δ is width of PFG, G is amplitude of PFG and Δ is time of separation of gradient pulses.

The above equation gives the diffusion coefficient of the mobile ionic species in the gradient field. It is quite successful method in the determination of diffusion coefficient and transference number of a large number of materials [1, 2, 271, 272].

(ii)   Light Scattering Technique:

Laser Raman spectroscopy technique was used by Chandra et al. (1986) [287, 289] to measure the diffusion coefficient of proton conductor such as H_3O^+ or H_2O in $MoO_3.2H_2O$ under d.c. bias. In this technique, the laser beam is allowed to strike on the electrolysed sample at different places between the cathode and anode. The concentration of the mobile species was evaluated from the intensity of peaks, characteristics of the species at different distances using a well-known solution of diffusion equation as derived above in mathematical eqn. 3.15. Since the concentration is proportional to peak intensity (I) of the Raman band, the diffusion coefficient can be evaluated from the slope of a plot between $\log I$ versus x^2 [287, 289].

3.1.3.4 Transport Number Measurement Techniques:

Transport or Transference number is defined as the ratio of the conductivity of a particular ion to the total conductivity [1, 2, 5, 271, 272, 289]. In ion conducting solid electrolytes having more than one conducting species, it is essential to know the contribution of each ion to the overall conductivity. The ionic transport number, t_{ion} can be expressed as,

$$t_{ion} = \frac{\sigma_{ion}}{\sigma_T} = \frac{I_{ion}}{I_T} \qquad \text{.... (3.18)}$$

whereas the electron/hole transport number $t_{e,h}$ can be written as,

$$t_{e,h} = \frac{\sigma_{e,h}}{\sigma_T} = \frac{I_{e,h}}{I_T} \qquad \text{.... (3.19)}$$

74

where σ_{ion}, $\sigma_{e,h}$, σ_T are the ionic, electronic/hole and total conductivity, respectively and I_{ion}, $I_{e,h}$, I_T are the ionic, electronic/hole and total current, respectively.

For a pure ionic conductor $t_{ion} = 1$ and $t_{e,h} = 0$ in ideal condition. The transference number lies between 0 and 1 for mixed conductors, which is partially ionic and partially electronic. In most of the liquids as well as ion conducting polymer gel electrolytes cations and anions both contribute significantly to the total ionic conductivity. Hence the cationic and anionic transport numbers (t_+ and t_-) are the important parameters to be evaluated in the study of transport number. Mathematically they can be expressed as:

$$t_+ = \frac{\sum I_+}{\sum (I_+ + I_-)} \qquad \ldots (3.20)$$

$$t_- = \frac{\sum I_-}{\sum (I_+ + I_-)} \qquad \ldots (3.21)$$

where $\sum I_+ + I_-$ is the total current expressed as the sum of the partial currents due to the mobile charged species (cations and anions) present in the electrolyte.

Various experimental techniques have been used to measure the transference number. Some of the techniques are described briefly in the following sections:

(a) Tubandt's Method

Tubandt was first to measure the ionic transport number in 1920. Tubandt's technique to measure the transport number is based on the Faraday's law of electrolysis [1,4]. The schematic diagram of the experimental arrangement is shown in Fig 3.7. On application of d.c. electric potential across the sample, the anions and cations will start migrating towards anode and cathode respectively. Depending on the extent of the ions transported to their respective electrodes the mass of cathode and anode would increase accordingly. Therefore by measuring
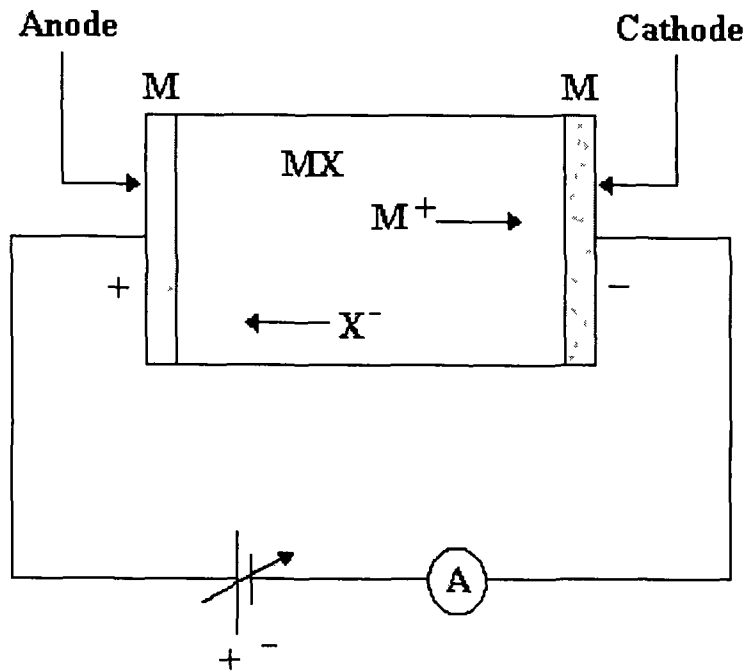
Fig 3.7:   Experimental set-up for measuring transference number by Tubandt's method.

the increase in mass of the respective electrodes and total charge passed through the electrolyte, the transport number can be easily calculated.

(b) Wagner's Polarisation Technique

Details of this technique have been given in section 3.2.1.2 (b).

(c) Electrochemical Potential Measurement Technique

Kiukkola and Wagner in 1957 used electrochemical cell voltage method for the determination of transport number [1]. According to this method, the ionic conductor is sandwiched between two electrodes having different chemical potentials, say, μ_1 and μ_2, as shown in Fig 3.8, an e.m.f. develops across the cell, which is given by,

$$E = \frac{1}{|Z|F} \int_{\mu_1}^{\mu_2} t_i \, d\mu = \frac{1}{|Z|F} t_i(\mu_2 - \mu_1) \qquad \dots (3.22)$$

where $|Z|$ is the absolute value of the valency of the mobile ion in the electrolyte, F is

76
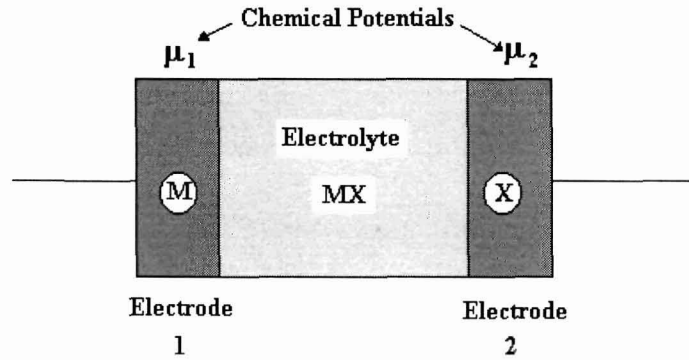
Fig 3.8: Experimental arrangement for the determination of transference number by electro-chemical potential measurement.

Faraday's number. For a pure ionic conductor (having $t_i = 1$), the theoretical value of e.m.f. is reduced to:

$$E_{theo} = \frac{\mu_2 - \mu_1}{|Z|F}$$ .... (3.23)

Therefore $E = t_i.E_{theo}$

Hence by measuring the e.m.f. E and a prior knowledge of E_{theo}, the value of t_i can easily be evaluated.

(d) A. C. Impedance Technique:

In 1982 Sorensen and Jacobsen [290] developed a novel technique of complex impedance spectroscopy for the measurement of transport number. In this technique a.c. impedance measurement is carried out on a cell in which the electrolyte is sandwiched between two non-blocking electrodes (i.e. electrode should be electroactive towards one of the mobile species, preferably the cation). The impedance of such a cell as a function of frequency is shown in Fig 3.9. The impedance plot of the cell consists of three arcs as given by Macdonald [291] which is distributed over a wide range of frequency as shown in Fig 3.9 (d). At very high frequency, there is a capacitive coupling between the electrodes (the geometrical capacitance of

the cell, C_g) shunted by electrolyte bulk resistance R_b. No charge transfer occurs at the electrode-electrolyte interface. The resulting equivalent circuit is shown in the Fig 3.9 (a).
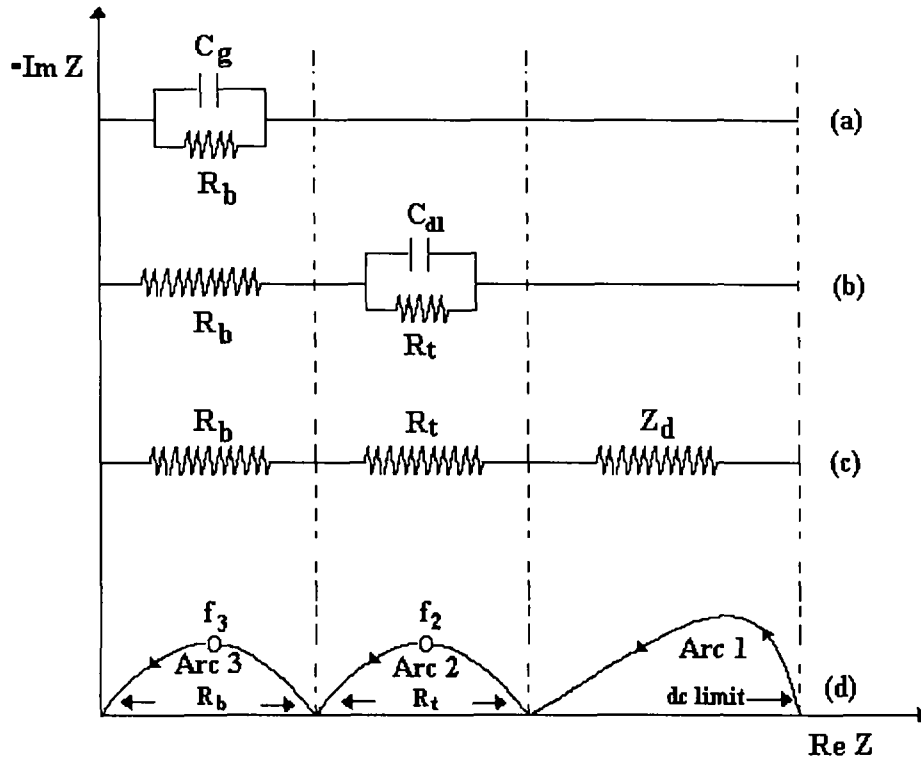
Fig 3.9:   *Impedance response of an electrochemical cell measured as a function of frequency, (a) the high frequency equivalent circuit, (b) the medium frequency equivalent circuit, (c) the low frequency equivalent circuit, and (d) the total impedance plot including all three arcs.*

The effect of the geometrical capacitance C_g is not significant at lower and intermediate frequencies. In this frequency range, the charge transfer occurs at the interface and the impedance of double layer becomes dominant. This region can be represented as a bulk resistance R_b in series with the parallel combination of the charge transfer resistance R_t and double layer capacitance, C_{dl} as shown in the Fig 3.9 (b). The $R_t–C_{dl}$ coupling is responsible for the arc 2, which is second semicircle in the complex impedance plots of Fig 3.9 (d). At very low frequencies, the amount of charge transferred in the electrode reaction during half a cycle is sufficient to produce concentration gradients in the electrolyte. When we further go towards

lower frequency region, the impedance of the cell approaches closely to a limiting d.c. value. This can be shown as a skewed semicircle in the lower frequency region of the impedance plots. In the complex impedance plots this is reflected in the linear part of the arc having a slope 1. At this lower frequency, concentration waves and quasi-steady state profiles may develop depending upon the thickness of the electrolyte. This causes the cell impedance to get inclined at an angle of 45^0 to the real axis [Fig 3.9 (d)]. The intercept at real axis (width of the skewed semicircle) arises from diffusion because of the concentration gradients within the electrolyte. The intercept at real axis is termed as Z_d (0). The equivalent circuit in this case is shown in Fig 3.9 (c).

According to MacDonald [291], the transport number can be represented as:

$$t_i = \frac{1}{1 + \frac{Z_d(0)}{R_b}} = \frac{R_b}{R_b + Z_d(0)} \qquad \dots (3.24)$$

Details have been given in the reference Sorensen and Jacobsen [290].

(e) D. C. Conductivity Technique

Blonsky et al. [292] and Bruce et al. [293] proposed excellent method of d.c. conductivity technique for the measurement of transport number. This method is based on the measurement of d.c. conductivity of a two-terminal cell consisting of the electrolyte sandwiched between the non-blocking electrodes.

When a constant potential difference is applied across the electrodes, initially a higher value of current flow occurs due to the migration of both cations and anions. As the time passes, the value of this initial current flow decreases and a steady state current flow is eventually observed due to the building up of a gradient in the salt concentration across the cell as a function of time. The establishment of this concentration gradient across the cell is responsible for (a) generating an e.m.f. that opposes the applied potential, (b) reducing and

finally stopping the net motion of the anions in the direction of the field due to the rate of anion

migration, and (c) accelerating the motion of the cations in the direction of the field, which

contributes to the eventual steady current.

The difference between the initial and final currents, I_0 and I_s, gives the cation transport

number which can be expressed mathematically as:

$$t_+ = \frac{I_{steady}}{I_{initial}} = \frac{I_s}{I_0} \qquad \dots (3.25)$$

In this way the transport number of cations (anions also) can be determined. This

method is quite useful but restriction is that, it is valid only for the ideal electrolytes in simple

cells in which convection is absent and the polarisation voltage is vanishingly small. Further

the relationship does not hold in cells where the electrode kinetics is not fast or when resistive

layers were present on the electrode surface.

(f) Combined D. C. / A. C. Techniques

The combined D. C. / A. C. technique has been proposed by Vincent et al. [294] and

Watanabe et al. [295] for the determination of transport number, which is described as follows:

(i) Vincent and Bruce Method:

Vincent and Bruce [294] used a.c. / d.c. technique for the determination of transport

number. According to this method a.c. impedance of a cell is recorded having a cell

configuration of M | MX (Electrolyte) | M and charge transfer resistance is evaluated.

Thereafter the cell is polarised by applying a small d.c voltage (~ 10 mV). The cation transport

number can be mathematically represented as:

$$t_+ = \frac{I_s(\Delta V - I_0 R_{01})}{I_0(\Delta V - I_0 R_{1s})} \qquad \dots (3.26)$$

where ΔV is the potential difference across the cell, t_+ is cationic transport number, I_0 and I_s are the currents before and after polarisation and R_{01} and R_{1s} are the charge transfer resistances before and after polarisation., details of which are given in references [293, 294].

(ii) Watanabe Method:

Another a.c. impedance / d.c polarisation technique for the determination of transport number was used by Watanabe and co-workers [295]. The experimental arrangement consists of cell having electrolytes sandwiched between two non-blocking i.e. reversible electrodes, which are electroactive towards one of the mobile ions, generally cation. In this case the cell assembly is thermally equilibrated at suitable temperature before measurement. First of all, the a.c. complex impedance of the cell is recorded upto low frequency region (upto few mHz) and the values of the bulk resistance (R_b) and the electrode-electrolyte charge transfer resistance (R_e) are recorded. Thereafter, the cell is polarised by applying a small d.c. potential (normally a few millivolts $\sim$ 10 mV). The d.c. polarisation of the cell with non-blocking electrodes provides a steady state current (I_s) with the passage of time. This value of current arises due to the contribution of cations (assuming electronic current is negligible).

According to Watanabe and co-workers [295], the transport number may be represented as:

$$t_+ = \frac{R_b}{\left(\dfrac{V}{I_s}\right) - R_e} = \frac{I_s R_b}{(V - I_s R_e)} \qquad \dots (3.27)$$

(iii) Transient Ionic Current Technique:

This technique of transport number measurement is based on "Transient Ionic Current (TIC)" measurement method, which was originally developed to detect the number of mobile ionic species and to evaluate their mobility [296, 297].

According to this technique, the sample is first polarized by applying a d.c. electric potential as shown in Fig 3.10. As a result the mobile ionic species start accumulating at their respective electrodes resulting in polarisation and subsequent reduction in current. On
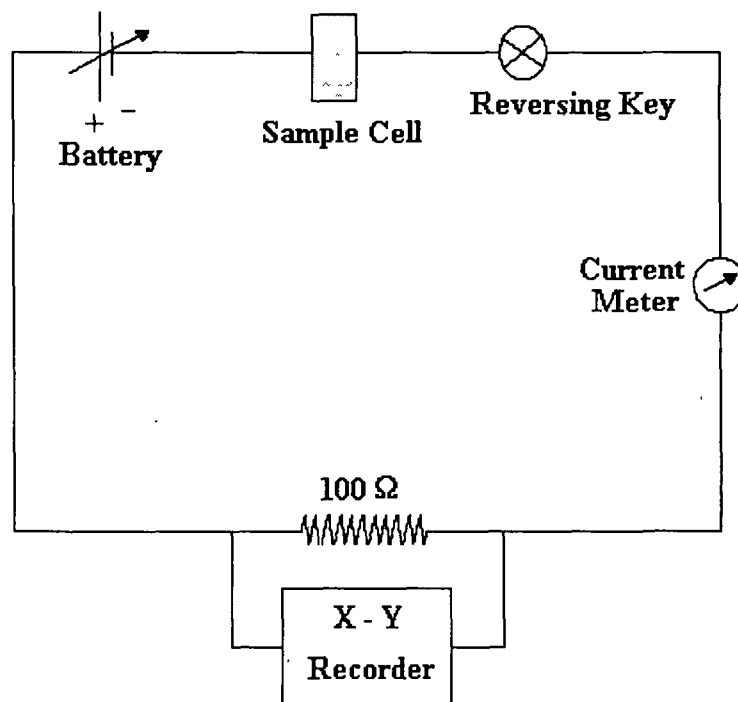
Fig 3.10: Schematic circuit diagram for transient ionic current (TIC) measurement.

reversing the polarity, these ionic species start moving in the reverse direction. When complete stripping of polarizing cloud is achieved a peak in the current vs time plot is obtained. Since the different types of ions have different mobilities, they will reach at the counter electrodes at different times. Thus different number of peaks would appear in the current vs. time plot depending on the types and number of mobile species present in the electrolyte during depolarisation. The ionic mobility (μ) is related to the time of flight (τ) for the mobile ions at which peak occurs by the mathematical relation:

$$\mu = \frac{d^2}{\tau . V}$$

.... (3.28)

where 'd' is sample thickness, 'V' is d.c. voltage applied and 'τ' is the time of flight of the ion.

To evaluate the cationic and anionic transport numbers, the values of cationic/anionic mobilities (μ_+ / μ_-) as evaluated from eqn. (3.28) are substituted in the following mathematical relations:

$$t_+ = \frac{\mu_+}{(\mu_+ + \mu_-)}$$ .... (3.29)

$$t_- = \frac{\mu_-}{(\mu_+ + \mu_-)}$$ .... (3.30)

3.1.4 Microscopic Studies:

The bulk properties of superionic solids are related to the microscopic dynamical phenomena. In order to design new and potentially technologically significant solid ion conductors in this field, it is quite important to characterize and understand the microscopic behaviour both
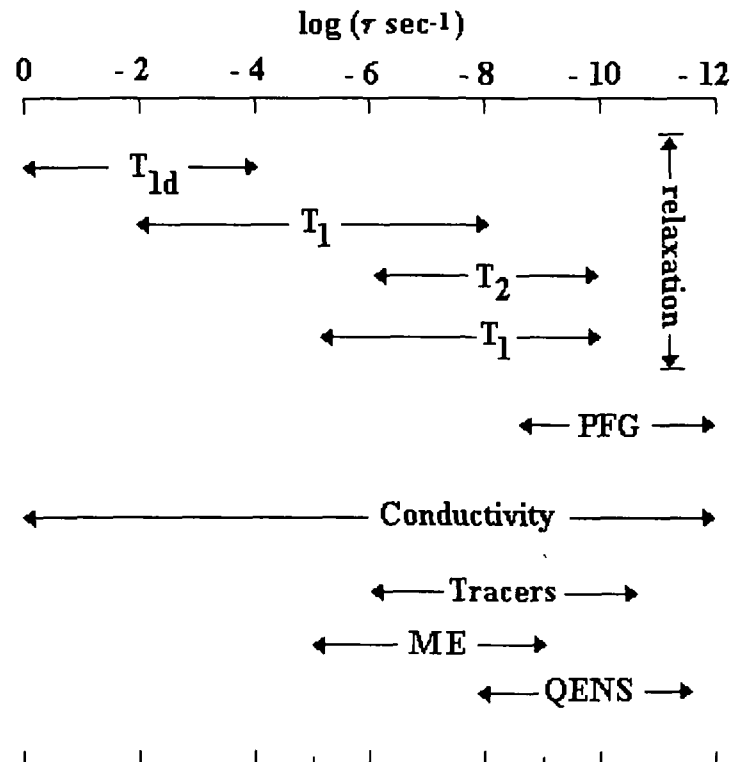
Fig 3.11: Motional time scales probed by a variety of experimental techniques.

from the structural and dynamical points of view. X-rays and neutron diffraction are powerful techniques for structural studies [298, 299]. The dynamical studies, in general, are sensitive to the elementary motional processes (e.g. the atomic jumps in the lattice). Fig 3.11 shows the time scales of motion for which various experimental measurements give useful information [300]. Some of the techniques widely used to study the superionic solids on the microscopic scale are listed below:

1. Nuclear Magnetic Resonance (NMR) [1, 271].

2. Vibrational spectroscopy (FTIR / Laser Raman) [1, 2, 271, 272].

3. Microwave conductivity (Dielectric Relaxation) [1,271].

4. Quasi-elastic neutron scattering (QNES) [1,271].

5. Diffuse X-ray and Neutron scattering [1,271].

6. Extended X-ray absorption fine spectroscopy (EXAFS) [1,271].

7. Light scattering experiments (Brillouin scattering / Ion backscattering) [1,271, 301].

8. Electron spin resonance (ESR) spectroscopy [1,271].

9. Electron hole burning spectroscopy [301, 302].

10. Inelastic electron tunnelling spectroscopy (IETS) [303].

These techniques are widely described in literature.

3.2 Experimental Techniques Used in the Present Studies

3.2.1 Techniques used for Preparation and Characterization of Gel Electrolytes:

3.2.1.1 Preparation of polymeric gel electrolytes:

The polymeric gel electrolytes have been synthesised using standard "Solution Cast Technique" [83, 84, 304-306] for their application in the fabrication of supercapacitors. The block diagram of the technique has been given in Fig 3.12. Two different types of gel electrolytes were prepared based on two different host polymers viz: poly (vinylidene fluoride-

co-hexafluoropropylene) (PVdF-HFP) and poly (methyl methacrylate) (PMMA). At first, the liquid electrolytes comprising of binary solvents, ethylene carbonate (EC) and propylene carbonate (PC) with different salts, lithium perchlorate (LiClO$_4$), sodium perchlorate (NaClO$_4$) and tetraethyl ammonium perchlorate (TEAClO$_4$) were prepared. The appropriate amount of
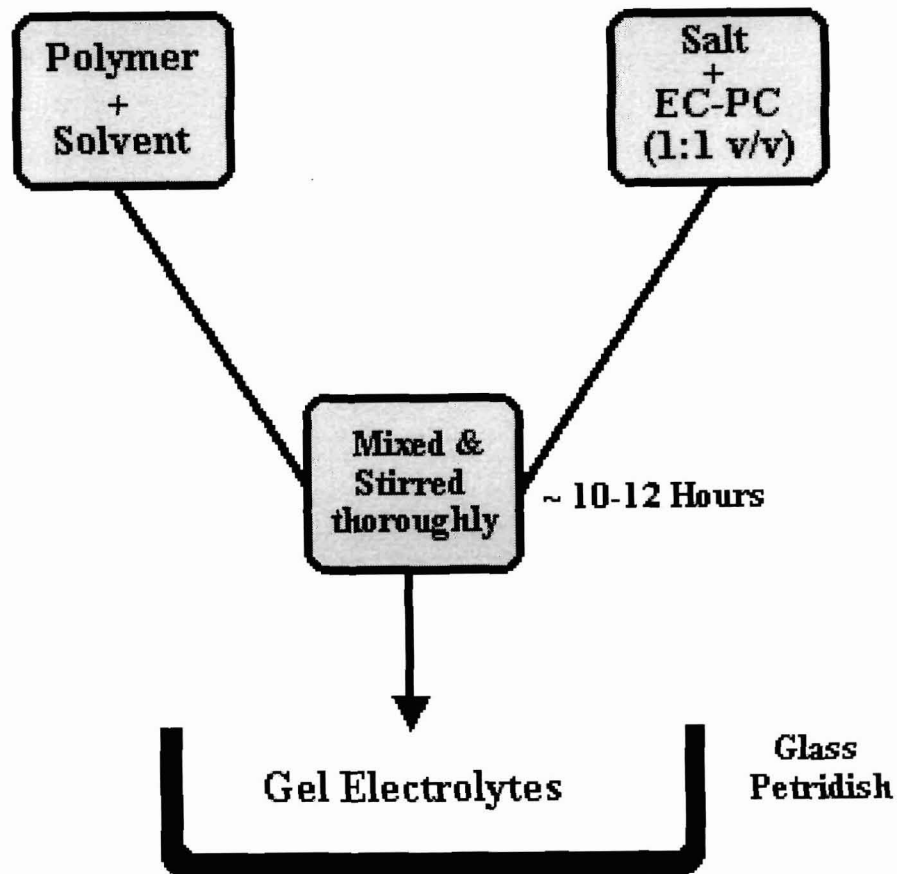
Fig. 3.12:   Schematic representation of "Solution Cast Techniques".

salts were dissolved in EC:PC mixture (1:1 V/V) by stirring thoroughly to get liquid electrolytes. The compositions of these electrolytes were optimised by electrical conductivity measurements.

The PVdF-HFP based gel electrolytes were prepared by immobilising the optimised liquid electrolytes. In this process, the host polymer, PVdF-HFP, was dissolved in tetrahydrofuran (THF) separately at 50^0C. The optimum composition of each liquid electrolyte was mixed with different appropriate amount of PVdF-HFP solution. The mixtures were then stirred thoroughly for about 10-12 hours, poured to glass petri-dishes and allowed to evaporate the intermediate solvent, THF. Finally, the freestanding highly and almost transparent films (~200-300 μm thick) of different compositions were obtained, as shown in Fig. 3.13.

The polymeric gel electrolytes comprising of PMMA-EC-PC-salts (LiClO$_4$, NaClO$_4$ and TEAClO$_4$) were prepared using a slightly different procedure. The optimum compositions of liquid electrolytes with different salts (i.e. 1.0 M salts in EC:PC mixture) were mixed with different appropriate amounts of PMMA. The mixtures were then kept in an
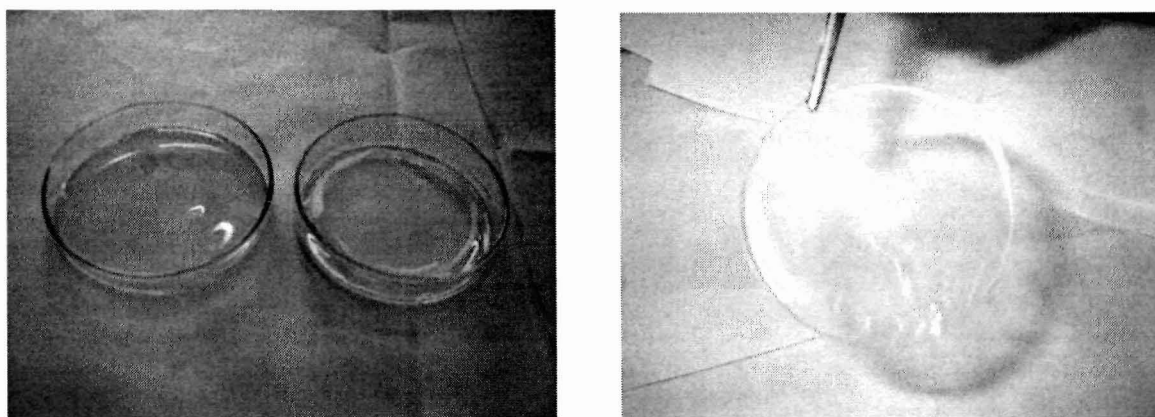
Fig. 3.13: Photograph of transparent polymeric film.

oven at ~70^0C for about 10-12 hours for gelling. Finally the soft, semi-transparent and flexible lump materials of different compositions were obtained.The PVdF-HFP (average M.W. 400,000), PMMA (average M.W. 120,000), EC, PC and salts, LiClO$_4$, NaClO$_4$ and TEAClO$_4$ were obtained from Aldrich and used as received.

3.2.1.2   Characterisation of polymeric gel electrolytes:

The gel electrolytes have been characterised using the following techniques:

(a) <u>Electrical Conductivity and Impedance Spectroscopy</u>

The electrical conductivity 'σ' is defined as:

$$\sigma = G.\frac{l}{A} = \frac{1}{R}\left(\frac{l}{A}\right) \qquad \qquad \dots (3.31)$$

where G (1/R) is the conductance of the sample, R is the resistance, l is the sample thickness or separation between electrodes and A is the area of the electrode.

The measurement of the electrical conductivity of the superionic solids is not as simple and straightforward as it is in the case of electronic conductors. In the case of electronic conductors, conductivity can be measured directly by applying d.c potential using either by two probe or four probe methods. But in the case of ionic conductors, we cannot apply d.c. potential as it leads to the fast interfacial polarisation, which results in the continuous increase in resistance as a function of time. In order to avoid this problem, two different methods have been adopted for the measurement of ionic conductivity of solids:

(i)   Direct Current (d.c.) methods, and

(ii)   Alternating Current (a.c.) methods.

(i) Direct Current (d.c.) methods:

In this method, a constant d.c. potential or current is applied across a cell comprising of electrolyte sandwiched between two non-blocking (reversible) electrodes and the resulting current or potential is monitored. In this case conductivity can be written as:

$$\sigma = \frac{I}{V}.\frac{l}{A} \qquad \qquad \dots (3.32)$$

where V is the voltage and I is the current.

Generally, two types of d.c. conductivity techniques are used to measure the ionic conductivity:

- Two probe and

- Four probe methods.

In two probe method, a known d.c. potential is applied across the cell (comprising of electrolyte material sandwiched between two reversible electrodes) and the resulting current is measured to determine the d.c. resistance. Whereas in the four probe method, a known d.c. current is applied between two outer electrodes and the potential is measured between two inner electrodes. Conductivity can be calculated by measuring the area of the two inner electrodes and the distance between them. The experimental set-up for the four-probe method is given in Fig 3.14.
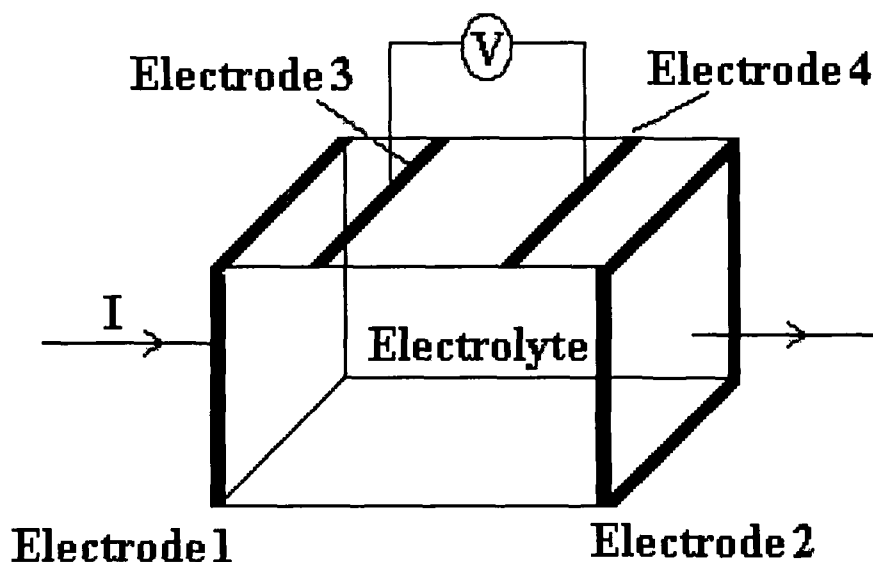
Fig. 3.14: Experimental set-up for four probes method [1].

Though the d.c. technique for the measurement of ionic conductivity appears to be simple, it possesses many practical difficulties such as, it is difficult to get reversible electrodes for both the cations and anions, there is also a contribution of electrode-electrolyte interfacial resistances to the overall conductivity, presence of grain boundary conduction, formation of a double layer due to concentration polarisation etc. Further, the interpretation of the electrical conductivity data is also very difficult due to the presence of more than one phase in the materials. Hence, the combination of all the above difficulties led the researchers to switch over to a.c. methods.

(ii)   Alternating Current (a.c.) methods:

The a.c. technique, also referred to as "Impedance Spectroscopy", is a method according to which a sinusoidal voltage is applied to a cell, comprising of an electrolyte sandwiched between two blocking or non-blocking electrodes, and the resulting cell current passing through the cell as a result of this perturbation is determined. The resulting current is related to the applied sinusoidal voltage by two different parameters, which are:

- the ratio of the voltage and current maxima, V_{max} / I_{max} (analogous to resistance in d.c. measurements), and

- the phase difference 'θ' between the voltage and the current.

The combination of these two parameters represents the impedance 'Z' of the cell. Both the magnitude of impedance ($|Z| = V_{max}/I_{max}$) and the phase angle 'θ' are the functions of applied frequency. The impedance of a cell is measured as a function of applied frequency over a wide range of frequencies, typically 1 mHz - 1 MHz. Impedance Spectroscopy enables us to evaluate and separate the contribution of different electrical parameters in different frequency

regions such as bulk phenomena, i.e. the migration of ions through the bulk and across the grain boundaries within the electrolyte, interfacial phenomena due to electrode reactions at the electrode/electrolyte interfaces etc. [291, 307]. This study was initially applied successfully for the study of dielectric properties of the materials by Cole and Cole [308]. Bauerly [309] was the first to propose a generalized complex impedance/admittance plot method to extract the true bulk conductivity of superionic conductors from the a.c. conductivity measurements.

Impedance of a cell is a complex quantity and it can be displayed in a complex plane in different forms [291, 307]:

Complex impedance, $Z^*(\omega) = Z' - j\,Z'' = R_s - j\,/\,\omega C_s$ ... (3.33)

Complex admittance, $Y(\omega) = Y' + j\,Y'' = 1\,/\,R_p + j\,\omega\,C_p = G(\omega) + j\,B(\omega)$ ... (3.34)

Complex modulus, $M(\omega) = 1\,/\,\varepsilon(\omega) = M' + j\,M'' = j\,\omega\,C_0\,Z(\omega)$ ... (3.35)

Complex permittivity (Dielectric constant), $\varepsilon(\omega) = \varepsilon' - j\varepsilon''$ ... (3.36)

Loss Tangent, $\tan\delta = \varepsilon''\,/\,\varepsilon' = M''\,/\,M' = -Z'\,/\,Z'' = Y'\,/\,Y''$ ... (3.37)

Complex resistivity, $\rho(\omega) = \rho' + j\,\rho'' = Z \times (C_0\,/\,\varepsilon_0)$ ... (3.38)

Complex conductivity, $\sigma(\omega) = \sigma' - j\,\sigma'' = Y \times (\varepsilon_0\,/\,C_0)$ ... (3.39)

Where $j = \sqrt{-1}$, C_0 is vacuum capacitance of the cell, G is the conductance and B is susceptance (subscripts s and p are for series and parallel combinations of the circuit elements, respectively).

Out of these parameters, the impedance and admittance plane representations provide useful information when various processes within the cell have different relaxation times as in the case with the solid electrolyte cells. In this regard, Randles [310] was the first to successfully show that the electrical processes occurring within the cell could be represented by

an electrical equivalent circuit comprising of resistors, capacitors, inductors and their series and parallel combinations. This equivalent circuit shows almost the same phenomenological processes within the cell. Practically the equivalent circuit mainly consists of resistors and capacitors in terms of which the charge migration and polarisation occurring within the cell can be represented. A general practice is to represent one charge polarisation or migration process by one parallel RC combination. Hence, a model of equivalent circuit for a general solid electrolyte consists of three parallel RC circuits connected in series. Each of the parallel combinations represents contributions due to the bulk properties of the material, electrode-electrolyte interfacial processes and grain boundary conduction in different frequency ranges, respectively, as shown in Fig 3.15.
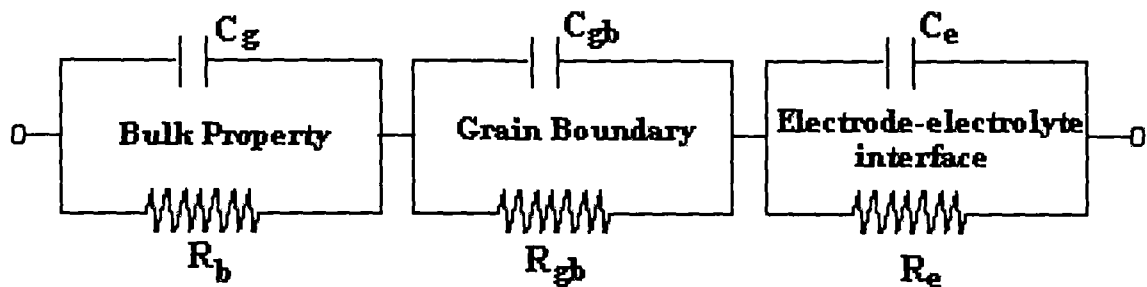
Fig. 3.15: Equivalent circuit model of a general electrolyte.

The impedance plots of some simple electrical circuit are shown in Fig 3.16.
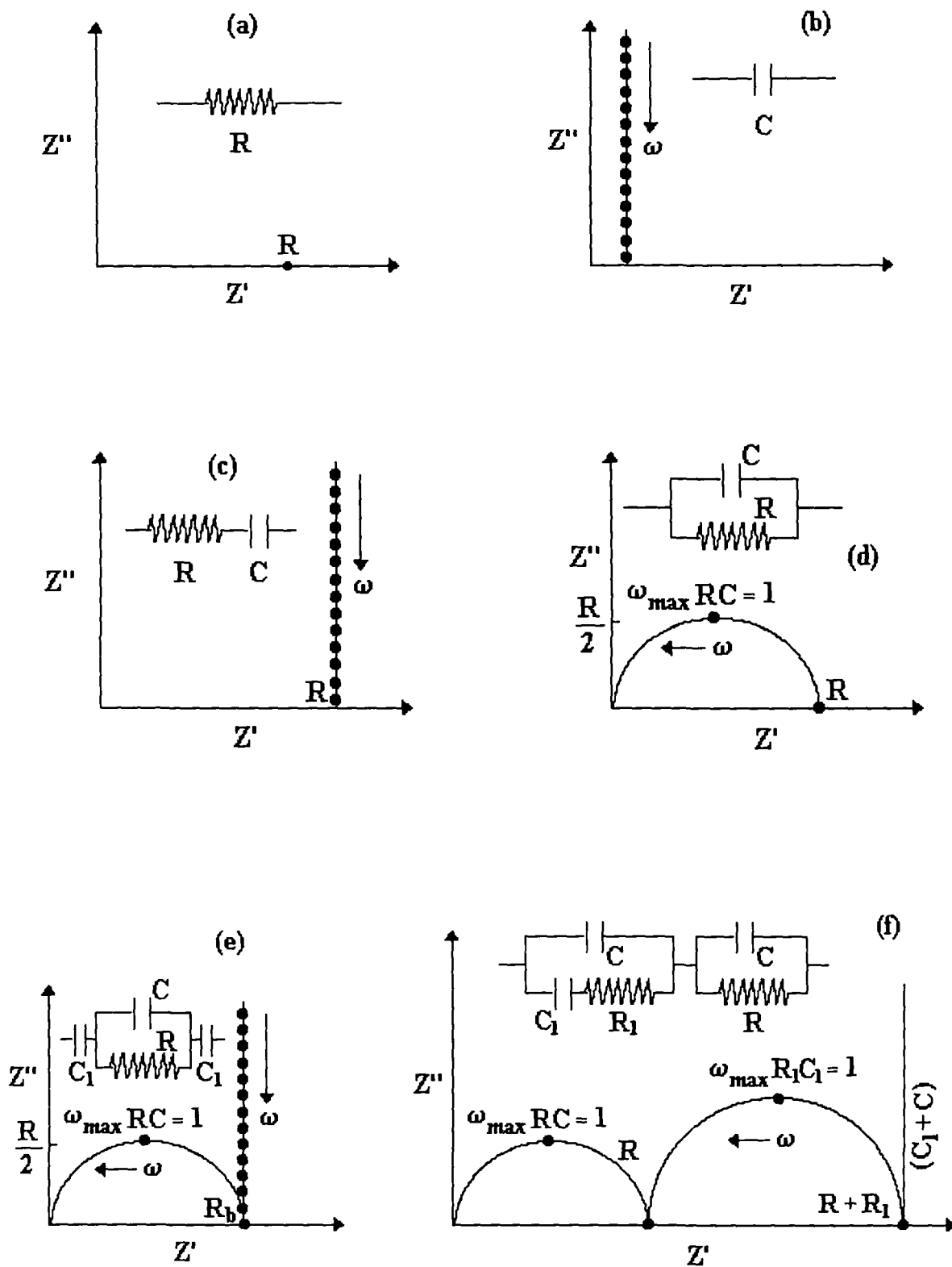
Fig. 3.16: Impedance plots of some simple RC circuits.

Depending on the types of electrodes used (i.e. either blocking or non-blocking electrodes) and types of electrolytes having single mobile ion species (in conventional solid electrolytes) or double mobile ion species (cations and anions both as observed in the liquid or polymer / gel electrolytes), the behaviour of the cells, their impedance patterns and hence their equivalent circuits are distinctly different which are described briefly as follows:

Blocking electrodes

Fig 3.17 shows the cell with blocking electrodes and single ion conducting electrolyte, its ideal impedance pattern and the equivalent circuit representing its a.c. response. The bulk polarisation and ion migration in the electrolyte is reflected as a semicircle in the impedance
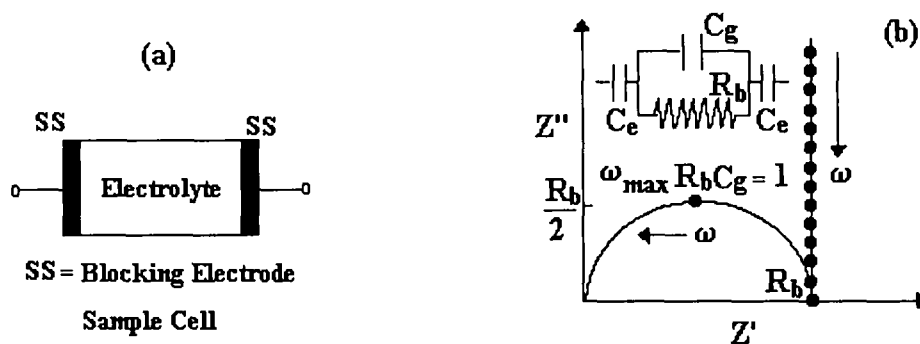
Fig. 3.17:   Schematic representation of (a) an electrochemical cell with blocking electrodes, (b) impedance plot. The equivalent circuit is represented in inset.

plot, generally observed in the middle/high frequency range. This semicircular spur indicates that the R_b (bulk resistance) and C_g (geometrical capacitance) are connected in parallel combination. The double layer capacitances (C_e) built up due to charge accumulation at the electrode-electrolyte interfaces, appear as a spike rising at right angle parallel to imaginary axis in the low frequency region of impedance plot [Fig 3.17 (b)] and connected in series with parallel combination of R_b and C_g [Fig 3.17 (b) inset].

It is generally observed that the middle/high frequency response gives information about the properties of the electrolyte, whereas the low frequency response carries information about the electrode-electrolyte interfaces. Overall, the magnitude of all the fundamental electrical properties of the cell may be obtained from the complete impedance data. Particularly R_b, the bulk resistance of the electrolyte can easily be evaluated by sandwiching the electrolyte between two blocking electrodes.

Non-blocking (reversible) electrodes

In the case of non-blocking or reversible electrodes, there is a finite reversible electrode reaction at the electrode-electrolyte interfaces, which allow the dissolution of mobile ionic species in the electrodes. Fig 3.18 shows the impedance plots of the cell consisting of (a) single ion conducting electrolyte, and (b) both the cation and anion conducting electrolyte (e.g. liquid / polymeric gel electrolyte). The equivalent circuits are shown in their corresponding insets.

In the case of single ion conducting electrolyte, the high frequency semicircle in the impedance plot is observed due to the parallel combination of R_b and C_g (representing bulk
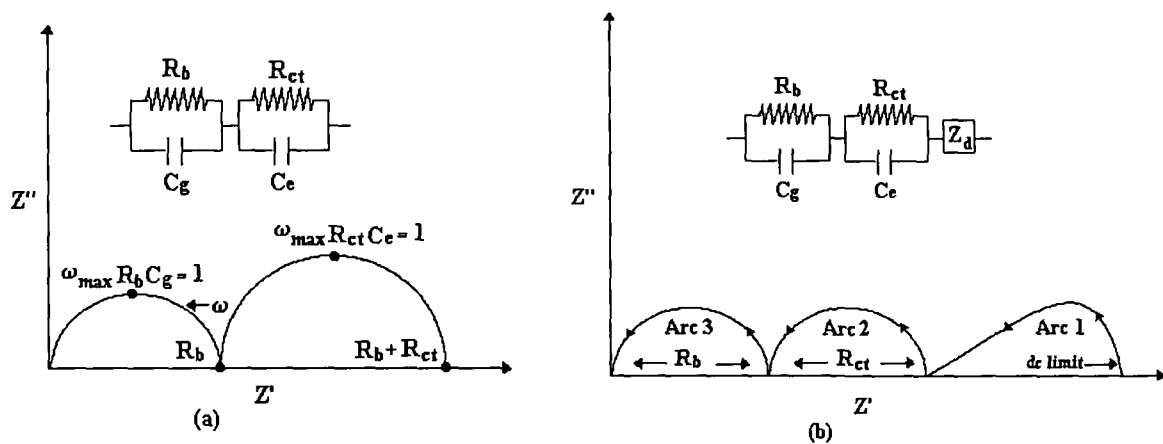
Fig. 3.18: Schematic representation of impedance plot for the cells with non-blocking electrodes consisting of (a) single ion conducting electrolyte, and (b) both the cation and anion conducting electrolyte (e.g. liquid/polymer gel electrolyte). The equivalent circuits are shown in their corresponding insets.

properties of the electrolyte) similar to the pattern as observed in the case of the cell with blocking electrodes. In addition to this, another semicircle is observed in the middle frequency region, which is the representation of a.c. response of the electrode/electrolyte interface. This is represented by a parallel combination of a finite charge-transfer resistance, R_e, and double layer capacitance, C_e.

On the other hand, in the case of an electrolyte having two (cation and anion) mobile ions, three semicircles are observed which are corresponding to the bulk (high frequency), electrode-electrolyte interfaces (middle frequency) and diffusion impedance due to the concentration gradient of anions developed at sufficiently low frequency, as shown in the Fig 3.18 (b). The low frequency semicircle is skewed and is inclined at an angle of 45^0 to the real axis. However, all the three features may not be observed in all the cases [307].

In actual practice, it is observed that there is a significant flattening of the ideal semi-circular pattern and tilting of the spike in the impedance spectrum contrary to the ideal spectrum obtained from the equivalent circuit model based on the processes within the electrolyte cell as shown in Fig 3.19.
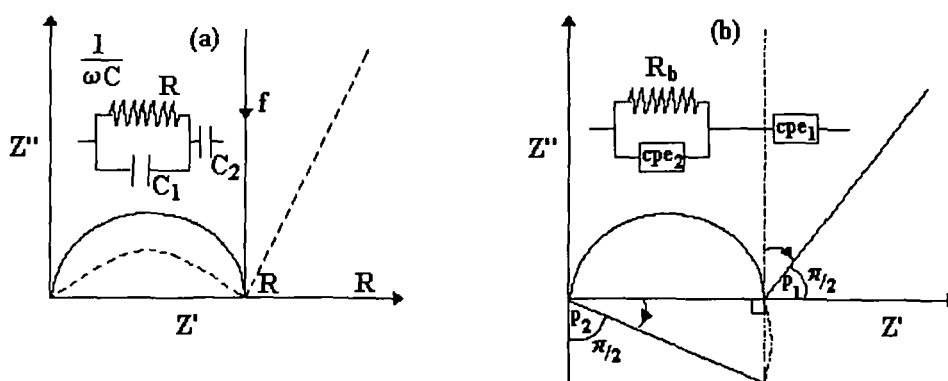
Fig. 3.19: (a) Equivalent circuit and impedance spectrum (bold line represents spectrum for ideal equivalent circuit. Dotted line represents experimental impedance spectrum for gel electrolytes), (b) Depression of semicircle and tilting of spike caused by replacing capacitors by constant phase elements.

Particularly in the case of polymer electrolytes, the effect may be related to the presence of crystalline non-conducting regions interlocked with the conducting amorphous materials within the spherulites of a polymer electrolyte system. The cell behaves as a "leaky capacitor" resulting in the semicircle flattening and spike tilting as shown in the Fig 3.19 (a). The effect has also been attributed to a variety of physical phenomena such as the multiple or coupled reaction sequences, roughening of the electrodes, and frequency dependent ohmic resistances caused by a non-uniform charging of the double layer [311]. In order to account for such effect, a generalised impedance element known as the "constant phase angle element (cpe)" is introduced into the equivalent circuit model as shown in the Fig 3.19 (b) as inset. The impedance of the constant phase angle element is given by:

$$Z_{cpe} = k \ (J\omega)^{-p} \ , \ 0 \le p \le 1 \qquad \qquad .... (3.40)$$

When $p = 0$, Z is frequency independent and 'k' represents the resistance R.

When $p = 1$, $Z = k \ / \ j\omega = -j \ / \ \omega k^{-1}$, in such a case Z is frequency dependent and k^{-1} represents the capacitance. For $0 \le p \le 1$, the 'cpe' acts, in a way, intermediate between a resistor and a capacitor, which is the case for polymeric materials.

In the present studies, the impedance measurement was carried out for the determination of true bulk conductivity of the polymeric gel electrolytes as a function of composition and temperature. Different types of sample holders and arrangement for impedance measurement at different temperature in the present studies are shown in Fig 3.20.
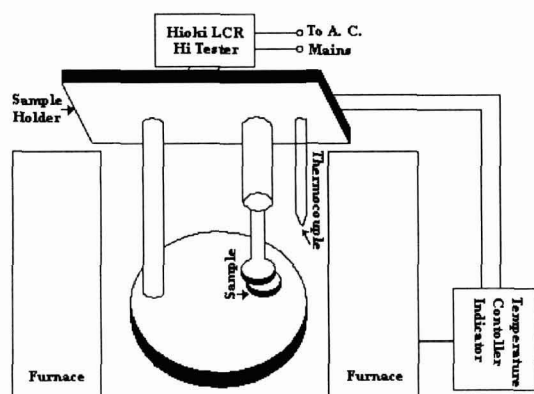
(a)

(b)
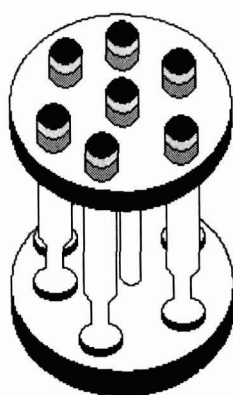
(c)
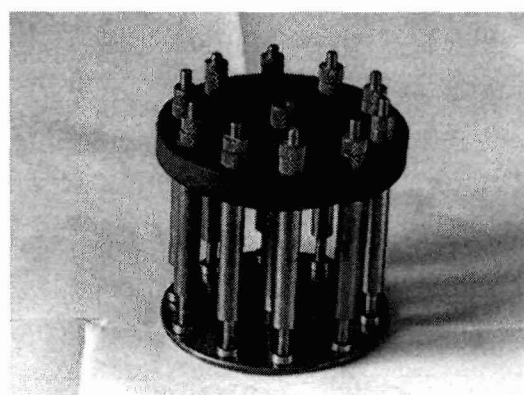
(d)

Fig. 3.20: Different types of sample holders used in the present studies.

(b)   Transport Number Measurement

Different studies for the measurement of transport number have been given in section 3.1.3.4. In the present studies, the polarization method [312, 313] was used for the determination of the ionic transport number of different gel electrolytes. The experimental arrangement is shown in Fig 3.21(a). According to this method a d.c. electric field is applied across the sample sandwiched between two blocking electrodes and the resulting current is monitored as a function of time. The nature of the curve is shown in Fig 3.21(b). The current at first decreases with time due to polarisation of charges at the respective electrodes, reaching a

residual constant value. The initial total current (I_T) is due to both electronic and ionic conduction, whereas the constant residual current is due to electronic conduction only.

(a)   (b)
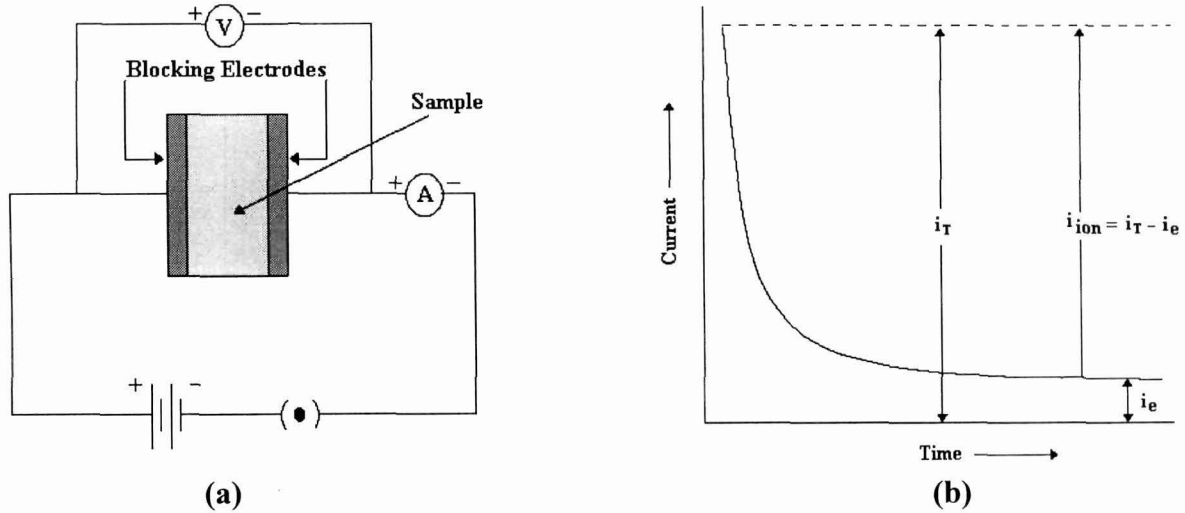
Fig 3.21:   Experimental arrangement for measuring transference number by polarization method.

The ionic transport number 't_{ion}' is expressed as:

$$t_{ion} = 1 - \frac{\sigma_e}{\sigma_T} = 1 - \frac{i_e}{i_T} \qquad\qquad .... (3.41)$$

where σ_e is the electronic conductivity and σ_T is the total conductivity, σ_{ion} ($= \sigma_T - \sigma_e$) is ionic conductivity.

Though this method is quite useful in the determination of transport number, it has certain limitations also such as, it fails to identify the types of ions responsible for the ion transport and hence we cannot determine whether the conduction is due to cations or anions. Moreover it is quite difficult to choose perfectly blocking electrodes for different ions like H^+, Li^+, Na^+ etc. though the platinum or stainless steel foils fulfil the requirement as blocking electrodes to some extent.

3.2.2 Technique used for the Preparation of Electrode Materials:

Two different types of solid state supercapacitor devices were constructed namely (i) electrical double layer capacitors (EDLCs), and (ii) redox supercapacitors, using gel electrolytes and the electrodes comprising of activated charcoal powder and the electrochemically deposited conducting polymer, polypyrrole, respectively. Details of the preparation of electrode materials are given below:

3.2.2.1 Preparation of Activated Charcoal Powder Electrodes:

The preparation method of activated charcoal powder electrodes is described in schematic diagram (Fig 3.22). A slurry of activated charcoal powder (Aldrich) and polymer (PMMA or PVdF-HFP) with a ratio 90 : 10 (w/w) in a common solvent, acetone was prepared by a thorough mixing. Fine films of electrodes were coated by spraying the slurry on carbon papers (Toray, Japan) followed by heating them in oven at ~70°C for 10-12 hours.
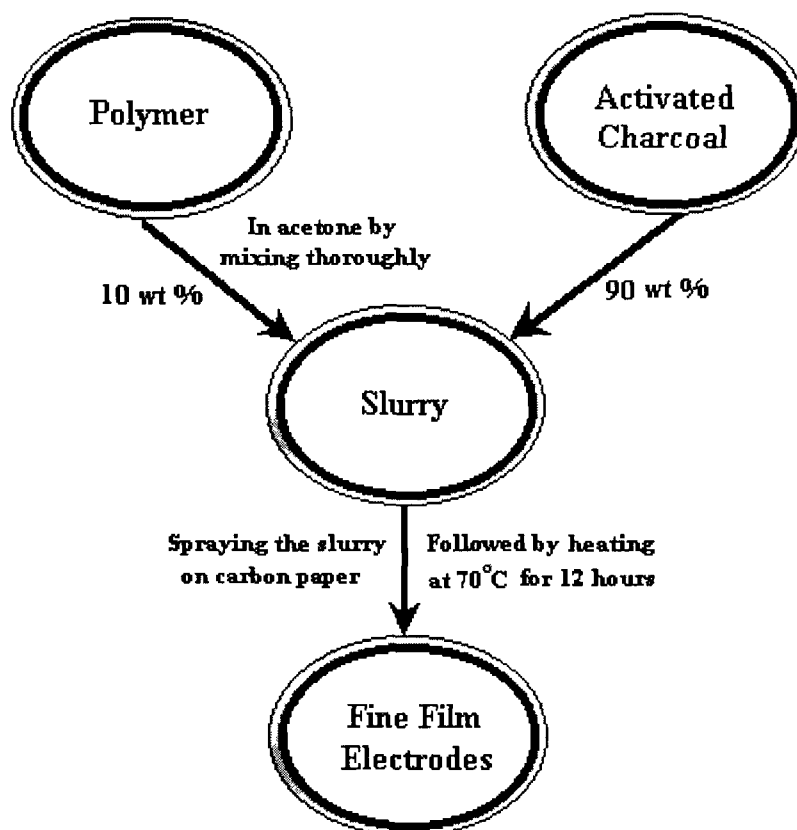
Fig. 3.22: Block diagram for the preparation of activated charcoal powder electrodes.

99

3.2.2.2   Preparation of Conducting Polymer Electrodes (p-doped Polypyrrole):

Polypyrrole (pPy) is one of the most studied conducting polymers because of its good electrical conductivity (100-300 S cm^{-1}), environmental stability and relative ease of synthesis. It is always available either in neutral or p-doped forms. The n-doped polypyrrole is highly unstable. It can be prepared either by chemical or electrochemical methods. In chemical methods, monomer (pyrrole) is mixed with different types of oxidants (e.g., ferric chloride, ferric perchlorate, etc.) and supporting salts (LiClO$_4$, TEABF$_4$, etc.). Consequently, blackish p-doped polypyrrole powder is obtained, which is washed thoroughly using suitable solvent(s) to eliminate excess impurities. This method is efficient, straightforward and useful in mass production. On the other hand, the electrochemical method of preparation of conducting polymers is a clean method as it restricts the incorporation of impurities to a larger extent. In this process, electrochemical polymerisation and doping is performed simultaneously in a suitable cell, consisting of common solvent + monomer + supporting electrolyte. The p- and n-doping occurs in anoding and cathodic regions, respectively. The electrochemical polymerisation can be performed in different modes of operation, such as potentiostatic, potentiodynamic, galvanostatic, etc. In the present studies, galvanostatic method for the synthesis of polypyrrole was used, described as follows:

The p-doped polypyrrole were deposited electrochemically in a three electrode one compartment cell on the indium tin oxide (ITO) conducting glass substrates (~80 Ω cm^2) (Fig.3.23). Electrosyntheses were carried out in the above cell containing 0.1 M pyrrole and 0.2 M supporting electrolyte LiClO$_4$ solutions in acetonitrile. The solutions were degassed by purging with dry nitrogen before electropolymerisation. The electro-depositions were made on ITO with a constant current of 2 mA for 10 minutes. The deposition area was limited to ~ 4 cm^2. The value of current used for the ITO substrate was selected in order to ensure a

CE : Counter Electrode
WE: Working Electrode
RE : Reference Electrode
SCE : Saturated Calomel Electrode
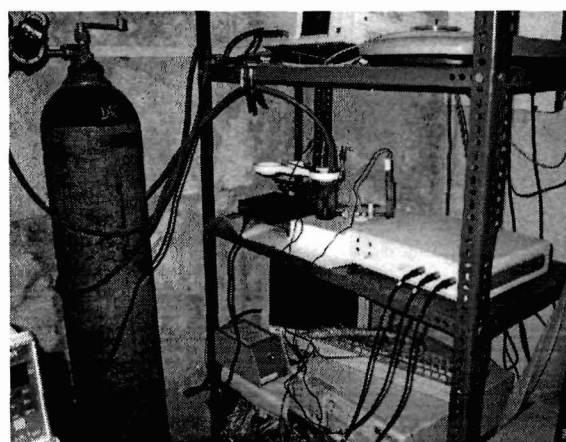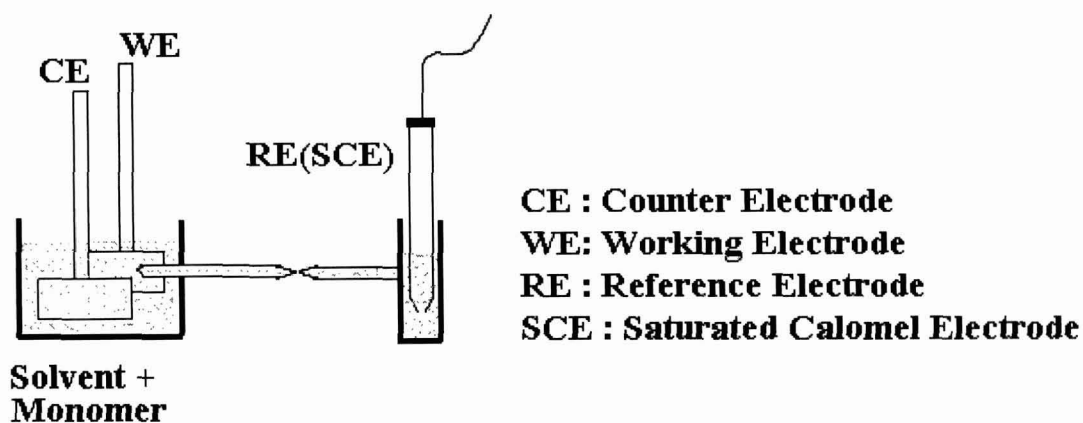
Fig. 3.23: Experimental set-up for the preparation of p-doped conducting polymer.

deposition potential greater than 800 mV with respect to a saturated calomel electrode (SCE). The polypyrrole films, so obtained, were used for the fabrication of redox supercapacitors.

3.2.3   Techniques used to Characterize Supercapacitors:

In order to characterise the supercapacitors, the physical techniques adopted were mainly, (i) a.c. impedance spectroscopy, (ii) linear sweep cyclic voltammetry and (iii) charge-discharge methods.

3.2.3.1 A. C. Impedance Spectroscopy

An electrochemical capacitor cell, as described previously, is generally fabricated from two identical electrodes with a liquid or a solid electrolyte separating them. Impedance

spectroscopy is an attractive method for characterising the electrochemical behaviour of such cells because of the direct connection between the real system and its idealised equivalent circuit consisting of discrete electrical components (R, C and L) in their series and parallel combinations. As described earlier, the real systems in the present context are electrochemical capacitor cells that employ either blocking / polarisable electrodes (called electrical double layer capacitors) or electroactive electrode materials (called redox supercapacitors). The blocking electrodes used in the capacitors have either planar geometry (e.g. high density graphite sheets, glassy carbon sheets etc.) or large surface area porous electrodes (activated carbon powder/ fabrics/ fibre etc.).

A schematic representation of the impedance behaviour of an ideal and a real capacitor cells are illustrated in Fig 3.24.
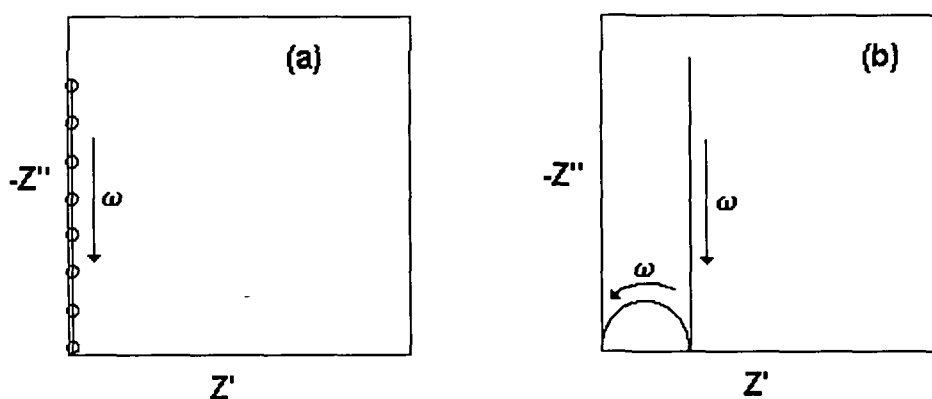
Fig 3.24: Impedance plots of (a) an ideal capacitor, and (b)a real capacitor

The impedance pattern of an ideal capacitor shows a steep rising dispersion line overlapping with imaginary axis of the impedance plot as shown in Fig 3.24 (a). The impedance pattern of a real capacitor [Fig 3.24 (b)] shows a semicircle representing a parallel combination of a bulk resistance R_b (resistive component owing to the ion migration owing to the bulk of electrolytes) and a geometrical capacitance C_g (due to dielectric polarisation of electrolyte under the influence of an electric field). The interfacial polarisation leads to the

formation of a double layer capacitor at the two identical interfaces, which is represented by a steeply rising spike in the low frequency region of the impedance spectra [Fig 3.24 (b)].

The equivalent circuit of capacitor cells with either rough or porous electrode in contact with the electrolytes can be represented in the form of a transmission line type distributed circuit which gives variable time constant. Conducting polymer electrodes (e.g. polypyrrole, polythiophene and their derivatives etc.) also show a similar pattern of impedance behaviour as the porous electrodes. The region of the impedance spectrum associated with a high capacitance at low frequencies is often interpreted in terms of a distributed R and C network due to ionic penetration throughout the polymer films or the porous electrodes.

In the present studies, the impedance measurements were carried out using computer controlled LCR HI TESTER (Model 3522-50, Hioki, Japan) in the frequency range from 10 mHz to 100 kHz. The signal level was kept at 10 mV. The overall capacitance of the cell can be evaluated from the relationship:

$$C = -\frac{1}{\omega Z''}$$
.... (3.42)

where ω is angular frequency and Z" is the imaginary part of the total impedance measured in low frequency range (say 100 mHz-10 mHz). The single electrode specific capacitance values were evaluated by multiplying the overall capacitance by a factor of two and divided by the mass of a single electrode material.

3.2.3.2   Linear Sweep Cyclic Voltammetry

The linear sweep cyclic voltammetry (CV) is another important experimental probe to characterise the capacitors. In CV, the potential applied to the working electrode of the cell is a triangle wave as a function of time. The potential of the working electrode is continuously swept back and forth between two set points, say, A and B at a constant sweep/scan rate. In CV, the initial potential is chosen to be a value where little or no electrode reaction occurs (near

zero current). Thus, the start and end potentials are usually not the same as A or B but often the equilibrium or open circuit potentials [201]. The nature of the current, which flows through the working electrode, is observed as a function of scanned potential. The reversal of the potential scan direction gives rise to a current flow due to the reaction of the products formed in the preceding scan period. A cyclic voltammogram is a plot of cell current (I) as a function of the electrode potential (V) [201].

In the case of supercapacitors, the cyclic voltammogram of an ideal capacitor (having negligible internal resistance) shows a perfect rectangular shape [Fig 3.25 (a)] and it is scan rate dependent. For real capacitors, the deviation from rectangular shape is observed [Fig 3.30 (b)], which is represented as a series combination of internal resistance R, and ideal capacitance C.
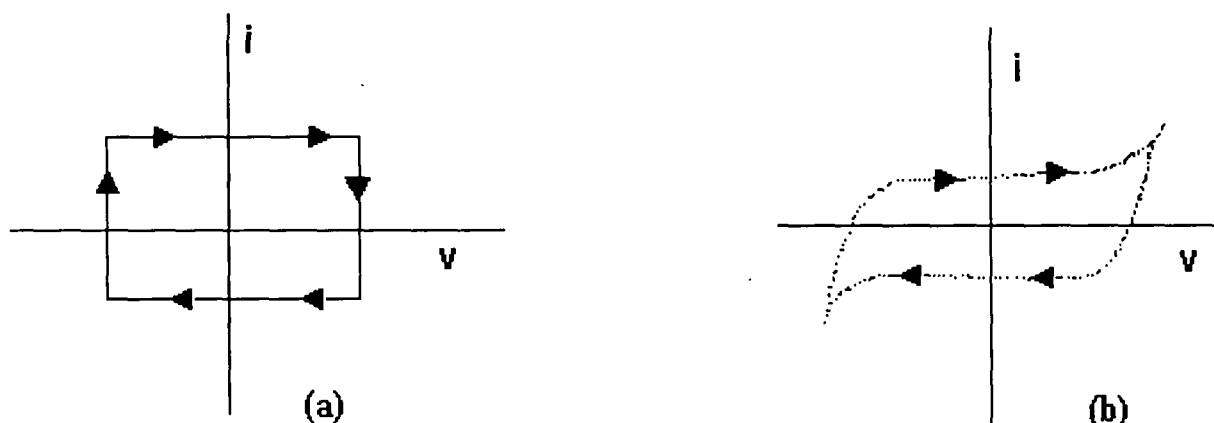
Fig. 3.25: Linear sweep voltammogram of (a) ideal capacitor, and (b) real capacitor

In the present studies all the cyclic voltammetry experiments was carried out with the help of Analytical Electrochemical Workstation (Model: AEW-2, Sycopel, U.K.).

The value of capacitance can be evaluated from the expression:

$$C = \frac{i}{s} \qquad \qquad \dots (3.43)$$

where 'i' is the voltammetric current and 's' is scan rate.

3.2.3.3 Charge-Discharge Studies

Information about an electrochemical system is generally gained by applying an electrical perturbation to the system and by observing the resulting changes in the characteristic behaviour of the system. In impedance spectroscopic measurements, an a.c. perturbation is applied, whereas a voltage ramp is applied in the case of linear sweep voltammetry. In the charge-discharge technique, for characterisation of a capacitor it is necessary to consider the behaviour of a real capacitor system represented by an ideal capacitor C_e connected with the internal resistance R_i in series. The perturbation can be either by potential step (potentiostatic method) or by current step (galvanostatic method).

(a) <u>Potentiostatic (Voltage Step) Method</u>

When a potential step is applied across the capacitor cell, the capacitor charges and an exponentially decaying current is obtained. The behaviour of the current 'i' with respect to time on application of the potential step V_0 can be expressed as:

$$i = \frac{V_0}{R} \exp\left(-t/\tau\right) \qquad \dots (3.44)$$

where '$\tau = RC$' is the time constant. The capacitor cells start discharging when the operation is reversed and the pattern of discharge curve is similar to the charging curve but with the reverse polarity of the current.

The charge-discharge curves can be integrated numerically to obtain the total charge stored or released from the cell. The capacitance 'C' can be evaluated by dividing the total charge by the applied voltage V_0, i.e.

$$C = \frac{\int i.dt}{V_0} \qquad \dots (3.45)$$

(b) Galvanostatic (Current Step) Method

When a capacitor cell is charged by a constant current 'i', the total voltage 'V' developed across the cell can be expressed as:

$$V = iR_i + \frac{\int i.dt}{C}$$
.... (3.46)

As the current is constant, the expression can be written as:

$$V = i\left(R_i + \frac{t}{C_e}\right)$$
.... (3.47)

Thus for a current step, the voltage across an ideal capacitor cell, whose capacitance value C_e, is expected to be constant, increases linearly with time. A schematic V-t curve showing the linear variation is shown in Fig 3.26 (a). After the full charging of the capacitor at the
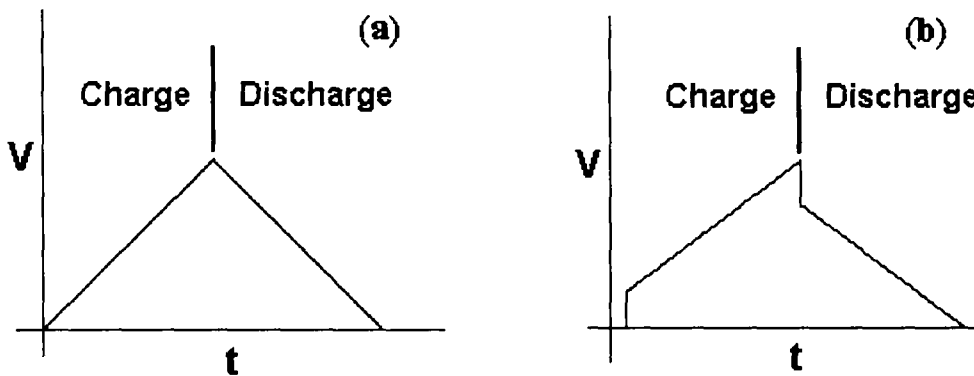
Fig. 3.26: Charge-discharge behaviour of (a) an ideal capacitor, and (b) a real capacitor

maximum permissible or desired voltage level, it can be discharged galvanostatically. The decrease in voltage across the cell is also linear with respect to time [Fig 3.26 (a)]. In the real capacitors, an initial sharp jump/fall in voltage while charging/discharging of the capacitor is observed [Fig 3.26 (b)], which is owing to an ohmic (iR) loss due to internal resistance of the cell.

The capacitance of the cell can be evaluated from the linear region of the curve following the relation:

$$C_e = i\frac{\Delta t}{\Delta V}$$ $$\ldots. (3.48)$$

where ΔV is the change in voltage for Δt interval of time. The charge-discharge experiment can be carried out for several cycles (10^3 to 10^5 cycles) to test the cyclic efficiency of the cell. It may be noted that the cyclic efficiency of supercapacitors is 100-1000 times larger than that of the rechargeable (e.g. Ni-Cd, Ni-metal hydride etc.) batteries. This aspect makes the supercapacitors more attractive as power source over the rechargeable batteries.

The coulombic efficiency can also be calculated easily from the results of galvanostatic charge-discharge experiment. When a constant current is used in charging and discharging, the coulombic efficiency 'η' can be described by:

$$\eta = \frac{\Delta t_D}{\Delta t_C} x100\%$$ $$\ldots. (3.49)$$

where Δt_C and Δt_D are time intervals for charging and discharging, respectively.

In the present studies to characterize the supercapacitor cells, galvanostatic charge-discharge method was adopted. For the purpose, a computer controlled constant current charge-discharge unit, suitable for charging and discharging of supercapacitors at different constant currents, was designed indigenously and tested successfully in our laboratory. The circuit diagram of the unit is shown in Fig 3.27.

The charge discharge experiment was performed by measuring the voltage as a function of time at constant currents of 100 µA - 1mA.
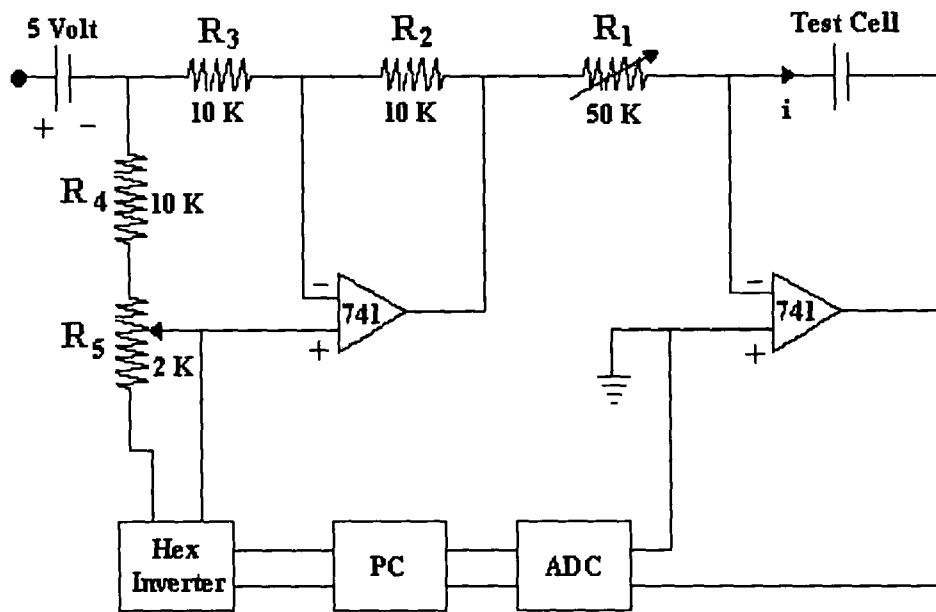
Fig 3.27: Circuit diagram of a computer controlled constant current charge-discharge unit

The performance parameters associated with the supercapacitors can generally be obtained by discharging a fully charged supercapacitor through a load resistance. The parameters along with their expressions and units are listed in Table 3.3.

Table 3.3: Performance parameter of Supercapacitors.

Parameters	Expression	Unit
Capacitance	$C = q/V$	Farad 'F'
Specific Capacitance	$C' = C/M$ $C'' = C/A$	$F g^{-1}$ $F\ cm^{-2}$
Stored Charge	$q = \int \left(\dfrac{V}{R_L} \right) dt$	Coulomb
Energy Density	$E = \dfrac{1}{M} \int \left(\dfrac{V^2}{R_L} \right) dt$ $= \dfrac{1}{2M} CV^2$	$J\ g^{-1}$ or Wh Kg^{-1}
Power Density	$P = \dfrac{V^2}{MR_L}$	$J\ g^{-1}\ s^{-1}$ or $W\ Kg^{-1}$

Chapter – 4

Polymer Gel Electrolytes: Electrical and Electrochemical Studies

POLYMER GEL ELECTROLYTES: ELECTRICAL AND ELECTRO-CHEMICAL STUDIES

The Present chapter is devoted to the studies on the polymer gel electrolytes based on the liquid electrolytes comprising of ethylene carbonate (EC) and propylene carbonate (PC) with the salts ($LiClO_4$, $NaClO_4$ and $TEAClO_4$), entrapped in two host polymers, namely: poly vinylidene fluoride-co-hexafluoropropylene (PVdF-HFP) and poly methyl methacrylate (PMMA). The preparation technique of the gel electrolytes is broadly described in chapter 3, section 3.2.1.1. The electrical and electrochemical characterisation of the gels and their optimisation have been carried out for their application in electrical double layer capacitors (EDLCs) and redox supercapacitors, described in chapters 5 and 6. The liquid electrolytes and the gel electrolytes have been optimised by studying their composition dependence of electrical conductivity. The temperature dependence of the conductivity of the gel systems has been studied and the results have been qualitatively correlated with the existing models. The transference number and electrochemical stability (working potential range) of the gels have also been estimated, which are useful data from the application point of view as electrolytes in electrochemical devices like supercapacitors, etc.

4.1 Electrical Conductivity

4.1.1 Composition Dependence of Electrical Conductivity: Liquid Electrolytes

In order to synthesize highly conducting polymeric gel electrolytes, which is an excellent alternative for the solvent free polymeric electrolyte systems [123, 314, 315], the primary need is to synthesize non-aqueous liquid electrolytes using different polar solvents. While choosing different solvents, few characteristics have to be taken into considerations, such as high ionic conductivity of the liquid electrolytes ($\sim 10^{-2}$) should be achieved at room temperature,

110

dielectric constant of the solvent should be as high as possible so that it facilitates the salt dissociation, low viscosity for better ion transport, high boiling point to furnish non-volatility within the system, low freezing point to prevent sudden decline in the value of conductivity at low temperatures, good chemical and electrochemical stability, chemical compatibility with different electrodes, good plasticising properties, good miscibility with the polymer [164] etc are quite essential. The donor-acceptor concept (acid and base reaction) between the salts and solvents has to be taken into considerations. Since the salts act as strong Lewis acids [316] such as $LiClO_4$, $NaClO_4$ etc., which furnish their small cations after dissociation, so the best way to anticipate the solvating power of the solvent is to consider the solvent Lewis basicity (electron donating ability) [102]. The greater is the electro-donor ability [mostly measured in terms of the donor number (DN)] of the solvent, the greater is the extent of solvation of the salt by the solvent. For instance, donor number of EC is 16.4 and that of PC is 15.1, therefore Li^+ ion is strongly complexed in EC than in PC [317]. Out of several solvents such as EC, PC, diethyl carbonate (DEC), dimethylformamide (DMF) etc., particularly EC shows the highest dielectric constant value of 95.3. Various parameters are given in Table 4.1 [318]. So it can be used for the synthesis of polymeric gel electrolytes, but as can be seen from the Table 4.1, EC suffers by two major problems from application point of view.

Table 4.1: Comparisons of various parameters of the solvents.

Solvent	Dielectric Constant (ε) 25^0C	Viscosity (η) (cSt) 25^0C	Boiling Point (^0C)	Melting Point (^0C)	Conductivity (S cm^{-1})
EC ($C_3H_4O_3$) F. wt = 88.06	95.3	1.406 (40^0c)	248	36.2	11.63 x 10^{-3}
PC ($C_4H_6O_3$) F. wt = 102.09	65.1	2.093	241-242	-48	7.96 x 10^{-3}
EC : PC (1:1 v/v)	80.2	1.696	-	-	9.35 x 10^{-3}

Firstly, the melting point of pure EC is relatively high ($\sim36.2^0C$), which reduces the conductivity of the electrolytes at low temperatures. Secondly, there is an absence of pure liquid phase for the electrolytes at lower concentrations of the salts, say less than 0.6 M concentration [317, 319]. Due to the above limitations, we have to go for some compromise with the pure EC solvent and seek some binary solvent as a substitute. For the purpose PC has been used, which fulfils the requirement and act as a good binary solvent. Hence the mixture of EC and PC shows the good agreement by possessing the intermediate characteristics of the two solvents (Table 4.1). The melting point and boiling point depends on the ratio of EC and PC solvents, but always lie in between the two. Thus the combination of all the above factors made us to choose binary solvent EC-PC (1:1 V/V) for the preparation of liquid electrolytes.

In order to optimise the molar concentration of the salts in liquid electrolytes, the conductivity measurements were performed at room temperature, by varying the concentration of salts from 0.1 M to 2.0 M in the solvent mixture of EC:PC (1:1 V/V). Fig. 4.1 shows a general trend of conductivity variation with respect to molar concentration of salts. It has been observed for all the liquid electrolytes that initially the ionic conductivity increases with the increase in salt concentration upto 1.0 M concentration of each salt, thereafter the conductivity either remains constant or starts decreasing at about 2.0 M concentration of each salts. Further increase in the salt concentration leads to the decrease in conductivity of the liquid electrolyte. The above behaviour of the liquid electrolyte can be explained in the following manner. Initially, as the salt concentration increases, the number of free mobile ions also increases, which leads to the increase in conductivity. At higher concentrations of the salt, ion-aggregation is likely to play a major role in limiting the ionic conductivity of the electrolyte [315, 316]. Finally we have chosen EC:PC (1:1 V/V) – 1.0 M salts (LiClO$_4$, NaClO$_4$ and TEAClO$_4$) as liquid electrolytes for the synthesis of polymeric gel electrolytes.
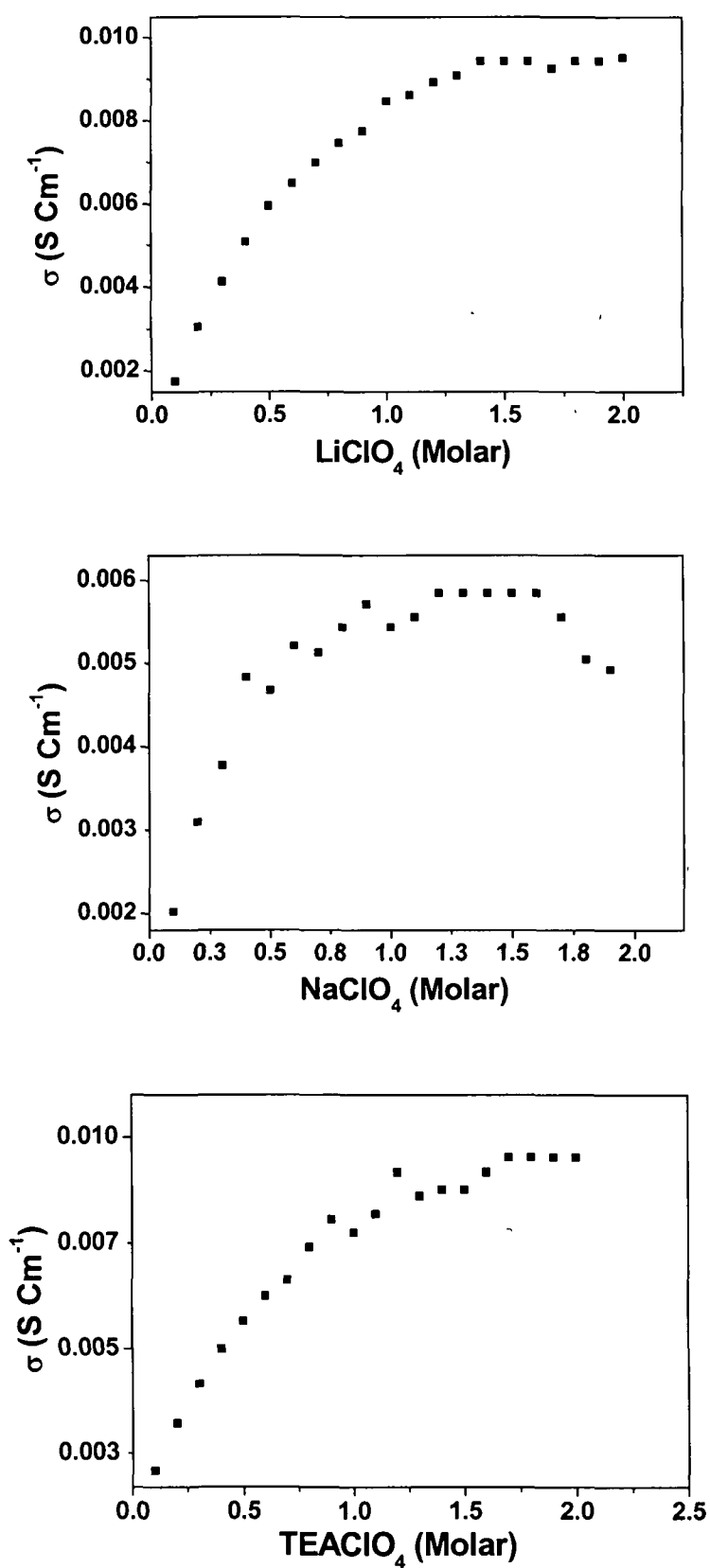
Fig 4.1: Variation of Electrical conductivity as a function of varying salt concentration in the solvent mixture EC:PC (1:1 V/V).

4.1.2 Composition Dependence of Electrical Conductivity: Polymer Gel Electrolytes

As it is well established that in the polymeric gel electrolytes, liquid electrolytes are immobilized in a polymer matrix in which the polymer acts as a container and gelling agent for liquid electrolytes and imparts high viscosity to the liquid electrolyte without affecting its ionic conductivity significantly [123, 320]. It is also important that upon incorporation of any polymer in non-aqueous liquid electrolyte, the resulting homogeneous gel should possess a mechanical stability comparable to that of solid electrolyte and simultaneously should retain a room temperature ionic conductivity of the order of 10^{-3} S cm^{-1}, which is comparable to that of liquid electrolytes [164, 321-323]. Further it is well known that the ion conduction in polymer electrolytes is confined to the amorphous regions of the polymeric material and that any tendency to crystallization leads to the decrease in ionic conductivity [147, 324]. In view of the above facts, in present investigations two polymers, namely, poly(vinylidene fluoride–hexa fluoro propylene) (PVdF-HFP) and poly (methyl methacrylate) (PMMA) have been selected as they possess larger content of amorphicity and have many of the desired above mentioned properties. The chemical structure of these polymers along with their other properties, are shown in Table 4.2.

Table 4.2: Polymers used in the present studies and their different characteristics:

PMMA	COOCH$_3$ | —(CH$_2$—C)$_n$ | CH$_3$	Molecular Weight = 1,20,000	$T_g = 114°C$.
PVdF-HFP	H F F CF$_3$ —(C—C)$_m$—(C—C)$_n$— H F F F	Molecular Weight = 4,00,000	$T_m = 140\text{-}145°C$.

PVdF alone has high degree of crystallinity due to the presence of single monomer throughout the polymer chain, which provides less free volume to the mobile ions, resulting in lower conductivity. In order to create disorder or amorphicity in PVdF polymer, another monomer HFP is introduced. Introduction of HFP in PVdF leads to the higher amorphicity in the copolymer due to the steric hindrance provided by CF_3 pendant group in HFP monomer units which is randomly mixed with the VDF ($-CH_2CF_2-$) monomers in the polymer chain. Higher amorphicity provides mobile ion greater free volume giving rise to higher conductivity. Apart from providing good mechanical stability to the electrolytes, the polymer plays a passive role in conduction and acts as a stiffener for the solvent which solvates the salt and also provides a continuous conduction path through the solvent for ion migration [320].

PMMA is a thermoplastic polymer, which act as a framework for gel electrolytes. It is an atactic polymer having an amorphous morphology that imparts a mechanical strength and dimensional stability to the gel electrolytes. Incorporation of PMMA polymer in liquid electrolytes enhances its macroscopic viscosity by several orders of magnitude thereby imparting mechanical stability to the system. Since the decrease in conductivity occurs only by a factor and not by an order, it is assumed that polymer addition does not alter the conduction mechanism that prevails in liquid electrolyte significantly. In view of the above mentioned properties of both the polymer viz. PVdF-HFP and PMMA, they are chosen as a host polymer matrix for the preparation of polymeric gel electrolytes.

Hence in the present studies the compositions of (PVdF-HFP / PMMA)-EC-PC-salts ($LiClO_4$, $NaClO_4$ and $TEAClO_4$) based gel electrolytes are first optimized to get high ionically conducting and mechanically stable materials. Fig 4.2 shows the typical variation of electrical conductivity (σ) of the gel systems as function of polymer content in liquid electrolytes (EC-PC-salts). The similar pattern of variation has been observed for the other polymeric gel
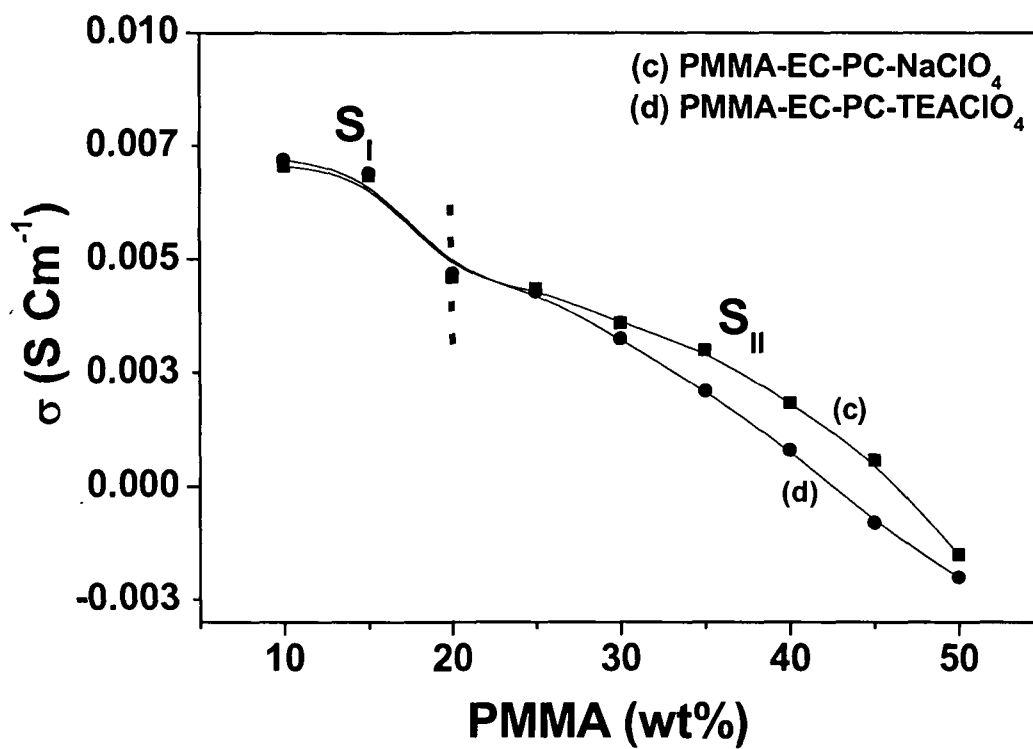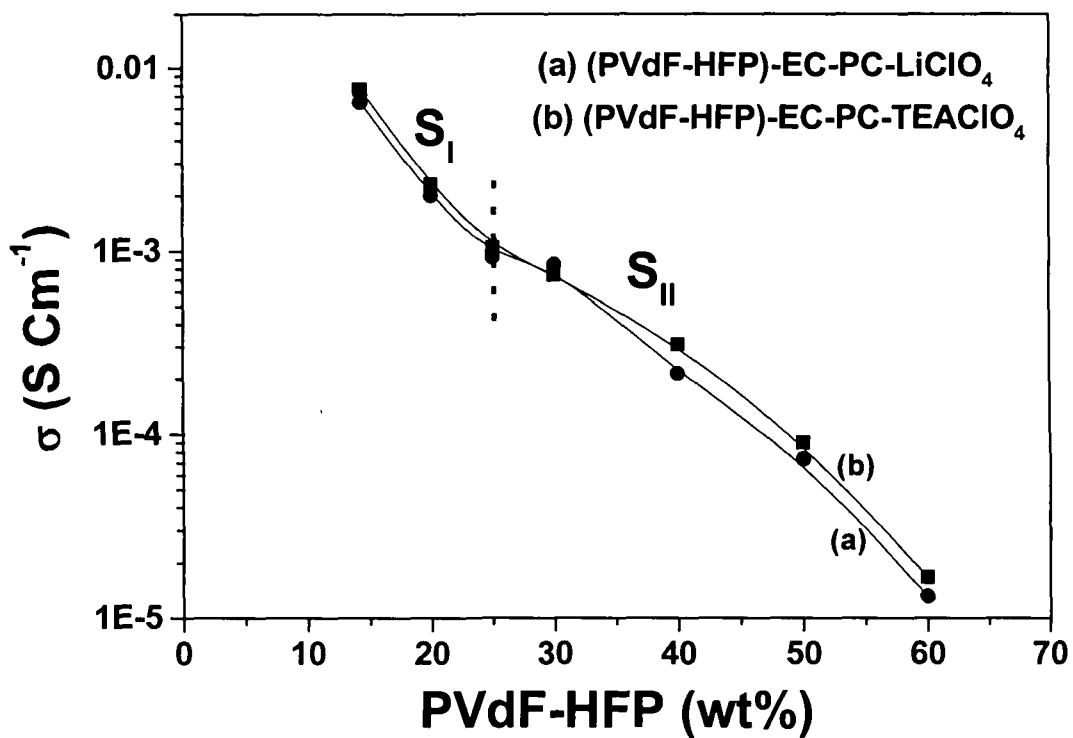
Fig 4.2: Effect of polymer addition on the ionic conductivity of gel electrolytes.

electrolytes under present investigation. The values of σ decrease substantially due to the addition of the host polymer PVdF-HFP or PMMA. The variation in conductivity can be divided in two regions S_I and S_{II} as indicated in Fig. 4.2. The decrease in conductivity in the lower polymer concentration region i.e. region S_I is steep as compared to higher polymer region S_{II}. This indicates that only a partial amount of liquid electrolyte could be utilized in gel formation while the excess of it remains phase separated in the region S_I (i.e. below 25 wt% PVdF-HFP content and below 20 wt% PMMA content). On addition of the host polymer beyond ~25 wt% for PVdF-HFP system and ~20 wt% for PMMA system, liquid electrolytes are fully utilised in the gel formation. On further addition of the host polymer, stiffening of the gel electrolytes occur which results in the continuous decrease in conductivity.

Further, an important point may be noted that the electrical conductivity of the gel electrolytes containing even upto 10 wt % of the host polymer is slightly higher than that of the liquid electrolytes, EC-PC-salts systems (Fig.4.2). Similar observations have recently been obtained and systematically studied by Chandra and co-workers [325, 326] in a different system of PMMA based gel electrolytes. Such observations have been found to be in full agreement with the "Breathing Chain model" proposed by Chandra et al [325, 326]. According to this model, polymeric gel is considered to consist of dissociated ions (free ions), ion pairs, undissociated ions, solvents and polymeric chains (folded or partially/fully unfolded chain). At low polymer concentration, the system behaves as a liquid electrolyte as a result of dissociation of salts. With an increase in polymer concentration, viscosity comes into picture and it tends to decrease conductivity by effectively decreasing the mobility of free ions. However, a competitive phenomenon is assumed to occur at microscopic level. The polymer chain 'breathes' while it opens or folds occupying different volumes in the process at different time span. Therefore folding and unfolding of polymeric chains lead to localized pressure

fluctuations in the surrounding volumes and this localised turbulent pressure leads to the dissociation of ion pairs and enhance mobility [325, 326].

The final compositions of the gel electrolytes, PVdF-HFP or PMMA (20 wt%)-EC:PC (1:1 V/V) - 1.0 M $LiClO_4/NaClO_4/TEAClO_4$ salts, were chosen for the construction of different supercapacitors (described in chapters 5 and 6). All these electrolytes possess the conductivity of the order of 10^{-3} S cm^{-1} at room temperature with good mechanical strength in the form of freestanding films for PVdF-HFP based gel electrolytes and flexible as well as semitransparent lump materials for PMMA based gel systems. This order of conductivity is acceptable for use in supercapacitors fabrication, as they offer low resistance, when used in the form of thin films of thickness about 100-200 micron.

4.1.3 Temperature Dependence of Electrical Conductivity: Polymer Gel Electrolytes

From the application point of view, one of the most important properties of solid electrolyte is the temperature dependence of the d.c. conductivity σ (T). The main objective of the present studies is to check the suitability of the polymeric gel electrolytes in different electrochemical devices such as supercapacitors over a substantial temperature range as these devices are normally required to be operated over a temperature range, from below freezing point to about $90^{0}C$ or so [327]. Generally the polymeric materials show some peculiar type of characteristics. The σ (T) curves for most of the polymer electrolytes show one of the five patterns of behaviour [72]:

- Vogel-Tamman-Fulcher (VTF) behaviour throughout the available temperature range, in which σ vs. 1/T plot shows a curved nature.

- Arrhenius behaviour for low temperatures showing linear σ vs. 1/T plot and VTF behaviour at higher temperatures.

- Arrhenius behaviour throughout, but with two different activation energies, high E_a closer to glass transition temperature, T_g, and a smaller E_a at higher temperatures.

- VTF behaviour for temperatures slightly greater than T_g, but Arrhenius behaviour at higher temperatures.

- Behaviour, which is very unlike either Arrhenius or VTF at all temperatures.

The temperature dependence of electrical conductivity i.e., σ vs. $1/T$ for all the polymeric gel electrolytes under present studies are shown in Fig. 4.3. As can be seen from the figures, the temperature dependence of conductivity indicates an activated process. Conductivity increases with increasing temperature and the Arrhenius behaviour often provides a good representation of the data [72, 73, 328]. On having minute inspection, it can be observed in the figure that there is a change in slope and curvature of the σ vs. $1000/T$ plots for all the polymeric gel electrolytes in present studies. This particular behaviour i.e. non-linearity of conductivity plots is typical of highly viscous and amorphous polymeric electrolytes [126, 147, 329]. When conductivity is plotted in Arrhenius coordinates, we may observe the pattern either straight or curved lines, which can be fitted in Arrhenius or Vogel-Tamman-Fulcher (VTF) forms [72, 147, 319, 328].

Arrhenius Equation $\quad \sigma = \sigma_0 \exp(-E_a/KT)$ $\qquad$ ....(4.1)

VTF Equation $\quad \sigma\, T^{1/2} = \sigma_0 \exp[-B/K\,(T-T_0)]$ $\qquad$ ....(4.2)

where, E_a is the activation energy of conduction in Arrhenius form, T_0 is the "ideal or equilibrium" glass transition temperature i.e. the temperature at which the free volume extrapolates to zero, σ_0 is pre-exponential factor, related to the number of charge carriers and k is the Boltzmann constant. B is a constant, whose dimensions are infact that of energy which is not simply interpreted as an activation term. VTF equation is basically an empirical
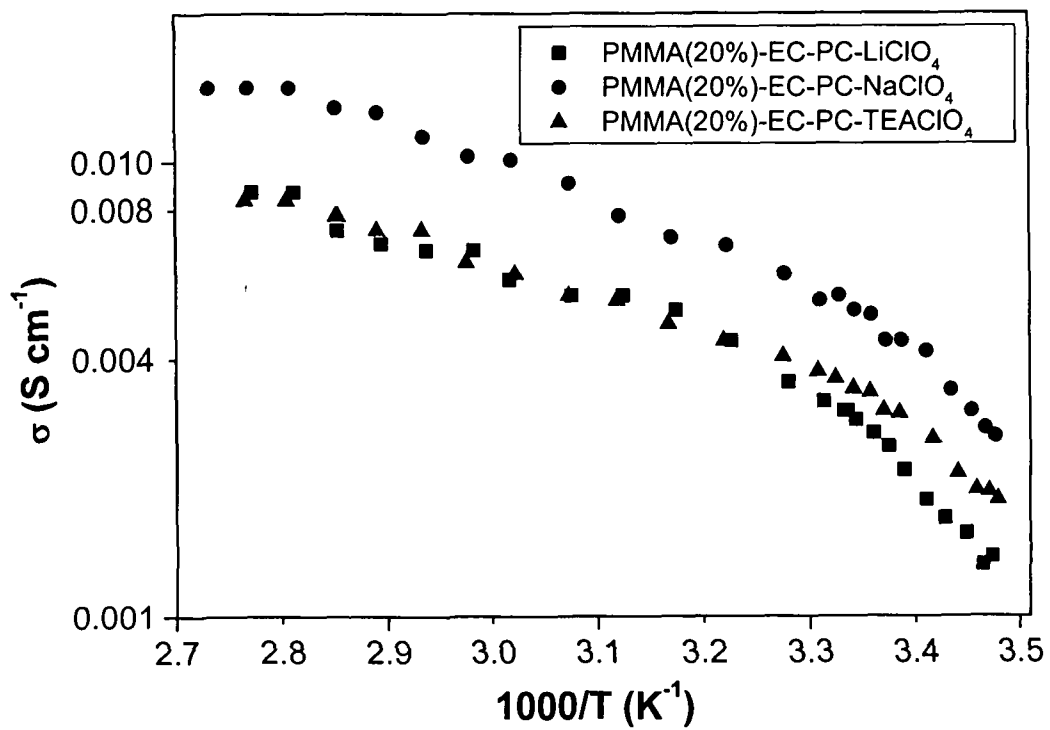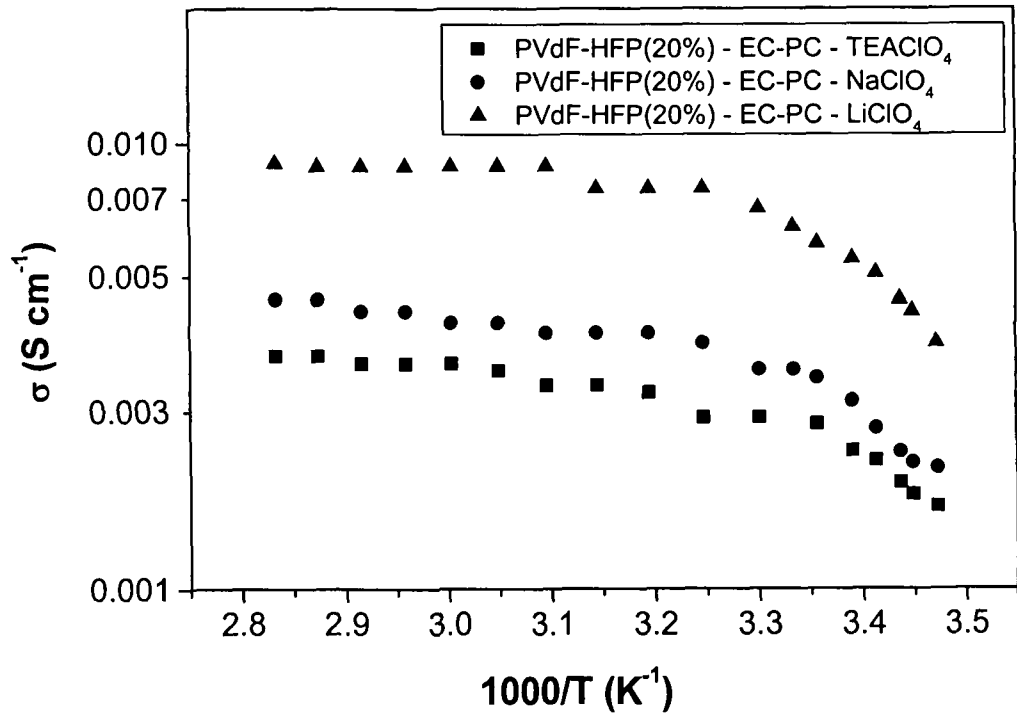
Fig 4.3: Temperature Dependence of electrical conductivity of the polymer gel electrolytes.

generalization, which is based on the free volume model and describes the temperature dependence of ionic conductivity adequately [72, 75, 328]. Free Volume model was given by Cohen and Turnbull [330], according to which the ionic motion is supposed to be a non-thermally activated process and occurs as a result of redistribution of free volume within the material. By increasing the temperature, the segmental motion of the polymeric materials gives rise to enhancement in the ion motion by making and breaking the coordination sphere of the solvated ion and by providing the local voids i.e. free volume which are generally created by the expansion of the polymeric materials into which the ion may diffuse under the influence of an electric field [96].

This phenomenological model is based on the considerations involving the critical role of the glass transition temperature (T_g) and of the so-called equilibrium glass transition temperature (T_0). Above T_g, the polymeric material becomes microscopically rubbery rather than glassy [328]. This can be well understood by considering that the local environment of any given polymer chain becomes liquid like at the glass transition temperature. Hence it is only the thermal energy, which in excess of the glass transition temperature provides the actual mobility of the local polymer chain segments. Thus the Arrhenius behaviour involving the inverse of the temperature is replaced by the VTF equation, which involves the inverse of $T - T_0$, where T_0 is the temperature at which all the free volume of the materials vanishes or at which all polymer segmental motion disappears. Generally T_0 lies 40-50 K below the actual glass transition temperature T_g [315, 316].

In the case of liquid electrolytes, cations and anions move with their solvent sheath intact and charge transport is related to the macroscopic viscosity of the electrolyte. Whereas in the case of gel electrolytes, which encompass high molecular weight polymers, the ion-transport is decoupled from the macroscopic viscosity of the electrolyte. The polymer chains

become increasingly entangled and cannot therefore move to a long distance with the ions [75].

In this case one point should be noted that the VTF model describes the motion of the polymer

chains whereas the conductivity refers to the migration of charged species i.e. the ions

introduced by the presence of salt. The ionic diffusion is closely related to the polymeric

motions but they are not exactly the same, as the pure polymer does not conduct, so that the

VTF behaviour for the ions does not immediately follow from the VTF behaviour for the

polymer [72].

In this regard, conductivity studies have been performed by Bohnke and co-workers

[147, 320] by varying the different weight ratios of the polymeric materials. They showed that

as the polymer is added, the effective area/length of the high conductivity path decreases.

Consequently, T_g, σ_0 and B (activation energy of conduction) increase and T_0 decreases.

Decrease in ionic conductivity was observed to be very small for gels containing less than 30

wt% of polymer. Whereas for gels with higher polymer content (greater than 30 wt% of the

polymer), the ionic conductivity decreases very rapidly. Gel electrolytes with lower polymer

content (less than 30 wt%) can be conveniently regarded as the liquid electrolytes encaged in a

polymer matrix. Ions can easily migrate through the solvent domain surrounding the polymer

matrix. As the activation energy increases very slightly upon addition of polymer, it was

concluded that the ion-migration is not severely influenced by the addition of polymer content.

These assumptions lead to a very small decline in conductivity upon polymer addition upto 30

wt%. All the polymeric gel electrolytes under present investigations as shown in the Fig. 4.3

exhibit distinct curved profiles thereby rendering them to be non-Arrhenius in nature and

therefore conductivity behaviour can be best expressed using the VTF equation. The

interconnection between Arrhenius and VTF conductivity versus temperature behaviour are

widely reported and discussed in literature [72]. The ionic conductivity for all polymer gel

electrolytes investigated in present studies increases as a function of temperature over the entire temperature under present studies. Conductivity increment occurs utmost by an order of magnitude. No colossal enhancement in conductivity was observed over the entire temperature range (280-370 K). This is an important and most advantageous property of polymeric gel electrolytes to be used in supercapacitors like devices. Lesser the magnitude of the change associated with the ion conducting properties of polymer electrolytes with temperature, greater is the feasibility for their useful practical applications.

4.2 Electrochemical Stability of Polymer Gel Electrolytes

The electrochemical stability of the electrolytes, which limits the working voltage range (i.e. electrochemical potential window) of the devices, including supercapacitors, is an important aspect to be evaluated. The potential windows of different gel electrolytes, in the present studies, were estimated by linear sweep voltammetry using symmetrical stainless steel like almost inert electrodes with two electrodes configuration. Fig. 4.4 illustrates the linear sweep voltammograms of different gel electrolytes at a voltage scan rate 2 mV sec^{-1}. The
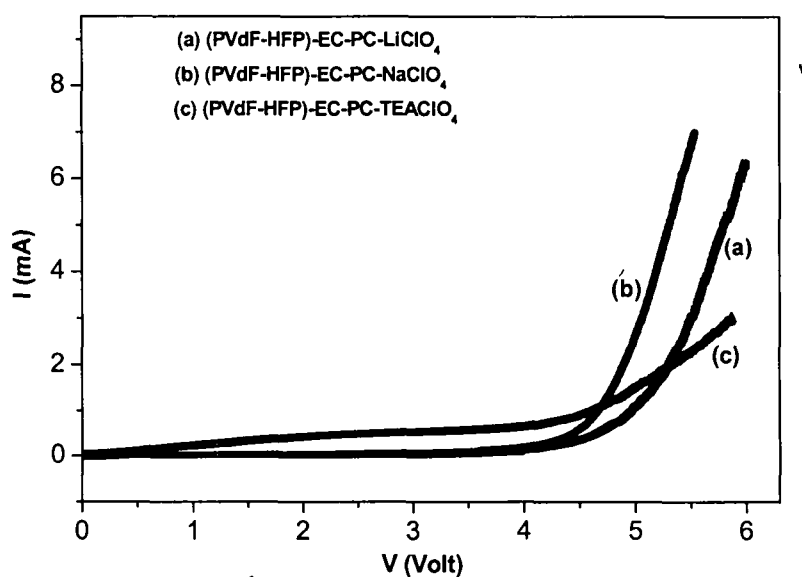
Fig 4.4: Linear sweep voltammograms of different gel electrolytes with two-electrode configuration of stainless steel at scan rate 2 mV sec^{-1}.

observed I-V characteristics are the combined effect of anodic and cathodic responses for the two electrodes configuration (Fig 4.4). For all the gel electrolytes under present studies, the values of current goes on increasing gradually with the increase in the applied voltage across the cells upto a certain voltage, which is termed as "Electrochemical Potential Window or Working Voltage", after that point current increases abruptly as shown in the Fig. 4.4. The abrupt increase in current takes place due to the decomposition of the electrolytes. It provides the information regarding the voltage level upto, which the electrolyte can function properly and safely. Almost all the gels under present studies show the same working voltage range (~ 4 V). The potential range of the electrochemical stability of liquid electrolytes is larger (> 4 V) as compared to that of the solid electrolytes. The wider range of working voltage is indicative of the liquid like characteristics of the gel electrolytes under present investigations.

4.3 Transport Number of Polymer Gel Electrolytes

As described earlier, the transport number is defined as the net number of moles of an ion that cross a reference plane fixed with respect to the solvent when one Faraday of current is passed between the electrodes. In pure polymeric systems, the transport number helps in distinguishing the ionic contribution from the electronic contribution towards total current. Total ionic transport number "t_{ion}" for all the gel electrolytes under present studies are determined using "Polarization method" as described in chapter 3, section 3.2.1.2 (b). The polarisation current versus time plots for all the polymeric gel electrolytes in present studies are shown in Figs. 4.5 and 4.6. The voltage applied across the cells was kept well within the electrochemical stability range of all the polymeric gel electrolytes. In the present case it has be chosen to 0.5 V. The values of ionic transport number have been evaluated using mathematical expressions 3.41 (chapter 3) and are listed in Table 4.3.
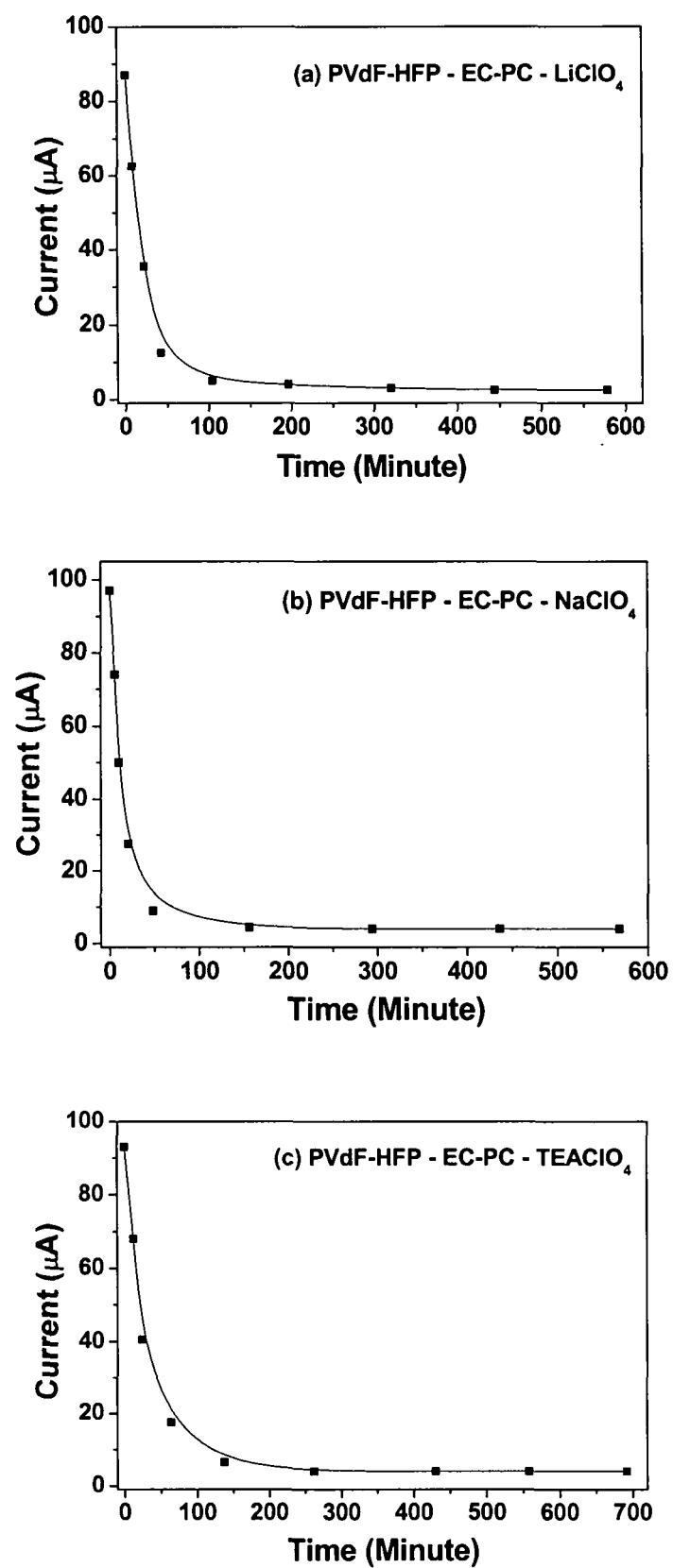
Fig 4.5: Polarisation Current as a function of time for different polymer gel electrolytes (Applied Voltage ~0.5 V).
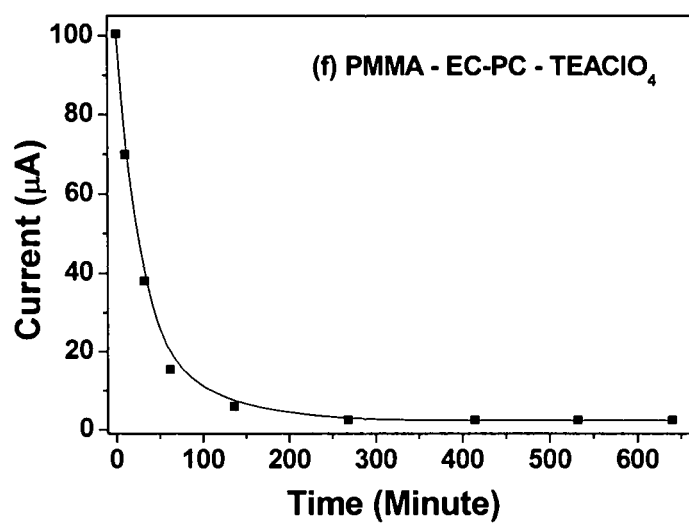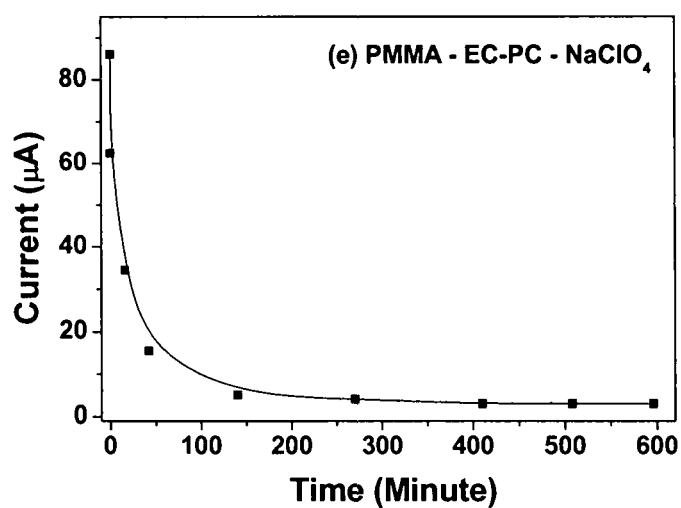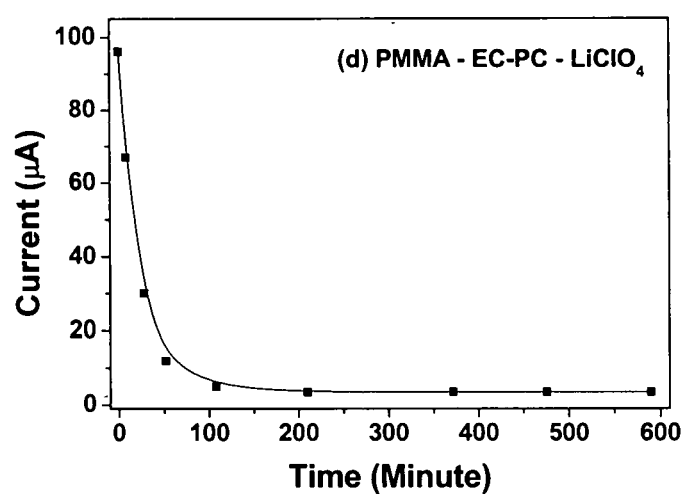
Fig 4.6: Polarisation Current as a function of time for different polymer gel electrolytes (Applied Voltage ~ 0.5 V).

From the Figures 4.5 and 4.6, it can be calculated that the values of transport number for all the polymeric gel electrolytes are in the range of 0.96-0.98, which shows that the charge transport is mainly due to the contribution of ions.

Table 4.3: Ionic transport number of different polymeric gel electrolytes.

Polymeric Gel Electrolyte Systems	Ionic Transport Number (t_{ion})
PVdF-HFP (20 wt%)-EC:PC (1:1 V/V)-1.0 M LiClO$_4$	0.97
PVdF-HFP (20 wt%)-EC:PC (1:1 V/V)-1.0 M NaClO$_4$	0.96
PVdF-HFP (20 wt%)-EC:PC (1:1 V/V)-1.0 M TEAClO$_4$	0.96
PMMA (20 wt%)-EC:PC (1:1 V/V)-1.0 M LiClO$_4$	0.96
PMMA (20 wt%)-EC:PC (1:1 V/V)-1.0 M NaClO$_4$	0.97
PMMA (20 wt%)-EC:PC (1:1 V/V)-1.0 M TEAClO$_4$	0.98

4.4 Conclusions

Combining all the above results, we may conclude that:

- 1M concentration of each salts i.e. LiClO$_4$, NaClO$_4$ and TEAClO$_4$ in binary solvent EC:PC (1:1 V/V) is sufficient for the preparation of polymeric gel electrolytes in order to achieve maximum conductivity of the order of 10^{-3} S cm^{-1} at room temperature.

- 20 wt% of the polymer content i.e. PVdF-HFP as well as PMMA is sufficient in order to achieve the acceptable value of conductivity of the gel electrolytes with good mechanical properties.

- All the polymer gel electrolytes show a wide electrochemical stability of ~ 4 Volt, indicative of liquid like behaviour.

- The ionic transport number 't_{ion}' has been found to be in the range of 0.96-0.98, which shows that the charge transport in the gel electrolytes is predominantly ionic in nature.

- The temperature dependence of electrical conductivity (i.e. σ vs 1/T) plots show the VTF behaviour over a temperature range of 280-370 K indicating that the polymeric gel electrolytes are thermally stable.

- All the polymeric gel electrolytes investigated are flexible enough to mould in the desirable area and thickness. The order of conductivity (10^{-3} S cm^{-1}) is also acceptable for use in supercapacitors application as they offer low resistance. Being the flexible materials, they are able to form proper interfacial contacts for the maximum accessibility of the active electrode materials.

Chapter – 5

Studies on Electrical Double Layer Capacitors (EDLC's) using Activated Charcoal Powder Electrodes and Polymeric Gel Electrolytes

STUDIES ON ELECTRICAL DOUBLE LAYER CAPACITORS (EDLCs) USING ACTIVATED CHARCOAL POWDER ELECTRODES AND POLYMERIC GEL ELECTROLYTES

As described in chapter 2, there exist two types of electrochemical supercapacitors, viz., electrical double layer capacitors (EDLCs) and redox supercapacitors, classified on the basis of nature of electrode materials employed and charge storage mechanism at the electrode-electrolytes interfaces [201, 203, 204, 206]. Particularly in EDLCs, various types of carboneous materials namely: activated carbon powder / fibres / fabrics [206, 211, 212, 331], activated carbon composites [332], carbon black [331], graphite powder / paper [211, 331], glassy carbon [203, 333], carbon aerogel [203, 334] etc. are reported to be employed for the construction of EDLCs. The activated charcoal powder, used in the present investigations, is a cheap and abundantly available material on the commercial scale, which is mostly used for medical purposes particularly as adsorbent of particles and gases in the body's digestive system. Its electrical properties such as high conductivity with large specific surface area make a possibility to use it as electrode material for the fabrication of cost effective EDLCs with almost same charge/power storage capability as compared to the reported devices based on other carboneous electrode materials.

Most of the EDLCs reported in literature are based on liquid electrolytes such as: PC-LiClO$_4$, aqueous KCl, KOH, H$_2$SO$_4$ solutions, acetonitrile solution with TEABF$_4$, PC-TEABF$_4$, etc. [201, 203, 204, 206]. These offer well-known disadvantages of:

- bulky design
- corrosion
- self-discharge
- electrolyte leakage, etc.

A major attention has recently been devoted by researchers globally to construct all-solid-state supercapacitors based on polymer/gel electrolytes [201, 203, 206, 211, 212, 332]. Such electrolytes play a common role of high ionic conductor and a separator along with their advantageous mechanical properties including high flexibility for proper electrode-electrolyte contact and ability to form thin films of desirable area. The all-solid-state EDLCs are not widely reported except a few recent reports which include the capacitors employing different polymer/gel electrolytes, for example PVdF-EC-PC-TEABF$_4$ [212], PMMA-PEO-PC-tetra alkyl ammonium salts [209], Nylon 6-H$_3$PO$_4$ [207], PVA-H$_3$PO$_4$ [206, 211], PEO-PEG-LiCF$_3$SO$_3$ [206, 211], potassium poly (acrylate)-KOH [332], etc. Some reports on EDLCs are based on "solvent-free polymer electrolytes" (Chapter 2, Table 2.4). These electrolyte offers generally lower electrical conductivity and less flexibility due to the use of poly (ethylene oxide) (PEO) like polymers, which contains substantially larger proportion of crystalline backbone. Some reports also exist based on different polymeric gel electrolytes, which have many advantageous properties, as described in chapter 4. The gel electrolytes show the combination of liquid like behaviour offering high electrical conductivity ($\sim 10^{-3}$-10^{-2} S cm^{-1}) with wider electrochemical potential window and solid like behaviour mechanically with high degree of flexibility suitable for proper electrode-electrolyte contact in supercapacitors / batteries like electrochemical devices. The polymeric gel electrolytes, therefore, are observed to be the most suitable substitute of liquid electrolytes as well as solvent free polymer electrolytes for the fabrication of supercapacitors.

The present chapter is devoted to the fabrication and characterization of solid state electrical double layer capacitors (EDLCs) based on activated charcoal powder as electrodes with the optimized ion conducting polymeric gel electrolytes having compositions (PVdF-HFP) or PMMA-EC-PC-salts, LiClO$_4$, NaClO$_4$ and (C$_2$H$_5$)$_4$NClO$_4$ (TEAClO$_4$). Details of the

131

preparation of flat electrode sheets of activated charcoal on carbon papers are given in Chapter-3, section 3.2.2.1. Details of the preparation and optimisation of the polymeric gel electrolytes are described in Chapter-4. These electrolytes are mechanically stable, highly flexible in the form of films and lumps offering high electrical conductivity and wider electrochemical potential window.

Six different EDLCs cells were constructed using the activated charcoal (AC) electrodes and the optimised polymeric gel electrolytes.

Cell A: AC | PVdF-HFP (20 wt%)-EC:PC (1:1 V/V)-1.0 M LiClO$_4$ | AC

Cell B: AC | PVdF-HFP (20 wt%)-EC:PC (1:1 V/V)-1.0 M NaClO$_4$ | AC

Cell C: AC | PVdF-HFP (20 wt%)-EC:PC (1:1 V/V)-1.0 M TEAClO$_4$ | AC

Cell D: AC | PMMA (20 wt%)-EC:PC (1:1 V/V)-1.0 M LiClO$_4$ | AC

Cell E: AC | PMMA (20 wt%)-EC:PC (1:1 V/V)-1.0 M NaClO$_4$ | AC

Cell F: AC | PMMA (20 wt%)-EC:PC (1:1 V/V)-1.0 M TEAClO$_4$ | AC

The gel electrolytes based on different salts of varying size of cations (Li$^+$, Na$^+$ and TEA$^+$) with common anion (ClO$_4^-$) were employed for a comparative study to see the effect of cations on the capacitive behaviour of the EDLCs / supercapacitors.

The performance characteristics of capacitor cells under present studies have been carried out using:

- a.c. impedance spectroscopy,

- linear sweep cyclic voltammetry,

- galvanostatic charge-discharge, and

- prolonged cyclic tests

5.1   Results and Discussion:

5.1.1   Linear Sweep Cyclic Voltammetry

As described earlier, the linear sweep cyclic voltammetry is an important electrochemical technique to characterize the supercapacitors, either in three-electrode configuration generally in the case of liquid electrolytes based systems or in two electrode configuration in the case of solid state devices. This technique gives different information, including nature of charge storage at the individual interfaces in the anodic and cathodic regions or the overall behaviour of the cells, too. Figs. 5.1 and 5.2 show the linear sweep cyclic voltammograms (in two electrode configuration) for all the capacitor cells (A-F) at different scan rates. In such sweep-reversal (cyclic) voltammetry at constant scan rates, the profile of current response is ideally a rectangle when capacitance is constant (i.e. potential independent). On the other hand, a peaked structured voltammogram is observed in case of potential dependent capacitance showing a differential profile. In the present studies, the cyclic voltammograms for all the capacitor cells (A-F) show almost featureless characteristics. Voltammograms are almost close to an ideal shape of rectangle even for the higher scan rates (more than 100 mV sec^{-1}), as shown in Figs. 5.1 and 5.2. The featureless characteristics of voltammograms for all the capacitor cells indicate that the electron transfer between the electrode and the polymeric gel electrolytes occurs at a constant rate, giving a fairly perfect mirror image of the current responses about the zero-current line between the charging and discharging processes of the capacitor cells. At higher scan rates a slight deviation from the rectangular shape has been observed for each capacitor cell, which is attributed to a substantial value of equivalent series resistance also referred as ESR, practically present in real capacitors. The response of each capacitor cell has been found to depend on scan rates, which is the characteristic of capacitor cells [201, 335]. The capacitance values for all the capacitor cells, as

Fig.5.1:   Cyclic voltammograms of different EDLC cells (a) Cell A: AC | PVdF-HFP-LiClO₄-
gel | AC, (b) Cell B: AC | PVdF-HFP-NaClO₄-gel | AC and (c) Cell C: AC | PVdF-
HFP-TEAClO₄-gel | AC at different scan rates. Scan rates (in mV sec⁻¹) are marked
on the figures.
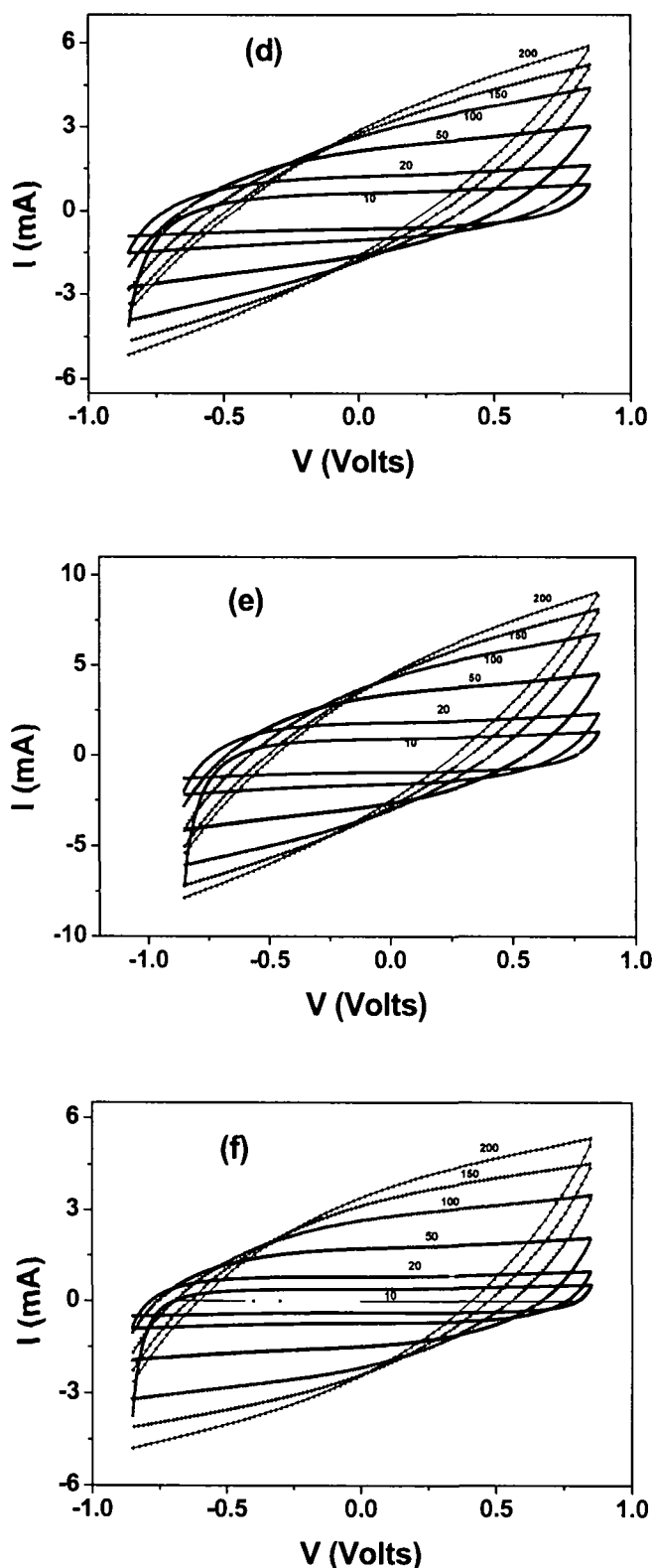
Fig.5.2:   Cyclic voltammograms of different EDLC cells (d) Cell D: AC | PMMA-LiClO₄-gel |
AC, (e) Cell E: AC | PMMA-NaClO₄-gel | AC and (f) Cell F: AC | PMMA-
TEAClO₄-gel \ AC at different scan rates. Scan rates (in mV sec⁻¹) are marked on
the figures.

calculated from the capacitive currents and scan rate (using eqn. 3.43), for different polymeric

gel electrolytes in the present studies, are in good agreement with the values obtained from the

charge-discharge measurements and impedance analysis (discussed later in section 5.1.2 and

5.1.3, respectively). The variation of capacitance values (evaluated using eqn. 3.43) as a

function of scan rates for all the capacitor cells (A-F) has been demonstrated in Fig.5.3. Initially
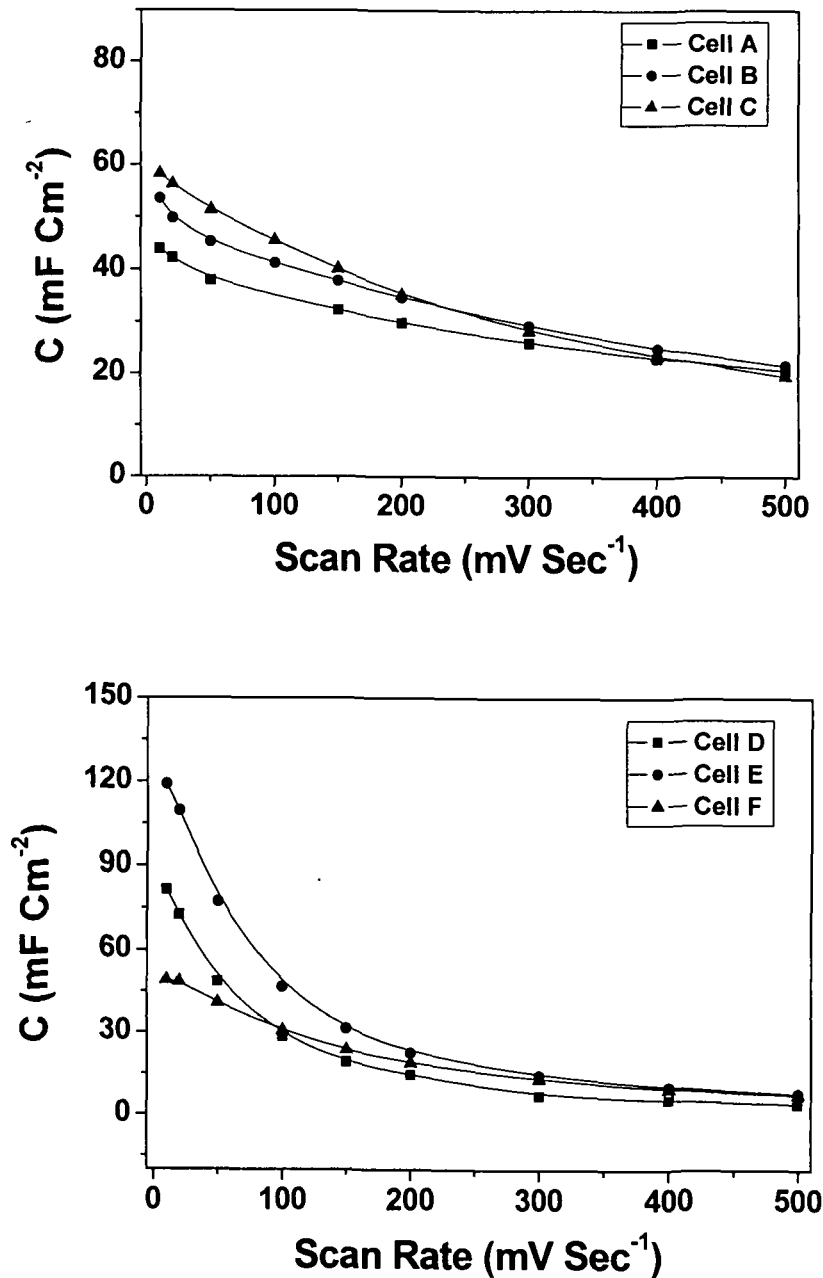
Fig.5.3: Variation of the capacitance of different EDLC cells as a function of scan rates.

a substantial decrease in the values of capacitance has been found at the lower scan rates. Thereafter almost stable and constant capacitance values have been observed even for higher scan rates which indicates the fast ion switching behaviour at the interfaces in such gel electrolytes based EDLCs. This confirms the suitability of gel electrolytes for their use in the fabrication of EDLCs / supercapacitors.

The reversibility for large number of charge-discharge cycles is one of the most important and attractive aspects of double layer capacitors over rechargeable batteries from the application point of view as an alternative/complementary power sources to the batteries. Fig. 5.4 depicts the variation of capacitance values as a function of voltammetric cycles
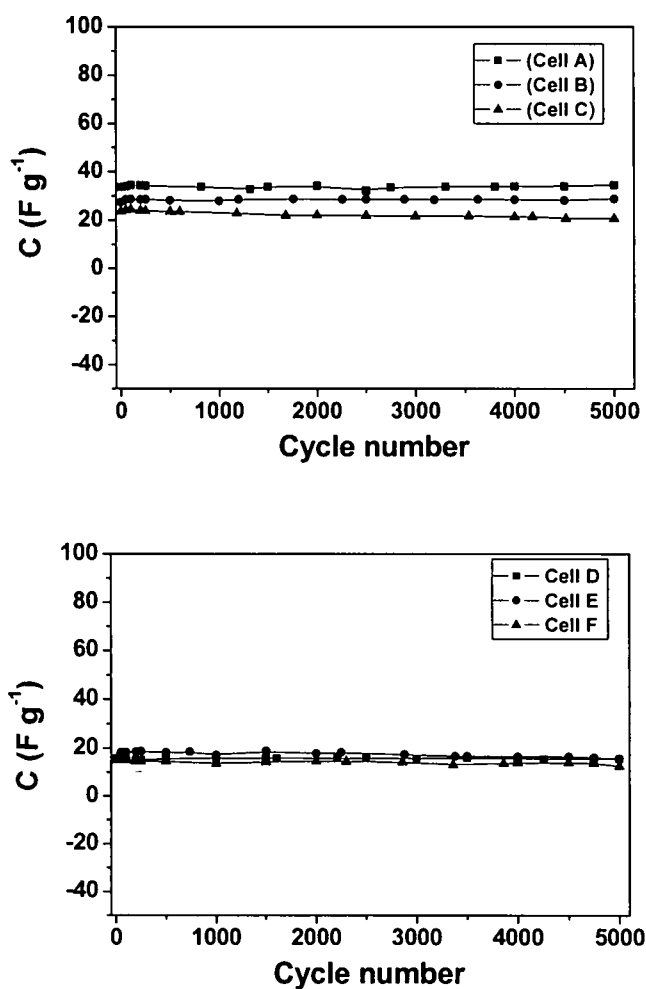
Fig.5.4:   Variation of the capacitance of different EDLC cells as a function of voltammetric cycles at a scan rate of 100 mV sec^{-1}.

137

between −850 mV and 850 mV recorded for all the capacitor cells (A-F) at a scan rate of 100 mV sec⁻¹. Reasonably stable and almost constant values of capacitance have been observed for each EDLC cells upto 5000 cycles, even more. A slight decrease (fluctuation) in capacitance values for a initial few cycles has been observed, which can be attributed to the irreversible charge consumption due to some faradic reaction(s) associated with possible oxidation and reduction of loosely bound surface groups (particularly hydroxyl group) at the electrode/electrolyte interfaces [201, 211].

5.1.2 Galvanostatic Charge Discharge Studies

Galvanostatic charge-discharge experiments have been performed for all the capacitor cells A-F. This is the most practical technique from the application point of view of capacitors as power sources. Figs. 5.5 and 5.6 show the typical charge-discharge characteristics of different capacitor cells at constant current. The cut-off voltage for the charging and discharging of the capacitor cells has been found to be ~1.0 V, which is within the voltage limit of electrochemical stability range of the gel electrolytes under the present studies. All the cells have been charged upto 1.0 V and the discharge characteristics have been found to be almost linear. This confirms the capacitive behaviour for all the cells (A-F) in the present studies. An initial sudden change in the voltage while charging and discharging of each cell has been observed, which is owing to the redistribution of charges within the pores of the electrode material apart from the ohmic loss across internal resistance (R_i, also referred to as equivalent series resistance, ESR) of the cells. The internal resistances have been calculated from these voltage drops. The discharge capacitance (C_d) values have been evaluated from the linear part of the discharge characteristics (Figs. 5.5 and 5.6) using eqn. 3.48. These values of internal resistance R_i and discharge capacitance C_d of different EDLC cells are listed in Tables 5.1 and 5.2. The values of the internal resistances and discharge capacitances of all the cells A-F have
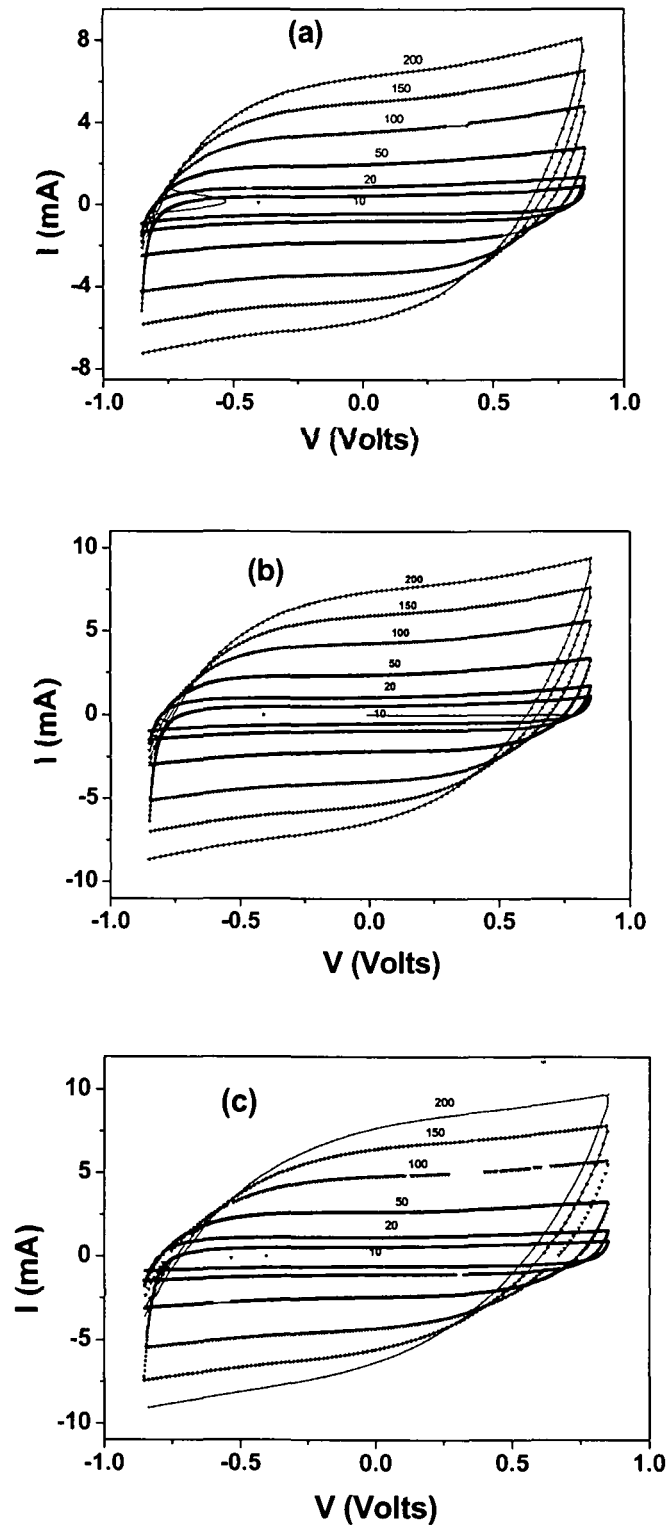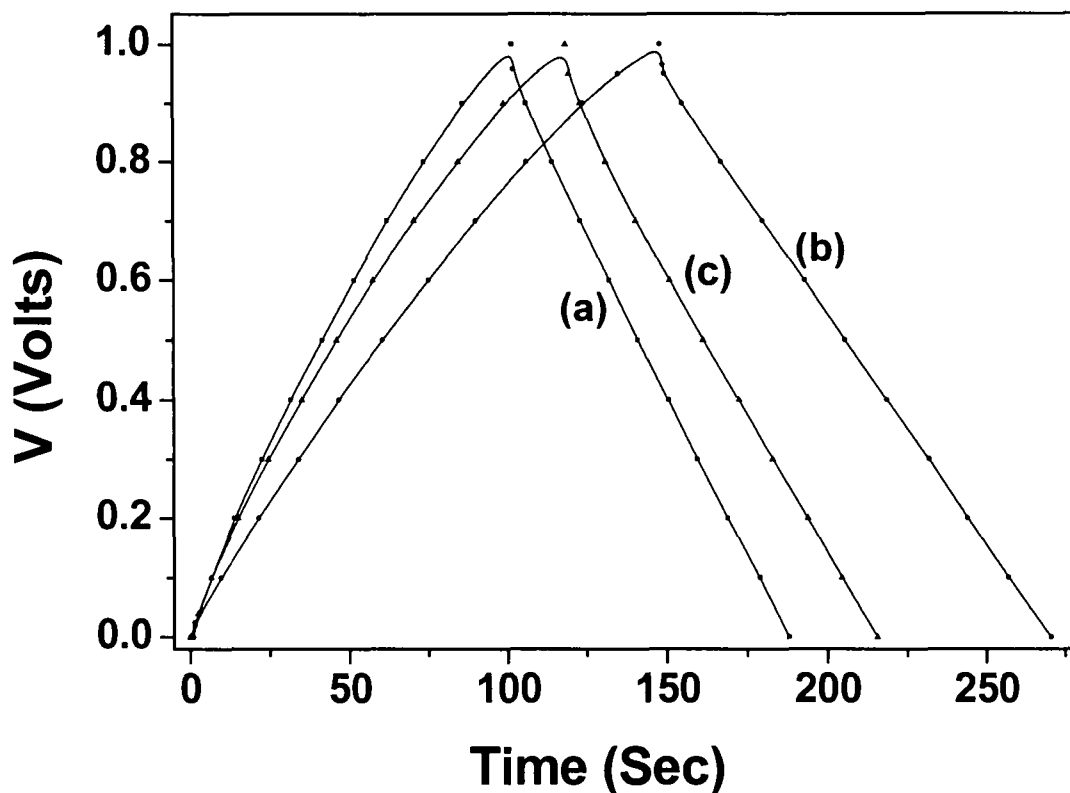
Fig.5.5: Charge-discharge curves of different EDLC cells (a) Cell A: AC | PVdF-HFP-LiClO₄-gel | AC, (b) Cell B: AC | PVdF-HFP-NaClO₄-gel | AC, (c) Cell C: AC | PVdF-HFP-TEAClO₄-gel | AC, at a constant current of 0.5 mA cm⁻².

Table 5.1. Typical charge-discharge characteristics of different capacitor cells at a current density of 0.5 mA cm^{-2}

Cells	R (Ω cm^2)	Discharge Capacitance, C_d (mF cm^{-2})*	(F g^{-1})**	Working Voltage (V)	Energy Density (Wh Kg^{-1})	Power Density (KW Kg^{-1})
A	90	44.89	43.80	1.0	6.1	0.26
B	70	64.71	47.06	1.0	6.6	0.20
C	110	53.3	38.07	1.0	5.3	0.20

* *Overall capacitance of the cells*
** *Single electrode capacitance*
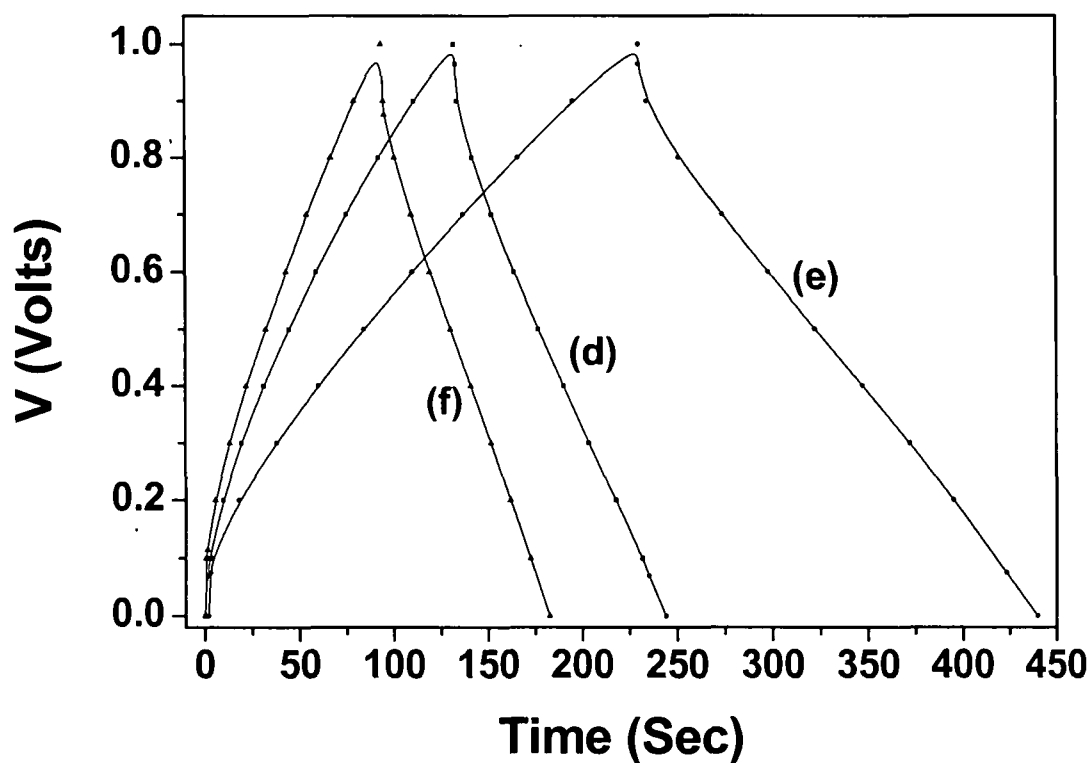
Fig.5.6: Charge-discharge curves of different EDLC cells (a) Cell D: AC | PMMA-LiClO₄-gel | AC, (b) Cell E: AC | PMMA-NaClO₄-gel | AC, (c) Cell F: AC | PMMA -TEAClO₄-gel | AC, at a constant current of 0.64 mA cm⁻².

Table 5.2: Typical charge-discharge characteristics of different capacitor cells at a current density of 0.64 mA cm⁻²

Cells	R $(\Omega\ cm^2)$	Discharge Capacitance, C_d (mF cm⁻²)*	(F g⁻¹)**	Working Voltage (V)	Energy Density (Wh Kg⁻¹)	Power Density (KW Kg⁻¹)
D	216	84.02	46.04	1.0	6.4	0.21
E	210	151.37	77.63	1.0	10.8	0.19
F	293	67.78	38.19	1.0	5.3	0.22

*   Overall capacitance of the cells
** Single electrode capacitance

been observed to be almost in the same range (Tables 5.1 and 5.2) and comparable with values obtained from the impedance studies (given later in Table 5.3).

Further, the value of discharge capacitance, C_d, has been found to almost stable after an initial slight decrease with the increasing current density for all the EDLCs under present studies (Figs. 5.7 and 5.8). Liu and Osaka [336] reported similar behaviour for capacitors, which comprised of PMMA-PAN-LiClO$_4$ gel electrolyte. This initial decrease is possibly attributed to charge consumption (loss) due irreversible possible reaction(s) while charging-discharging with loosely bound surface groups at the interfaces. The internal resistance, R_i, of each cell shows the similar trend of variation with substantial initial decrease with respect to the increase in current density. This indicates a substantial improvement in the electrode-electrolyte contacts at the interfaces at the higher current densities.

The coulombic efficiency (η) was calculated using eqn. 3.49 and its values were found to be in the range of 90-95% for all the capacitor cells, suggesting liquid like behaviour of all the polymeric gel electrolytes in the present studies. The energy and power densities of all the capacitor cells have also been evaluated and listed in Tables 5.1 and 5.2. The values of energy density of these solid state EDLCs, which are observed in the range of 5-10 Wh Kg^{-1}, are quite lower than the conventional rechargeable batteries. The limited working voltage range (i.e. ~1.0 V, observed in the present cases) appears to be the main reason of lower values of energy densities. The power densities, observed about ~0.2 kW Kg^{-1}, are higher values as compared to conventional batteries, but the values are lower than many reports on EDLCs based on liquid electrolytes. This is because of relatively higher values of ESR. Further investigations are still required in order to enhance the working voltage range, to reduce the ESR (internal resistance) and hence to enhance the power density by improving upon the electrode and electrolyte characteristics.
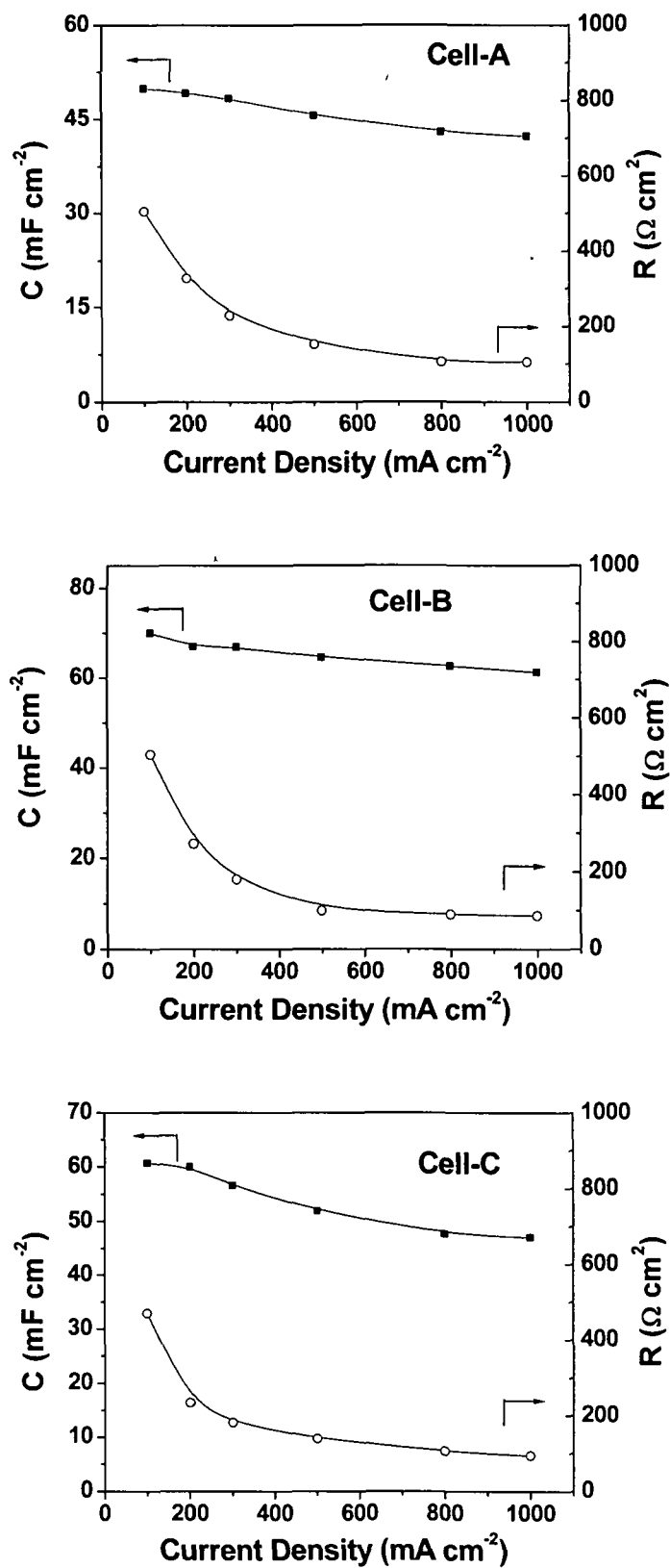
Fig. 5.7   Variation of discharge capacitance, C_d and internal resistance R_i of different capacitor cells, as a function of current density.
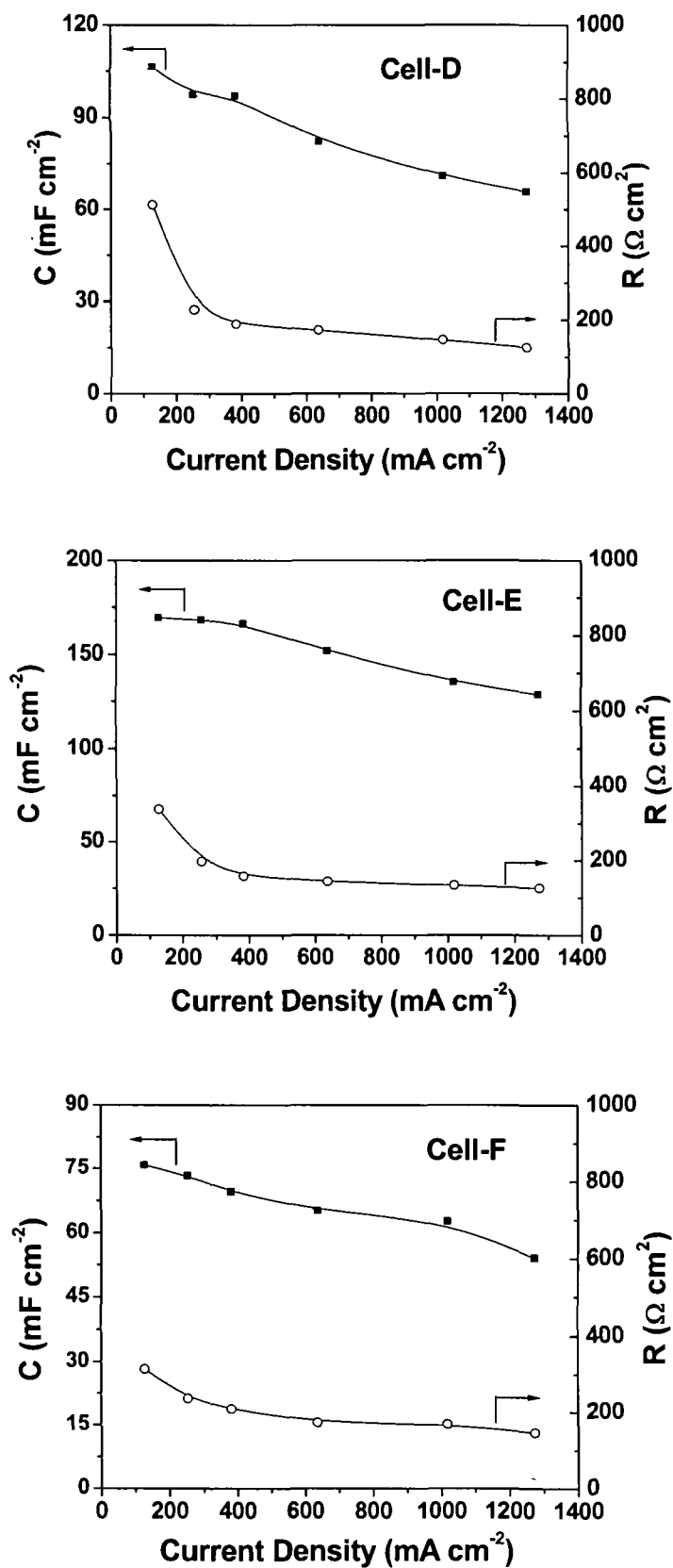
Fig. 5.8   Variation of discharge capacitance, C_d and internal resistance R_i of different capacitor cells, as a function of current density.

5.1.3 Impedance Spectroscopy

Figs. 5.9 and 5.10 show the typical impedance plots (also called as Nyquist plots), for all the capacitor cells (A-F). As mentioned earlier, impedance spectroscopy is a valuable technique for electrical characterization of supercapacitors, which enables the various parameters associated with bulk properties of electrolytes and electrode-electrolyte interfaces including equivalent series resistance (ESR) of overall capacitors, potential dependent faradic resistances, low frequency capacitance etc. to be evaluated separately in different frequency ranges [201, 206]. It should be noted that the impedance behaviour of an ideal capacitor is observed as straight line parallel to the imaginary axis of the complex impedance plots. But, in real capacitors, the steep rising capacitive impedance response is observed in low frequency region accompanied with high frequency semicircular features owing to the bulk and interfacial properties of the capacitor cells. In the present studies, the activated charcoal powder electrode material shows a capacitive behaviour with all the gel electrolytes under present studies as reflected from the steep rising behaviour in the lower frequency range. The high frequency semicircular spurs have also been distinctly observed for all the capacitors cells, as typically shown in expanded plot (Fig 5.11). This reflects the bulk properties of the polymeric gel electrolytes and the charge transfer process at electrode-electrolyte interfaces. The values of bulk resistance R_b and interfacial charge transfer resistance R_{ct} of the different capacitor cells could be easily evaluated from the intercepts on the real axis of the complex impedance response. In addition to these impedance features, a straight line making a phase angle of ~45^0 has also been observed for the capacitor cells in the middle frequency range, typically shown in Fig. 5.11. In cyclic voltammetry and a.c impedance, the measured capacitance of real capacitors (as in the present studies) always shows slight scan rate or frequency dependence predominantly in this middle frequency range, which an ideal capacitor would not show. This
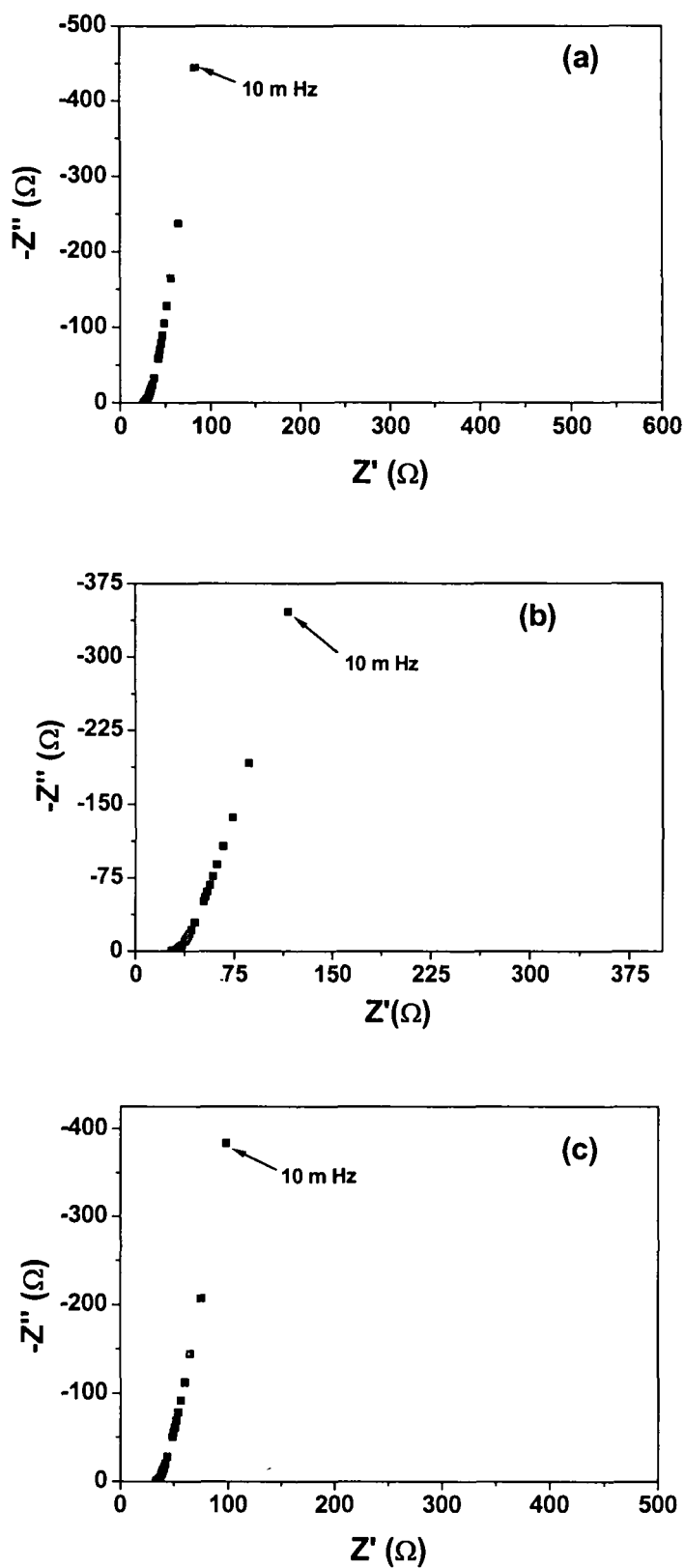
Fig.5.9: Typical Nyquist plots of different EDLC cells (a) Cell A: AC | PVdF-HFP-LiClO₄-gel | AC, (b) Cell B: AC | PVdF-HFP-NaClO₄-gel | AC and (c) Cell C: AC | PVdF-HFP-TEAClO₄-gel | AC.
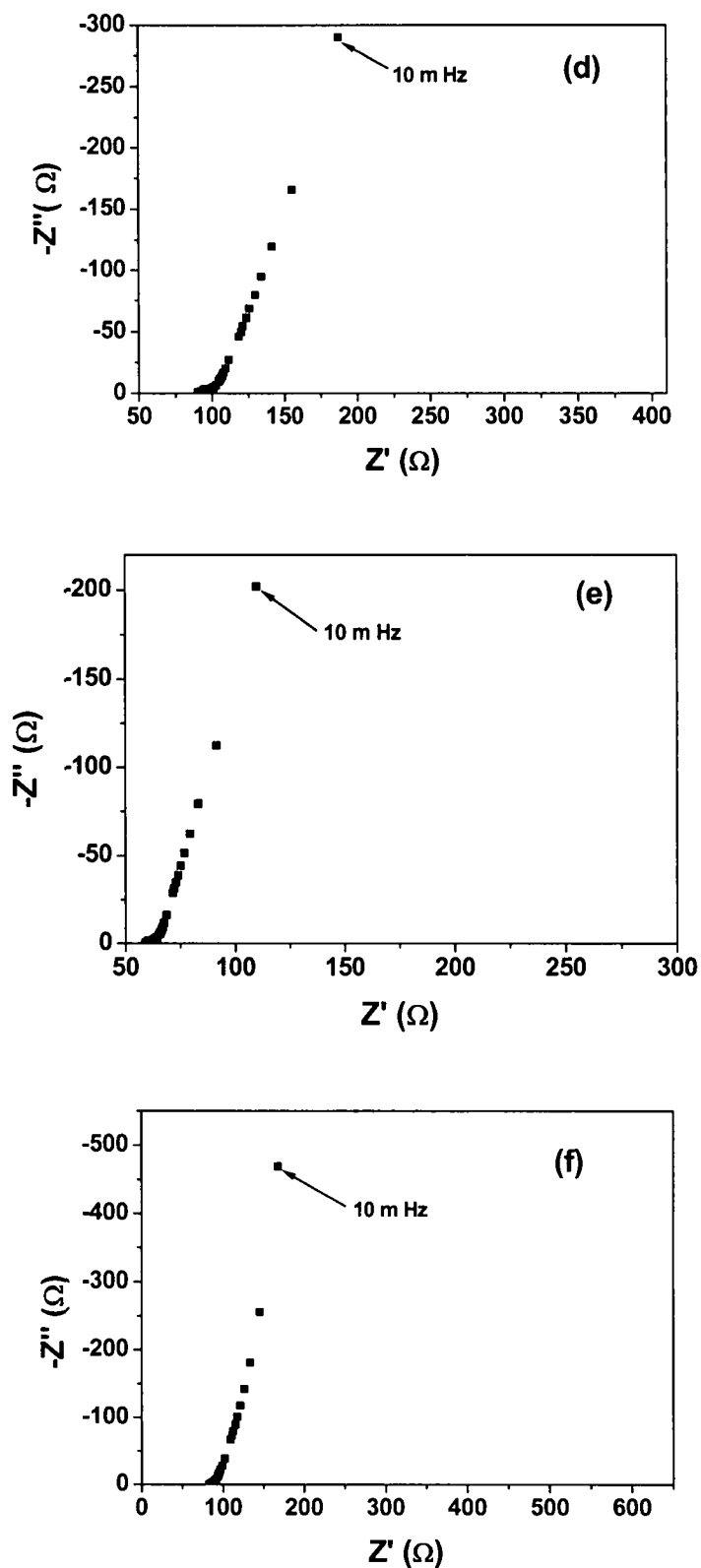
Fig.5.10: Typical Nyquist plots of different EDLC cells (d) Cell D: AC | PMMA-LiClO₄-gel | AC, (e) Cell E: AC | PMMA-NaClO₄-gel | AC and (f) Cell F: AC | PMMA-TEAClO₄-gel | AC.
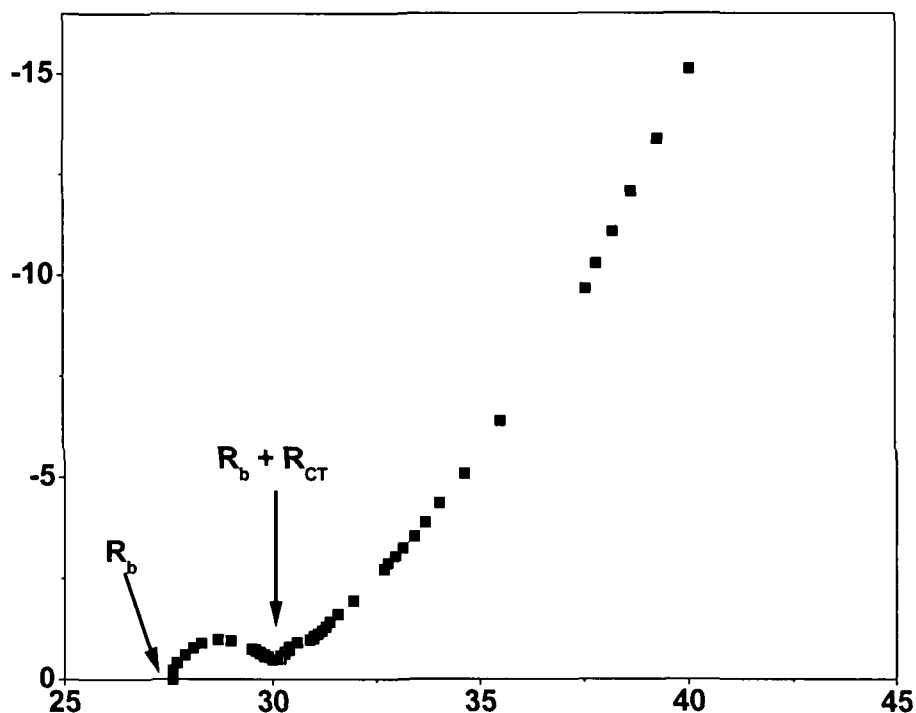
Fig. 5.11: Typical expanded plot of high frequency semicircular spur.

dispersion feature of impedance plots represents diffusion/ migration concentration gradients in the electrolyte [337-339], or charging of deep pores of electrodes [340-342] or as a minor effect, resulting from thermal and stochastic effects[343-346]. This response is mainly associated with the interfacial characteristics having specific porous structure of the electrode material in contact with the highly flexible and mechanically stable polymeric gel electrolytes in the present studies. The impedance response of various possible geometries for the porous structure of the electrode materials has been described theoretically by some workers [201, 340]. In this regard, the first theoretical work was started by de Levie [347, 348]. The model of an element of a porous electrode, as treated by de Levie [347, 34], is shown in Fig. 5.12. Accordingly, the network represents in a crude way the equivalent circuit of a porous high-area capacitor device. The equivalent circuit of a single pore is assumed to be a circularly cylindrical with a radius r_0. Solution resistance R and double-layer capacitance C are assumed to be

147

Distributed interfacial capacitance and
distributed internal resistance ΣR_i with R_s
(porous electrode, transmission line model)

(a)

(b)

(c)
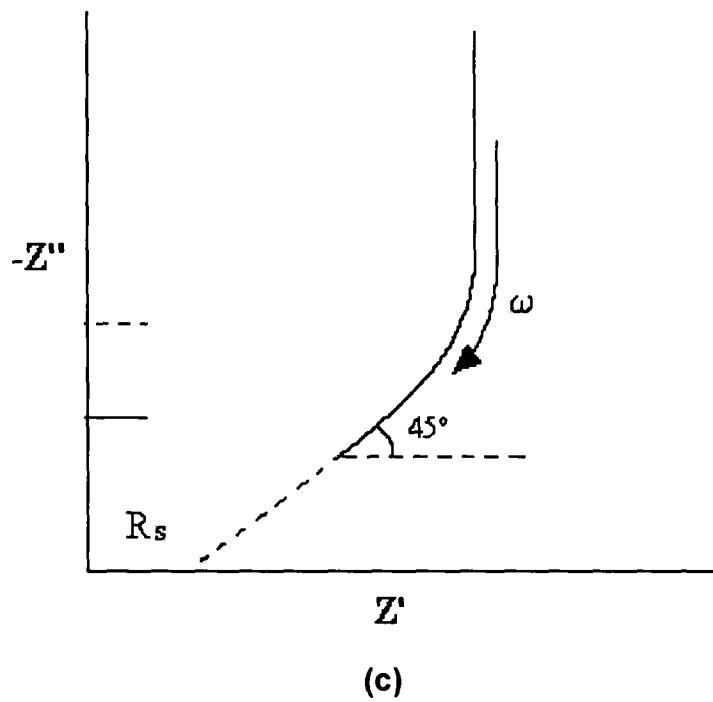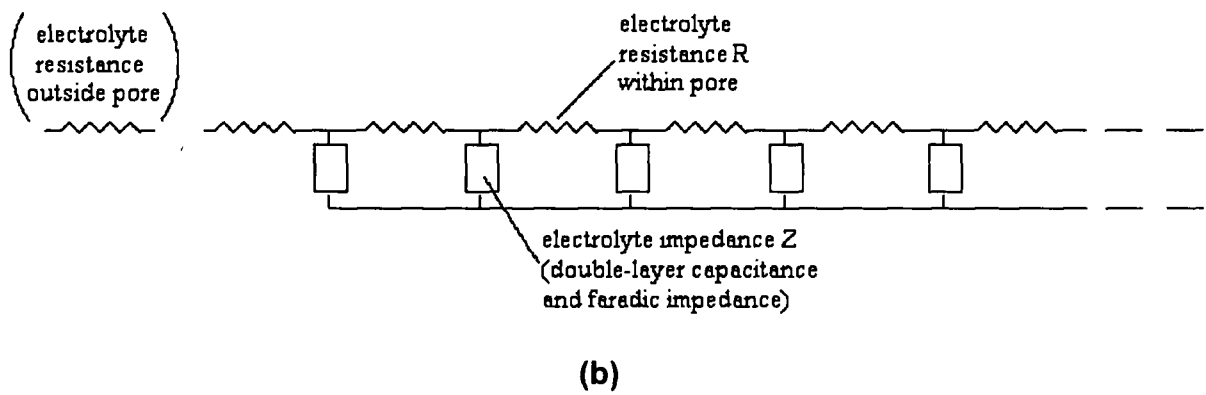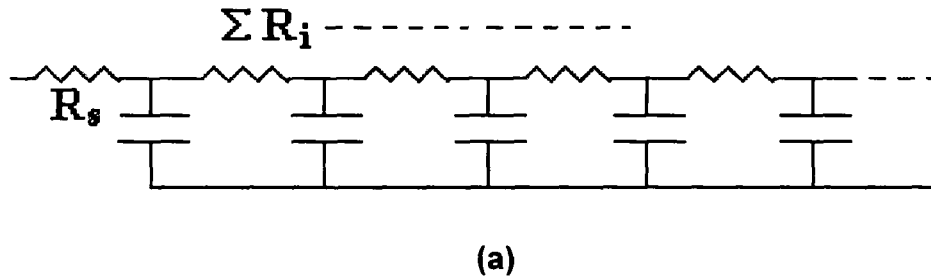
Fig. 5.12: The equivalent circuit of a pore invaded by a conducting electrolyte and having a distributed RC network (transmission line model). Typical –Z" vs. Z' response as f(ω) also shown.

uniformly distributed down the pore, both having values expressed per unit length down the pore in the direction z, where z is measured from the orifice of the pore at z = 0. The overall frequency-response behaviour approximates that of a transmission line that exhibits a -45^0 phase angle over a wide range of frequencies, such as the Warburg impedance involved in a diffusion-controlled Faradic reaction. Out of the rigorous theoretical analysis [347, 348], the general conclusion has been drawn, especially with regard to:

(a) distribution of charging rates or RC time constants down a pore, having penetration depth, represented in terms of the parameter $(\omega RC/2)^{1/2}$; and

(b) the frequency-independent phase angle of 45^0 characteristic of transmission-line-like behaviour.

The theoretical work by de Levie [347, 348] was taken further by Keiser et al. [340], who derived relations for the impedance as a function of frequency for various geometries of a single pore and applied the results to the case of a porous electrode. By means of comparisons calculated for various electrical models in relation to the overall impedance curve, they showed that the average pore structure of a porous electrode could be estimated. Again the mathematics is quite complex. Essentially, the transmission-line equivalent circuit was used and various pore shapes, as illustrated in Fig. 5.13, were investigated. They gave rise to a characteristic series of complex-plane curves of Z" vs. Z' for selected parameters [Fig. 5.13] representing different form-factors for the pores. Form-factor is defined as a quantity l / λ, where l is the length of the pore and λ is defined by equation (5.1):

$$\lambda = \frac{1}{2}\sqrt{\frac{rk}{\omega C}} \qquad \qquad \ldots. (5.1)$$

where, r is the radius and k is the specific conductance of the invading electrolyte. The values of form factors depend on the shape of the pores.

A comparison with the impedance response observed in the present case indicates that the activated charcoal powder electrode possesses almost cylindrical geometry of the pores accessible to the gel electrolytes. For such cylindrical pore of length l and radius r with a uniformly distributed double-layer capacitance at a smooth surface, the electrical properties may be regarded as made up of RC elements in a transmission line arrangement along a length variable x. The resulting impedance behaviour for an assumed 30 to 40-element circuit can be derived computationally, shown as curve 1 in Fig. 5.13. The form factor for such a cylindrical pore is approximately equal to unity.
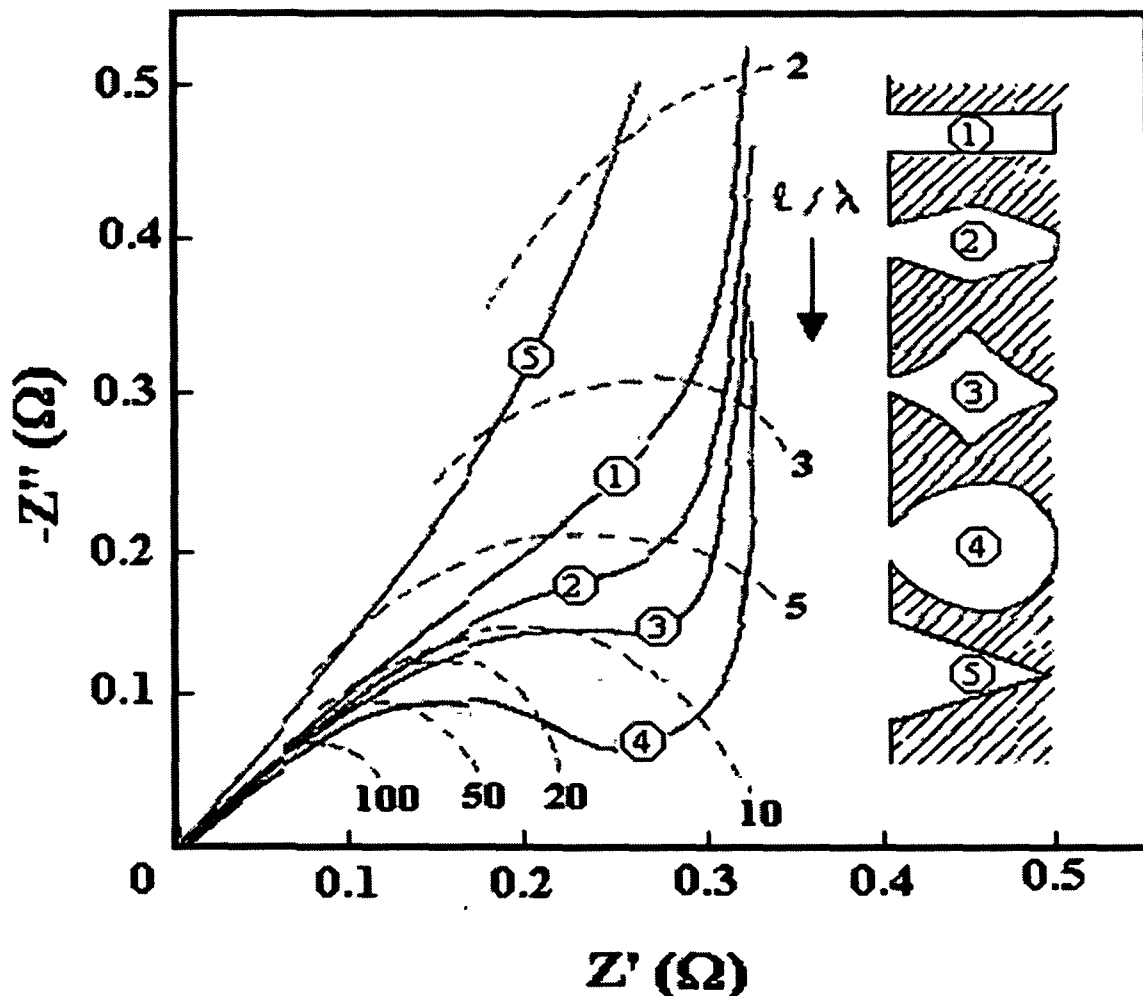
Fig.5.13: Pore shapes treated by Keiser et al. and corresponding complex-plane impedance plots[201, 340].

Thus the overall impedance response of the present solid-state EDLCs based activated charcoal powder electrode and gel electrolytes can be divided into different regions indicating different characteristics of the cells:

- High frequency region: (slightly depressed semi-circular spur) Bulk electrolyte properties followed by interfacial charge transfer behaviour.

- Middle frequency range: (linear curve with phase angle of 45^0) the characteristics of porous electrodes.

- Lower frequency region: (steep rising curve almost parallel to the Z" axis) High capacitance of EDLCs with ESR in series.

The equivalent circuit for such impedance response is most suitably represented by a modified Randles circuit, as shown in Fig.5.14 [349]. The slightly depressed semicircle,

R_b = Bulk Electrolyte Resistance
R_{ct} = Charge-Transfer Resistance
C_{dl} = Double Layer Capacitance
Z_w = Warburg Impedance
C_L = Limit Capacitance
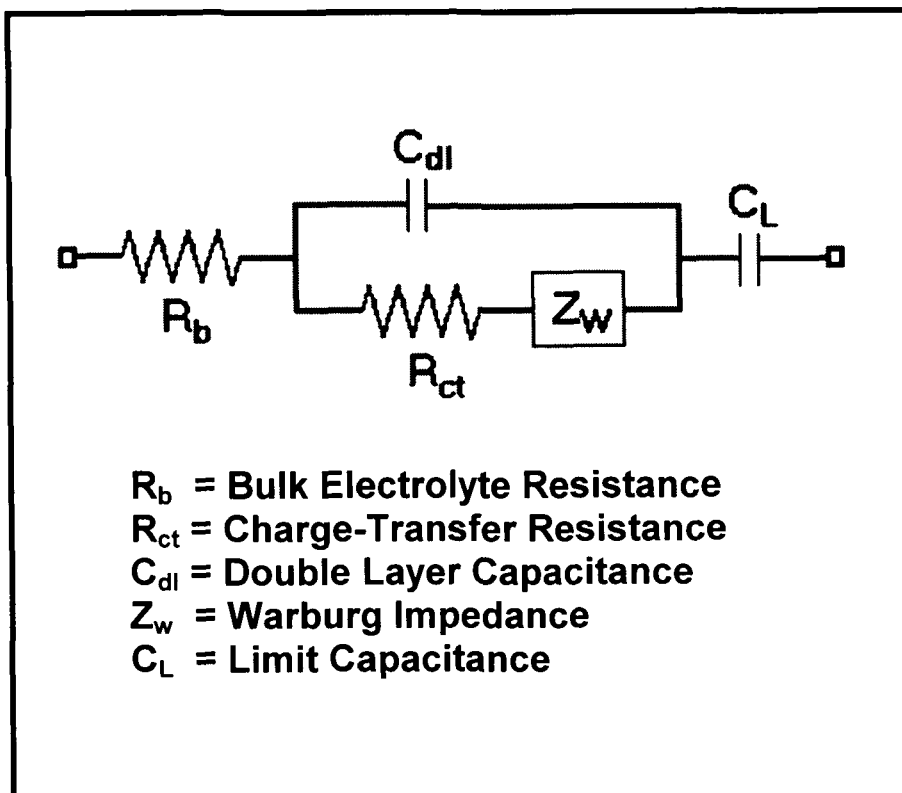
Fig. 5.14: Modified Randles Circuit representing an equivalent circuit for the capacitor cells.

151

which is observed in high frequency region, is attributed to the parallel combination of double layer capacitance C_{dl} and charge-transfer resistance R_{ct} in series with a Warburg impedance/constant phase element (cpe). The Warburg impedance Z_W is associated with the ionic diffusional process in the electrolytes, which is observed in intermediate (middle) frequency regime. The values of bulk resistance R_b and charge transfer resistance R_{ct} have been evaluated from the intercepts on the real axis of the complex impedance response. These parameters along with the total resistance R and the capacitance values (evaluated from eqn. 3.42) at frequencies 100 mHz and 10 mHz are listed in Table 5.3. Few parameters associated with the Warburg impedance, e.g. constant phase element etc., could not be evaluated due to the lack of facilities / softwares.

Table 5.3. Electrical parameters of different capacitor cells from impedance analysis.

Cells	R_{ct} (Ω cm^2)	R_b (Ω cm^2)	100mHz			10 mHz		
			R (Ω cm^2)	C (mF cm^{-2})*	(F g^{-1})**	R (Ω cm^2)	C (mF cm^{-2})*	(F g^{-1})**
A	3-9	26-40	50-100	21-28	21-27	90-180	35-39	35-37
B	3-7	27-30	40-52	31-42	20-30	66-117	45-51	28-37
C	3-4	32-35	42-49	32-41	22-28	71-98	40-51	30-34
D	8-11	48-90	70-144	31-45	17-23	150-220	59-70	33-36
E	4-6	46-51	56-66	46-71	28-37	86-111	64-100	38-52
F	5-6	65-95	86-113	25-36	17-21	132-159	37-52	25-30

* *Overall capacitance of the cells*
** *Single electrode capacitance*

A comparison indicates that the activated charcoal powder electrode shows almost similar capacitive characteristics with the PVdF-HFP and PMMA based gel electrolytes having different cationic (Li^+, Na^+ and TEA^+) perchlorate salts. The capacitance values have also been observed to be in the same range for all the gel electrolytes under the present studies as can be seen from the Table 5.3. Although the gel electrolytes that are based on the salts of substantially different cationic sizes ($Li^+ < Na^+ < TEA^+$) with common anion (ClO_4^-) have been employed, it does not make any substantial difference in the capacitive behaviour and capacitance values of EDLCs. This indicates the possible predominant role of anions in the capacitive nature of such polymer/gel electrolytes based solid state EDLCs. Another attractive aspect of the present studies is that the EDLCs fabricated using activated charcoal electrodes, in combination with different polymeric gel electrolytes, offer relatively smaller values of charge-transfer, bulk and overall resistances in the range of 3-11 ohm cm^2, 26-95 ohm cm^2 and 66-220 ohm cm^2 respectively (Table 5.3). These lower resistances, which mainly contribute to equivalent series resistance (ESR), lead to relatively higher power densities of all solid state EDLCs. In general, the lower values of resistances of the order of mΩ cm^2 to a few Ω cm^2 are observed with liquid electrolytes based EDLCs [201, 203, 204, 206], but relatively larger values of resistances have been reported for the solid state EDLCs based on other carboneous electrodes [206, 211, 212, 331]. The present studies indicate the proper contact between activated charcoal electrodes and the highly flexible and conducting polymer gel electrolytes, which make a vast improvement in interfacial properties leading to the high capacitance values and lower ESR. Further, the value of capacitance of the cell comprising of liquid electrolytes is expected to be quite large as compared to that of the polymer/gel electrolyte based capacitors. This difference is possibly due to inaccessibility of the solid polymer/gel electrolytes to form the complete interfacial contact with the electrode materials.

5.2 Conclusions:

In this chapter the possibility of application of activated charcoal powder as electrode material in the fabrication of solid state electrical double layer capacitors (EDLCs) has been examined. All solid-state EDLCs with activated charcoal powder electrodes using PMMA and PVdF-HFP based polymeric gel electrolytes with different cationic salts ($LiClO_4$, $NaClO_4$ and $TEAClO_4$) having same perchlorate anions have been constructed and characterised using a.c impedance analysis, cyclic voltammetry and charge discharge techniques. Comparing all the above results, it may be concluded that:

- The gel electrolytes PVdF-HFP or PMMA (20 wt%) - EC:PC (1:1 V/V) - 1.0 M $LiClO_4$ / $NaClO_4$ / $TEAClO_4$ salts, showing the room temperature conductivity of the order of 10^{-3} S cm^{-1}, have been found to be suitable electrolytes for the fabrication of solid state EDLCs.

- The overall capacitance values have been observed to be 70-152 mF cm^{-2} (equivalent to single electrode specific capacitance of 40-78 F g^{-1} of activated charcoal powder).

- The working voltage of each capacitor cell has been found to be 1.0 V. This corresponds to the energy densities in the range of 5.3-10.8 W h Kg^{-1} and corresponding power densities in the range of 0.19-0.22 kW Kg^{-1}.

- The relatively smaller values of 210-293 ohm cm^2 for the cell resistances have been observed, which is an attractive aspect of the solid state EDLCs. Further improvement is still required.

- For each capacitor cell, reasonably stable capacitance value has been observed for about 5000 or more voltammetric. Some initial fluctuations in the capacitance values have been observed, which is possibly due to some irreversible faradic reactions associated with some loosely bound surface groups, most likely hydroxyl groups.

- The comparative studies of different capacitor cells show that anions in the polymeric gel electrolytes play a predominant role in the capacitive behaviour of the solid state EDLCs over the cations.

- Coulombic Efficiency of these capacitor cells is measured to be in the range of 90-95%, indicating liquid like properties of the gel electrolytes.

Chapter – 6

Solid State Redox Supercapacitors based on Polypyrrole Electrodes and Polymeric Gel Electrolytes

SOLID STATE REDOX SUPERCAPACITORS BASED ON POLYPYRROLE ELECTRODES AND POLYMERIC GEL ELECTROLYTES

Electronically conducting polymers (e.g. polypyrrole, polythiophene, polyaniline, etc.), in general, opened new field of interest from a theoretical and academic point of view and created expectations for a large number of practical applications, e.g. batteries, sensors, electrochromic displays, electromagnetic shields, artificial muscles, etc. [349-354]. Recently, conducting polymers have been shown to be promising electrode materials for redox supercapacitors because they offer several advantageous properties over the other noble metal oxides and carbon electrode materials [201, 206, 240, 355, 356-358], as discussed in detail in Chapter 2. These include their low cost, easy chemical or electrochemical preparation in desirable extended area thin films and large capability of charge storage ($\sim$ 500 C g^{-1}) throughout their volume. Particularly for electrochemical capacitors, the ability to charge (or discharge) through the whole volume is a most attractive aspect of conducting polymers compared to the large area carbon materials [240, 358].

In most of the studies on the conducting polymers based redox supercapacitors, liquid electrolytes have been used as separators. These include acetonitrile (ACN)-Me$_4$NCF$_3$-SO$_3$, ACN-Et$_4$NBF$_4$, ACN-Bu$_4$NPF$_6$ [240, 358], propylene carbonate (PC)-LiClO$_4$, PC-TEABF$_4$ [355, 356], ACN-Me$_4$NCF$_3$SO$_3$ [201, 206] etc. A limited number of solid state systems have also been studied with polymer/gel electrolytes e.g. poly(ethylene oxide) (PEO)-PC-Et$_4$NBF$_4$, poly(ethylene glycol) (PEG)-Et$_4$NBF$_4$ [244], poly (methyl methacrylate) (PMMA)-PC-ethyl carbonate (EC)-LiClO$_4$ [241, 359] etc. All solid-state redox supercapacitors are in the early

stages of development and require improvements in their capacitance values, reduction of internal resistance and enhancement in the electro-chemical stability range of potential.

The present chapter is devoted to the studies on fabrication and characterization of all solid-state redox supercapacitors using electrochemically deposited polypyrrole and optimized polymeric gel electrolytes having compositions PVdF-HFP or PMMA (20 wt%)-EC:PC(1:1V/V)- (1M) salts (LiClO$_4$, NaClO$_4$, (C$_2$H$_5$)$_4$NClO$_4$ (TEAClO$_4$). Details of the polypyrrole preparation have been given in Chapter-3, section 3.2.2.2. The preparation and optimisation of gel electrolytes have been described in Chapter-4. As mentioned earlier, all these gel electrolytes possess the conductivity of the order of 10^{-3} S cm^{-1} at room temperature with good mechanical strength, flexible enough to mould in the desirable area and thickness. The order of conductivity is acceptable for use in capacitor applications as they offer low resistance, when used in the form of films of the thickness order ~100-200 μm. Being the flexible materials, these are able to form proper interfacial contacts for the maximum accessibility of the active electrode materials.

Six different model capacitor cells have been constructed for the comparative studies, by varying the size of cations of the salts used in the preparation of gel electrolytes with two different polymers. The characteristics of the capacitors have been critically examined and compared on the basis of different nature and size of cations of the salts (with common anion ClO$_4^-$) incorporated in the gel electrolytes.

Cell A: pPy | PVdF-HFP (20 wt%)-EC:PC (1:1 V/V)-1.0 M LiClO$_4$ | pPy

Cell B: pPy | PVdF-HFP (20 wt%)-EC:PC (1:1 V/V)-1.0 M NaClO$_4$ | pPy

Cell C: pPy | PVdF-HFP (20 wt%)-EC:PC (1:1 V/V)-1.0 M TEAClO$_4$ | pPy

Cell D: pPy | PMMA (20 wt%)-EC:PC (1:1 V/V)-1.0 M LiClO$_4$ | pPy

Cell E: pPy | PMMA (20 wt%)-EC:PC (1:1 V/V)-1.0 M NaClO$_4$ | pPy

Cell F: pPy | PMMA (20 wt%)-EC:PC (1:1 V/V)-1.0 M TEAClO$_4$ | pPy

The performance of the different capacitor cells have been characterized using a.c. impedance analysis, linear sweep voltammetry, charge-discharge at constant current and prolonged cyclic tests.

6.1   Results and Discussions:

6.1.1   Linear Sweep Cyclic Voltammetry

Figs. 6.1 and 6.2 show the linear sweep cyclic voltammograms for all the capacitor cells (A-F) at different scan rates between floating potentials -850 mV and 850 mV. The voltammograms were recorded for the two-electrode configuration of the cells. In such sweep-reversal (cyclic) voltammetry at constant scan rates, the profile of current response is ideally a rectangle when capacitance is constant (i.e. potential independent). On the other hand a peaked structured voltammogram is observed in the case of potential dependent capacitance showing a differential profile. In the present studies, the cyclic voltammograms for all the capacitor cells (A-F) show a featureless structure (without any peak) and are almost close to an ideal shape of rectangle even for higher scan rates (100 mV sec^{-1}) [Figs. 6.1 and 6.2]. This is characteristic of capacitive behaviour and is indicative of fast switching rate of ions at the sites of electrode-electrolyte interfaces. At higher scan rates (more than 100 mV sec^{-1}) a slight deviation from the rectangular shapes has been observed for each cell. This is attributed to a substantial value of equivalent series resistance (ESR), which is practically present in the real capacitors. Further, the response of each capacitor cell has been found to depend on scan rates, which is also expected and is a characteristic of capacitor cells [201, 335, 356]. The capacitance values were calculated using eqn. 3.43 and found to be in good agreement with the values obtained from impedance spectroscopy as described later in section 6.1.3.
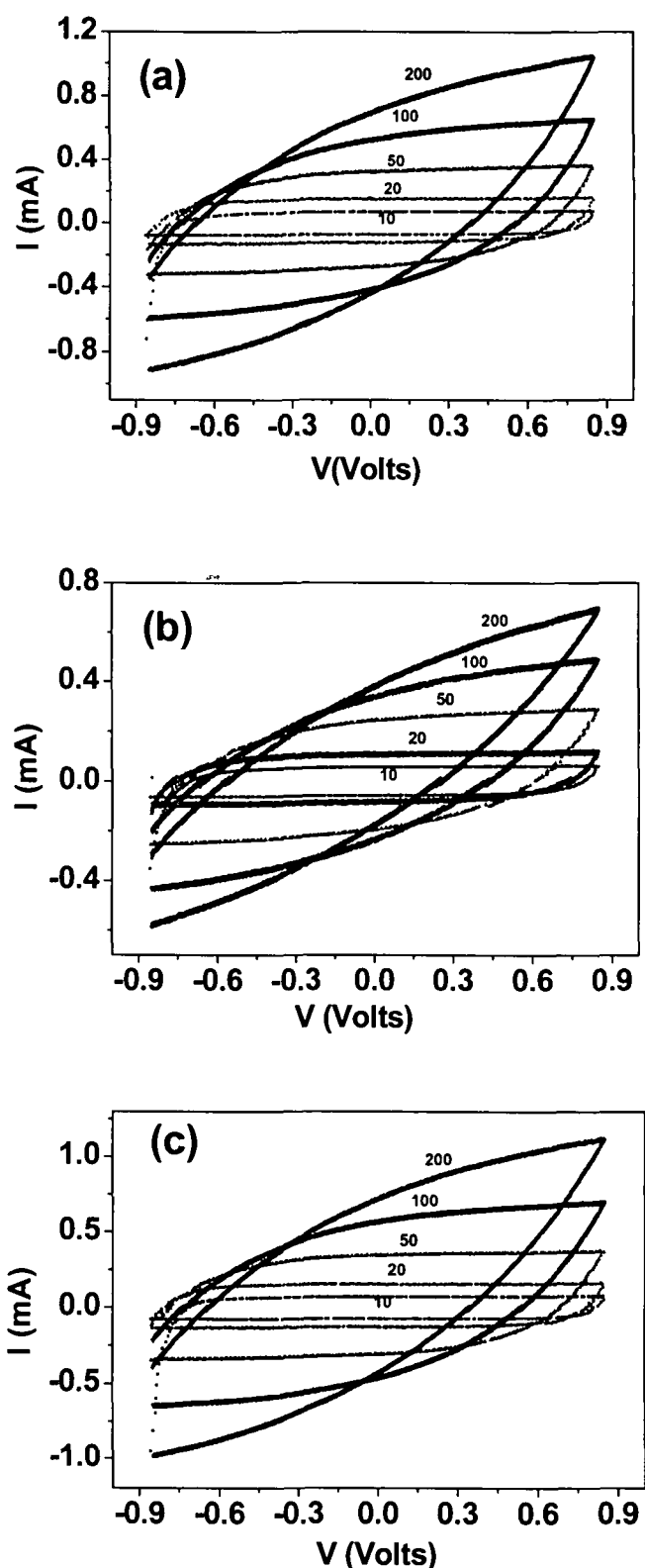
Fig.6.1:   *Cyclic voltammograms of different capacitor cells (a) Cell A: pPy | PVdF-HFP-LiClO₄-gel | pPy, (b) Cell B: pPy | PVdF-HFP-NaClO₄-gel | pPy and (c) Cell C: pPy | PVdF-HFP-TEAClO₄-gel | pPy at different scan rates. Scan rates (in mV sec⁻¹) are marked on the figures.*
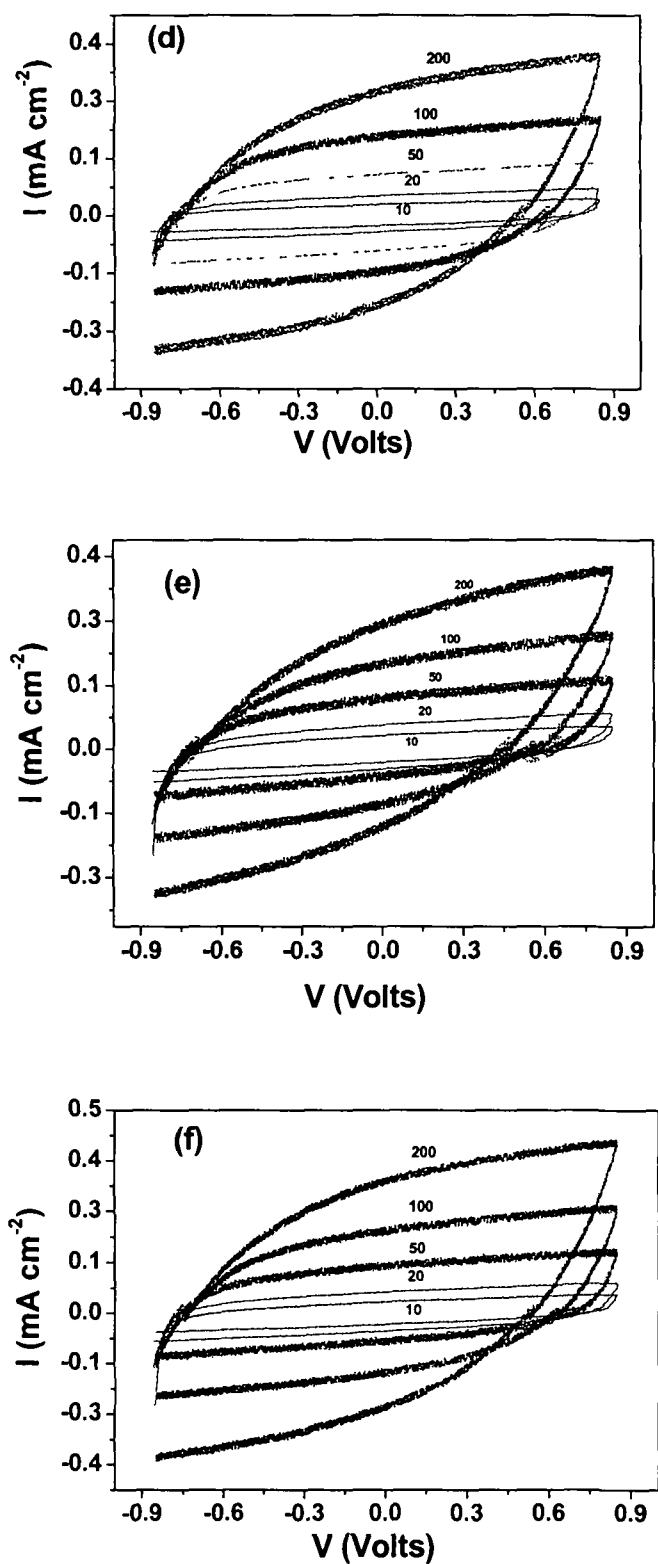
Fig.6.2: Cyclic voltammograms of different capacitor cells (d) Cell D: pPy | PMMA-LiClO₄-gel | pPy, (e) Cell E: pPy | PMMA-NaClO₄-gel | pPy and (f) Cell F: pPy | PMMA-TEAClO₄-gel | pPy at different scan rates. Scan rates (in mV sec⁻¹) are marked on the figures.

One of the most important and attractive aspect of supercapacitors over rechargeable batteries is the cyclic efficiency i.e., their reversibility for large number of charge-discharge cycles. Fig. 6.3 refers the variation of capacitance values as a function of voltammetric cycles
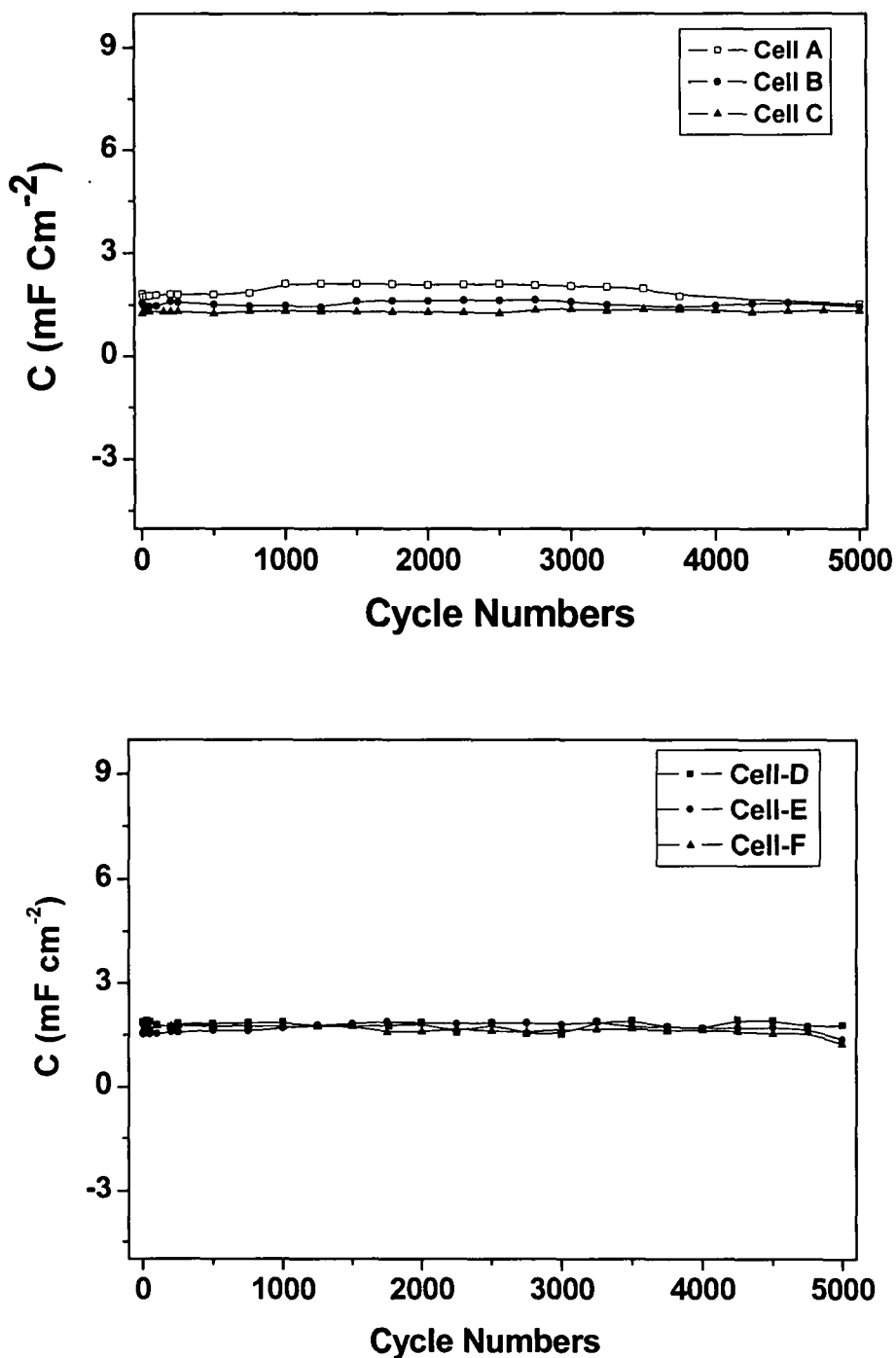
Fig.6.3:   Variation of the capacitance of different capacitor cells as a function of voltammetric cycles at the scan rate 100 mV sec⁻¹.

between -850 mV and 850 mV recorded for all the cells (A-F) at scan rate 100 mV sec^{-1}. Reasonably stable and almost constant values of capacitance have been observed for each capacitor cell upto 5000 cycles. A slight decrease (fluctuation) in capacitance for initial few cycles has been observed, which is attributed to the charge loss due to some possible faradic reaction(s) with loosely bound surface groups (e.g. OH- groups etc.) at the electrode electrolyte interfaces [201].

6.1.2 Galvanostatic Charge Discharge Studies

The capacitor cells have also been tested with the galvanostatic (constant current) charge-discharge methods. The typical charge-discharge characteristics of all the capacitor cells are shown in Figs. 6.4 and 6.5. All the cells were charged up to 1.0 V, which is the maximum voltage limit for doping-dedoping of polypyrrole electrodes [240, 242, 243, 251, 355, 356]. The voltage limit of the electrochemical stability of the polymeric gel electrolytes is wide enough (more than 4.0 V) for such devices as discussed in chapter 4. The linear portions of the discharge characteristics confirm the capacitive behaviour of all the cells. In general, a real capacitor is represented by an equivalent circuit comprising of an ideal capacitor in series with the internal resistance (R_i). The initial sudden change in voltage response with respect to time while charging and discharging has been found to be due to ohmic loss across the internal resistance, also known as ESR, of the cells. The internal resistances of the cells have been estimated from this voltage loss. The values of discharge capacitances have been evaluated from the linear part of the discharge characteristics using eqn. 3.48. The values of discharge capacitance C_d internal resistance R_i and coulombic efficiency η (evaluated using eqn. 3.49) are listed in Tables 6.1 and 6.2. The capacitance and internal resistance values are consistent with the values obtained from impedance analysis (Table 6.3). The energy density of each capacitor cell has been estimated from their corresponding values of the capacitance and the working
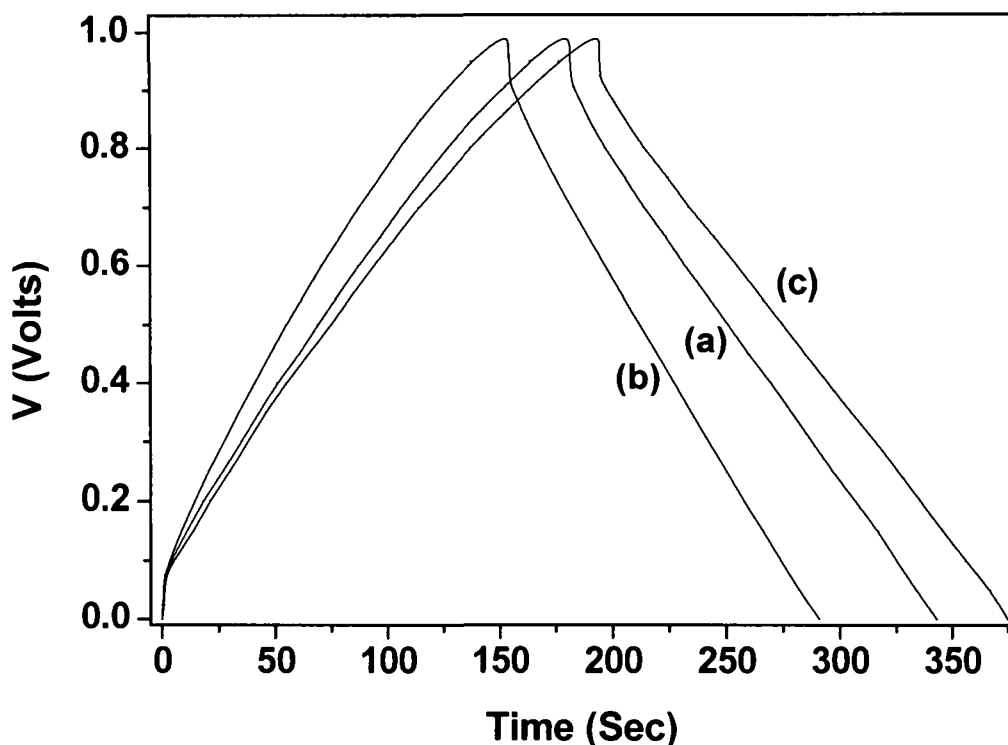
Fig.6.4: Typical charge-discharge curves of different capacitor cells, (a) Cell A: pPy |
PVdF-HFP-LiClO₄-gel | pPy, (b) Cell B: pPy | PVdF-HFP-NaClO₄-gel | pPy and
(c) Cell C: pPy | PVdF-HFP-TEAClO₄-gel | pPy at constant current density 0.15
mA cm⁻².

Table 6.1. Typical Charge-discharge characteristics of different capacitor cells at current
density of 0.12 mA cm⁻²

Cells	R (Ω cm²)	Discharge Capacitance, C_d		Working Voltage (V)	Energy Density (Wh Kg⁻¹)	Power Density (kW Kg⁻¹)
		(mF cm⁻²)*	(F g⁻¹)**			
A	508-810	20.6-25.2	112-137	1.00	15.6-19.0	0.35-0.38
B	710-800	18.0-22.0	98-120	1.00	13.6-16.7	0.36-0.44
C	630-900	14.4-25.0	78-136	1.00	10.8-18.9	0.22-0.38

*   *Overall capacitance of the cells*
** *Single electrode capacitance*
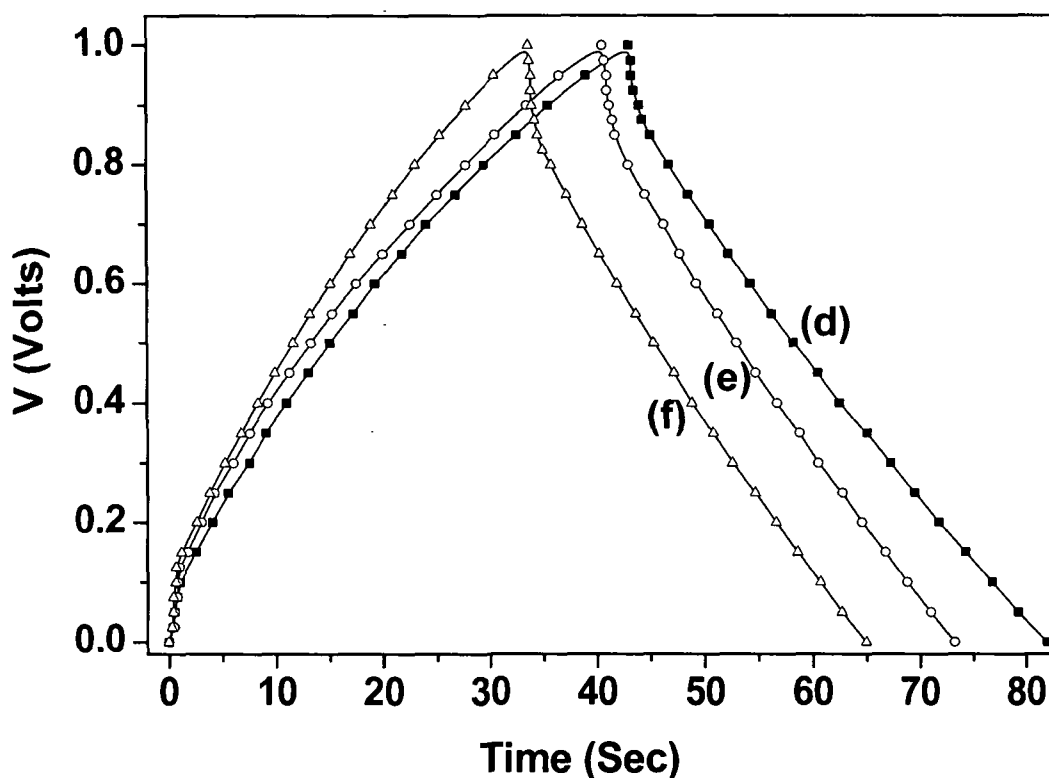
Fig.6.5: Typical charge-discharge curve of different capacitor cells, (d) Cell D: pPy | PMMA-LiClO₄-gel | pPy, (e) Cell E: pPy | PMMA-NaClO₄-gel | pPy and (f) Cell F: pPy | PMMA-TEAClO₄-gel | pPy at constant current density 0.38 mA cm⁻².

Table 6.2. Typical Charge-discharge characteristics of different capacitor cells at current density of 0.38 mA cm⁻²

Cells	R (Ω cm^2)	Discharge Capacitance, C$_d$ (mF cm^{-2})*	(F g^{-1})**	Working Voltage (V)	Energy Density (Wh Kg^{-1})	Power Density (kW Kg^{-1})
D	320-458	15.8-18.5	124-145	1.00	17.2-20.2	1.6-1.9
E	420-445	15.5-18.7	122-147	1.00	17.0-20.5	1.9-2.3
F	280-430	15.3-22.5	120-178	1.00	16.7-24.7	1.9-2.8

* Overall capacitance of the cells
** Single electrode capacitance

voltage (1.0 V in the present case of polypyrrole). The power density values have been evaluated by dividing the energy density values by the discharge time of the cells [241]. The energy and power density values are also listed in Tables 6.1 and 6.2. Although the energy density values are comparatively lower than that of the rechargeable batteries, but the power density values make such supercapacitor devices attractive from the application point of view as power sources for the peak requirements [201, 203, 205, 206]. As far as the all solid-state redox supercapacitor cells are concerned under the present studies, their energy and power density values have been found to be lower as compared to the liquid electrolyte based cells. The primary reason is the limited accessibility of solidus gel electrolytes over the liquid electrolytes. These solid state devices can further be improved for their suitable applications as power sources by: (i) choosing the conducting polymers / conducting polymer composites having more charge density, better activity and porosity. Porosity is important for the better accessibility of electrolytes and faster switching of ions at the electrode-electrolyte interfaces, (ii) improving the electrical conductivity and mechanical flexibility of the gel electrolytes, which would result the reduction of ESR, and (iii) choosing the type-III configuration (as described in chapter 2), which will enhance the potential range of the redox capacitor cells. But the rare availability of stable n-dopable conducting polymers is the limitation.

The coulombic efficiency, which is the ratio of charging capacitance to the discharge capacitance is another important parameter associated with the charge-discharge behaviour of the supercapacitors. The coulombic efficiency of each capacitor cells has been found to be in the range of 95-100%. In general the polypyrrole shows the columbic efficiency close to 100% for the liquid electrolytes based batteries and capacitors [360]. The values observed for the polypyrrole and solid polymer electrolytes capacitors have been reported to be limited to 60-80% [242, 243]. The present studies indicate that the improvement in the columbic efficiency is

166

owing to the possible improvement in interfacial properties of the solid-state capacitor cells due to the application of highly flexible gel electrolytes, which offer the liquid like properties.

Figs. 6.6 and 6.7 represents variation of discharge capacitance, C_d and internal resistance, R_i with respect to the varying current density for all the capacitor cells under present studies. It can be seen that almost stable values of C_d and R_i for different current densities have been observed after an initial slight decrease in the values [Figs. 6.6 and 6.7]. This decrease in the capacitance values is associated with the possible charge loss during the charge-discharge at the initial stage due to irreversible faradic reaction(s) with the foreign surface groups (most possibly hydroxyl groups) present at the electrode- electrolyte interfaces. The initial decrease in the internal resistances indicates the slight improvement in the electrode-electrolyte contacts during the initial charging-discharging of the different capacitor cells under present studies.

The almost similar variations in the capacitance values for all the capacitor cells indicate that the different cationic sizes of the salts used in the preparation of gel electrolytes do not affect substantially on the capacitance values / behaviour and the internal resistance of the cells. This further confirms the possibility of the predominant role of anions in the interfacial properties of the different capacitor cells under the present studies.
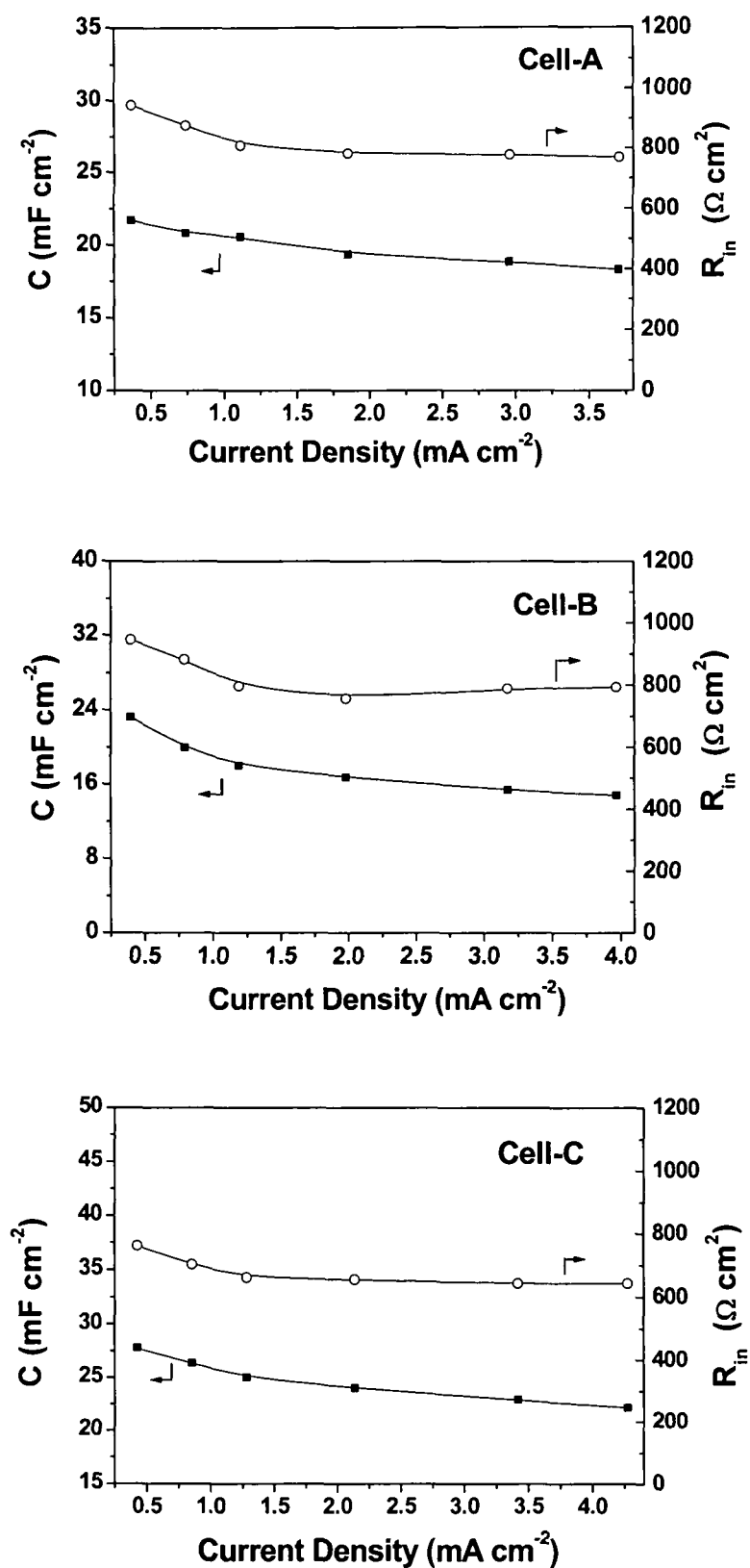
Fig.6.6: *Variation of discharge capacitance, C_d and internal resistance R_i of different capacitor cells as a function of current density.*
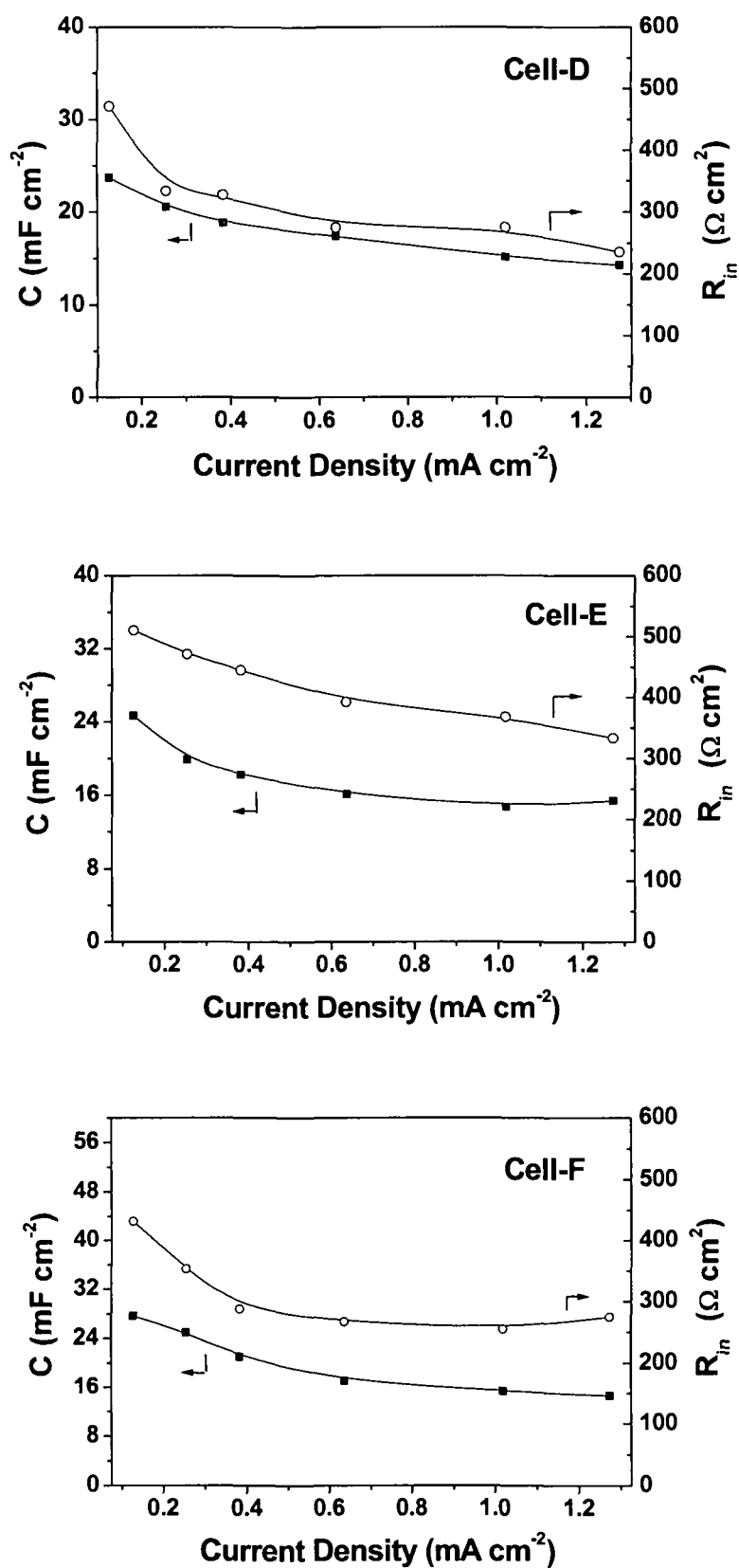
Fig.6.7: Variation of discharge capacitance, C_d and internal resistance R_i of different capacitor cells as a function of current density.

6.1.3 Impedance Spectroscopy Studies

The complex impedance plots of different capacitor cells (A-F) are illustrated in Figs. 6.8 and

6.9. As described in previous Chapters 3 and 5, a.c. impedance spectroscopy is a powerful and

widely applicable technique for the electrical/electrochemical characterization of

electrochemical cells, e.g. batteries / supercapacitors. Particularly for supercapacitors different

parameters associated with the bulk properties of the electrolyte, electrode-electrolyte

interfaces, equivalent series resistance (ESR) of overall capacitor cells, their potential

dependent faradic resistances, low frequency capacitance etc. can be evaluated separately in

different frequency ranges. It should be noted that an ideal impedance response for a pure

capacitor is a straight line parallel to the imaginary axis of the complex impedance plots. But in

real capacitors, the steep rising capacitive impedance response is observed in low frequency

region accompanied with high frequency semicircular features owing to the bulk and interfacial

properties. The polypyrrole shows the capacitive behaviour (i.e. steep rising response of Z"

almost parallel to Z"-axis for approximately constant value of Z') in the lower frequency range

up to 10 mHz, even below this frequency, with each gel electrolyte employed to fabricate redox

capacitors in the present studies (Figs. 6.8 and 6.9). The expanded portion of the higher

frequency response is shown typically in Figs. 6.10 (a and b)], which is the characteristic of

bulk electrolyte and electrode-electrolyte interfacial properties. The high frequency

semicircular spurs are observed (followed by almost linear portions in the middle frequency

range) in the cases of all the capacitor cells with the PVdF-HFP based gel electrolytes [Fig.

6.10 (a)]. Whereas the cells based on PMMA [Fig. 6.10 (b)] shows no such semicircular

features, which represent bulk properties and interfacial characteristics. This feature could be

observed in further higher frequency region (beyond 100 kHz), but this could not be done due

to lack of the impedance analyser of higher frequency range in our laboratory.
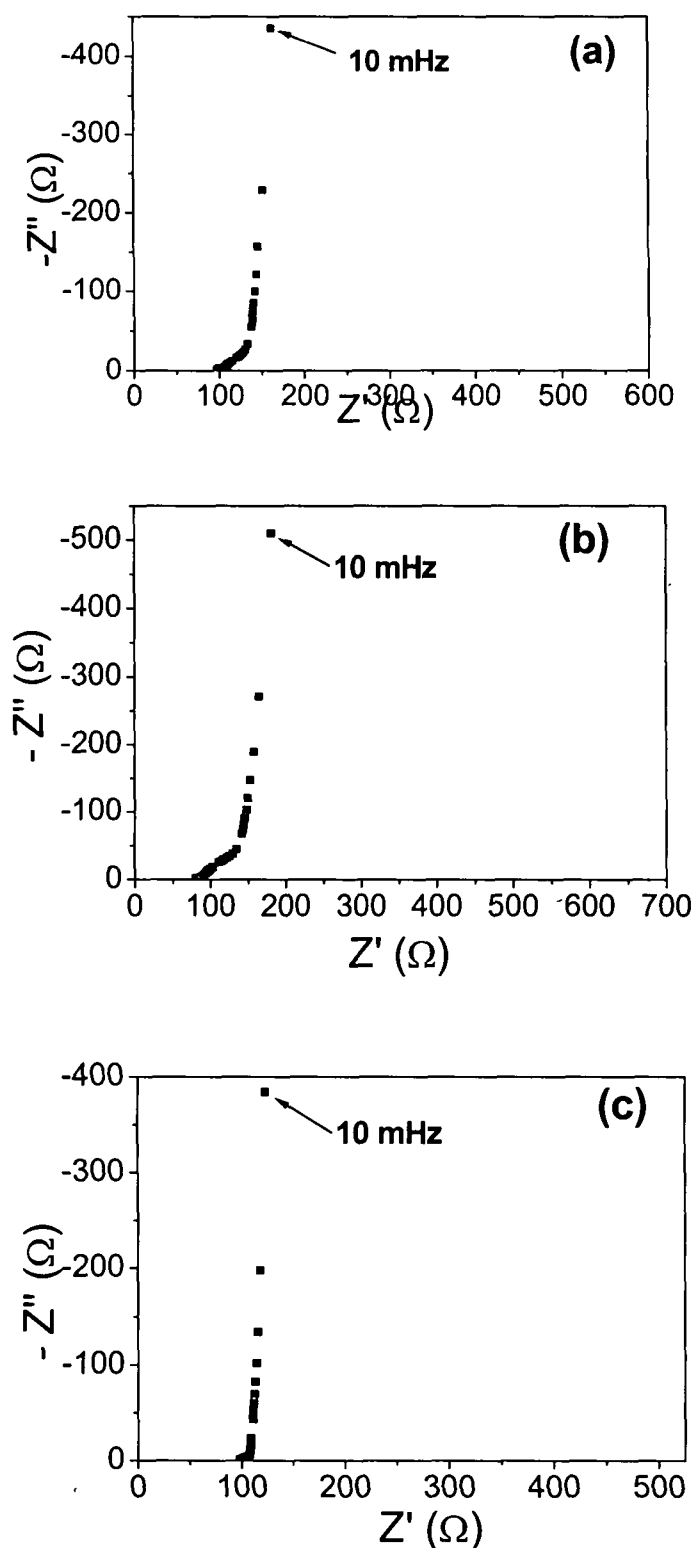
Fig.6.8: Typical impedance plots of different capacitor cells, (a) Cell A: pPy | PVdF-HFP-LiClO₄-gel | pPy, (b) Cell B: pPy | PVdF-HFP-NaClO₄-gel | pPy and   (c) Cell C: pPy | PVdF-HFP-TEAClO₄-gel | pPy recorded at room temperature in the frequency range 100 kHz to 10 mHz.
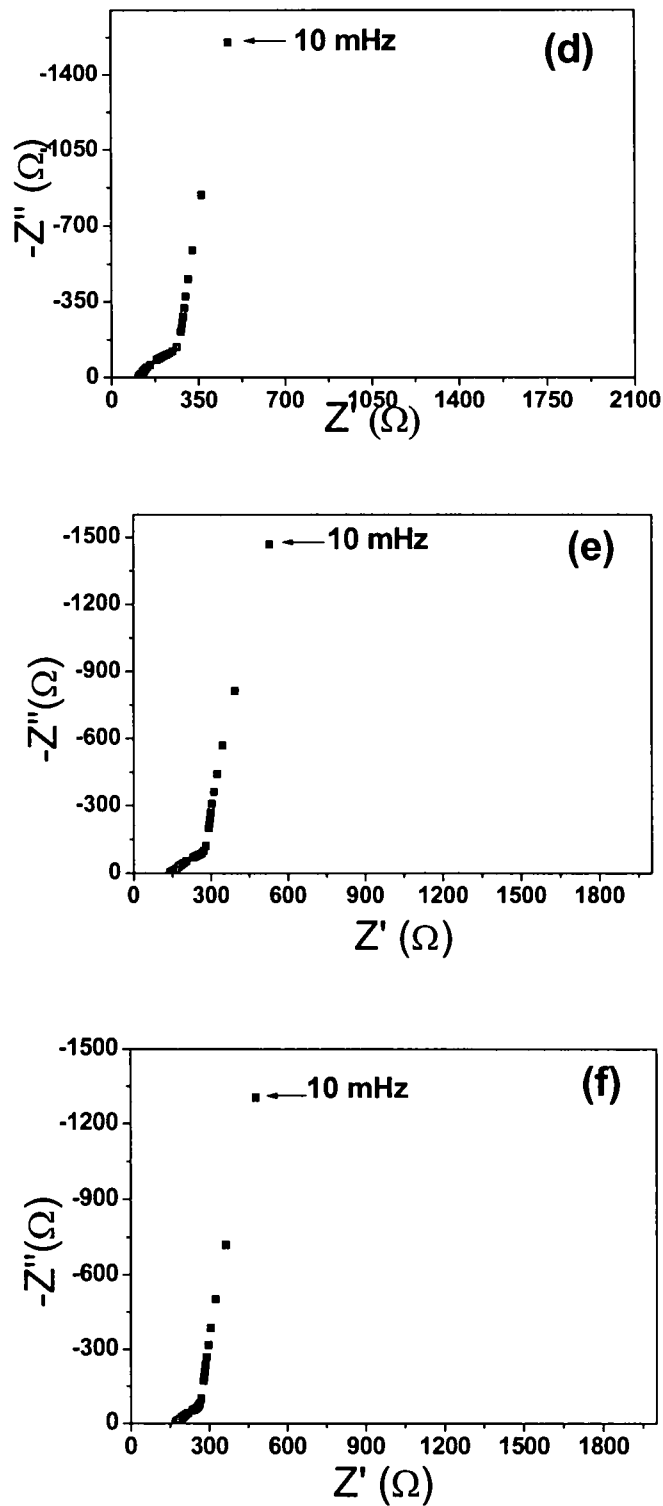
Fig.6.9: Typical impedance plots of different capacitor cells, (d) Cell D: pPy | PMMA-LiClO₄-gel | pPy, (e) Cell E: pPy | PMMA-NaClO₄-gel | pPy and (f) Cell F: pPy | PMMA-TEAClO₄-gel | pPy recorded at room temperature in the frequency range 100 kHz to 10 mHz.

It can be emphasised that almost linear impedance (Z" vs. Z') response has been observed in * the middle frequency range i.e. between higher frequency semicircular spur and lower frequency steep rising capacitive response [Figs. 6.10 (a and b)]. This response is associated
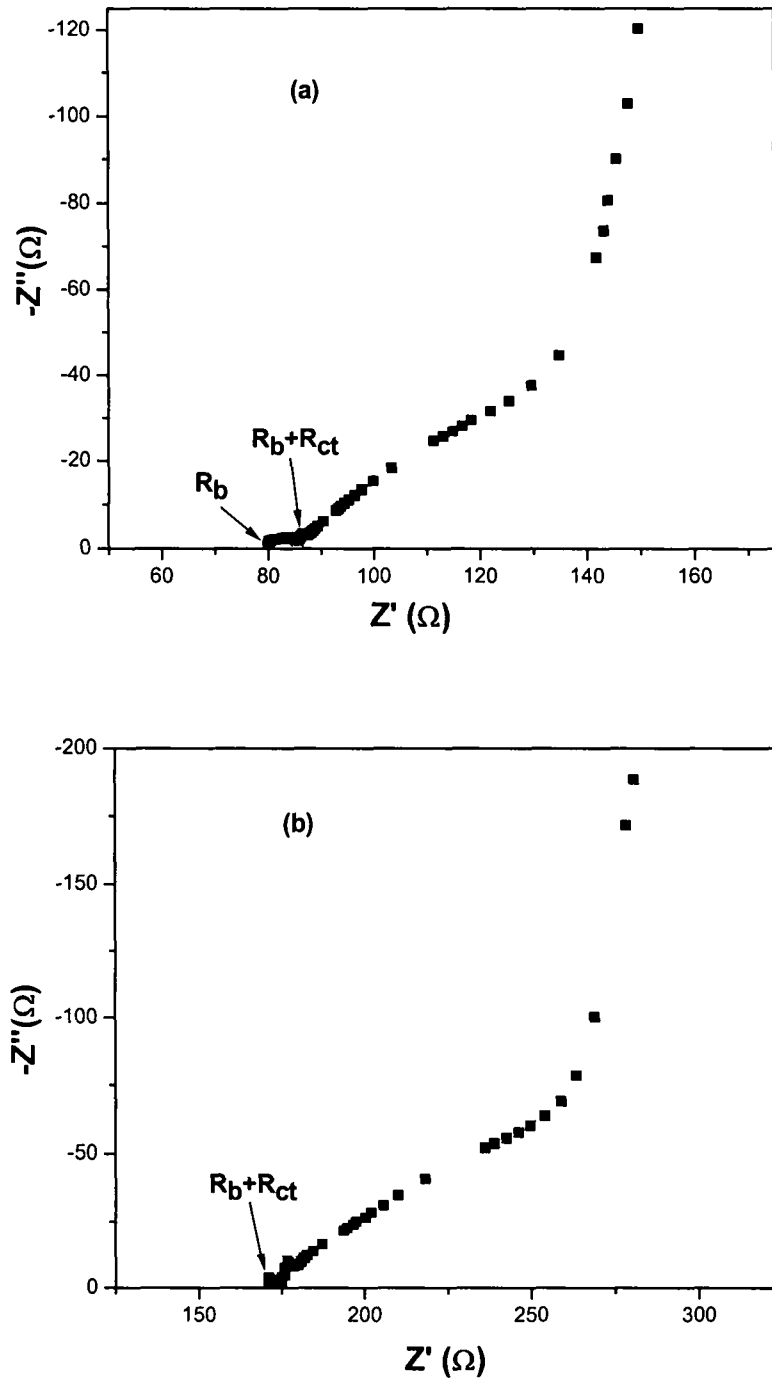
Fig.6.10: *Typical expanded plot of high frequency semicircular spur.(a) PVdF-HFP based gel electrolytes; (b) PMMA based gel electrolytes.*

with the interfacial characteristics having specific porous structure of the electrode material in contact with the highly flexible gel electrolytes. Some workers [201, 340] described the theoretical approach of the impedance response considering different possible geometries of pore structure of the electrodes as described in section 5.1.3 [Fig. 5.13]. A comparison with the present experimental observations indicates that the electrochemically deposited polypyrrole on ITO conducting glass substrates possesses almost cylindrical geometry of the pores accessible to the gel electrolytes.

Thus, it can be summarised that the overall impedance response of the present solid-state redox supercapacitors comprises of: (i) high frequency semicircle representing bulk electrolyte and interfacial charge transfer characteristics, (ii) intermediate (middle) frequency almost linear impedance response representing porous electrode characteristics, and (iii) steep rising capacitive response. This indicates that the equivalent circuit should be represented by a modified Randles circuit [355], as described in section 5.1.3 (Fig.5.14). The semicircle, which is observed to be slightly suppressed towards the real axis, is attributed to the parallel combination of double layer capacitance, C_{dl} and charge transfer resistance, R_{ct} in series with Warburg impedance. The Warburg impedance is related with the diffusional process of ions at the porous electrode-electrolyte interface, which corresponds to the transmission line type RC equivalent circuit [201].

Various electrical parameters such as bulk resistance R_b, interfacial charge transfer resistance R_{ct}, total resistance R and capacitance C at frequencies 100 mHz and 10 mHz are summarised in Table 6.3. In the cases of capacitor cells with PMMA based gels, the values R_b and R_{ct} could not be evaluated separately due to the absence of semicircular spurs.

Table 6.3. Electrical parameters of different capacitor cells from impedance analysis.

| Cells | R_{ct} (Ω cm^2) | R_b (Ω cm^2) | 100mHz | | | 10 mHz | | |
			R (Ω cm^2)	C (mF cm^{-2})*	(F g^{-1})**	R (Ω cm^2)	C (mF cm^{-2})*	(F g^{-1})**
A	92-130	140-330	250-485	10.6-12.1	57-66	320-535	13.5-16.7	75-98
B	96-132	170-201	305-357	9.4-10.5	52-57	395-456	12.4-14.1	67-77
C	25-90	265-355	300-465	13.6-14.2	74-77	330-415	15.4-16.3	84-89
D	-	-	220-410	7.0-10.0	55-78	370-550	12.0-13.0	94-102
E	-	-	230-280	9.0-10.00	70-86	415-560	13.0-16.0	102-125
F	-	-	200-265	9.0-12.0	70-94	375-500	12.0-16.0	94-125

*   *Overall capacitance of the cells*
** *Single Electrode Capacitance*

The values of $R_b + R_{ct}$, evaluated from the intercept of impedance curves on real (Z')-axis in the higher frequency range [Fig. 6.10 (b)], have been found to be in the range of 85-145 Ω cm^2. Various parameters associated with Warburg impedance could not be evaluated due to lack of the facilities in our laboratory.

The values of bulk electrolyte resistance, R_b and interfacial charge transfer resistance, R_{ct} have been evaluated from the intercepts of the impedance response on real (Z')-axis, as illustrated in Figs. 6.8 and 6.9 (inset). The values of capacitance at lower frequencies 100 mHz and 10 mHz have been calculated from eqn. 3.42 for each cells and was observed to be in the range of 12-16.7 mF cm^{-2} (equivalent to the single electrode specific capacitance of 70-125 Fg^{-1} mass of polypyrrole). For the estimation of total mass deposited, the thickness of the pPy films,

was evaluated following the procedure given by Holdcroft and Funt [361] and Roncali et al. [362], respectively. An attractive aspect of the present studies is that the values of charge transfer and overall resistances have been observed to be in the range of 25-200 Ω cm^2 and 320-560 Ω cm^2 respectively, which are comparatively smaller than the values for the solid state capacitors based on the conventional solid polymer electrolytes, observed in the order of kilo ohms cm^2 [242, 243, 251]. This indicates the substantially proper contact between polypyrrole electrodes and highly flexible and conducting gel electrolytes. Further, the capacitance values are comparatively lower than the liquid electrolyte based capacitors with the same electrodes [206, 240, 355], but reasonably higher than that of the capacitors using solid conventional PEO or PVA based polymer electrolytes [242, 243, 251]. This difference is associated with the accessibility limit of the electrolytes to form interfacial contact with the active electrodes like polypyrrole. This has further been confirmed from a comparison of charge transfer and overall resistances (Table 6.3) with the liquid electrolytes and solid conventional polymer electrolytes based capacitors [206, 242, 243, 251, 355]. The application of gel electrolytes in the capacitors leads to a substantial improvement in the capacitance and resistance values over the solid conventional polymer electrolytes based capacitors due to their highly flexible nature and higher conductivity. Further, the capacitance and resistance values have been observed to be almost in the same range for all the cells employing different gel electrolytes in the present studies (Table 6.3). It is striking to be noted that though the difference in cationic sizes of the salts in gel electrolytes is substantially larger (TEA$^+$ > Na$^+$ > Li$^+$), it does not affect much on the capacitive behaviour and capacitance values of different redox capacitor cells. This indicates that possibly anion is playing predominant role in giving the capacitive nature in all the solid-state redox supercapacitors.

6.2 Conclusions:

In this chapter, a comparative studies have been carried out for electrochemically deposited polypyrrole based redox supercapacitors with gel electrolytes PVdF-HFP and PMMA-EC-PC-salts $LiClO_4$, $NaClO_4$ and $TEAClO_4$ using various techniques such as, a.c. impedance analysis, linear sweep voltammetry and charge-discharge studies. Combining all the above experimental studies, the following important conclusions have been drawn:

- The (PVdF-HFP) or (PMMA)(20 wt%)-(EC-PC)(1:1 V/V)-salts, $LiClO_4$, $NaClO_4$ and $TEAClO_4$ based polymeric gel electrolytes, having room temperature conductivity of about 10^{-3} S cm^{-1} are the suitable electrolytes for the fabrication of all solid state redox supercapacitor with polypyrrole as conducting polymer electrodes.

- The size of the cations of the salts used in polymeric gel electrolytes does not make substantial difference in the capacitive properties of the redox supercapacitors based on polypyrrole, rather the predominant role of anions is possible.

- The overall capacitance values of about 14-25 mF cm^{-2} (equivalent to a single electrode specific capacitance of 78-178 F g^{-1} of polypyrrole), which corresponds to the energy density of 11-25 W h Kg^{-1} and power density of 0.22-2.80 kW Kg^{-1}, have been obtained for the capacitor cells under the present studies.

- The internal/overall resistance of each cell based on gel electrolytes has been found to be in the order of few hundreds ohm cm^2, which is comparatively lower than that of the solid state capacitor cells based on conventional solid polymeric electrolytes. Further improvement is still required.

- All the capacitors show the stable capacitance values for about 5000 voltammetric cycles and even more. The initial fluctuation in capacitance values is associated with the

irreversible charge consumption during faradic electrochemical reactions with the loosely bound surface groups.

- The coulombic efficiency of these gel electrolytes based capacitor cells, which is about 95-100%, is equivalent to liquid electrolytes based cells, confirming the liquid like behaviour of the gel electrolytes.

Chapter – 7

Summary and Conclusions

SUMMARY AND CONCLUSIONS

The present thesis is devoted to the fabrication and characterization of ion conducting polymeric gel electrolytes based solid-state supercapacitors. In order to achieve the objectives, ion conducting polymeric gel electrolytes comprising of PVdF-HFP or PMMA (20 wt%) – EC:PC (1:1 V/V) – salts (namely: LiClO$_4$, NaClO$_4$, TEAClO$_4$) have been synthesized. The materials have been characterized and optimized using various electrical and electrochemical methods such as impedance spectroscopy, electrical conductivity measurements as a function of composition and temperature, transport number measurement etc. The optimised materials have been used for the fabrication of solid-state electrical double layer capacitors (EDLCs) based on activated charcoal powder electrodes and electrochemically deposited polypyrrole based redox supercapacitors. The performance characteristics of the supercapacitors have been characterised using various techniques such as a.c. impedance spectroscopy, linear sweep cyclic voltammetry, galvanostatic charge-discharge and prolonged cyclic tests. In the present chapter, work done and the conclusions drawn from the results of the present thesis are summarised.

7.1   Experimental techniques used in the present studies:

7.1.1   Materials Preparation:

(a) Preparation of Electrolyte Materials:

Polymeric gel electrolytes were synthesized using standard solution cast techniques for the fabrication of different types of supercapacitors as described in section 7.1. The standard "solution cast" technique was used for the preparation of all the polymeric gel electrolytes under present studies.

(b) Preparation of Electrode Materials:

Two types of electrode materials were prepared for the fabrication of supercapacitors: (i) activated charcoal powder electrodes for the development of electrical double layer capacitors, and (ii) conducting polymer electrodes namely, p-doped polypyrrole for the development of redox supercapacitors.

(i) <u>Preparation of Activated Charcoal Electrodes</u>

A slurry of activated charcoal powder and polymer (PMMA or PVdF-HFP) with the ratio 90 : 10 (w/w) in a common solvent, acetone was prepared by a thorough mixing. Fine films of electrodes were coated by spraying the slurry on carbon papers (Toray, Japan) followed by heating them at 70^0C for 10-12 hours. The prepared electrodes were used for the fabrication of solid-state electrical double layer capacitors.

(ii) <u>Preparation of Conducting Polymer Electrodes</u>

Electronically conducting p-doped polymer, polypyrrole films were deposited electrochemically (galvanostatically) in a three electrode one compartment cell on indium tin oxide (ITO) conducting glass substrates. Suitable supporting electrolyte $LiClO_4$ or $NaClO_4$ having 0.2 M concentration has been added in the mixture of acetonitrile (ACN) and 0.1 M pyrrole to obtain p-doped polypyrrole. The prepared polypyrrole electrode materials were then used in the fabrication of solid state redox supercapacitors.

7.1.2 Physical Characterisation

In order to optimise the polymeric gel electrolytes, various experimental techniques were used, which are summarised as follows:

1) The "Impedance Spectroscopy" was used to evaluate the electrical conductivity of the liquid as well as polymeric gel electrolytes as a function of composition and temperature.

2) The polarisation technique was used to determine the ionic transport number of the polymeric gel electrolytes under present investigations.

3) The cyclic voltammetry was used to determine the electrochemical stability of the polymeric materials.

Two types of supercapacitors, namely EDLCs and redox capacitors were constructed using activated charcoal powder and polypyrrole electrodes, respectively, with the optimised polymeric gel electrolytes.

Different electrical and electrochemical measurements were used to study the performance characteristics of the supercapacitors.

(i)   a.c. impedance spectroscopy.

(ii)   Linear sweep cyclic voltammetry.

(iii) Galvanostatic charge discharge method.

(iv)   Prolonged cyclic tests.

7.2   Studies on Polymeric Gel Electrolytes:

As mentioned above, different experimental techniques were used in order to optimise the polymeric gel electrolytes for the fabrication of solid-state supercapacitors. For the purpose systematic studies have been carried out.

1) Composition dependence of liquid electrolytes has been carried out by varying the concentration of salts in EC:PC (1:1 V/V) mixture and it was found that the 1 M concentration of each salt is sufficient in order to achieve highest room temperature conductivity of the order of 10^{-3} S cm^{-1}.

2) Composition dependence of polymeric gel electrolytes has also been made in order to optimise the contents of polymer. It is found that 20 wt% of both the polymer i.e. PVdF-HFP and PMMA are optimised content for having acceptable conductivity at

182

room temperature ($\sim 10^{-3}$ S cm^{-1}) and mechanical property for their application in supercapacitors.

3) Temperature dependence of electrical conductivity of polymeric gel electrolytes has been studied and it is found that the polymeric gel under present study is quite stable over a temperature range varying from 280 K-370 K. The σ vs. 1/T variation shows predominantly VTF behaviour.

4) Polarisation technique has been adopted to calculate the transport number of the polymeric gel electrolytes. It has been found the ionic transport number to be in the range of 0.96 - 0.98, showing predominantly ionic nature of all the electrolytes under the present studies.

5) Electrochemical stability of the polymeric material has been tested and is found to be of the order of $\sim$ 4 Volts. This value of potential window is sufficient enough and acceptable from supercapacitor fabrication point of view.

6) The gel electrolytes based on three type of salts, namely, $LiClO_4$, $NaClO_4$ and $TEAClO_4$ were chosen with the aim to keep the size of anions constant by varying cationic size in order to see the effect of cations on the capacitive behaviour at the electrode-electrolyte interfaces of the supercapacitors.

7.3   Studies on Electrical Double Layer Capacitors (EDLCs):

Possibility of activated charcoal powder has been examined for its application as electrode material in the fabrication of all solid-state electrical double layer capacitors (EDLCs). The EDLCs have been fabricated using optimised gel electrolytes for the comparative studies. The following results have been obtained from different studies:

1) The overall capacitance values have been observed to be 70-152 mF cm^{-2} (equivalent to a single electrode specific capacitance of 40-78 F g^{-1} of activated charcoal powder).

183

2) The working voltage for each capacitor cell has been found to be 1.0 V, which corresponds to the energy densities of 5.3-10.8 W h Kg^{-1} and corresponding power density in the range of 0.19-0.22 kW Kg^{-1}.

3) Internal resistance of the cell has been observed to be 210-293 Ω cm^2, which is the attractive aspect of solid state EDLCs. Further improvement is still required.

4) Almost stable values of capacitance have been observed for each capacitor cells under present investigations for about 5000 cycles and even more.

5) Coulombic efficiency has been found to be in the range of 90-95% for each capacitor cells, showing liquid like electrochemical behaviour of all the gel electrolytes under present studies.

6) Comparative studies of all the capacitor cells show that the anions in the polymeric gel electrolytes play pre-dominant role in the capacitive behaviour of the solid state EDLCs, rather than the cations.

7.4 Studies on Redox Supercapacitors:

Comparative studies have also been carried out for electrochemically deposited polypyrrole based symmetric redox supercapacitors with all the sets of optimised polymeric gel electrolytes under present investigations. On the basis of studies using a.c. impedance spectroscopy, linear sweep cyclic voltammetry, charge discharge and prolonged cyclic tests, the following results have been observed:

1) The overall capacitance values have been found to be in the range of 14-25 mF cm^{-2}, which is equivalent to a single electrode specific capacitance of 78-178 F g^{-1}.

2) The working voltage for all the capacitor cells is limited to 1.0 V, owing to the limitation of working voltage of polypyrrole beyond 1.0 V. This voltage limit

corresponds to the energy density of 11-25 W h Kg^{-1} and their corresponding power density of the order of 0.22-2.80 kW Kg^{-1}.

3) Internal resistance is found to be in the order of hundreds of ohm cm^2, which is comparatively lower than that of the conventional polymer electrolytes based capacitors.

4) The capacitor cells show the stable capacitance values for about 5000 voltammetric cycles and even more, showing excellent cyclic efficiency for all the capacitor cells under present studies.

5) Coulombic efficiency is found to be of the order of 95-100% comparable to that of liquid electrolytes based capacitor cells. This again confirms the liquid like electrochemical behaviour of all the gel electrolytes under present studies.

6) Comparative studies again show that the types of cation of the salts used in the polymeric gel electrolytes hardly affect the capacitive properties of the redox supercapacitors under present investigations, rather predominant role of anions is possible.

7.5   Scope of Future Work:

Apart from the studies and investigations carried out in the present thesis, there is a vast scope for future work in this field, which is summarised as follows:

1) Some more polymeric gel electrolytes having high ionic conductivity at room temperature with good mechanical and electrochemical stability have to be explored for their practical applications.

2) Polymeric gel electrolytes have to be explored in depth using some other experimental techniques at their microscopic as well as macroscopic level in order to deeper insight

into the ion transport mechanism and test their suitability from device fabrication point of view.

3) Composites of electrode materials, such as blends of charcoal powder and amorphous manganese dioxide etc. can be explored as alternative electrode materials for the development of supercapacitors with improved performance.

4) n-doped conducting polymer is yet to be achieved under ambient conditions, so that working potential of the supercapacitor can be improved.

5) Some hybrid supercapacitors would be looked into in order to enhance their several electrical and electrochemical performances, such as specific capacitance, energy density, power density, working potential of the device and reduce the internal resistance of the devices for higher power density etc.

6) After having proper optimisation and encapsulation, commercialisation of these supercapacitors is practically possible for their low and high energy density applications.

References

REFERENCES

1. S. Chandra, "Superionic Solids: Principles and Applications", North Holland, Amsterdam, 1981.

2. T. Kudo, K. Fueki, "Solid State Ionics", VCH Publ., U.K, 1990.

3. Y. F. Y. Yao, J. T. Kummer, J. Inorg. Nuclear Chem., 29 (1967) 2553.

4. C. Tubandt, Z. Anorg. Allgem. Chem., 115 (1921) 105.

5. P. Hagenmuller, W. Van Gool, "Solid Electrolytes", Academic Press, New York, 1978.

6. J. Hladik, "Physics of Electrolytes", Vol. 1 and 2, Academic Press, New York, 1976.

7. E. C. Subba Rao, "Solid Electrolytes and their Applications", Plenum Press, New York, 1980.

8. A.L. Laskar, S. Chandra, "Superionic Solids and Solid Electrolytes: Recent Advances", Acad. Press, NY, 1989.

9. W. Van Gool, (ed.), "Fast Ion-Transport in Solids: Solid State Batteries and Devices", North Holland, Amsterdam, 1973.

10. P. Vasistha, J. N. Mundy, G. K. Shenoy, (eds.), "Fast Ion Transport in Solids: Electrodes and Electrolytes", North Holland, New York, 1979.

11. C. Julien, G. A. Nazri, "Solid State Batteries: Materials, Design and Optimization", Kluwer Acad. Publ., Boston, 1994.

12. B. V. R. Chowdari, S. Radhakrishna, "Solid State Ionic Devices", World Scientific Publishing Co., Singapore, 1988.

13. B. V. R. Chowdari, K. Lal, S. A. Agnihotri, N. Khare, S. S. Sekhon, P. C. Srivastava, S. Chandra, (eds.), "Solid State Ionics: Science & Technology", World Scientific Publishing Co. Singapore, 1998.

14. D. Kunze, "Fast Ion Transport in Solids-Solid State Batteries and Devices", W. Van Gool, (ed.), North Holland, Amsterdam, p.405, 1973.

15. K. W. Browall, J. S. Kasper, J. Solid State Chem., 15 (1975) 54.

16. B. A. Boukamp, G. A. Wiegers, Solid State Ionics, 9 & 10 (1983) 1193.

17. G. W. Mellors, D. V. Luzos, J. Electrochem. Soc., 118 (1971) 846.

18. B. Scrosati, F. Papeleo, G. Pistoia, M. Lazzari, J. Electrochem. Soc., 122 (1975) 339.

19. H. Wada, M. Ishii, M. Onoda, M. Tansho, A. Sato, Solid State Ionics, 86-88 (1996) 159.

20. N. Machida, S. Nishida, T. Shigematsu, H. Sekai, M. Tatsumisago, T. Minami, Solid State Ionics, 136-137 (2000) 381.

21. J. B. Goodenough, H. Y. P. Hong, J. A. Kafalas, Materials Research Bulletin, 11 (1976) 203.

22. W. Wang, J. Huang, "Solid State Ionic Materials", B. V. R. Chowdari et. al. (eds.) World Scientific Publishing Co., Malaysia, 1994, p. 179.

23. G. Vitins, J. Grins, T. Horlin, Solid State Ionics, 86-88 (1996) 119.

24. S. Yoshikado, Y. Michiue, Y. Onoda, M. Watanabe, Solid State Ionics, 136-137 (2000) 371.

25. B. A. Boukamp, R. A. Huggins, Phys. Lett., 58A (1976) 231.

26. J. Schoonman, J. Electrochem. Soc., 123 (1976) 1772.

27. C. E. Derrington, A. Linder, M. O. Keefee, J. Solid State Chem., 15 (1975) 171.

28. I. Murin, A. Peceliunaite, A. Kezionis, R. Mizaras, A. Orliukas, Solid State Ionics, 86-88 (1996) 247.

29. B. Kumar, L. G. Scanlon, R. J. Spry, J. Power Sources, 96 (2001) 337.

30. F. Banino, M. Lazzari, J. Power Sources, 1 (1976) 103.

31. C. A. Angel, Solid State Ionics, 18-19 (1986) 72.

32. E. Robinel, B. Carette, M. Ribes, J. Non-Crystalline Solids, 57 (1983) 49.

33. T. Minami, T. Shimizu, J. Chem. Soc., Japan. Chem. and Ind. Chem., p. 420, 1986.

34. T. Minami, T. Shimizu, M. Tanaka, Solid State Ionics, 9-10 (1983) 577.

35. J. M. Reau, B. Tanguy, J. J. Videau, J. Portier, P. Hagenmuller, Solid State Ionics, 28-30 (1988) 792.

36. K. Hariharan, R. Kaushik, J. Mater. Sci., 22 (1987) 3335.

37. J. P. Malugani, G. Robert, C. R. Acad. Sci. Paris C., 290 (1980) 251.

38. C. C. Hunter, M. D. Ingram, Solid State Ionics, 14 (1984) 31.

39. A. Magistris, G. Chiodelli, M. Duclot, Solid State Ionics, 9-10 (1983) 611.

40. J. P. Malugani, R. Mercier, B. Fahys, G. Robert, Solid State Chem., 45 (1982) 309.

41. A. Kone, M. Ribes, J. L. Souquet, Phys. Chem. Glasses, 23 (1982) 18.

42. M. D. Ingram, M. A. Machenzie, W. Muller, M. Torgge, Solid State Ionics, 28-30 (1988) 677.

43. S. Susman, C. J. Delbecq, J. A. McMillan, M. F. Roche, Solid State Ionics, 9-10 (1983) 667.

44. S. Chandra, A. Chandra, Proc. of the National Academy of Sciences, India, LXIV (1994) 141.

45. P. E. Bean, M. Tomozaw, Solid State Ionics, 18-19 (1986) 1219.

46. T. Minami, J. Non-Crystal. Solids, 56 (1983) 15.

47. R. C. Agrawal, R. Kumar, "Solid State Ionic Materials", B. V. R. Chowdari et. al. (eds.), World Scientific Publishing Co., Malaysia, 1994, p. 295.

48. T. Saito, N. Torata, M. Tatsumisago, T. Minami, Solid State Ionics, 86-88 (1996) 491.

49. S. S. Sekhon, S. Chandra, J. Mater. Sci. Lett., 18 (1999) 635.

50. V. K. Deshpande, F. C. Raghuwanshi, K. Singh, Solid State Ionics, 18-19 (1986) 378.

51. A. V. Deshpande, V. K. Deshpande, "Ion Conducting Materials: Theory and Applications", A. R. Kulkarni, P. Gopalan (eds.), Narosa Publishing House, New Delhi, 2001, p. 159.

52. H. S. Maiti, A. R. Kulkarni, A. Paul, Solid State Ionics, 9-10 (1983) 605.

53. Y. Kawamoto, I. Nohara, J. Fujiwara, Y. Umetani, Solid State Ionics, 24 (1987) 327.

54. B. V. R. Chowdari, G. V. Subba Rao, G. Y. H. Lee, Solid State Ionics, 136-137 (2000) 1067.

55. C. C. Liang, J. Electrochem. Soc., 120 (1973) 1289.

56. C. C. Liang, A. V. Joshi, W. E. Hamilten, J. Appl. Electrochem, 8 (1978) 445.

57. C. Liquan, Z. Zong – Yuan, L. Zirong, Kexue Tongbao, 26 (1981) 308.

58. M. A. K. L. Dissanayake, M. A. Careem, Solid State Ionics, 28 - 30 (1988) 1093.

59. K. Shahi, J. B. Wagner, J. Solid State Chem., 42 (1982) 107.

60. K. Shahi, J. B. Wagner, Jr., J. Phys. Chem. Solids, 43 (1982) 713.

61. V. B. Tare, "Materials for Solid State Batteries", B. V. R. Chowdari, & S. Rdhakrishna, (eds.), World Scientific Publishing Co., Singapore, p. 477, 1986.

62. J. Maier, "Transport – Structure Relations in Fast Ion and Mixed Conductors", F. W. Poulsen, N. Anderson Hessel, K. Clausen, S. Skaarup, Toft, O. Sorensen, (eds.), RISO National Laboratory, p. 153, 1985.

63. J. Maier, Phys. Chem. Solids, 46 (1985) 300.

64. P. W. S. K. Bhandarnayake, B. E. Mellander, Mat. Res. Bull., 14 (1979) 661.

65. N. Lakshmi, K. Pandey, P. K. Singh, S. Chandra, "Solid State Ionics: Science & Technology", B. V. R. Chowdari, K. Lal, S. A. Agnihotri, N. Khare, S. S. Sekhon, P. C. Shrivastava, S. Chandra, (eds.), World Scientific Publishing Co., Singapore, p.65, 1998.

66. D. E. Fenton, J. M. Parker, P. V. Wright, Polymer, 14 (1973) 589.

67. P. V. Wright, British Polymer J., 7 (1976) 319.

68. M. B. Armand, J. M. Chabagno, M. J. Duclot, Extended Abstr., 2nd International Conference on Solid Electrolytes, St. Andrews, Scotland, 1978.

69. M. B. Armand, J. M. Chabagno, M. J. Duclot, "Fast Ion Transport in Solids", P. Vasistha, J. N. Mundy, G. K. Shenoy, (eds.), North Holland, Amsterdam, p.131, 1979.

70. B. Papke, M. A. Ratner, D. F. Shriever, J. Electrochem. Soc., 129 (1982) 1682.

71. M. B. Armand, Annual Rev. Mater. Sci., 16 (1986) 245.

72. J. R. MacCallum, C. A. Vincent, "Polymer Electrolyte Reviews", Elsevier applied Science, London, Vol.-I, 1987 and Vol.-II, 1989.

73. F. M. Gray, "Solid Polymer Electrolytes: Fundamentals and Technological Applications" VCH Publishers Inc., USA, 1991.

74. R. G. Linford (ed.), "Electrochemical Science and Technology of Polymers-I", Elsevier Science, London, 1987.

75. P. G. Bruce, (ed.), "Solid State Electrochemistry", Cambridge University Press, 1995.

76. C. A. Vincent, Progress in Solid State Chem., 17 (1987) 1485.; 88 (1989) 109.

77. M. C. Wintersgill, J. J. Fontanella, J. P. Calme, M. K. Smith, T. B. Jones, S. G. Greenbaum, K. J. Adamic, A. N. Shetty, C. G. Andeen, Solid State Ionics, 18-19 (1986) 326.

78. S. G. Greenbaum, K. J. Adamic, Y. S. Pak, M. C. Wintersgill, J. J. Fontanella, Solid State Ionics, 28-30 (1988) 1042.

79. A. Magistris, G. Chiodelli, K. Singh, P. Ferloni, Solid State Ionics, 38 (1990) 235.

80. K. S. Sidhu, S. S. Sekhon, S. A. Hashmi, S. Chandra, J. Mater. Sci. Lett., 12 (1993) 346.

81. T. M. A. Abrantes, L. J. Alcacer, C. A. C. Sequeiraz, Solid State Ionics, 28 –30 (1993) 315.

82. S. Chandra, S.A. Hashmi, M. Saleem, R. C. Agrawal, Solid State Ionics, 67 (1993) 1.

83. K. K. Maurya, N. Srivastava, S. A. Hashmi, S. Chandra, J. Mater. Sci., 27 (1992) 135.

84. S. A. Hashmi, A. Kumar, K. K. Maurya, S. Chandra, J. Phys. D.- Appl. Phys., 23 (1990) 1307.

85. K. K. Maurya, S. A. Hashmi, S. Chandra, J. Phys. Soc. Japan, 61 (1992) 1709.

86. S. Clancy, D. F. Shriver, L. A. Ochrymowyez, Macromolecules, 19 (1986) 606.

87. A. J. Pollak, "Conductive Polymers and Plastics", J. M. Margolis (ed.), Chapman & Hall, NY, London, p.41, 1989.

88. S. A. Hashmi, S. Chandra, Mater. Sci. & Engg, B., 34 (1995) 18.

89. M. Watanabe, M. Rikukawa, K. Sanui, N. Ogata, H. Kato, T. Kobayashi, Z. Ohtaki, Macromolecules, 17 (1984) 2902.

90. K. M. Abraham, "Solid State Ionics-Materials and Applications", B. V. R. Chowdari, S. Chandra, S. Singh, P. C. Srivastava, (eds.), World Scientific, Singapore, p.277, 1992.

91. P. Mustarelli, E. Quartarone, C. Tomasi, A. Magistris, Solid State Ionics, 135 (2000) 81.

92. P. S. S. Prasad, M. Z. A. Munshi, B.B. Owens, W. H. Smyrl, Solid State Ionics, 40-41 (1990) 959.

93. N. Srivastava, S. Chandra, Eur. Polymer J., 36 (2000) 421.

94. M. M. Doeff, L. Edman, S. E. Sloop, J. Kerr, L. C. D. Janghe, J. of Power Sources, 89 (2000) 227.

95. G. B. Appetecchi, S. Passerini, J. Electrochem. Soc., 149 (7) (2002) A891.

96. D. F. Shriver, P. G. Bruce, "Solid State Electrochemistry, Chemistry of Solid State Materials", (Ed.), P. G. Bruce, Cambridge Univ. Press, U.K., 1999, p. 95.

97. D. M. Ivory, G. G. Miller, J. M. Sowa, L. W. Schacklette, R. R. Chance, R. H. Boughman, J. Chem. Phys., 71 (1979) 1506.

98. L. C. Hardy, D. F. Shriver, J. Am. Chem. Soc., 108 (1986) 2887.

99. J. R. Owens, "Fast Ion-Transport in Solids: Solid State Batteries and Devices", W. Van Gool, (ed.), North Holland, Amsterdam, 1973.

100. K. E. Doan, S. Ganapathiappan, K. Chen, M. A. Ratner, D. F. Shriver, "Solid State Ionics", G. Nazri, R. A. Huggins, D. F. Shriver, (eds.), Materials Research Society, Pittsburgh, Vol. 135, p.343, 1989.

101. B. Scrosati, C. A. Vincent, MRS Bull., March (2000) 28.

102. C. A. Angell, C. Liu, E. Sanchez, Nature, 362 (1993) 137.

103. C. A. Angell, J. Fan, C. Liu, Q. Liu, E. Sanchez, K. Xu, Solid State Ionics, 69 (1994) 343.

104. F. M. Gray, "Polymer Electrolytes", RSC Materials Monographs, (Ed.), J. A. Cannor, The Royal Society of Chemistry, Cambridge, U. K., 1997, p. 31.

105. J. Weston, B. C. H. Steele, Solid State Ionics, 7 (1982) 75.

106. W. Wieczorek, Mat. Sci. and Engg. B, 15 (1992) 108.

107. J. Przyluski, W. Weiczorek, "Solid State Ionic devices", B. V. R. Chowdari, S. Radhakrishna, (eds.), World Scientific, Singapore, p. 475, 1988.

108. B. K. Choi, K. H. Shin, Solid State Ionics, 86-88 (1996) 303.

109. S. Skaarup, K. West, B. Z. Christiansen, Solid State Ionics, 28-30 (1988) 975.

110. A. Dabrowska, W. Wieczorek, Mat. Sci. and Engg. B, 22 (1994) 117.

111. G. B. Appetecchi, S. Passerini, Electrochim. Acta, 45 (2000) 2139.

112. F. Croce, G. B. Appetecchi, L. Persi, B. Scrosati, Nature, 394 (1998) 456.

113. R. A. Vaia, S. Vasudevan, W. Krawiek, L. G. Scanlon, E. P. Giannelis, Adv. Mater., 7 (1995) 154.

114. D. P. Almond, A. R. West, Solid state Ionics, 23 (1987) 27.

115. J. Plocharski, W. Wieczorek, J. Przyluski, K. Such, Appl. Phys. A, 49 (1989) 55.

116. D. P. Almond, A. R. West, Solid State Ionics, 9-10 (1983) 277.

117. W. Wieczorek, K. Such, H. Wycislik, J. Plocharski, Solid State Ionics, 36 (1989) 255.

118. C. W. Nan, D. M. Smith, Mater. Sc. & Engg. B, 10 (1991) 99.

193

119. W. Wieczorek, M. Seikierski, J. Appl. Phys., 76(4) (1994) 2220.

120. W. Wieczorek, A. Zalewska, M. Seikierski, J. Przyluski, Solid State Ionics, 86-88 (1996) 357.

121. M. Nakamura, Phys. Rev. B, 29 (1984) 3691.

122. J. W. Lorimer, J. Power Sources, 26 (1989) 491.

123. O. Bohnke, C. Rousselot, P. A. Gillet, C. Truche, J. Electrochem. Soc., 139(7) (1992) 1862.

124. B. R. Scrosati, "Solid State Ionics: Materials and Applications", (Eds.), B. V. R. Chowdari, S. Chandra, S. Singh, P. C. Srivastava, World Scientific Co., Singapore (1992) 321.

125. J. Y. Sanchez, Solid State Ionics: Materials and Applications, (Eds.) B. V. R. Chowdari, S. Chandra, S. Singh, P. C. Srivastava, World Scientific Co., Singapore, 1992, p. 159.

126. S. A. Agnihotry, Pradeep, S. S. Sekhon, Electrochim. Acta., 44 (1999) 3121.

127. E. Cazzanelli, G. Mariotto, G. B. Appetechi, F. Croce, Ionics, 2 (1996) 81.

128. M. Kono, E. Hayashi, M. Watanabe, J. Electrochem. Soc., 146 (5) (1999) 1626.

129. M. Watanabe, M. Kanaba, K. Nagaoka, I. Shinohara, J. Polym. Sci., Polym. Phys. Edition, 21 (1983) 939.

130. E. Tsushida, H. Ohno, K. Tsunemi, Electrochim. Acta, 28 (1983) 591.

131. K. Tsunemi, H. Ohno, E. Tsushida, Electrochim. Acta, 28 (1983) 833.

132. J. M. Tarascon, A. S. Gozdz, C. Schmutz, F. Shokoohi, P. C. Warren, Solid State Ionics, 86 (1993) 49.

133. D. Peramungae, D. M. Pasquariello, K. M. Abraham, J. Electrochem. Soc., 142 (6) (1995) 1789.

134. T. Osaka, X. Liu, M. Nojima, T. Momma, J. Electrochem. Soc., 146 (5) (1999) 1724.

135. D. Fauteux, A. Massucco, M. McLin, M. V. Buren, J. Shi, Electrochim. Acta., 14 (13-14) (1995) 2185.

136. Y. Saito, C. Capiglia, H. Yamamoto, P. Mustarelli, J. Electrochem. Soc., 147 (2000) 1645.

137. J. M. Tarascon, M. Armand, Nature, 414 (2001) 359.

138. B. Scrosati, "Solid State Ionics - New Developments", B. V. R. Chowdari, M. Yahaya, I. A. Talib, M. M. Salleh (eds.), World Scientific, Singapore, p.411, 1996.

139. H. G. H. Sunder, S. W. Martin, C. A. Angell, Solid State Ionics, 18-19 (1986) 437.

140. A. M. Voice, J. P. Southall, V. Rogers, K. H. Matthews, G. R. Davies, J. E. McIntyre, I. M. Ward, Polymer, 35 (1994) 3363.

141. Y. Saito et. al., Solid State Ionics, 131 (2000) 291.

142. H. Tsutsumi, Y. Nakgawa, K. Tamura, Solar Energy Materials and Solar Cells, 39 (1995) 341.

143. H. M. Upadhyaya, R. K. Yadav, A. K. Thakur, S. A. Hashmi, "Ion Conducting Materials: Theory and Applications" Narosa Publishing House, New Delhi, p. 111, 2000.

144. S. S. Sekhon, N. Arora, "Solid State Ionics: Materials & Devices", B. V. R. Chowdari, Wenji Wang, (eds.), World Scientific Publishing Co., Singapore, p. 443, 2000.

145. K. M. Abraham, M. Alamgir, J. Electrochem. Soc., 137 (1990) 1657.

146. M. Alamgir, K. M. Abraham, J. Electrochem Soc., 140 (1993) L 96.
147. O. Bohnke, G. Frand, M. Rezrazi, C. Rousselot, C. Truche, Solid State Ionics, 66 (1993) 97, 66 (1993) 105.

148. P. E. Stallworth, J. Li, S. G. Greenbaum, F. Croce, S. Slane, M. Salomon, Solid State Ionics, 73 (1994) 119.

149. B. K. Choi, H. K. Lee, Y. W. Kim, Solid State Ionics, 113-115 (1998) 493.

150. K. M. Abraham, M. Alamgir, D. K. Hoffman, J. Electrochem. Soc., 142 (1995) 683.

151. C. A. Edmondson, M. G. Wintersgill, J. J. Fontanella, F. Gerace, B. Scrosati, S. G. Greenbaum, Solid State Ionics, 85 (1996) 173.

152. S. Panero, A. Clemente, E. Spila, Solid State Ionics, 86-88 (1996) 1285.

153. B. Huang, Z. Wang, G. Li, H. Huang, R. Xue, L. Chen, F. Wang, Solid State Ionics, 85 (1996) 79.

154. D. Ostrovskii, L. M. Torell, G. B. Appetecchi, B. Scrosati, Solid State Ionics, 106 (1998) 19.

155. P. E. Stallworth, J. J. Fontanella, M. C. Wintersgill, C. D. Scheidler, J. J. Immel, S. G. Greenbaum, A. S. Gozdz, Journal of Power Sources, 81-82 (1999) 739.

156. P. Periasamy, K. Tatsumi, M. Shikano, T. Fujieda, T. Sakai, Y. Saito, M. Mizuhata, A. Kajinami, S. Deki, Solid State Ionics, 126 (1999) 285.

157. A. M. Grillone, S. Panero, B. A. Retamal, B. Scrosati, J. Electrochem. Soc., 146 (1) (1999) 27.

158. M. Morita, F. Araki, K. Kashiwamura, N. Yashimoto, M. Ishikawa, Eletrochim. Acta, 45 (2000) 1335.

159. H. Ericson, C. Svenbereg, A. Brodin, A. M. Grillone, S. Panero, B. Scrosati, P. Jacobsson, Electrochim. Acta, 45 (2000) 1409.

160. C. Capiglia, Y. Saito, H. Kataoka, T. Kodama, E. Quartarone, P. Mustarelli, Solid State Ionics, 131 (2000) 291.

161. P. Periasamy, K. Tatsumi, M. Shikano, T. Fujieda, T. Sakai, Y. Saito, T. Sakai, M. Mizuhata, A. Kajinami, S. Deki, J. Power Sources, 88 (2000) 269.

162. C. S. Kim, S. M. Oh, Electrochim. Acta, 46 (2001) 1323.

163. J. Vondrak, M. Sedlarikova, J. Velicka, B. Klapste, V. Novak, J. Reiter, Electrochim. Acta, 46 (2001) 2047.

164. M. Deepa, N. Sharma, P. Varshney, R. Chandra, S. A. Agnihotry, "Ion Conducting Materials: Theory and Applications", A. R. Kulkarni, P. Gopalan (eds.), Narosa Publishing House, New Delhi, 2001, p. 74.

165. Nobuko Yoshimoto, Shin Yakushiji, Masashi Ishikawa, Masayuki Morita, Electrochim. Acta, 48 (2003) 2317.

166. S. S. Sekhon, H. P. Singh, Solid State Ionics, 175 (2004) 545.

167. H. P. Singh, S. S. Sekhon, Electrochim. Acta, 50 (2004) 621.

168. S. S. Zhang, M. H. Ervin, K. Xu, T. R. Jow, Solid State Ionics, 176 (2005) 41.

169. K. S. Kim, S. Y. Park, Sun-Hwa Yeon, Huen Lee, Electrochim. Acta, 2005, in press.

170. Jaephil Cho, Meilin Liu, Electrochim. Acta, 42 (1997) 1481.

171. K. West, B. Z. Christiansen, T. Jacobsen, S. Skaarup, Solid State ionics, 28-30 (1988) 1128.

172. R. Koksbang, J. Barker, H. Shi, M. Y. Saidi, Solid State Ionics, 84 (1996) 1.

173. B. D. Mc Nicol, D. A. J. Rand, "Power Sources for Electric Vehicles", Elsevier Science, Amsterdam, 1984.

174. M. Z. A. Munshi, B. B. Owens, "Superionic Solids and Solid Electrolytes: Recent Trends", A. L. Laskar, S. Chandra, (eds.), Academic Press Inc., 1989, p.631.

175. M. Z. A. Munshi, (ed.), "Hand Book of Solid State Batteries and Capacitors", World Scientific Publishing Co., Singapore, 1995.

176. D. A. J. Rand, R. Woods, R. M. Dell, "Batteries for Electric Vehicles", John Wiley & Sons Inc., 1998.

177. J. B. Bates, N. J. Dudney, B. Neudecker, A. Vedaa, C. D. Evans, Solid State Ionics, 135 (2000) 33.

178. S. Kondo, "Lithium Ion Batteries: Fundamentals and Performance", M. Wakihara,   O. Yamaamoto, (eds.), Kodansha, Wiley-VCH, 1998, p.199.

179. Michael Krumplet, Romesh Kumar, K. M. Myles, J. Power Sources, 49 (1994) 37.

180. A. K. Shukla, R. Manoharan, K. V. Ramesh, Bull. Mat. Sci., 5 (1983) 267.

181. A. Kuver, I. Vogel, W. Vielstich, J. Power Sources, 52 (1994) 77.

182. J. T. Wang, J. S. Wainright, R. F. Savinell, M. Litt., J. Appl. Electrochem., 26 (1995) 751.

183. C. G. Granqvist, "Handbook of Inorganic Electrochromic Materials", Elsevier Science B. V., Amsterdam, Netherlands (1995) 1.

184. C. M. Lampert, Sol. Energy Mater., 6 (1981) 1.

185. S. Chao, M. S. Wrighton, J. Am. Chem.,Soc., 109 (1987) 2197.

186. Y. Sadaoka, Y. Sakai, H. Akiyama, "A humidity sensor using alkali-salt-PEO hybrid films", J. Mater. Sci., 21 (1986) 235.

187. W. Shimizu, K. Komoric, M. Egashira, J. Electrochem. Soc., 136 (1989) 2256.

188. S. Kuwata, H. Miura, N. Yamazoe, Chem. Lett., (1988) 1197.

189. H. Auer, G. Winkler, U. S. Patent # 4,984,342 (1991).

190. S. Tsuchiya, Y. Kudoh, T. Kojima, M. Fukuyama, and S. Yoshimura, U. S. Patent # 4,943,892, (1990).

191. K. Suguro, U. S. Patent # 4,959,745, (1990).

192. F. Jonas, G. Heywang, W. Schmidtberg, U. S. Patent # 4,910,645, (1990).

193. M. Waidhas, K. Pantel, G. Richter, U. S. Patent # 5,189,770, (1993).

194. K. Naitoh, Y. Arakawa, T. Ikezaki, S. Yabe, Y. Yokoyama, Y. Hamaguchi, Y. Roppongi, U. S. Patent # 4,889,536, (1989).

195. H. Von Helmholtz, Ann. Phys. (Leipzig), 89 (1853) 211.

196. G. Guoy, Ann. Phys., Paris, 7 (1917) 129; J. de Phys., 9 (1910) 457.

197. R. H. Fowler, E. A. Guggenheim, Statistical Thermodynamics, Cambridge University Press, (1939) 77.

198. O. Stern, Zeit. Elektochem., 30 (1924) 508.

199. D. L. Chapman, Phil. Mag., 25 (1913) 475.

200. D. O. Raleigh, J. Phys. Chem. 70 (1966) 689.

201. B. E. Conway, Electrochemical Supercapacitors: Scientific Fundamentals and Technical Applications, Kluwer Academic/Plenum Publishers, 1999.

202. F. M. Delnick, D. Intersoll, X. Andriew, K. Naoi (eds.), Electrochemical Capacitors II, Electrochem. Soc. Proc. Ser. Penington, NJ, 1997.

203. R. Kotz, M. Carlen, Electrochim. Acta, 45 (2000) 2483.

204. A. Nishino, J. Power Sources, 60 (1996) 137.

205. S. Sarangapani, B.V.Tilak, C. P. Chen, J. Electrochem. Soc., 143 (1996) 3791.

206. S.A.Hashmi, National Acad. Sci. Lett., 27 (2004) 27.

207. J.C. Lassagues, J. Grondin, T. Becker, L. Servant, M. Hernandez, Solid State Ionics, 77 (1995) 311.

208. S. Shiraishi, H.Kurihara, Lan Shi, T. Nakayama, A. Oya, *J. Electrochem Soc.*, 149 (2002) A855.

209. M. Ishikawa, M. Morita, M. Ihara, Y. Matsuda, *J. Electrochem Soc.*, 141 (1994) 1730

210. M. Ishikawa, M. Ihara , M. Morita, Y. Mabada, *Electrochim. Acta* 40 (1995) 2217.

211. S.A.Hashmi, R.J.Latham, R.G.Linford and W.S. Schlindwein, J. Chem. Soc., Faraday Trans, 93 (1997) 4177.

212. T. Osaka, X. Liu, M. Nojima, T. Mmomma, *J. Electrochem Soc.*, 146 (1999) 1724.

213. H. Nagakawa, A. Shudo and K. Miura, J. Electrochem. Soc., 147 (2000) 38.

214. C. Portet, P. L. Taberna, P. Simon, E. Flahaut, J. Power Sources, 139 (2005) 371.

215. T. Osaka, X. Liu, M. Nojima, J. Power Sources, 74 (1998) 122.

216. A. Matsuda, H. Honjo, M. Tatsumisago, T. Minami, Solid State Ionics, 113 (1998) 97.

217. Y. Matsuda, K. Inone, H. Takeuchi, Y. Okuhama, Solid State Ionics, 113 (1998) 103.

218. Y. Sakata, A. Muto, Md. Azaharruddin, N. Yamada, C. Marumo, S. Ibaraki, K. Kojima, Electrochemical and Solid State Letters, 3 (2000) 1.

219. F. C. Wu, R. L. Tseng, C. C. Hu, C. C. Wang, Journal of Power Sources, 144 (2005) 302.

220. A. B. Fuertes, G. Lota, T. A. Centeno, E. Frackowiak, Electrochima Acta, 50 (2005) 2799.

221. M. Kodama, J. Yamashita, Y. Soneda, H. Hatori, S. Nishimura, K. Kamegawa, Mater. Sci. and Engg. B, 108 (2004) 156.

222. I. Tanahashi, A. Yoshida, A. Nishino, Bull. Chem. Soc. Japan, 63 (1990) 3611.

223. Y. Guo, J. Qi, Y. Jiang, S. Yang, Z. Wang, H. Xu, Mater. Chem. & Phys., 80 (2003) 704.

224. C. Emmenegger, P. Mauron, P. Sudan, P. Wenger, V. Hermann, R. Gallay, A. Zuttel, J. Power Sources, 124 (2003) 321.

225. W. Li, H. Probstle, J. Fricke, J. Non-Crystalline Solids, 325 (2003) 1.

226. M. Ue, M. Taked, T. Takahashi, M. Takehorra, Electrochem. and Solid State Letters, 5 (2002) A119.

227. J. M. Pernaut, G. Goulart, J. Power Sources, 55 (1995) 93.

228. S. T. Mayer, R. W. Pakela, J. L. Kaschmitter, J. Electrochem. Soc., 140 (1993) 446.

229. H. Shi, Electrochimica Acta, 41 (1996) 1633.

230. H. Nakagawa, A. Shudo, K. Miura, J. Electrochem. Soc., 147 (2000) 38.

231. H. J. Bang, W. Lu, F. Cao, J. Prakash, Electrochem. Comm., 2 (2000) 653.

232. P. Gouerec, H. Talbi, D. Miousse, F. T. Van, C. H. Duo, K. H. Lee, J. Electrochem. Soc., 148 (2001) A 94.

233. P. V. Adhyapak, T. Maddanimath, S. Pethkar, A. J. Chandwadkar, Y. S. Negi, K. Vijayamohanan, J. Power Sources, 109 (2002) 105.

234. N. L. Wu, S. Y. Wang, J. Power Sources, 110 (2002) 233.

235. Y. R. Nian, H. Teng, J. Electrochem. Soc., 149 (2002) A1008.

236. H. Yang, M. Yoshio, K. Ison, R. Kuramoto, Electrochem. and Solid State Letters, 5 (2002) A141.

237. J.P. Zheng, T. R. Jow, J. Electrochem. Soc., 142 (1995) L6.

238. K-C. Liu, M. A. Anderson, *J. Electrochem Soc.,* 143 (1996) 124.

239. V. Srinivasan, J.W. Weidner, *J. Electrochem Soc.,* 147 (2000) 880.

240. A. Rudge, J. Davey, I Raistrick, S. Gottesfeld, J. Power Sources, 47 (1994) 89.

241. A. Clemente, S.Panero, E. Spila, B. Scrosati, Solid State Ionics, 85 (1996) 273.

242. S.A.Hashmi, R.J.Latham, R.G.Linford, W.S. Schlindwein, Polymer- International, 47 (1998) 28.

243. S.A.Hashmi, R.J.Latham, R.G.Linford, W.S. Schlindwein, Ionics, 3 (1997) 177.

244. C.Arbizzani, M. Mastragostino, L. Meneghello, Electrochim. Acta, 40 (1995) 2223.

245. J.C.Carlberg, O.Inganas, J. Electrochem. Soc., 144 (1997) L61.

246. J. H. Park, J. M. Ko, O. Ok Park, D-W.Kim, J. Power Sources 105 (2002) 20.

247. K.S.Ryu, K. M. Kim, Y.J.Park, N-G. Park, M.G.Kang, S. H. Chang, Solid State Ionics, 152-153 (2002) 861.

248. S. A. Hashmi, H.M. Upadhyaya, *Ionics,* 8 (2002), 272

249. A. Balducci, W. A. Henderson, M. Mastragostino, S. Passerini, P. Simon, F. Soavi, Electrochima Acta, 50 (2005) 2233.

250. Y. Gang Wang, Zi – Dong Wang, Y. Y. Xia, Electrochimica Acta, (2005) in press.

251. S. A. Hashmi, H.M. Upadhyaya, *Solid State Ionics,* 152-153 (2002) 883.

252. K. Rajendra Prasad, N. Munichandraiah, J. Electrochem. Soc., 149 (2002) A1393.

253. M. Mastragostino, R. Paraventi, A. Zanelli, J. Electrochem. Soc., 147 (2000) 3167.

254. D. Belanger, X. Ren, J. Davey, F. Uribe, S. Gottesfeld, J. Electrochem. Soc., 147 (2000) 2923.

255. M. Mastragostino, C. Arbizzani, F. Soavi, J. Power Sources, 97 (2001) 812.

256. E. Frackowiak, K. Jurewicz, S. Delpeun, F. Beguin, J. Power Sources, 97 (2001) 822.

257. F. Fusalba, P. Gouerec, D. Villers, D. Belanger, J. Electrochem. Soc., 148 (2001) A1.

258. J. H. Park, O. O. Park, J. Power Sources, 111 (2002) 185.

259. K. Rajendra Prasad, N. Munichandraiah, J. Power Sources, 112 (2002) 443.

260. K. Naoi, S. Suematsue, A. Manago, *J. Electrochem Soc.,* 147 (2000) 420.

261. S. A. Hashmi, S. Suematsue, K. Naoi, J. Power Sources, 137 (2004) 145.

262. R. Ma, B. Wei, C. Xu, J. Liang, D. Wu, Bull. Chem. Soc., Japan, 73 (2000) 1813.

263. Y. Sato, K. Yomogide, T. Nanaumi, K.Kobayakawa, Y. Ohsawa, M. Kawai, Electrochem. and Solid State Letters, 3 (2000) 113.

264. Y. U. Jeong, A. Manthiram, Electrochem. and Solid State Letters, 3 (2000) 205.

265. F. Cao, Jai Prakash, J. Power Sources,, 92 (2001) 40.

266. Y. U. Jeong, A. Manthiram, J. Electrochem. Soc., 148 (2001) A189.

267. N. L. Wu, S. L. Kuo, M. H. Lee, J. Power Sources, 104 (2002) 62.

268. H. Kim, B. N. Popov, J. Power Sources, 104 (2002) 52.

269. W. Sugimoto, T. Shibutani, Y. Murakami, Y. Takasu, Electrochem. and Solid State Letters, 5 (2002) A170.

270. Y. G. Wang, L. Cheng, Y. Y. Xia, J. Power Sources, (2005) in press.

271. R. G. Linford, S. Hackwood, Chem. Rev., 81 (1981) 3127.

272. D. Brinkmann, "Solid State Ionic Devices", B. V. R. Chowdari and S. Radhakrishna, (eds.), World Scientific Publishing Co., Singapore, 1988.

273. Goldstein, "Scanning Electron Microscopy and X-ray Microanalysis", 2nd edition, Plenum Press, NY, 1992.

274. E. R. Weiss, J. H. Guentherodt (eds.), "Scanning Tunneling Microscopy" I & II, Springer Series in Surface Sciences, Springer-Verlag, NY, 1992, Vol. 20 & 28.

275. D. A. Bonne, "Scanning Tunneling Microscopy and Spectroscopy: Theory, Techniques and Applications", VCH, NY, 1993.

276. J. A. Stroscio, W. J. Kaiser (eds.), "Scanning Tunneling Microscopy: Methods in Experimental Physics", Academic Press Inc., San Diego, CA, Vol. 27, 1995.

277. L. M. Brown (ed.), "Electron Microscopy and Analysis", Inst. Of Physics Conf. Series No. 90, 1987.

278. R. L. Darrel, B. A. Parkinson, Annal. Chem., 88 (1994) 64 R.

279. W. H. Freeman, " X-ray diffraction in Crystals, Imperfect Crystals and Amorphous bodies", A. Guinier, San Fransisco, 1963.

280. G. E. Bacon, "Neutron Diffraction", 2nd ed., Oxford: Clarendon press, 1962.

281. B. D. Cullity, "Elements of X-ray diffraction", 2nd ed., Addission-Wesley Publishing Co., NY, 1978.

282. R. A. Vargas, M. B. Salamon, C. P. Flynn, Phys. Rev. B, 17B (1978) 269.

283. R. A. Vargas, M. B. Salamon, C. P. Flynn, Phys. Rev. Lett., 37 (1976) 1550.

284. K. Arribart, J. F. Gouyet, B. Saporal, "Fast-Ion Transport in Solids", P. Vasistha, J. N. Mundy, J. K. Shenoy (eds.), North-Holland, NY, 569, 1979.

285. M. B. Salamon, Top. Current Phys., 175 (1979) 1.

286. R. F. Speyer, "Thermal Analysis of Materials", Marcel Dekker, NY, 1994.

287. S. Chandra, N. Singh, B. Singh, A. L. Varma, S. S. Khatri, T. Chakraty, J. Phys. Chem. Solids, 48 (1987) 1165.

288. E. O. Stejskal, J. E. Tanner, J. Chem. Phys., 42 (1965) 288.

289. S. Chandra, N. Singh, S. A. Hashmi, Proc. of Ind. Natl. Sci. Acad., 52 (1986) 338.

290. P. R. Sorensen, T. Jacobsen, Electrochim. Acta, 27 (1982) 1671.

291. J. R. Mac Donald, "Impedance Spectroscopy", John Wiley & Sons, Inc. NY, 1987.

292. P. M. Blonsky, D. F. Shriver, P. Austir, H. R. Allock, Solid State Ionics, 18/19 (1986) 258.

293. P. G. Bruce, C. A. Vincent, J. Electroanal. Chem. Interfacial Electrochem., (1987) 225.

294. J. Evans, C. A. Vincent, P. G. Bruce, Polymer, 28 (1987) 2324.

295. M. Watanabe, S. Nagano, K. Sanui, N. Ogata, Solid State Ionics, 28-30 (1988) 911.

296. M. Watanabe, M. Rikukawa, K. Sanui, N. Ogata, J. Appl. Phys., 58 (1985) 736.

297. S. Chandra, S. K. Tolpadi, S. A. Hashmi, Solid State Ionics, 28-30 (1988) 651.

298. S. M. Shapiro, F. Reidinger, "Physics of Superionic Conductors", M. B. Salamon (ed.), Berlin Heidelberg: Springer, 1979, p. 45.

299. H. Schulz, H. Zucker, Solid State Ionics, 5 (1981) 41.

300. R. C. T. Slade, "Solid State Protonic Conductors III" eds, J. B. Goodenough, J. Jensen, A. Potier (Odense Univ. Press, Denmark) (1985) 112.

301. W. E. Morener, (ed.), "Persistent Spectral Hole-Burning: Science and Applications", Springer-Verlag, Berlin, 1988.

302. S. Matsuo, H. Yugami, M. Ishigame, in "Solid State Ionics: New Developments", B. V. R. Chowdari et. al, (eds.), World Scientific Publishing Co., Singapore.

303. M. J. Line, R. G. Pritchard, R. Pynenburg, R. J. Latham, R. G. Linford, Surface and Interface Analysis, 23 (1995) 565.

304. S. A. Hashmi, A. K. Thakur, H. M. Upadhyaya, Eur. Polymer J., 34 (1998) 1277.

305. A. K. Thakur, H. M. Upadhyaya, S. A. Hashmi, A. L. Varma, Ind. J. Pure & Appl. Phys., 37 (1999) 302.

306. S. A. Hashmi, H. M. Upadhyaya, A. K. Thakur, Ionics, 6 (2000) 248.

307. P. G. Bruce in: "Polymer Electrolyte Reviews-I", J. R. MacCallum, C. A. Vincent (eds.), Elsevier Science, p.237, 1987.

308. K. S. Cole, R. H. Cole, J. Chem. Phys., 9 (1941) 341.

309. J. E. Bauerle, J. Chem. Phys., 45 (1969) 2657.

310. J. E. B. Randles, Discuss. Faraday Soc., 1 (1947) 11.

311. I. D. Raistrick, J. R. Macdonald, D. R. Franceschetti, in: "Impedance Spectroscopy characterizing Solid Materials and analysis", J. R. Macdonald (ed.), Chap. 2, John Wiley & Sons, Inc., New York 1987.

312. J. B. Wagner, in: "Electrode Processes in Solid State Ionics", M. Kleitz and M. Dupuy, (Eds.), Reidel, Holland, (1976) 185.

313. C. Wagner, Prog. Solid State Chem., 10 (1975) 3.

314. H. Gao, C. Fang, Y. Zhang, Solid State Ionics: Materials and Applications, (Eds.) B. V. R. Chowdari, S. Chandra, S. Singh, P. C. Srivastava, World Scientific Co. Singapore (1992) 539.

315. F. Croce, G. B. Appetechi, P. Mustarelli, E. Quartarone, C. Tomasi, E. Cazzanelli, Electrochim. Acta, 10-11 (1998) 1441.

316. M. Armand, W. Gorecki, R. Andreani, Second International Symposium on Polymer Electrolytes, (Ed.), B. Scrosati, Elsevier, London, U.K (1990) 91.

317. S. Tobishima, A. Yamaji, Electrochim. Acta, 29 (1984) 267.

318. Merck Catalogue for Reagents, Chemicals and Diagnostics (1996).

319. M. C. Smart, B. V. Ratnakumar, S. Surampudi, J. Electrochem. Soc., 146 (1999) 486; ibid, 149 (2002) A185.

320. O. Bohnke, G. Frand, M. Rezrazi, C. Rousselot, C. Truche, Solid State Ionics, 66 (1993) 97.

321. G. Frand, C. Rousselot, O. Bohnke, Proc. Photo-Opt. Instrum. Eng., 1728 (1992) 157.

322. H. Hong, C. Liquan, X. Tongjian, Solid State Ionics: Materials and Applications, (Eds.), B. V. R. Chowdari, S. Chandra, S. Singh, P. C. Srivastava, World Scientific Co. Singapore (1992) 199.

323. F. Croce, S. D. Brown, S. G. Greenbaum, S. M. Slane, M. Salomon, Chem. Mater. 5 (1993) 1268.

324. P. G. Bruce, Synth. Met. 45 (1991) 267.

325. S. Chandra, S. S. Sekhon, N. Arora, Ionics, 6 (2000) 112.

326. S. Chandra, S. S. Sekhon, Ritu Shrivastava, N. Arora, Solid State Ionics, 154-155 (2002) 6099.

327. I. I. Olsen, R. Koksbang, J. Electrochem. Soc., 143 (1996) 570.

328. M. A. Ratner, D. F. Shriver, Chem. Rev. 88 (1988) 109.

329. S. A. Agnihotry, Nidhi, Pradeep, S. S. Sekhon, Solid State Ionics, 136-137 (2000) 573.

330. M. H. Cohen, D. Turnbull, J. Chem. Phys. 31 (1959) 1164.

331. Kim Kinoshita and Xi Chu, Proc. Symp.Electrochem. Capacitors, The Electrochem. Soc. Proc., 95-29 (1997) 171-180.

332. C. Iwakura, H. Wada, S. Nohara, N. Furukawa, H. Inoue, M. Morita, Electrochem and Solid State Lett., 6 (2003) A37.

333. M. G. Sullivan, B. Schnyder, M. Bartsch, D. Alliata, R. Imhof, R. Kotz, J. Electrochem Soc. 147 (2000) 2636.

334. H. Probstle, C. Schmitt, J. Fricke, J. Power Sources, 105 (2002) 189.

335. V. Barsukov, S. Chivikov, Electrochim. Acta, 41 (1996) 1773.

336. X. Liu, T. Osaka, J. Electrochem. Soc. 144 (1997) 3066.

337. M. F. Mathias, O. Haas, J. Phys. Chem, 97 (1993) 9217.

338. R. P. Buck, M. B. Madaras, R. Mackel, J. Electroanal. Chem., 362 (1993) 33.

339. W. J. Albery, A. R. Mount, J. Electroanal. Chem., 388 (1995) 1.

340. H. Keiser, K. D. Beccu, and M. A. Gutjahr, Electrochim. Acta, 21 (1976) 539.

341. R. de Levie, "Advances in Electrochemistry and Electrochemical Engineering, Vol. 6", Interscience Publishers, New York (1967).

342. F. M. Delnick, C. D. Jaeger, S. Levy, Chem. Engg. Commun., 35 (1985) 231.

343. H. Scher, M. Lax, Phys. Rev. B, 7 (1973) 4502.

344. V. M. Kenkre, E. W. Montroll, M. F. Schlesinger, J. Stat. Phys., 9 (1973) 45.

345. K. Takahashi, Electrochim. Acta., 13 (1968) 1609.

346. R. G. Linford, "Electrochemical Science and Technology of Polymers, Vol. 2", Elsevier Applied Science, London (1990).

347. R. de Levie, Electrochim. Acta, 8 (1963) 751.

348. R. de Levie, Electrochim. Acta, 9 (1964) 1231.

349. A.G. MacDiarmid, Rev. Mod. Phys. 73, 701 (2001).

350. B. Scrosati, Prog. Solid State Chem., 18 (1988) 1.

351. S. Skaarup, M. Careem, K. West, in "Solid State Ionics - Materials and Applications," B.V.R. Chowdari, S. Chandra, Shri Singh and P.C. Srivasta, Eds., World Scientific, Singapore, 1992, p. 219.

352. K.P. Vidanapathirana, M.A. Careem, S. Skaarup, K. West, Solid State Ionics 154-155 (2002) 331.

353. S. Skaarup, Lasse Bay, Kamal Vidanapathirana, Susanne Thybo, Pentti Tofte, K. West, Solid State Ionics, 159 (2003) 143.

354. R.H. Baughman, Synth. Met., 78 (1996) 339.

355. C.Arbizzani, M. Mastragostino, L. Menegheta, Electrochim. Acta, 41 (1994) 21.

356. C.Arbizzani, M. Catellani, M. Mastragostino, C.Mingazzini, Electrochim. Acta, 40 (1995) 1871.

357. C. Arbizzani, M. Mastragostino, M. Meneghello, R. Paraventi., Adv. Mat. 8 (1996) 331.

358. A. Rudge, J. Davey, I. Raistrick, S. Gottesfeld., Electrochimica Acta., 39 (1994) 273.

359. S. Panero, A. Clemente, E. Spila., Solid State Ionics., 86-88 (1996) 1285.

360. P. Novak, K. Muller, K.S.V. Santhanam, Chem. Rev., 97 (1997) 207.

361. S. Holdcroft, B.L.Funt, J. Appl. Electrochem., 18 (1988) 619.

362. J. Roncali, A. Yassar, F. Garnier, J. Chem. Soc.: Chem. Comm., (1988) 581.

LIST OF PUBLICATIONS

Papers published / communicated in Refereed Journals:

1) Experimental studies on Solid State Electrical Double Layer Capacitors using Activated Charcoal Powder Electrodes and Poly Vinylidine fluoride-co-Hexa Fluropropylene based Gel Electrolytes.
   S.A.Hashmi, Ashok Kumar and S.K.Tripathi
   Ionics (Germany), **10** (2004) 213-220

2) Investigations on electrochemical supercapacitors using polypyrrole redox electrodes and PMMA based gel electrolytes
   S. A. Hashmi, Ashok Kumar and S. K. Tripathi.
   European Polymer Journal (U.K), **41** (2005) 1373-1379

3) Solid State Redox Supercapacitors using PVdF- HFP based Polymeric Gel Electrolyte and Polypyrrole as conducting polymer Electrodes.
   S.K.Tripathi, Ashok Kumar and S.A.Hashmi.
   Solid State Ionics, communicated

Papers presented in conferences:

1) Studies on Ion-Conducting Polymeric Gel Electrolyte based All-Solid-State Electrical Double Layer Supercapacitors.
   S.K.Tripathi, Ashok Kumar and S.A.Hashmi
   Presented for ISCA Young Scientist Award in 91st Indian Science Congress Association held at Panjab University, Chandigarh in Materials Science section of the conference from January 03-07, 2004.

2) Polymeric Gel Electrolytes Based Solid State Electrochemical Redox Supercapacitors
   S. K. Tripathi, Ashok Kumar and S. A. Hashmi
   Presented in 6th National Conference on Solid State Ionics-04 held at Jadavpur University, Kolkata from October 05-07, 2004.
   (Received "Prof. Suresh Chandra Medal" for best paper presention)

3) Electrochemical Supercapacitors using Polypyrrole and Polypyrrole-cobalt Oxide Electrodes with PMMA based Gel Electrolytes
   S. A. Hashmi, Ashok Kumar and **S. K. Tripathi**
   Presented in International Conference on Electroactive Polymers: Materials and Devices (ICEP-2004) held at Dalhausie, Himachal Pradesh, India from November 01-05, 2004.

4) Electrochemical Supercapacitors based on Amorphous MnO_2 Electrodes and Golymeric gel Electrolytes
   S.K.Tripathi, Ashok Kumar and S.A.Hashmi
   Presented for ISCA Young Scientist Award in 92nd Indian Science Congress Association Conference held at Nirma University of Science & Technology, Ahmedabad, Gujrat, India in Materials Science section of the conference from January 03-07, 2005.
   (Received "ISCA Young Scientist Award")